SORBONNE UNIVERSITE

ÉCOLE DOCTORALE SCIENCES DE L'ENVIRONNEMENT D'ILE DE FRANCE

UNIVERSIDAD NACIONAL AUTÓNOMA DE MÉXICO

POSGRADO EN CIENCIAS DEL MAR Y LIMNOLOGÍA

ACCUMULATION AND PRESERVATION OF ORGANIC CARBON IN MANGROVE SEDIMENTS AT RAMSAR SITES IN MEXICO OVER THE LAST 100 YEARS

Doctoral thesis in Marine Sciences

Presented by

JUPIN Johanna

Under the supervision of SIFEDDINE Abdelfettah et RUIZ FERNÁNDEZ Ana Carolina

Defended on the 20th of June 2024

In front of the Jury:

Dr.	TURCQ Bruno (HDR, IRD-LOCEAN)	President of the Jury
Dr.	PROISY Christophe (HDR, IRD-AMAP)	Reviewer
Dr.	AGRAZ HERNANDEZ Claudia Maricusa (Inv. C, UAC)	Reviewer
Dr.	CARDOSO MOHEDANO José Gilberto (Inv. C, UNAM)	Examiner
Dr.	SIFEDDINE Abdelfettah (HDR, IRD-LOCEAN)	Thesis Supervisor
Dr.	RUIZ FERNÁNDEZ Ana Carolina (Inv. C, UNAM)	Thesis Supervisor

ACKNOWLEDGEMENTS

I am deeply grateful for the support provided by the Posgrado en Ciencias del Mar y Limnología and L'école doctorale des Sciences de l'Environnement d'Ile de France N°129 throughout my doctoral studies. I acknowledge with gratitude the financial support from the Consejo Nacional de Ciencia y Tecnología de México (CVU 1102000), as well as the mobility grants awarded by both the Universidad Nacional Autónoma de México through the PAPIIT-DGAPA IN102821 project, the Instituto de Ciencias del Mar y Limnología, and the Centro de Estudios Mexicanos UNAM-Francia, and by the Institut de Recherche pour le Développement through the international network DEXICOTROP. Additionally, I express my sincere gratitude to the laboratories that hosted me for geochemical analysis: the laboratorio Geoquímica Isotópica y Geocronología from the Instituto de Ciencias del Mar y Limnología, Unidad Académica Mazatlán; the facilities of the Alysés platform in Bondy, France; and the Laboratoire GéoHydrosystèmes COntinentaux at the Université de Tours, Tours, France. Their collaboration was fundamental to the success of my research.

I would like to express my deep gratitude to my two tutors for their unwavering support during this doctoral study. I am deeply grateful for Ana Carolina Ruiz Fernández's invaluable assistance in developing this doctoral project, including her efforts in finding collaborators and securing funding. Additionally, her dedication to reviewing all my articles and her willingness to answer my questions provided me with the necessary guidance and freedom to fully explore and develop my creativity. J'aimerais également remercier Abdel Sifeddine, sans qui ce projet n'aurait pas pu voir le jour. Son accueil chaleureux et son soutien indéfectible m'ont permis de croire en la réalisation de toutes mes idées. J'espère avoir l'opportunité de poursuivre la collaboration sur de grands projets au Brésil.

I am grateful to my advisors and the other members of my Thesis Jury, Christophe Proisy, Bruno Turcq, José Gilberto Cardoso Mohedano, and Claudia Maricusa Agraz Hernández, as well as Francisco Javier Flores De Santiago, who provided valuable advice throughout my Ph.D. Je souhaite également remercier les membres de mon comité de suivi à Sorbonne Université, Mohammed Boussafir et François Colas, ainsi que ma référente, Juliette Mignot, qui m'ont soutenu pour obtenir ma cotutelle et continuer en dernière année de thèse.

I am deeply grateful to A. Garcia-López, F. Briceño-Zuluaga, J.A. Sanchez-Cabeza, J.G. Flores-Trujillo for their invaluable contributions to the completion of this doctoral research. I greatly appreciate the collaboration of A. Grant for the English edition of the scientific articles. I am grateful for the invaluable technical support of L.H. Pérez-Bernal for conducting the ^{210}Pb analyses; M.A. Gómez-Ponce for assistance in sampling tasks and sample preparation; of L.F. Álvarez-Sánchez for support in data curation; of C. Súarez-Gutiérrez for computer support; M. Mendez-Millan and I. Djouraev for conducting isotopic and elemental composition analyses; and Le-Milbeau, and R. Boscardin for conducting Rock-Eval analyses.

INDEX

ABBREVIATIONS

^{210}Pb: Lead-210

CO_2: carbon dioxide

C_{org}: organic carbon

CP: Candelaria-Panlau

EV: El Verde Camacho Lagoon

MAR: mass accumulation rate

MO: organic matter

NDCs: National Determined Contributions

PDE: Palizada-Del-Este

SAR: sediment accumulation rate

TL: Terminos Lagoon

UNFCCC: United Nations Framework Convention on Climate Change

URB: Usumacinta River Basin

$\delta^{13}C_{org}$: isotopic composition of organic carbon

$\delta^{15}N$: isotopic composition of nitrogen

SUMMARY

This doctoral project analyzed the spatial and temporal variability (~100 years) of the origin, accumulation, stocks, composition, and preservation of organic carbon (C_{org}) in mangrove sediments from the Terminos Lagoon, Campeche, and El Verde Camacho Lagoon, Sinaloa, Mexico. This variability was interpreted using environmental indicators, such as precipitation, sedimentation, river discharge, sea-level rise, population growth, land-use change, and deforestation rates. The results showed a progressive increase in sediment and C_{org} accumulation from 1900 to 2021 in the mangroves. This increase was primarily attributed to a rise in continental erosion that occurred parallel to land-use change caused by demographic expansion in the study regions. The eroded organic material was transported by rivers to the mangrove area, where it accumulated and formed stocks of terrestrial-derived C_{org} particularly resistant to degradation. In the river basins that flow into the study lagoons, a decrease in precipitation was recorded from 1959 to 2018. The increase in fluvial fluxes of water, sediment, and C_{org} was not directly related to precipitation trends, but rather to anthropogenic activities that modified sediment dynamics in the basin. This study highlights the adaptability and resilience of mangroves, which accumulated external inputs and, in certain mangrove areas, increased their local C_{org} production to cope with sea-level rise over the past century. These ecosystems are efficient and long-term sinks of C_{org}, and their conservation significantly contributes to mitigating climate change.

Key words: Mangrove, Blue carbon, Organic carbon, Lead-210, Precipitation, Coastal lagoon, Ramsar.

RESUMEN

Esta investigación doctoral analizó la variabilidad espacial y temporal (~ 100 años) del origen, acumulación, inventarios, composición y preservación del carbono orgánico (C_{org}) en sedimentos de manglar de la Laguna de Términos, Campeche, y El Verde Camacho, Sinaloa, México. Se utilizaron diversos indicadores ambientales, como la precipitación, sedimentación, descarga de ríos, nivel del mar, crecimiento poblacional, y cambio de uso de suelo, para interpretar esta variabilidad. Los resultados revelaron un aumento gradual en la acumulación de sedimentos y C_{org} desde 1900 hasta 2021 en los manglares estudiados. Este aumento se atribuyó principalmente al incremento en la erosión continental, en sincronía con el cambio de uso de suelo impulsado por la expansión demográfica. El material orgánico erosionado en la cuenca fue transportado por los ríos hasta la zona de manglar, donde se acumuló y formó inventarios de C_{org} principalmente de origen terrestre y particularmente resistente a la degradación. En las cuencas de los ríos que desembocan en la Laguna de Términos y el Verde Camacho, se registró una disminución en la precipitación desde 1959 a 2018. El aumento en los aportes de agua, sedimentos y C_{org} por estos ríos hacia la zona costera no estaba directamente relacionado con las tendencias de precipitación, sino más bien con las actividades antrópicas que modificaron las dinámicas hídricas y sedimentarias dentro de la cuenca. Este estudio destaca la capacidad de adaptación y la resiliencia del manglar, que progresivamente aumentó su acumulación en material externo y, en ciertos sitios, su producción local en C_{org}, lo que le permitió hacer frente al aumento del nivel del mar durante el último siglo. Estos ecosistemas son sumideros eficientes y a largo plazo de C_{org} y su conservación contribuye significativamente a la mitigación del cambio climático.

Palabras claves: Manglar, Carbono azul, Carbono orgánico, Plomo-210, Precipitación, Laguna costera, Ramsar.

RÉSUMÉ

Cette thèse de doctorat porte sur la variabilité spatiale et temporelle (~100 ans) de l'origine, de l'accumulation, des stocks, de la composition et de la préservation du carbone organique (C_{org}) dans les sédiments de mangroves de la lagune de Términos, Campeche, et la lagune de El Verde Camacho, Sinaloa, au Mexique. Divers indicateurs environnementaux, tels que la précipitation, la sédimentation, le débit des rivières, le niveau de la mer, la croissance démographique et le changement d'usage des sols ont été utilisés pour interpréter cette variabilité. Les résultats ont révélé une augmentation progressive de l'accumulation des sédiments et du C_{org} de 1900 à 2021 dans les mangroves étudiées. Cette augmentation a principalement été attribuée à l'érosion continentale, intensifiée par le changement d'usage des sols résultant de l'expansion démographique. Le matériel organique érodé a été transporté par les rivières jusqu'aux mangroves, où il s'est accumulé et a formé des stocks de C_{org} principalement d'origine terrestre, particulièrement résistants à la dégradation. Une diminution des précipitations a été enregistrée de 1959 à 2018 dans les bassins versants des fleuves qui se jettent dans les lagunes étudiées. L'augmentation des débits d'eau, de sédiments et de C_{org} par le fleuve vers la zone côtière n'était pas directement liée aux tendances des précipitations, mais plutôt aux activités anthropiques qui ont modifié l'hydrodynamique et la sédimentation dans le bassin. Cette étude met en évidence la capacité d'adaptation des mangroves, qui a favorisé l'accumulation en apports externes et la production locale de C_{org}, leur permettant ainsi de faire face à l'augmentation du niveau marin au cours du dernier siècle. Ces écosystèmes constituent des puits à long terme de C_{org} et leur conservation contribue à l'atténuation du changement climatique.

Mots clés : Mangrove, Carbone bleu, Carbone organique, Plomb-210, Précipitation, Lagune côtière, Ramsar.

INTRODUCTION

Mangrove forests are widely recognized as among the most efficient and long-term sinks of blue carbon (i.e., carbon stored in coastal ecosystems), owing to their high productivity, their ability to receive autochthonous and allochthonous inputs of organic carbon (C_{org}), and their high sedimentation rates (Alongi, 2020). Under the framework of the Paris Agreement (2016), signatory countries committed to accounting for their carbon dioxide (CO_2) emissions, conducting an inventory of greenhouse gases, and developing plans to reduce emissions at a national level and adapt to the effects of climate change through Nationally Determined Contributions (NDCs) (Herr and Landis, 2016). As a result, several countries, including Mexico, have integrated mangrove conservation and restoration into their climate change mitigation and adaptation strategies within their NDCs. In its most recent update of its NDC to the United Nations Framework Convention on Climate Change (UNFCCC), Mexico has reaffirmed its priority to develop a 'National Blue Carbon Strategy' for the protection of blue carbon ecosystems such as mangroves (INECC–SEMARNAT, 2022).

The implementation of mangrove protection and restoration actions worldwide is urgent, as these ecosystems face considerable pressure due to high population density and increasing demand for space and resources in coastal areas. It is estimated that nearly 40% of the world's population resides between the coastline and 100 km inland, and population growth in coastal areas is projected to increase between 10% and 22% (14% in Mexico), depending on the countries, between 2020 and 2035 (Maul and Duedall, 2019). Mangroves are often associated with communities with limited economic resources, limited social and food security, and where the exploitation of these ecosystems is high due to the lack of adequate natural resource management policies (Glaser et al., 2010). Between 2010 and 2016, globally, 3,363 km^2 (2.1%)

of mangroves were lost, and 62% of this loss was attributed to land-use change, mainly due to mangrove conversion to aquaculture and agriculture areas (Goldberg et al., 2020). Therefore, anthropogenic activity and its repercussions are the main factors behind mangrove loss worldwide.

Mangrove degradation leads to the loss of all their ecosystem services (e.g., coastline stabilization, nutrient regulation; Primavera et al., 2019) and, in particular, their role as a C_{org} sink. The majority of the C_{org} stocks in mangroves is found within the sediments, constituting up to 90% of the total stocks (e.g., Phang et al., 2015). This high proportion of sedimentary C_{org}, compared to aerial stocks, is primarily due to regular flooding and predominantly anoxic conditions of mangrove sediments, which favor C_{org} preservation. As a result, C_{org} can accumulate over extended periods (centuries to millennia) and constitute substantial and stable stocks (Jennerjahn, 2020). However, destabilizing these sedimentary stocks through anthropogenic activities (e.g., converting mangroves to agricultural areas) would expose sedimentary C_{org} to atmospheric oxygen, leading it to oxidize into CO_2, which would then be added to the greenhouse gas flux in the atmosphere and contribute to climate change (Breithaupt et al., 2012).

While some studies debate the role of mangrove forests as potential sources of greenhouse gases (CO_2, methane, and nitrous oxide) to the atmosphere (e.g., Borges et al., 2003; Purvaja and Ramesh, 2001; Rosentreter et al., 2018) derived from the waters surrounding the mangrove (Bouillon et al., 2003; Koné and Borges, 2008), others demonstrate that mangrove forests act as efficient and long-term sinks of atmospheric CO_2, thus mitigating climate change (Alongi, 2008; Bouillon et al., 2008; E. Kristensen et al., 2008b). This divergence is due to the strong spatial and temporal heterogeneity of the processes associated with mangrove C_{org} accumulation and degradation, leading to uncertainty regarding the magnitude and implications of these variations (Rosentreter et al., 2018). The current debate on the potential role as sinks

or sources of atmospheric CO_2 requires a better understanding of the variability of C_{org} accumulation and fluxes in mangrove sediments. Since mangroves are diverse, complex, and dynamic ecosystems, their study and monitoring requires a multi-temporal (short and long-term), multidimensional (local, regional, global), and multidisciplinary perspective (economic, environmental, and social) (Glaser et al., 2010; Atwood et al., 2017).

Several studies have addressed the identification of possible impacts of climate change on mangroves (e.g., Gilman et al., 2008; Alongi et al., 2016; Ward et al., 2016) and the climatic factors (e.g., precipitation, temperature, and storm occurrence) influencing the growth and distribution of mangrove trees (Alongi, 2009; Simard et al., 2019). Precipitation plays a role in the transport of sediments, carbon, and nutrients in river systems (Soria-Reinoso et al., 2022) and a significant correlation has been found between global precipitation and C_{org} stocks worldwide (Sanders et al., 2016). Depending on the region, potential changes in precipitation patterns due to climate change could impact mangrove distribution, extent, and growth (Ward et al., 2016). An increase in tropical regions due to climate change could result in more frequent and prolonged periods of flooding in coastal wetlands, reducing oxygen inputs to sediment and favoring the preservation of sedimentary C_{org} stocks (Davidson and Janssens, 2006; Sanders et al., 2016). However, precipitation patterns can be highly variable at local and regional scales, as they are influenced by topography and atmospheric circulation, which can be particularly complex in regions like Mexico. For example, in Central America, reductions in precipitation, alterations in rainy seasons, and increases in the occurrence of extreme precipitation events have been recorded in recent decades (Hidalgo et al., 2017, 2013). Decreased precipitation could reduce freshwater input to mangroves, causing high salinity and reduced flooding, which in turn could limit mangrove distribution, extent, and growth (Gilman et al., 2008). However, to date, no integrated study has been conducted addressing the multi-decadal variability of

precipitation and its potential impacts on the dynamics of C_{org} accumulation and preservation in mangrove sediments.

To accurately quantify the accumulation of sediments and C_{org} over time in mangroves, it is necessary to have a reliable time frame. The use of sediment records to reconstruct recent environmental changes in aquatic systems is well established (Emeis et al., 2000; Smith, 2001) and the most commonly used method for dating recent sediments in marine or lacustrine environments is based on the study of profiles of Lead-210 (^{210}Pb) (Koide et al., 1973), a natural radionuclide ($T_{1/2}$ = 22.23 ± 0.12 yr; DDEP, 2012) member of the Uranium-238 chain. ^{210}Pb is formed from the decay of Radon-222 and is supplied to sediments by atmospheric deposition, runoff, or production in the water column and within sediments. ^{210}Pb is an ideal marker for dating sediments in the last 100 years, a period during which appreciable environmental changes have occurred due to global change. In areas where bioturbation, physical mixing, or sediment erosion is minimal, chronology with ^{210}Pb provides the ideal temporal framework for interpreting records of temporal changes in sediment accumulation rate, C_{org} burial rates, and preservation of organic compounds of interest (Sanchez-Cabeza and Ruiz-Fernández, 2012).

C_{org} Burial rates (i.e., velocity at which C_{org} accumulates in the sediment column) and stocks (i.e., C_{org} mass per unit area at a defined depth) are common metrics used to quantify the temporal and spatial C_{org} retention capacity of mangroves (Jennerjahn, 2020). Through stoichiometric relationships, C_{org} stocks can be used to estimate potential CO_2 emissions in case the ecosystem is disturbed (Howard et al., 2014). The accumulation of C_{org} in mangrove ecosystems depends on a variety of interrelated factors, including mangrove community structure, hydrodynamics (e.g., influence of tides, rivers, and currents), local climate (e.g., precipitation and temperature), sediment accumulation rates, C_{org} origin (allochthonous vs. autochthonous), and the efficiency of C_{org} degradation during diagenetic processes (Twilley et al., 1992; Woodroffe et al., 2005; Rovai et al., 2018). By comparing variations in C_{org} burial

rates and stocks with environmental indicators, it becomes possible to reconstruct past conditions that influenced C_{org} accumulation in mangroves.

In particular, to understand the spatial and temporal heterogeneity of C_{org} stocks, it is important to identify the source of C_{org}, i.e., whether it results from local productivity or allochthonous supply (terrestrial and/or marine) (Kusumaningtyas et al., 2019a). The origin of C_{org} can be elucidated through the analysis of (1) the elemental ratio of C_{org} and nitrogen (C:N), which varies, for example, between 4 and 10 for algae, or can be ≥ 20 for vascular plants (Meyers, 1994); and (2) the isotopic composition of C_{org} ($\delta^{13}C_{org}$) and nitrogen ($\delta^{15}N$) which allows for estimation of the proportion between C3 and C4 terrestrial plants, and marine material (Gonneea et al., 2004; Bao et al., 2013; Ranjan et al., 2015). The mangrove-derived C_{org} can represent the majority (~58%) of the C_{org} stored in the mangrove sedimentary stocks (Alongi, 2014). However, allochthonous inputs, which include remains of marine organisms (e.g., micro and macroalgae, seagrasses, transported by tidal currents) and terrestrial (e.g., plant residues carried by surface runoff) (Bouillon et al., 2004; Alongi et al., 2005), can represent significant contributions in mangroves influenced by tides and river discharges (Adame et al., 2012; Bouillon et al., 2003).

Microbial decomposition of organic matter (OM) can occur through aerobic or anaerobic pathways, involving a variety of electron acceptors (Kristensen et al., 2008a). The efficiency of degradation depends on various environmental factors, such as temperature, moisture, pH, and aeration (Rovira and Ramón-Vallejo, 2002), as well as intrinsic properties such as compound type, size, and shape of organic detritus (Osono et al., 2008; Ono et al., 2015). To understand the potential of mangrove sediments as a sink or source of CO_2, it is essential to know the composition and stability of accumulated C_{org}. The C_{org} stability refers to its ability to degrade, from labile (easily degradable) to refractory (difficult to degrade) (Disnar et al., 2003). The composition and stability of C_{org} can be determined through (1) Rock-Eval pyrolysis analysis,

which allows the identification of sources, composition, and preservation state of C_{org} (Espitalié et al., 1985a, 1985b), and (2) palynofacies analysis that quantifies and identifies organic compounds according to their origin (i.e., terrestrial or aquatic), characteristics (i.e., biogenic, anthropogenic, or fossil), and/or formation process (i.e., biodegradation, oxidation, or combustion) (Combaz, 1964; Tyson, 1995).

Mexico ranks 4th among the 125 countries and territories with the largest mangrove cover, although it is also one of the countries with the highest rates of mangrove loss (3.5 million hectares between 1970-80 and 2015; CONABIO, 2017) due to population growth and industrialization. The Terminos Lagoon (TL), Campeche, in the southern Gulf of Mexico, and the El Verde Lagoon (EV), Sinaloa, at the entrance of the Gulf of California, are two examples of coastal areas that possess significant mangrove cover at a regional scale (143,045 ha and 1,300 ha, respectively; CONABIO, 2020). TL can be separated into two subsystems (Fig. 1), Palizada-Del-Este (PDE) in the western zone of the lagoon and Candelaria-Panlau (CP) in the central and eastern zones of the lagoon. PDE contributes to 75% of freshwater discharge to TL from the Palizada River and is characterized by well-mixed, low-salinity waters, muddy sediments, and well-developed, tall fringe mangroves. The CP system contributes to a lower proportion of freshwater input (15% of the total) to TL from the Candelaria River. It has shallow, with predominantly calcareous sediments and fringe mangroves with a tendency towards edge growth (Ramos-Miranda and Villalobos-Zapata, 2015). TL has been significantly altered by human activity, particularly by shrimp farming (since the 1950s) and oil exploitation (since the 1970s), leading to the construction of road networks, pipelines, and canals in the wetlands (Ochoa, 2003). The EV system (Fig. 1) is a coastal lagoon, predominantly closed off throughout the year but with open communication to the ocean during the rainy season (June to October) due to the breaking of the sandy barrier by the combined effects of the Quelite River flow, high tides, and occasional tropical storms and hurricanes (Flores-Verdugo et al., 1995).

The beach and wetlands of EV have been relatively well-preserved in the past, although in recent years, the extent of native vegetation has diminished due to changes in land-use (tourism development, construction of intensive aquaculture ponds, and population settlement growth) (Briseño-Dueñas, 2003).

Due to their significance as habitats of high biodiversity, bird migration, and breeding grounds for many coastal species and the imperative need to protect mangroves from various anthropogenic alterations, both TL and EV have been designated as internationally important wetlands by the Ramsar Convention (TL: site 1356; EV: site 1349; RSIS, 2024a, 2024b). The PDE, CP, and EV systems share similar mangrove species but exhibit contrasting climatic, hydrological, and anthropic characteristics. No previous studies have investigated the temporal variation in C_{org} accumulation and preservation in TL and EV mangrove sediments associated with the anthropogenic and natural pressures experienced in these lagoons.

This doctoral research constitutes the first reconstruction of temporal changes (~100 years) in variables associated with C_{org} dynamics (concentration, origin, accumulation, composition, and preservation) in mangrove sediments, through the study of ^{210}Pb-dated cores from the TL and EV systems. The temporal trends of C_{org} variables were compared with trends in indicators of climate change (e.g., precipitation, sea-level) and anthropogenic interventions (e.g., population growth, land-use change). The results of this study allowed for the reevaluation of the role of mangroves as sinks for atmospheric CO_2 and justified the importance and urgency of preserving and restoring these ecosystems both in Mexico and the rest of the world.

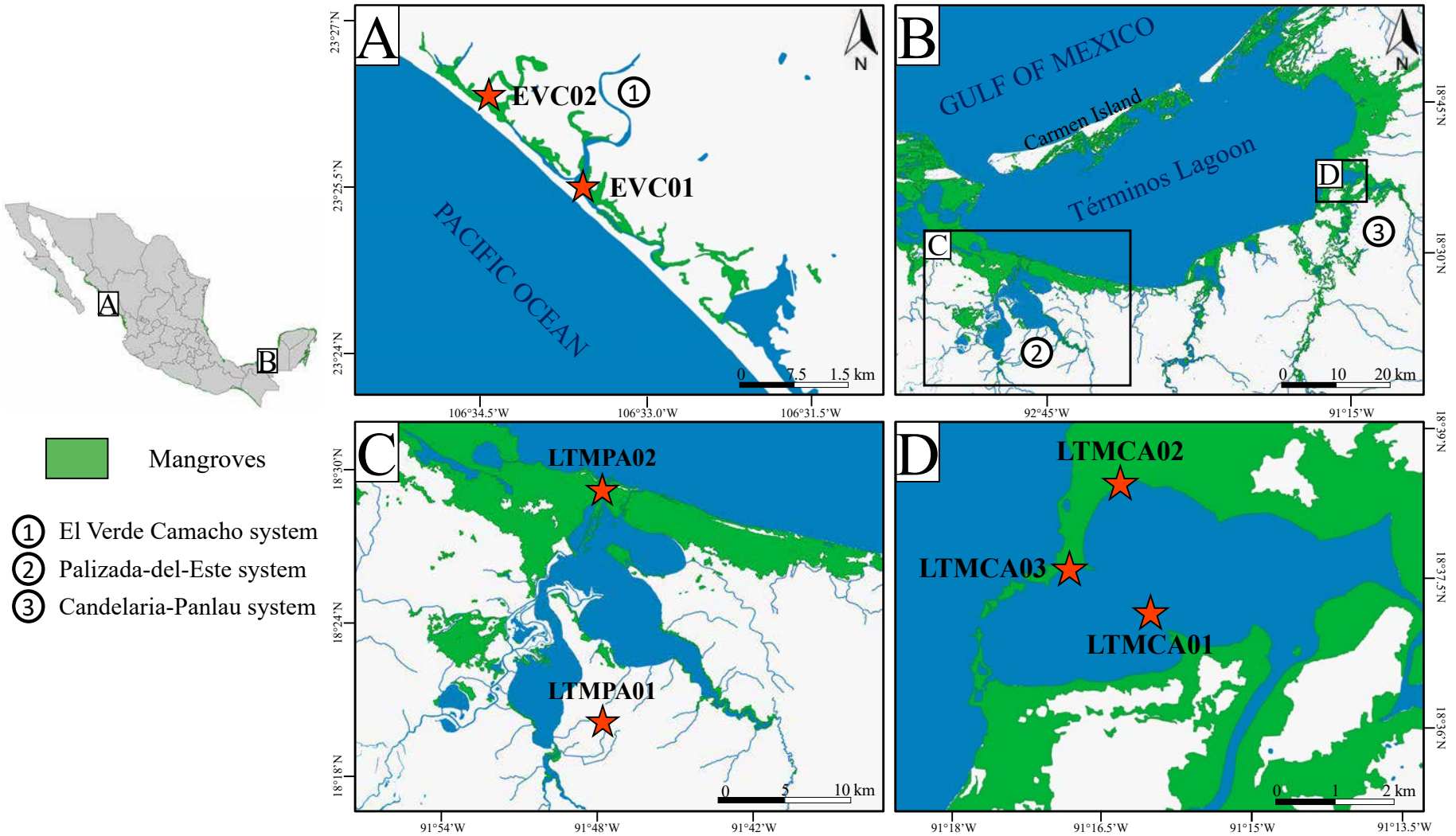

Figure 1. Location of the study sites. A: El Verde Camacho Lagoon, Sinaloa; B: Terminos Lagoon, Campeche, C: Palizada-Del-Este, and D: Candelaria-Panlau. Mangrove cover was sourced from CONABIO (2020).

LITTERATURE REVIEW

The studies on the carbon cycle in the marine environment date back to the 19th century, with early investigations initially focused on the contribution of phytoplankton to the carbon cycle (Riley, 1944). As the 20th century progressed, attention shifted towards understanding the significance of seagrasses and macrophytes as carbon sinks, leading to the initial estimations of their contribution to atmospheric CO_2 sequestration (Boysen-Jensen and Station, 1915; Duarte and Cebrián, 1996; Smith, 1981). The UNFCCC, established in New York on May 9, 1992 (coming into effect on March 21, 1994), was the first international agreement on climate change (Herr and Landis, 2016). It not only formally acknowledged the reality of climate change and humanity's responsibility in its causation but also set forth objectives to stabilize concentrations of greenhouse gases in the atmosphere and underscored the imperative to protect natural CO_2 sinks. Since then, various studies (e.g., Breithaupt et al., 2012; Chmura et al., 2003; Howard et al., 2014) have provided quantitative information on the contribution of blue carbon ecosystems to CO_2 sequestration, long-term burial capacity of C_{org} in blue carbon ecosystem sediments, and the relevance of mangroves among ecosystems with the highest C_{org} storage capacity.

The literature on C_{org} dynamics in mangrove sediment records is extensive and includes estimates of C_{org} burial rates (e.g., Breithaupt et al., 2012; Breithaupt and Steinmuller, 2022; Conrad et al., 2019; MacKenzie et al., 2016), C_{org} stocks (e.g., Kusumaningtyas et al., 2019; Liu et al., 2014), C_{org} origin (e.g., Bouillon et al., 2003; Letourneur et al., 2018; Ray et al., 2018), processes of C_{org} degradation (e.g., Bao et al., 2013; Dittmar et al., 2001; Marchand et al., 2005), and CO_2 and methane emissions to the atmosphere from sediments (e.g., Kristensen et al., 2008b; Rosentreter et al., 2018). However, there often remains a dearth of precision and standardization in methodologies (e.g., variations in sampling methods, observational errors,

instrument imprecision, and inaccuracies in data calculations and reporting) to determine C_{org} sources and burial rates, as well as in understanding the factors influencing C_{org} storage in these ecosystems (Sidik and Friess, 2021). Uncertainties persist regarding mangrove responses to climate-induced factors (e.g., droughts, floods, hurricanes) and anthropogenic interventions (e.g., land-use changes), which have spatially variable impacts worldwide (Macreadie et al., 2019).

Global databases include wide ranges of C_{org} burial rates (ranging from 2.3 to 1750 g m^{-2} yr^{-1}, Breithaupt and Steinmuller, 2022) and stocks (ranging from 72 to 936 Mg ha^{-1}; Atwood et al., 2017), reflecting the high spatial variability in C_{org} accumulation in mangrove sediments. Global patterns and interpolations in these metrics can be biased in regions or countries lacking data (Sidik and Friess, 2021). In Mexico, in particular, the study of blue carbon is relatively recent, and studies on temporal variations in C_{org} sources, burial rates, and stocks in mangrove sediments are still scarce. The synthesis by Herrera-Silveira et al. (2017) on carbon storage and fluxes in Mexican mangroves is based on 48 studies on above-ground C_{org} storage in mangrove forests and, although valuable, is limited by the scarcity of sediment data, which is very relevant, given that most of the stored carbon is found in this compartment (e.g., Phang et al., 2015). Furthermore, in general, the data used are not comparable and are derived from estimates with reported/recommended factors in the international literature rather than locally measured values. The study by Herrera-Silveira et al. (2020) included 196 sediment cores collected around the Mexican coasts and showed high interregional variability in C_{org} stocks at a depth of 1 meter (10-1952 Mg ha^{-1}); however, these sediment cores lacked a chronological framework, and sediment accumulation rates (which can be highly variable) were not reported, implying that accumulated stocks over various periods of time were compared. Generating additional data using ^{210}Pb-dated sediment cores in Mexico is imperative to improve estimates of C_{org} storage and fluxes.

In Mexico, only three studies on C_{org} storage in mangrove sediment areas dated with the ^{210}Pb method were found during literature review. Gonneea et al., (2004) estimated the temporal variations of C_{org} burial rates in sediment cores within channels surrounded by mangroves in the Celestún (55–70 g m^{-2} yr^{-1}), Chelem (35–104 g m^{-2} yr^{-1}), and Terminos (33–117 g m^{-2} yr^{-1}) lagoons in the Yucatan Peninsula; they reported a decrease in C_{org} burial rates towards the present in all three lagoons, which coincided with a decrease in mangrove production. Aldana-Gutiérrez et al. (2021) estimated C_{org} burial rates (8.5 ± 5.2–284.9 ± 48.2 g m^{-2} yr^{-1}) and C_{org} stocks at 1 m depth (375.1 ± 14.2–445.1 ± 11.2 Mg ha^{-1}) in mangrove sediment cores from the Estero de Urías lagoon, in Mazatlan, Sinaloa, Mexico, whereas Vazquez-Molina (2019) estimated C_{org} burial rates (26.1–374.7 g m^{-2} yr^{-1}) and stocks (272–490 ± 1.4 Mg ha^{-1}) in mangrove sediment cores from Puerto Morelos, Quintana Roo, Mexico. In these latter two studies, a general increase in C_{org} burial rates over the past 100 years was observed, primarily attributed to land-use change in the studied regions. In Puerto Morelos, it was found that C_{org} in sediment records mainly originated from terrestrial sources corresponding to C3 plants (Vazquez-Molina, 2019). Additionally, in the vicinity of TL, stocks at 30 cm depth have been evaluated in the Pom-Atasta system (80–236 Mg ha^{-1}; Guerra-Santos et al., 2014) and stocks at 30 and 60 cm depth southeast of Isla del Carmen (12–222 Mg ha^{-1}; Cerón-Bretón et al., 2011); however, these values were calculated with undated sediment samples, so it is unknown whether these C_{org} stocks have comparable formation periods.

In EV, few environmental studies on mangroves and different aspects of carbon dynamics (source, transport, and degradation) were conducted between the 1980s and 1990s, providing information on the main autochthonous sources of OM including the white mangrove *Laguncularia racemosa*, phytoplankton, and the seagrass *Ruppia maritima* (Flores-Verdugo, 1985; González-Farias, 1985); the seasonal variation of *in situ* decomposition of mangrove leaves, which was higher during the rainy season (Flores-Verdugo et al., 1987); laboratory

biodegradation of mangrove leaves from EV which was very slow due to the presence of tannin (González-Farías and Mee, 1988); and the carbon import and export in the system that varied over time and space, depending on hydrological conditions (river discharge, mouth opening and closure, precipitation) (Flores-Verdugo et al., 1995). There are no previous studies on sedimentary C_{org} burial rates and stocks in this ecosystem.

According to the literature, there has been no previous study in Mexico or globally on the relationship between temporal variations in precipitation and indicators of C_{org} dynamics in mangrove sediments over the past century. Furthermore, there is a lack of information regarding burial rates, stocks, composition, and preservation of C_{org} in ^{210}Pb-dated mangrove sediment cores at any of the study sites (EV, PDE, and CP).

JUSTIFICATION AND SIGNIFICANCE

This study is relevant because it provides quantitative information on C_{org} burial rates and stocks in mangrove sediments, which is necessary to improve databases aimed at estimating CO_2 emissions resulting from mangrove disturbances and assessing CO_2 emission reduction through the implementation of conservation or restoration programs for these ecosystems. Determining whether mangroves act as sinks or sources of atmospheric CO_2 is crucial for justifying mangrove conservation as nature-based strategies for mitigating climate change. Additionally, it provides justification for the inclusion of this ecosystem in countries' NDCs worldwide, which is especially significant for Mexico, where the paucity of data complicates the inclusion of contributions from mangrove ecosystems in greenhouse gas emission inventories.

The generation of data on sediment accumulation rates, and C_{org} burial rates and stocks at the study sites, where information was previously unavailable, is crucial for defining patterns of C_{org} accumulation in mangrove sediments at a more detailed scale. This is particularly significant given the complexity and dynamism of mangrove ecosystems. Furthermore, this study uses standardized methods and reliable dating techniques that facilitate inter-comparability between data, both globally and in the specific context of Mexico.

Reconstructing the influence of climatic and anthropogenic disturbances on the origin, accumulation, and preservation of C_{org} in mangroves at a centennial scale is fundamental for predicting in the future how these ecosystems might respond to such changes and anticipating their socio-economic repercussions. The study of precipitation variability and trends holds significant importance as it elucidates its potential impact on the dynamics of C_{org} accumulation and preservation in mangrove sediments. Additionally, the findings regarding precipitation trends are of considerable interest to policymakers and stakeholders for planning and

implementing adaptive measures aimed at mitigating the potential impacts of droughts and floods on populations, ecosystems, and economic activities within these regions.

RESEARCH QUESTIONS

This doctoral research work addresses the following questions:

(1) Are there differences in the variability and trends of precipitation over the study period (~100 years) among the study areas?

(2) Are there differences in sediment accumulation rates over the study period (~100 years) in sediment cores from the study sites?

(3) Are there differences in the sources, burial rates, and stocks value of C_{org} over the study period (~100 years) among the study areas?

(4) Are there differences in the composition and stability of C_{org} (~100 years) among the study areas?

OBJECTIVES

General objective

To evaluate the recent temporal variability (~100 years) of concentration, stocks, burial rates, origin, composition, and preservation of C_{org} in mangrove sediment cores from coastal Ramsar sites in Mexico (TL, Campeche, and EV, Sinaloa), through the analysis of sediment cores dated using the ^{210}Pb method.

Specific objectives

(1) To assess precipitation variability at the study sites and relate it to indicators of climate variability.

(2) To estimate sediment age models and accumulation rates over the past 100 years in sediment cores using the ^{210}Pb method.

(3) To evaluate the temporal variability of C_{org} origin (autochthonous *vs.* allochthonous), concentration, burial rates, and stocks in mangrove sediments over the past 100 years at the study sites.

(4) To assess the composition and stability of C_{org} over the past 100 years at the study sites.

CHAPTER 1

PRECIPITATION VARIABILITY AND ITS RELATIONSHIP WITH CLIMATE VARIABILITY INDICATORS

The first chapter focuses on evaluating precipitation variability at the study sites over the past century and its relationship with indicators of climate variability. The analysis of temporal and spatial precipitation patterns at a regional scale requires long-term observations with sufficiently high temporal resolution and adequate spatial coverage. This chapter is primarily based on the results and interpretations derived from the analysis of precipitation data from the Usumacinta River Basin (URB), which drains into the PDE system and the LT through the Palizada River. The selection of this region was based on the methodology employed, which requires an adequate spatial and temporal density of meteorological stations and precipitation data, according to the thresholds defined by the "climatol" homogenization model and the research objectives (to obtain the longest possible series in order to compare with geochemical variables from sediment cores). These criteria, which are fundamental to conducting a relevant analysis of precipitation trends, were not met in the Candelaria River (CP system) and Quelite River (EV system) basins, preventing a comprehensive study of these regions. As a result, this chapter is split between an article titled "Precipitation Homogenization and Trends in the Usumacinta River Basin (Mexico-Guatemala) from 1959 to 2018," published in open access in December 2023 in the *International Journal of Climatology*, and an additional section addressing precipitation variability in the Candelaria and Quelite River basins.

In the article, the variability and trends of precipitation were evaluated over the most extended available period (1959-2018) using precipitation series from 60 meteorological stations located within the URB in Mexico and Guatemala. Precipitation series often present

missing data and suspicious values, behaviors, or trends induced by non-climatic external factors, generated during the measurement or data digitization process, or by changes in instruments, calibration, or station location. These alterations (or inhomogeneities) could lead to erroneous interpretations. To ensure that the observed precipitation values reflect only climatic processes, the climatol homogenization algorithm was used to perform quality control, homogenization of the precipitation series, and completion of missing data. The corrected and completed series were grouped to investigate the temporal and spatial factors controlling precipitation variability in the URB during the analyzed period. To analyze precipitation trends in the URB, different indicators were used, including the Mann-Kendall tests and Sen's slope, the 30-year precipitation normals, and the Standardized Precipitation Index to quantify the occurrence of dry years.

The novelty of this work, compared to previous studies on precipitation variability in the URB, lies in (1) the inclusion of data from meteorological stations in both countries (Mexico and Guatemala), allowing for a more comprehensive representation of precipitation patterns in the URB; (2) the use of climatol, a recent and flexible tool for performing quality control, homogenization, and filling in missing data in precipitation series; and (3) the identification of precipitation regions and the analysis of long-term trends (1959-2018), which has significant practical implications for sustainable planning and adaptation in the region.

1.1. A CASE STUDY OF THE USUMACINTA RIVER BASIN

Received: 19 May 2022 | Revised: 9 October 2023 | Accepted: 18 November 2023

DOI: 10.1002/joc.8318

International Journal of Climatology | RMetS

RESEARCH ARTICLE

Precipitation homogenization and trends in the Usumacinta River Basin (Mexico-Guatemala) over the period 1959–2018

Johanna L. J. Jupin[1,2] | **Alan A. Garcia-López**[3,4] | **Francisco J. Briceño-Zuluaga**[5] | **Abdelfettah Sifeddine**[2,6] | **Ana Carolina Ruiz-Fernández**[7] | **Joan-Albert Sanchez-Cabeza**[7] | **José Gilberto Cardoso-Mohedano**[8]

[1]Posgrado en Ciencias del Mar y Limnología, Universidad Nacional Autónoma de México, Ciudad de México, Mexico

[2]Institut de Recherche pour le Développement (LOCEAN-IPSL), Sorbonne Université, Paris, France

[3]Departamento de Investigación y Servicios Meteorológicos, Instituto Nacional de Sismología, Vulcanología, Meteorología e Hidrología-INSIVUMEH, Ciudad de Guatemala, Guatemala

[4]Department of Earth and Environmental Sciences, Columbia University, New York, USA

[5]Faculty of Basic and Applied Sciences, New Granada Military University (UMNG), Bogotá, Colombia

[6]ERC2-Université de Quisqueya, Port au Prince, Haiti

[7]Unidad Académica Mazatlán, Instituto de Ciencias del Mar y Limnología, Universidad Nacional Autónoma de México, Mazatlán, Mexico

[8]Estación el Carmen, Instituto de Ciencias del Mar y Limnología, Universidad Nacional Autónoma de México, Ciudad del Carmen, Mexico

Correspondence
Ana Carolina Ruiz-Fernández, Unidad Académica Mazatlán, Instituto de Ciencias del Mar y Limnología, Universidad Nacional Autónoma de México, 82040 Mazatlán, Sin., Mexico.
Email: caro@ola.icmyl.unam.mx

Abstract

The precipitation variability and trends were investigated in the Usumacinta River Basin (URB) for the period 1959–2018, based on imputed and homogenized data records from 60 meteorological stations in Mexico and Guatemala. The homogenization process played a crucial role in enhancing the quality of the original precipitation series, reducing regional inconsistencies and improving temporal and spatial coherence. The dataset reliably captured large-scale climate variations, revealing three regions with similar precipitation variability and trends in the URB. Notably, maximum precipitation occurred at 636 m a.s.l., while minimum precipitation was at 1531 m a.s.l., indicating an orographic effect in the region. Extreme precipitation events were linked to El Niño–Southern Oscillation. Although the Mann–Kendall test showed statistically significant negative trends in only 18% of the stations, integration of Sen's slope analysis and 30-year normals and dry year occurrences highlighted a progressive shift towards dryer conditions throughout the study period in the URB. These drier conditions could notably affect regions with higher precipitation, requiring special attention due to possible socioeconomic impacts associated with drought events. By identifying these vulnerable regions, policymakers and stakeholders can proactively plan and execute adaptive measures to mitigate the potential impacts of droughts on communities, ecosystems, and economic activities within the basin.

KEYWORDS

Central America, climatol, drought, homogenization, precipitation, trend

Funding information
Consejo Nacional de Ciencia y Tecnología-Mexico, Grant/Award Number: CVU1102000; Universidad Nacional Autónoma de México, Grant/Award Number: DGAPA/PAPIIT-IN102821; Institut de Recherche Pour le Développement, Grant/Award Number: DEXICOTROP

1 | INTRODUCTION

Precipitation is one of the most studied hydroclimatic variables because of its important social, economic and ecological implications. Variations in global or local rainfall (i.e., amount, intensity, frequency) can lead to extreme hydrological events (i.e., drought and floods) and affect water availability and management, and agricultural activities, particularly in developing countries (Kotz et al., 2022). Information related to these events is vital in the current scenario of climate change, especially since recent global climate models predict changes in local precipitation patterns, in particular, reduced precipitation and altered rainfall seasons in the Central America region, and a higher number per year of extreme precipitation events (IPCC, 2022). As a result, Central America is considered a region expected to suffer significant agricultural, ecological and hydrological impacts of climate change (Hannah et al., 2017; Hidalgo et al., 2013).

The Usumacinta River Basin (URB) in the southeast of Mexico and northern Guatemala is in the eastern part of the Grijalva-Usumacinta fluvial system, the second largest to flow into the Gulf of Mexico (after the Mississippi River) and the largest river basin in Mexico, accounting for 30% of the surface runoff of the country (CONAGUA, 2018). The URB belongs to one of the world's regions with the greatest biodiversity, as it is home to the Lacandon Jungle, which has the highest biodiversity in the Tropics (Soasores & Garcia-Garcia, 2017). The basin hosts ~2 million inhabitants, belonging to one of the most marginalized populations of Mexico and Guatemala, with the prevalence of indigenous people, who live mainly from crop cultivation and livestock, with low production and high impact on the environment (March-Mifsut & Castro, 2010).

The average annual precipitation in the URB ranges from 1500 mm·year^{-1} in the Mexican lowlands (García, 1998) to 3500 mm·year^{-1} in the Guatemalan highlands (INSIVUMEH, 2016). In this region, precipitation is influenced by easterly waves (Serra et al., 2010), cyclonic activity (NOAA, 2022), polar fronts (Zárate-Hernández, 2013) and the complex topography of the region, resulting in marked contrast in the annual precipitation cycle between the Caribbean and the Pacific slopes (Alfaro, 2002; Giannini et al., 2000; Maldonado et al., 2017; Taylor & Alfaro, 2021). Previous studies have analysed annual precipitation trends based on climate indices from meteorological station series over three decades in the Mexican part of the URB (Aguilar et al., 2005; De la Barreda et al., 2020; Montero-Martínez et al., 2018), and from reanalysis data in the URB region (Andrade-Velázquez & Medrano-Pérez, 2020), and in Mexico (Murray-Tortarolo, 2021); however, most results differed between stations, and precipitation did not show general trends. Furthermore, no studies have examined the variability of rainfall in the URB, including meteorological stations in the Guatemalan portion of the basin, which, however, constitutes the largest area of the URB and experiences a high precipitation variability. This can be explained by the restricted spatial and temporal availability of data in northern Guatemala, which is constrained by the poor infrastructure of the network of meteorological stations due to the difficulty of access (e.g., absence of highways, low population, presence of a jungle; Fuentes, 2021). However, precipitation data from the upper basin is essential for understanding the hydrological processes, water availability and impacts of climate change in the entire river basin.

To calculate climate normals and trends, it is highly recommended to perform quality control and homogenization of the dataset and to ensure that the dataset is complete with no missing or erroneous values (WMO, 2017). Among the datasets that can be considered to study the URB, global satellite and reanalysis data have become increasingly available; however, many of these datasets are not always calibrated with rain gauge information for Mexico and Guatemala (Morales-Velazquez et al., 2021). Satellite datasets typically cover a relatively short-term record, mainly since the 1980s, while reanalysis datasets, generated through data assimilation techniques (Parker, 2016), provide broader temporal coverage, but may exhibit a greater bias in estimating precipitation in complex mountainous regions and tend to overestimate lighter precipitation events while underestimating heavier ones (e.g., Izadi et al., 2021; Jiang et al., 2021). Rain gauge time-series have longer periods of availability, and certain Mexican records have been available since the beginning of the twentieth century (SMN-CONAGUA, 2022). However, these data series are usually limited by gaps in the data and by dubious values, behaviours or trends owing to nonclimatic

external factors, generated during the measurement process or data digitization or by changes in instrument, calibration or station location (Peterson et al., 1998; WMO, 2017). These alterations (inhomogeneities) could lead to erroneous interpretations (Guijarro, 2018). Among the various methods that aim to guarantee that the observed values correspond only to climatic processes, the neighbour-based homogenization algorithm "climatol" (Guijarro, 2019) has outstanding accessibility, flexibility to adapt to any climatic variable, its high tolerance of missing data and capability to deal with any temporal resolution (e.g., day, month or year). In the last few years, climatol has been widely applied to homogenize a variety of daily and monthly climate databases. In particular, it has shown its efficiency in studying air temperature, precipitation, and wind speed series worldwide (e.g., Chile, Meseguer-Ruiz et al., 2018; Australia, Azorin-Molina et al., 2019; Israel, Yosef et al., 2019; Ireland, Coll et al., 2020; Domonkos et al., 2020; Iran, Javanshiri et al., 2021; Canada, James et al., 2022) and is recommended as one of the top homogenization methods (Coll et al., 2020; Guijarro et al., 2023).

This study used a meteorological station dataset over the period 1959–2018 to construct a homogenized and complete precipitation dataset for the URB region, identify the main precipitation regions and the possible factors that explained the spatiotemporal precipitation variability, and conduct a trend analysis at station and precipitation region scale over the study period. It aims to improve upon previous research conducted in the region by introducing several novel aspects: (1) incorporated data from meteorological stations situated in both the Mexican and Guatemalan territories to capture a broader representation of the precipitation patterns and climatic conditions within the URB; (2) the use of one of the most widely used and recent software (climatol) for quality control, homogenization and imputation of missing data to obtain valuable insights into long-term precipitation trends (1959–2018) in the URB; (3) the identification of precipitation regions within the URB to find the main precipitation characteristics and examine long-term temporal trends at yearly scales, which have significant practical implications for sustainable planning and adaptation strategies, particularly for stakeholders and policymakers in the URB region.

2 | MATERIALS AND METHODS

2.1 | Study site

The URB extends from 14.90°N to 18.70°N and from 92.71°W to 89.13°W, and its 77,183 km^2 is shared by Mexico (~46%), Guatemala (~54%) and Belize (<1%). The water source is in the upper basin, in the northwestern highlands of Guatemala (Huehuetenango and El Quiche departments, with a maximum altitude of 3800 m a.s.l). The Usumacinta River runs off through the Mexican states of Chiapas, Tabasco and Campeche before reaching the Gulf of Mexico, with a river flow estimated at 1700 $m^3 \cdot s^{-1}$ (Cotler-Ávalos, 2010). The Köppen climate classification was modified by García (1973) for Mexico, based on temperature and precipitation, and divides the basin into three altitude levels (lower, middle, and upper), for which the climatic types are warm-humid in the lower basin (Am2 (x'); Am(f)) and middle basin (Am), and semi-warm humid in the upper basin ((A)C(m)(f); (A)C(m)). Considering the latitude and altitude ranges of the URB, snow is not considered in the region.

2.2 | Database management

The boundaries of the URB used in this study were geographically defined by Solorza-Gómez (2017) (bold black line in Figure 1). The daily precipitation database for URB was compiled with data from the Mexican states of Campeche, Tabasco, and Chiapas (period 1942–2019) from the database of SMN-CONAGUA (2022), and Guatemala (period 1969–2018) from the National Weather Service (INSIVUMEH, 2021). Precipitation time series from 77 meteorological stations were found in the URB: 70 in Mexico and 7 in Guatemala. Daily data missing from the stations within Mexico were calculated over the respective networks' operating period from this study's database. Daily data missing over its operating period from Guatemalan stations were calculated by Fuentes (2021). As a first step, only time series with ≤20% of daily missing data and ≥10 years of continuous data were selected, that is, 54 in Mexico and 6 in Guatemala (Figure 1 and Table S1, Supporting Information).

For further analyses, monthly accumulated precipitation was computed from daily data. To compute valid monthly accumulates, the daily data had to fulfil two requirements set by the World Meteorological Organization (WMO, 2017): (1) there cannot be 10 days with missing data in a month and (2) there cannot be ≥4 consecutive days with missing data in a month. The neighbour-based homogenization algorithm R-package climatol version 3.1.2 (Guijarro, 2019) was used for quality control of the data, time-series homogenization and imputation of missing data by comparing each time series with a reference series estimated from an average of nearby stations.

2.2.1 | Data availability and homogenization

Climatol requires a minimum of three (ideally five or more) data at every time step (here monthly). Data

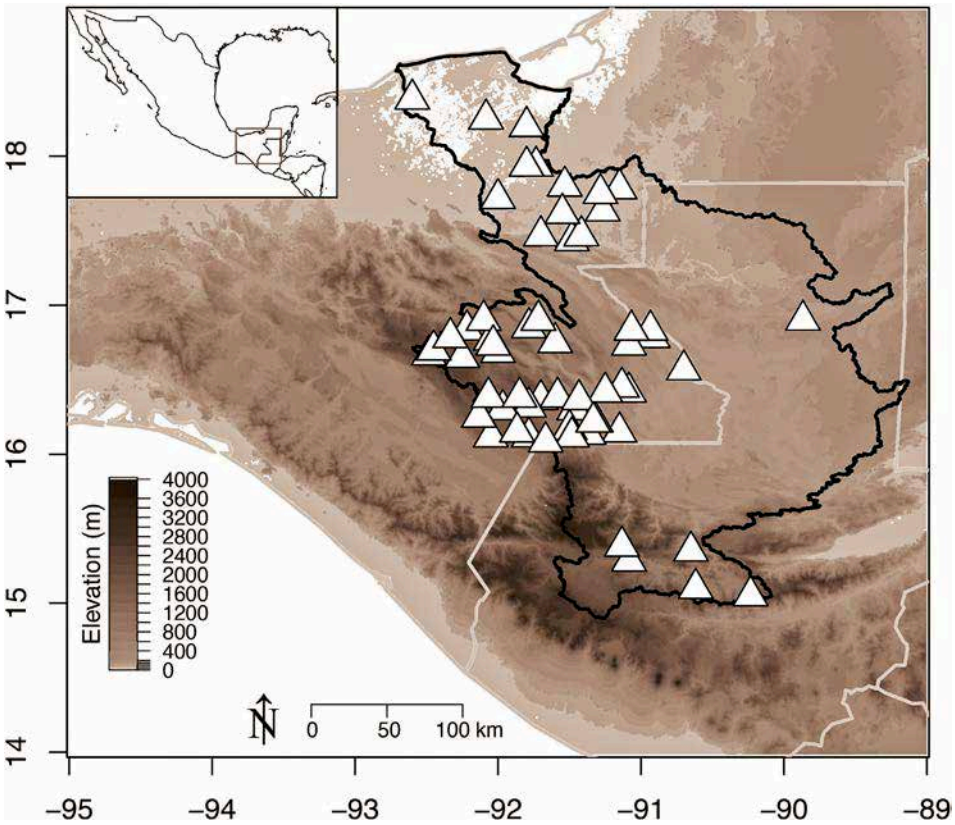

FIGURE 1 Meteorological stations (Δ) used for the analysis of precipitation patterns and trends in the Usumacinta River Basin (bold black line), in southern Mexico and northern Guatemala [Colour figure can be viewed at wileyonlinelibrary.com]

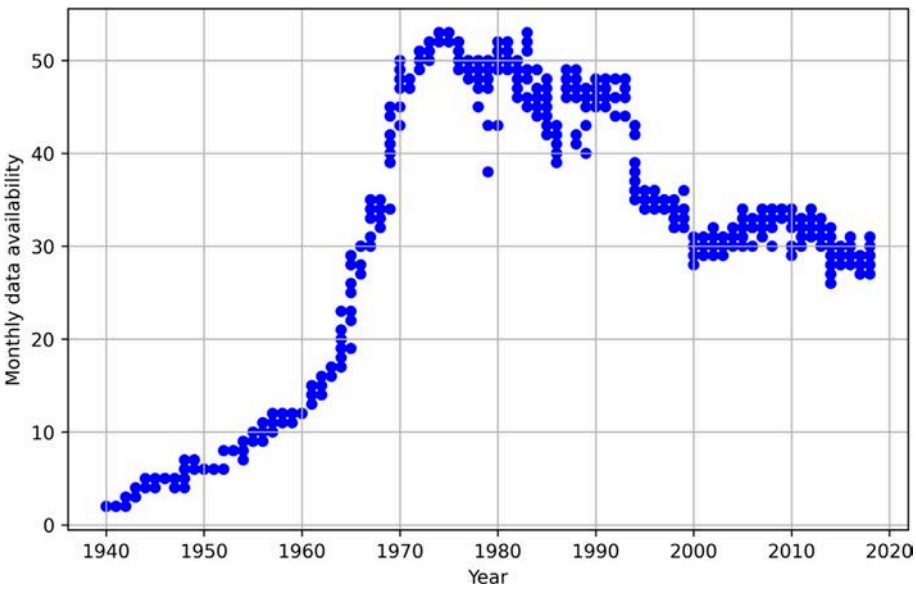

FIGURE 2 Monthly data availability per station in the meteorological stations of the Usumacinta River Basin (1959–2018) [Colour figure can be viewed at wileyonlinelibrary.com]

availability was lowest (3–14 data per month) between 1940 and 1959 and highest (36–51 data per month) between 1970 and 1990 and ranged from 14 to 51 during the period 1959–2018 (Figure 2). To minimize errors stemming from data gaps in the initial decades and enhance the accuracy of infilled data, the monthly accumulated precipitation data were limited to the period 1959–2018 and prepared using the approach outlined by Guijarro (2019). This period allowed the study of two 30-year periods (1959–1988 and 1989–2018) to calculate climate normals and compute consistent trends (WMO, 2017).

From the preliminary run of climatol, the following parameters were determined for quality control, homogenization, and imputation: (i) the minimum and maximum limits for the standardized anomalies that allowed the exclusion of outliers and (ii) the thresholds of the Standard Normal Homogeneity Test (SNHT;

Alexandersson, 1986) that verified the homogeneity of the series, dividing the series at a break-point (i.e., sudden shifts in the means) when the SNHT statistics were more significant than the prescribed threshold, and filling missing data before and after a break-point. To prevent negative values, average ratio normalization was applied to the raw data to indicate that precipitation has a natural zero lower limit. Afterward, climatol was run in full mode with the previously defined thresholds, and complete monthly precipitation series were obtained for each climatological station. The station density was checked to validate the statistical homogeneity of the results (Gubler et al., 2017), and higher weights were assigned to the closest station series during the imputation process. Spearman correlation coefficients between each pair of precipitation series assessed both the strength and direction of the relationship between time-series data before and after the homogenization process and allowed the identification of reference stations for homogenization (Aguilar et al., 2003).

The performance evaluation metrics used for evaluating the impact of the homogenization process on the data quality included: (1) the break-points detection by the homogenization process that indicates when occurred sudden shifts in the means of the station precipitation series (i.e., data irregularities in the series), leading to a break and correction of the series by climatol; (2) the comparison of monthly median accumulated precipitation for raw, imputed and homogenized data, calculating for all the available data in the homogenization process and indicating the monthly distribution of the original data compared to the reconstructed data; (3) the mean absolute difference (in mm) and the bias percentage (in %) for each station, indicating the deviation magnitude and orientation (i.e., under- or over-estimation) of the reconstructed data compared to the original data; and (4) the bias time-series percentage between the means of original and the reconstructed data throughout the study period.

2.2.2 | Precipitation regions and extreme precipitation events

The subsequent analyses were conducted using annual precipitation data calculated specifically for the period from May to October, which corresponds to the 6 months of the highest annual precipitation in the region (i.e., the rainy season; Figure 3), in order to focus on long-term series independently from the impact of seasonal variability. The Gap statistic (Tibshirani et al., 2001) was used to estimate the optimal number of meteorological station clusters, and a hierarchical cluster analysis identified major station groups that shared a similar temporal pattern of annual precipitation (Kolde, 2019).

In order to define dry and wet periods, the Standardized Precipitation Index (SPI; McKee et al., 1993) at a 6-month scale (May–October) was used to quantify the anomalies (Beguería & Vicente-Serrano, 2017) from normal precipitation conditions for each station and cluster. Annual values of 6-month SPI ≤ -1 were considered dry, and annual values of 6-month SPI ≥ 1 were considered wet, between values of 0.99 to −0.99, defined as close to normal (WMO, 2012) (Table S2). The Niño3.4 index (CPC, 2021) was calculated for the period from May to October of each year (using the period of the rainy season defined by SPI; Figure 3) to describe annual ENSO sea surface temperature anomalies in the central Equatorial

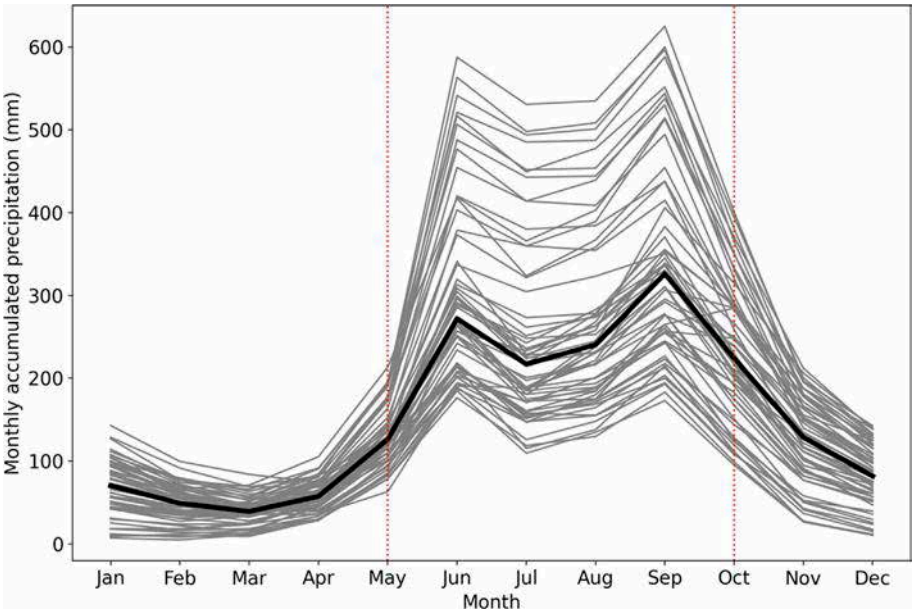

FIGURE 3 Annual cycle of the monthly mean accumulated precipitation for each station in the Usumacinta River Basin (1959–2018). Bold line is the median. Within the dotted lines is found the period of highest annual precipitation in the region (May–October) [Colour figure can be viewed at wileyonlinelibrary.com]

Pacific Ocean (5°N–5°S, 170°E–120°W) and was compared to the occurrence of extremes precipitation events in the 6-month SPI series of each cluster.

2.2.3 | Trends analysis

As precipitation does not follow a normal distribution, the Mann–Kendall nonparametric test (Kendall, 1975; Mann, 1945) and Sen's slope estimator (Sen, 1968) were applied, at a 95% confidence level, to the stations and the cluster series, aiming to detect potential trends within the series and precipitation region. These methods are widely used in analysing hydrological data trends as they are less sensitive to extreme values or outliers (e.g., Aditya et al., 2021; Aswad et al., 2020; Gan & Kwong, 1992; Gocic & Trajkovic, 2013; Hirsch et al., 1982). In particular, Sen's slope analysis offers an estimation of the trend's magnitude (expressed in this study in mm·year^{-1}), enabling the interpretation of both the direction and extent of the trend, even in cases where the Mann–Kendall test does not yield statistically significant results (e.g., Aditya et al., 2021; Aswad et al., 2020; Gocic & Trajkovic, 2013; Stefanidis & Stathis, 2018).

To complete the previous trend analyses, 30-year precipitation normals were calculated and compared for the periods 1959–1988 and 1989–2018. The 30-year normals were derived by averaging the monthly normals for each year of the precipitation series and then computing the mean of the annual normals over the respective 30-year intervals, following the guidelines outlined by the World Meteorological Organization (WMO, 2017). Climate normals have proven to be valuable tools for identifying and quantifying precipitation trends (e.g., Grigorieva & de Freitas, 2014; Kuya et al., 2022). Additionally, the occurrence of dry years based on 6-month SPI values below −1 (WMO, 2012) was compared between the two 30-year periods for each station and precipitation region, aiming to investigate potential changes in extreme drought events over time. The SPI has been previously used for drought monitoring and trend analysis (e.g., Guimarães Santos et al., 2019; Montero-Martínez et al., 2018; Naresh Kumar et al., 2009; Saada & Abu-Romman, 2017).

3 | RESULTS

3.1 | Homogenization and reliability of the imputation

Most of the meteorological stations (50) showed no break-points (splits) through the homogenization process. A total of 13 splits were observed in the time series of 10 stations, with each station experiencing either one or two splits due to anomalous changes in their mean (Figure 4). From the 1980s to 2000s, there was a notable surge in the number of data splits per year, indicating a substantial increase in data inconsistencies. This rise in splits coincided with the progressive decline of data availability in the region (Figure 3).

Considering the entire study period, the mean distance to the closest stations with available data used in the imputation process was 63 km (46–122 km) and 93.33% of stations exhibited a mean value below 100 km (Figure S1), indicating sufficient data within a 100-km radius to perform the imputation and homogenization process. The median Spearman correlation coefficient obtained for time-series from stations within 100 km was 0.81 (0.64–0.92 at a 95% confidence interval) before homogenization and 0.87 (0.75–0.95 at a 95% confidence interval) for the homogenized data (Figure 5). The monthly medians of the raw, imputed and homogenized were compared to gain insights into the potential biases introduced by the homogenization and imputation procedures (Figure 6). In general, the imputed data demonstrated higher median monthly precipitation values (+10.2 mm; +4.5%) compared to the raw data. The difference was more pronounced during the rainy season from May to October (+13.5 mm; +4.8%) compared to the dry season from November to April (+7.0 mm; +4.2%). The homogenized data consistently exhibited higher values (+5.2 mm; +3.4%) than the raw data, both during the rainy season (+4.0 mm; +2.4%) and the dry season (+6.5 mm; +4.4%). However, the homogenized data still remained lower than the imputed data, suggesting that the homogenization process effectively adjusted the dataset and preserved the statistical distribution of the original data, as evidenced by the relationship between the raw and homogenized data, which displayed a high degree of significance with a strong determination coefficient ($R^2 = 0.95$; Figure 7). Among the Mexican stations, stations 7089 and 7006 exhibited noteworthy deviations from the regression line (Figure 7; see detailed discussion in section 4.1).

The absolute differences between the means of monthly precipitation data before and after homogenization were within a narrow range for a majority of the stations, as absolute difference values were below 5 mm for 68% of the stations, below 10 mm for 80% of the stations and below 15 mm for 94% of the stations (Figure 8). The evaluation of bias percentages demonstrated that the majority of stations exhibited minimal bias, with values that were within the range of −5% to +5% for 80% of the stations and between −10% and +10% for 97% of the stations. The comparison between the means of raw and homogenized data over the study period indicated a bias per year that ranged from

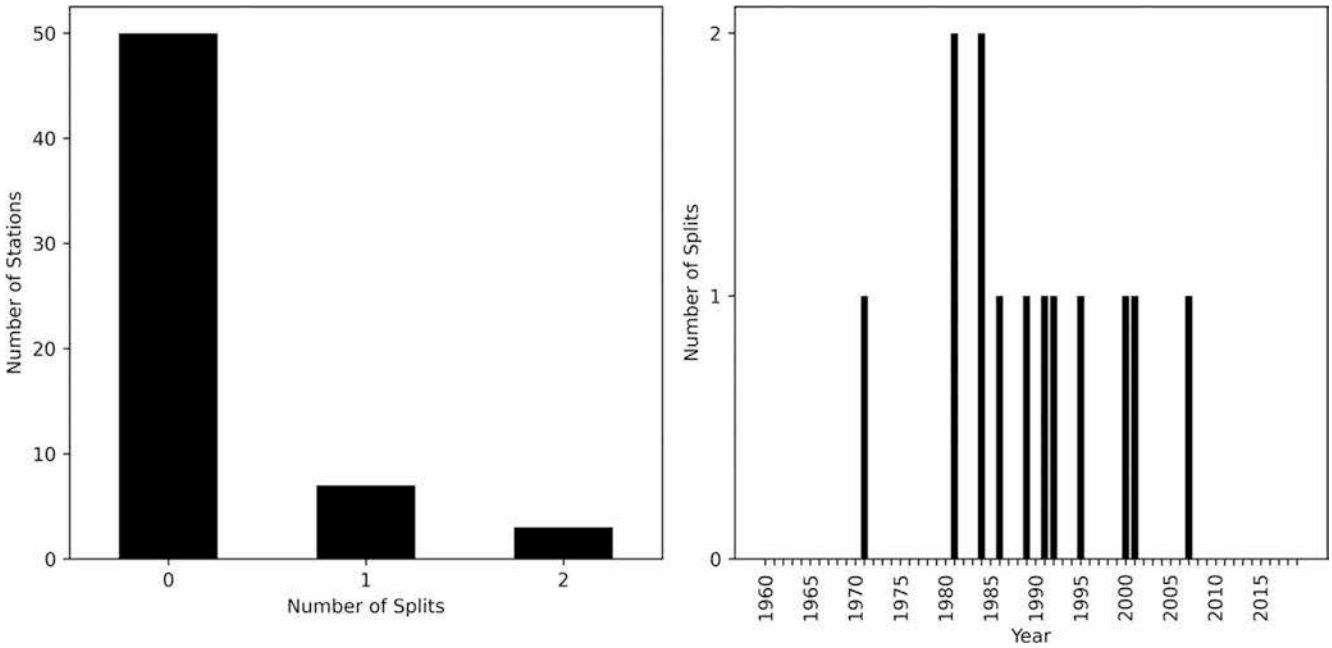

FIGURE 4 Number of splits per station (left) and per year (right) in precipitation series accounted during the homogenization process in meteorological stations from the Usumacinta River Basin (1959–2018)

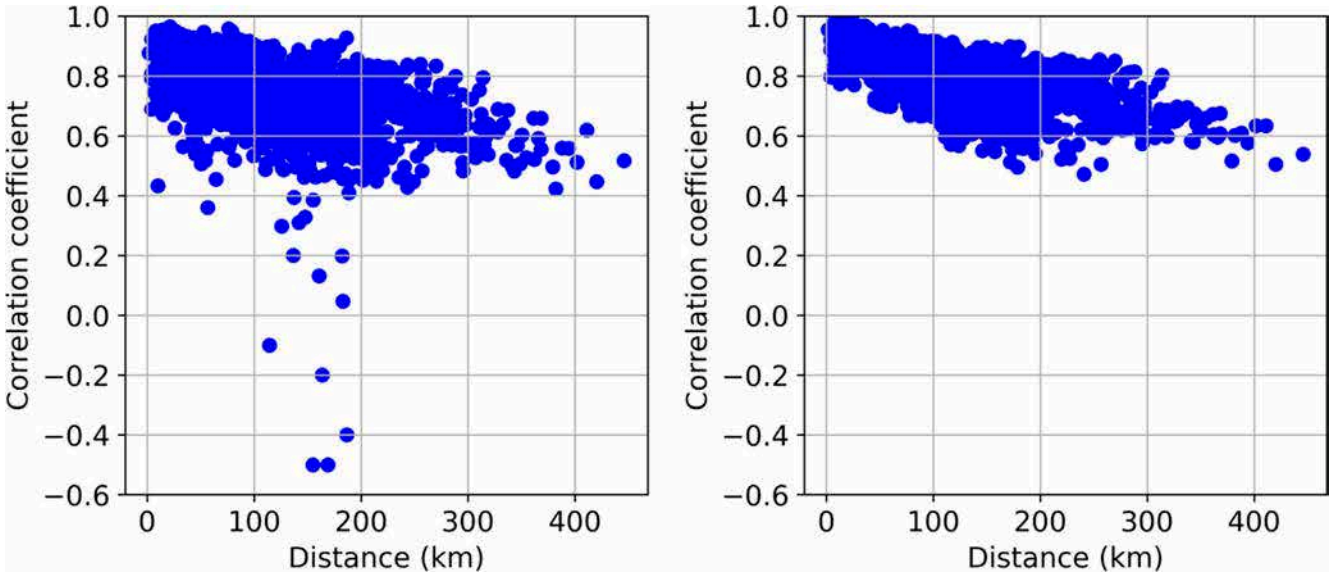

FIGURE 5 Spearman correlation coefficient for time series between stations against their distance for the raw (left) and homogenized data (right) in the Usumacinta River Basin (1959–2018) [Colour figure can be viewed at wileyonlinelibrary.com]

−5.1% to 6% for the period 1959–1988 and from 5% to 21% during the second 30-year period (Figure 9).

3.2 | Data clustering and precipitation anomalies

The median annual precipitation in the URB was 1384 mm·year^{-1} over 1959–2018 (IQR: 1025–1879 mm·year^{-1}) and the median altitude of the stations was 777 m a.s.l. (IQR: 122–1258 m a.s.l.) (Table 1). The data clustering was done on the homogenized data. The Gap statistic identified three main clusters for the study period that suggested the presence of three main precipitation regions within the URB. A composite series of annual precipitation with the average of all stations per cluster was computed (Ci: Cluster i, $i = [1, 3]$; Figure 10 and Table 1). The highest accumulated annual precipitation

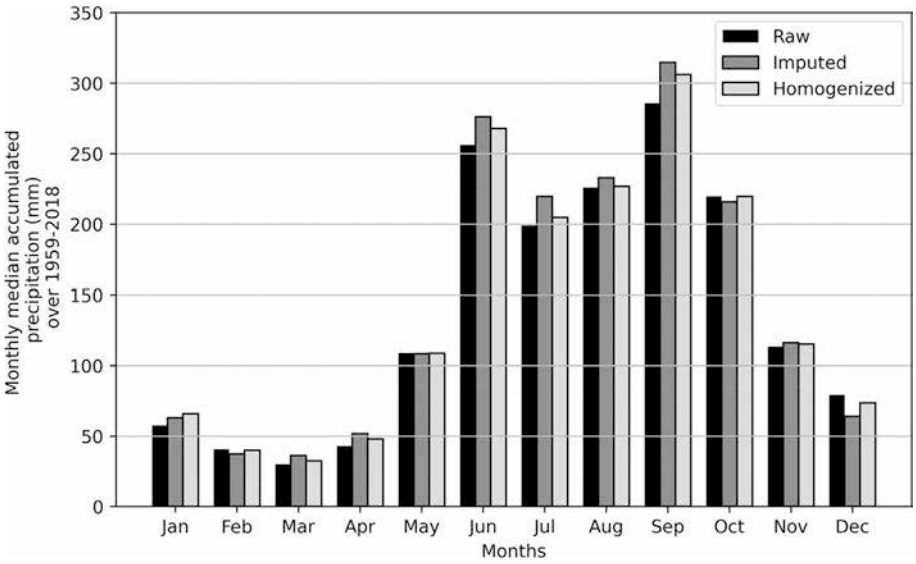

FIGURE 6 Monthly median accumulated precipitation of raw, imputed and homogenized data calculated for all the available data in the Usumacinta River Basin (1959–2018)

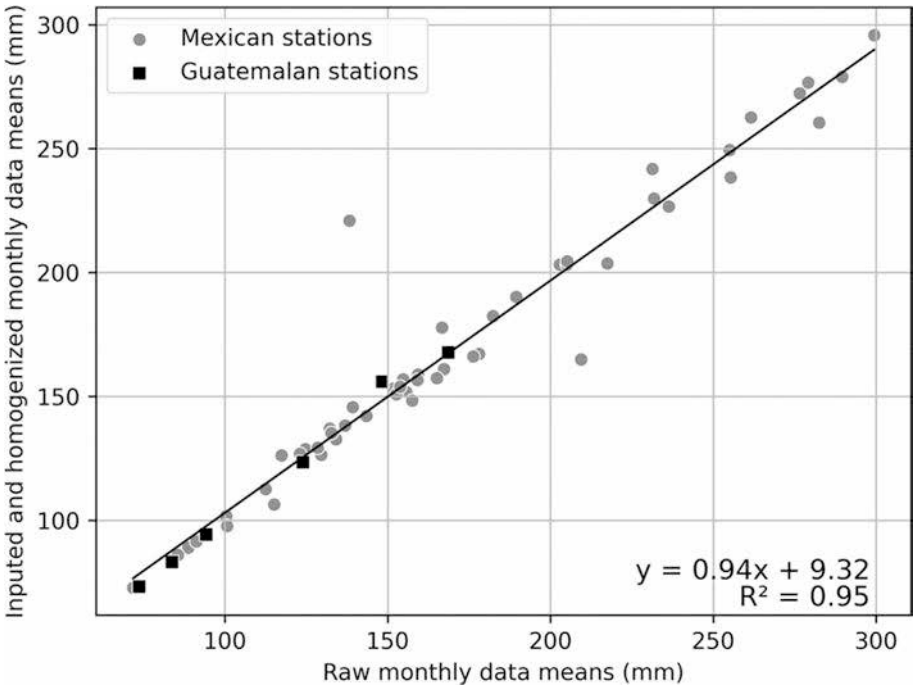

FIGURE 7 Monthly means of accumulated precipitation for raw and homogenized data in the Mexican and Guatemalan meteorological stations from the Usumacinta River Basin (1959–2018)

was in C1 (IQR: 1957–2688 mm·year^{-1}; $n = 15$), which grouped stations in a restricted area of Chiapas (average distance between stations of 62 km) with a mean altitude range of 636 m a.s.l. Precipitation values were intermediate in C2 (IQR: 1160–1604 mm·year^{-1}; $n = 32$) with a lower mean altitude (536 m a.s.l.). Precipitation was lowest in C3 (IQR: 874–1035 mm·year^{-1}; $n = 13$) in the mountains of Chiapas and northwestern Guatemala, including the highest mean altitude (1531 m a.s.l.).

The 6-month SPI analysis revealed similar values among the three clusters, with shared common dry years (6-month SPI ≤ -1; 1994, 2004, 2015, 2016 and 2018) and common wet years (6-month SPI ≥ 1; 1960, 1969, 1981, 1984, 1999, 2010, 2013 and 2017) (Figure 10). Significant ($p < 0.05$) positive Spearman's correlations were found between the 6-month SPI time series of the clusters ($0.81 \leq r \leq 0.88$) and significant ($p < 0.05$) negative correlations were observed between the cluster and Niño3.4 index time series ($-0.40 \leq r \leq -0.31$) (Table 2).

3.3 | Trend analysis

The application of the Mann–Kendall test to the raw data revealed significant ($p \leq 0.05$) trends, both positive and negative, in eight stations across the basin (Figure 11).

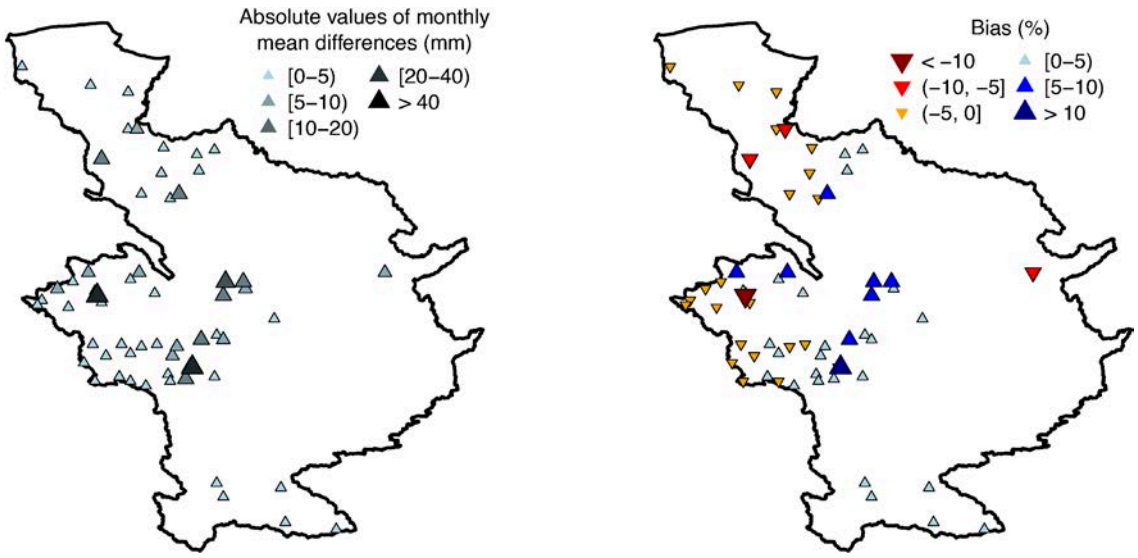

FIGURE 8 Mean absolute difference (left) and bias percentages (right) between the raw and homogenized data at monthly scale in meteorological stations from the Usumacinta River Basin (1959–2018) [Colour figure can be viewed at wileyonlinelibrary.com]

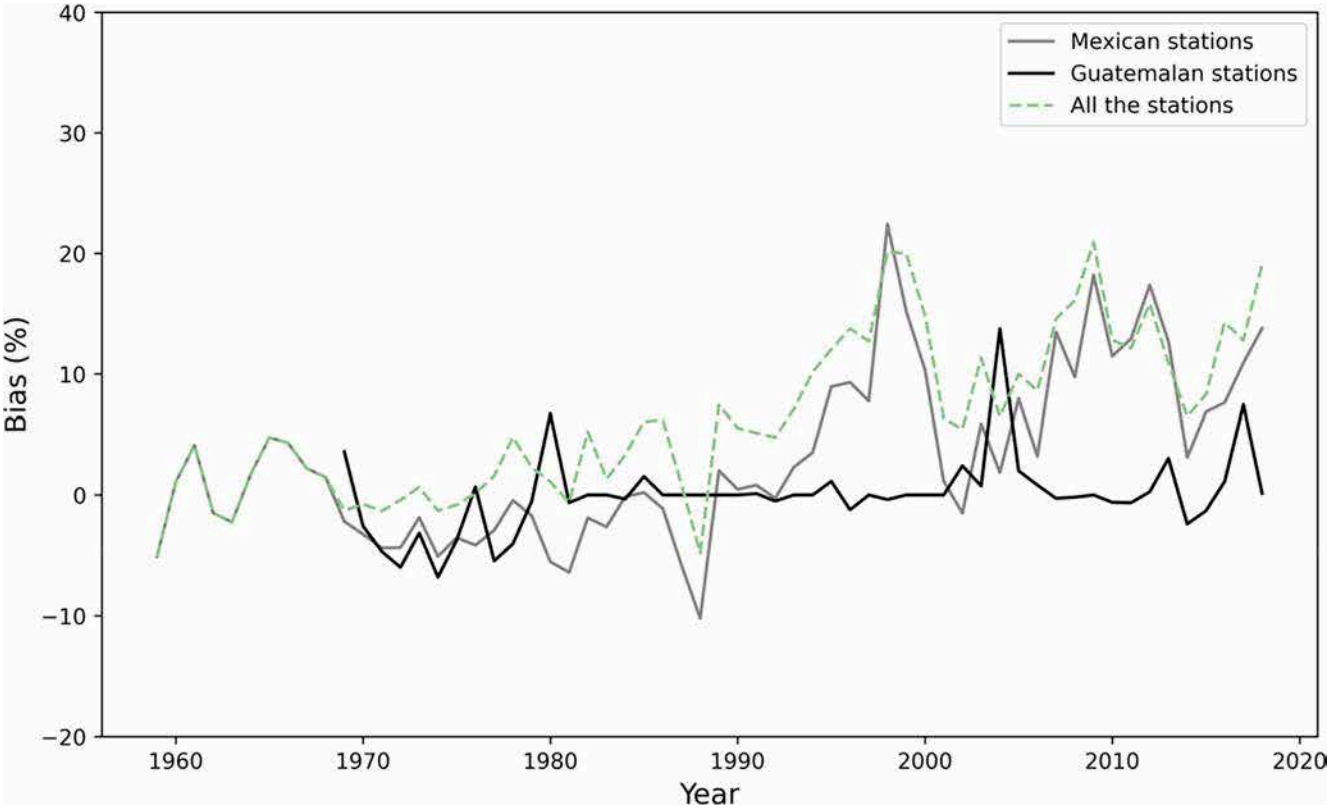

FIGURE 9 The yearly mean bias percentage between the raw and homogenized data from the Usumacinta River Basin (1959–2018) [Colour figure can be viewed at wileyonlinelibrary.com]

The median Sen's slope, indicating the magnitude of the observed trends, was calculated as −0.12 mm·year^{-1} (−0.51 to 0.26 mm·year^{-1}). When comparing the 30-year normals, the results revealed that 35 stations exhibited values of difference ranging from −10% to 7% in 1989–2018 compared to 1959–1988, while the remaining stations recorded values below −10%. Moreover, among all the stations, 32 stations displayed an increase of 1–4 dry years (6-month SPI values ≥1) during the second period. Fourteen stations showed no

TABLE 1 Annual precipitation, station altitude, and trend analysis in clusters grouping meteorological stations from the Usumacinta River Basin (1959–2018)

Stations clustering	All stations	Cluster 1	Cluster 2	Cluster 3
Number of stations	60	15	32	13
Median annual precipitation (mm·year^{-1})	1384	2311	1364	874
Precipitation interquartile range (mm·year^{-1})	1025–1879	1957–2688	1160–1604	874–1035
Mean altitude (m a.s.l.)	777	636	536	1531
Altitude interquartile range (m a.s.l.)	122–1258	265–712	19–963	1180–1750
Trend analyses				
Kendall's tau	−0.08	−0.10	−0.09	−0.10
p-value	0.36	0.31	0.45	0.41
Sen's slope (mm·year^{-1})	−2.33	−3.89	−2.10	−1.95
Difference in climate normals (%)[a]	−4.70	−4.77	−4.65	−2.60
Increase in dry year[b]	+4	+6	+7	+4

Abbreviation: m a.s.l., meters above sea level.
[a]Comparing the two 30-year periods of 1959–1988 and 1989–2018.
[b]Based on the number of dry years (defined as 6-month-SPI values >1) in 1989–2018 compared to 1959–1988.

change, while another 14 experienced a reduction of one or two dry years from 1989 to 2018 when compared to the 1959–1988 period.

After homogenization of the station series, the Mann–Kendall test revealed significant ($p \leq 0.05$) negative trends in 11 stations from the central-western region of the URB, which exhibited negative Sen's slopes values (−4 to −6 mm·year^{-1}), a notable difference between the 30-year normals (−22% to −10%) and a higher number of dry years (+6 to +11 dry events) during the second period compared to the first. At the scale of the basin, the Sen's slope value was negative for 82% of the stations (median: −2.33 mm·year^{-1}) and the difference between the 30-year normals was negative for 81% of the stations (−4.70%). The analysis of the 6-month SPI revealed an increase in the number of dry years during the second 30-year period, observed in 92% of the meteorological stations. More than half of them (52%) experienced an additional 4–11 dry years occurring during the second period.

At the scale of the precipitation regions, the Mann–Kendall test on homogenized data assessed negative values of a nonsignificantly ($p \geq 0.05$) monotonic trend in the cluster time series of the URB (−0.09 to −0.10) (Table 1). Sen's slope estimated the magnitude of that trend, accounting for −3.89 mm·year^{-1} in C1, −2.10 mm·year^{-1} in C2, and −1.95 mm·year^{-1} in C3. The discrepancy in climate normals exhibited a negative trend across all three precipitation regions, with C1 displaying a higher disparity compared to the other clusters. Over the second period (1989–2018), a noticeable rise in dry years was observed, showing an increase ranging from +4 to +7.

4 | DISCUSSION

4.1 | Reliability of the imputation and homogenization process

Studying temporal and spatial precipitation patterns at a regional scale requires long-term observations at sufficiently high temporal resolution and enough spatial coverage (Easterling, 2013). However, these conditions are challenging in the URB region. Indeed, data were scarce in Mexico before 1960 (3–14 data per month) and nonexistent in Guatemala before 1970 (Figure 2); this was due to the paucity of meteorological stations during earlier times, as was the case in most of the countries of Central America (e.g., Aguilar et al., 2005; INSIVUMEH, 2016). The declining data availability in Mexico, starting in the 1980s and accelerating after the 1990s, is likely due to budgetary constraints (CONAGUA, 2012) because many climatological stations in Mexico that were operative in the 1950s were progressively suspended (SMN-CONAGUA, 2022): of 5880 stations that were once operative in Mexico, only 3348 remain operational in the country (CONAGUA, 2018). Results suggested that the restructuring of the station network in Mexico may have compromised the quality of data from the 1980s to the 2000s, resulting in a noticeable rise in data inconsistencies and irregularities during this timeframe (Figure 4). The station INS-110104 (Flores) in Guatemala exhibited data inconsistencies in 2000 that can be ascribed to localized alterations introduced during the measurement or data digitization process, which may occur in the Guatemalan station network, as reported in Fuentes (2021).

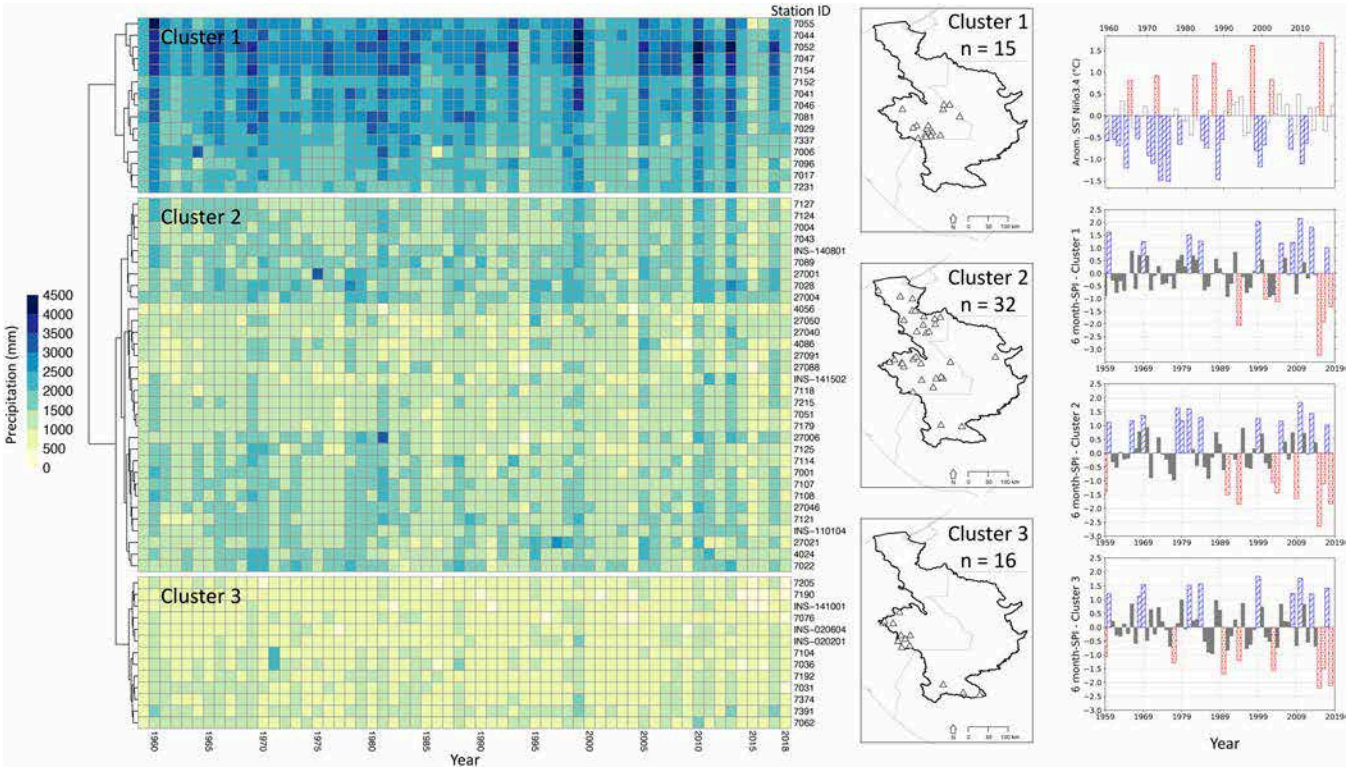

FIGURE 10 Heatmap of annual precipitation for each station grouped by cluster (left); station localization (Δ) (centre); time series of the Niño3.4 index and the 6-month Standardized Precipitation Index (SPI) for each cluster (right) in the Usumacinta River Basin (1959–2018). On the right, hatched bars represent the occurrence of wet years (6-month SPI > 1) and La Niña events (Niño3.4 index ≤0.5°C), whereas dotted bars represent dry years (6-month SPI < 1) and El Niño events (Niño3.4 index ≥0.5°C) [Colour figure can be viewed at wileyonlinelibrary.com]

TABLE 2 Spearman's correlation coefficients between the time-series of 6-month SPI in clusters and the Niño3.4 index in the Usumacinta River Basin (1959–2018)

	Cluster 1	Cluster 2	Cluster 3	Niño3.4
Cluster 1	1	0.88	0.81	−0.31
Cluster 2		1	0.81	−0.40
Cluster 3			1	−0.47
Niño3.4				1

Note: Values shows significant correlations (95% of confidence level, $p < 0.05$); $n = 60$.

The imputation process, relying on a reference precipitation series derived from an average of neighbouring stations, was made possible over the study period due to low mean distances from the closest station with available data (46–122 km) (Figure S1) and the strong correlation observed among their time-series (Figures 5 and S1). The homogenization process improved the correlation coefficients among precipitation time-series, as indicated by an increase from a median value of 0.81–0.87 (Figure 5) and a diminution of the bias percentage of monthly median accumulated precipitation between the raw and imputed data (Figure 6), demonstrating the efficacy of the homogenization process in enhancing the quality of the data compared to its pre-homogenization state. Overall, the monthly means of the two datasets exhibited a strong relationship ($R^2 = 0.95$; Figure 7), and the absolute differences and the bias between the means of nonhomogenized and homogenized series were low for the majority of the stations (Figure 8), indicating a high level of accuracy and agreement between the nonhomogenized and homogenized data. Throughout the study period, the bias time-series percentage between the raw and homogenized data remained consistently low (Figure 9), indicating the successful preservation of the temporal distribution of average precipitation despite the homogenization process. In the second 30-year period for the Mexican stations, bias values increased slightly (ranging from 5% to 21%) due to a higher correction of artificial precipitation values and trends through the homogenization process after the break-point detection (Figure 4).

Despite the presence of a unique station in the northern part of Guatemala (INS-110104), the closest stations that served as references for its missing data imputation were located within a 122 km radius (Figure S1) and the

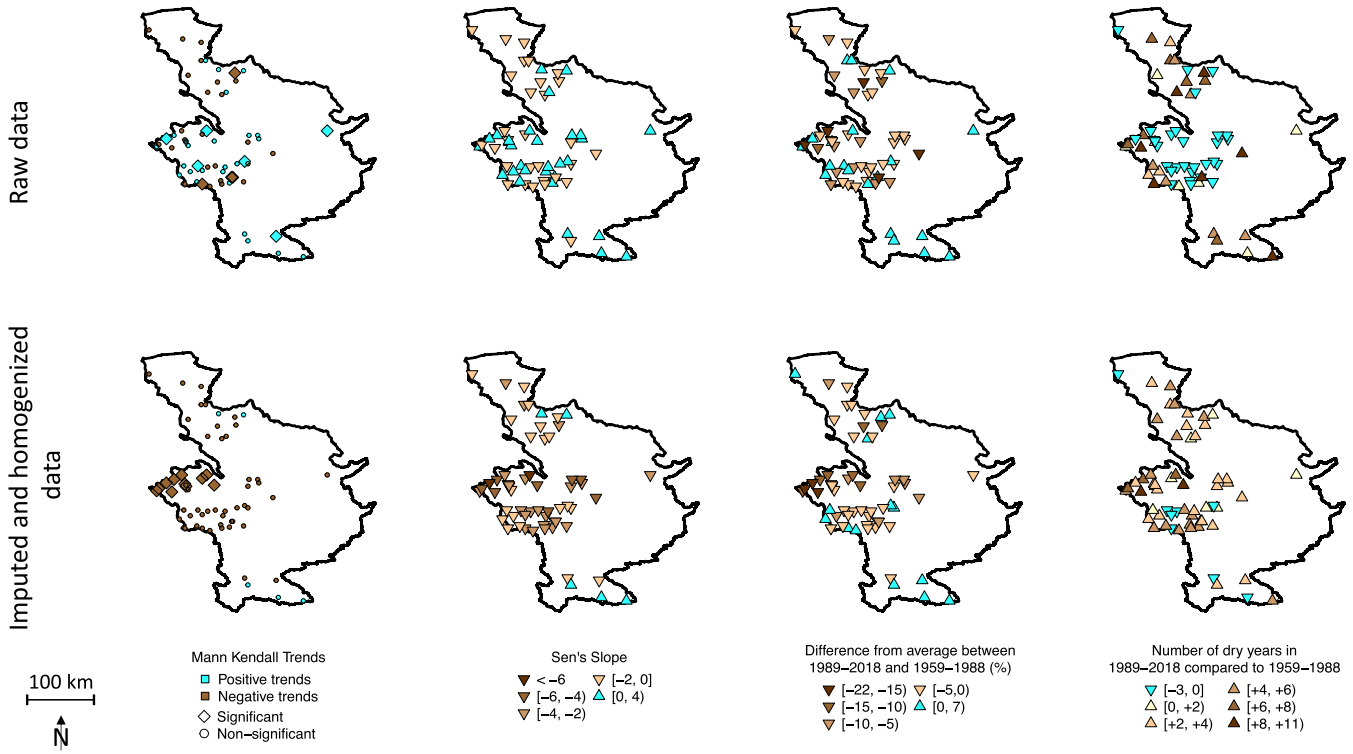

FIGURE 11 Trend analysis over the station series (Mann–Kendall and Sen's slope) and the difference normals and the number of dry years between the two 30-year periods (1959–1988 and 1989–2018) for nonhomogenized and homogenized data in the Usumacinta River Basin [Colour figure can be viewed at wileyonlinelibrary.com]

correlation coefficients between the station INS-110104 and other stations were relatively high (76–78, 95% confidence interval), indicating sufficient data for the infilling procedure and good correspondence with other station series. Moreover, station INS-110104 presented a minimal amount of missing data (2%) during its operational period (Fuentes, 2021) and its reconstructed data was reliable, as demonstrated by low absolute difference (7.6 mm) and bias percentage (−5.2%) values compared to the original data (Figures 7–9).

Among the Mexican stations that were analysed, the two stations 7089 and 7006, stood out from the others for showing noticeable deviations from the regression line (Figure 7) and relatively high absolute difference values (7089: 44 mm; 7006: 83 mm; Figure 8), although the correlation coefficients were high before homogenization (7089: 0.86; 7006: 0.82), indicating a similar temporal variability with other stations. This was explained by the presence of significant shifts in precipitation series detected by the SNHT test, which were attributed to nonclimatic external errors, likely resulting from changes in the instrument or calibration. These alterations affected the recorded precipitation values after the breakpoints. For instance, station 7089 showed a transition from mean monthly values around 220–110 mm after the breakpoint. Similarly, station 7006 displayed anomalous high precipitation values during the period December 1986–August 1989 compared to nearby stations, leading to the detection of two breaks before and after this period.

The different used parameters have demonstrated the reliability of climatol in imputing and homogenizing the precipitation series of each station, successfully rectifying data inconsistencies as observed in stations 7006 and 7089. Following homogenization, the station series presented improved temporal and spatial coherence compared to the nonhomogenized series.

4.2 | Precipitation regions

The three clusters of meteorological stations, each corresponding to different precipitation regions, exhibited well-defined and distinct precipitation ranges. The C1 stations, situated at intermediate altitudes, exhibited the highest median precipitation, while the C3 stations, located at the highest altitudes, experienced the lowest median precipitation. Thus, the spatial distribution of clusters was primarily influenced by altitude, where the highest precipitation was observed at a mean elevation of 636 m a.s.l., represented by C1, and the minimum precipitation occurred at a mean elevation of 1531 m a.s.l, as shown by C3. The wide altitude range of the C2 stations (19–963 m a.s.l) reflected the influence of other factors, such as the source and direction of wind and humidity

(windward/leeward mountainsides) and the distance to the ocean (Houghton, 1979).

The relationship between elevation and precipitation is the result of the orographic effect occurring in the Tropics, a combination of the cooling of moist air ascending along the mountains and the decreasing air moisture with altitude (Daly et al., 1994; Fernández et al., 1996; Houghton, 1979), that produces an increase in precipitation until a particular elevation (belt of maximum precipitation) after which precipitation declines with higher elevation. Finding a belt of maximum precipitation is a frequent phenomenon in the mountains of the Tropics and subtropics (Hastenrath, 1967) and has been found around the world, such as India (Puvaneswaran & Smithson, 1991), Costa Rica (Chacón & Fernandez, 1985; Fernández et al., 1996) and Morocco (Abahous et al., 2018). The belt of maximum precipitation of this study defined as 265–712 m a.s.l. and based on C1 stations (Table 1) was found at a lower altitude than other studies in Central America, such as on the Pacific escarpment of the Guatemala Highlands (900 m a.s.l.; Hastenrath, 1967) and on the Pacific and the Caribbean coasts (~1000 m a.s.l.; Fernández et al., 1996) and in the Reventazón River Basin (1700 m a.s.l.; Chacón & Fernandez, 1985) in Costa Rica. This level varies in Central American mountains; it depends on each region's topographic and meteorological conditions but is generally reported to occur at intermediate elevations.

Certain events of El Niño (Niño3.4 index ≥0.5°C) and La Niña (Niño3.4 index ≤0.5°C) were associated with changes in URB precipitation in the last decades (Figure 10; hatched bars for dry years and El Niño events; dotted bars for dry years and La Niña events). All the clusters showed mild to severe drought SPI categories ($-1 \leq$ 6-month SPI < -1.5) in the URB linked to the El Niño medium intensity event of 2002–2003 and linked to the very intense El Niño event of 2015. The strong La Niña events of 1999 and 2010 were associated with severely wet conditions (6-month SPI ≥ 1.5), and the moderate event of La Niña in 1984 was related to the moderate wet conditions (6-month SPI ≥ 1) in the URB. In particular, these events were also evident in the temporal bias (Figure 9), where they resulted in a notable increase in variability among the station series. Specifically, we observed a higher bias during La Niña events and a lower bias during El Niño events, compared to the original series. The significant negative correlation ($-0.47 \leq r \leq -0.32$; $p < 0.05$) found between the time-series of the clusters and the Niño3.4 index (Table 2) is consistent with results from previous studies in the URB region (Andrade-Velázquez & Medrano-Pérez, 2020; INSIVUMEH, 2016) and in Central America (Alfaro, 2002; Maldonado et al., 2018), as a result of the impact of El Niño events on the moisture transport for Central American precipitation (Durán-Quesada et al., 2017). In addition, evidence of a relationship between drought and El Niño events has been found in southern Mexico (Magaña et al., 2003; Salas-Flores et al., 2014; Salas-Flores & Jones, 2014). The possible further increases in the frequency and intensity of extreme El Niño events related to climate change (Cai et al., 2022; Wang et al., 2019) may lead to future drought conditions in the URB and associated socioeconomic consequences, although further research and consideration of various factors are required to better understand and project the future behaviour of ENSO under the influence of anthropogenic climate change (Cai et al., 2022).

4.3 | Trend analysis at station and precipitation region scale

Based on the Mann–Kendall test results, a small number of meteorological stations presented statistically significant trends over 1959–2018 in both non-homogenized (8 stations) and homogenized (11 stations) data, suggesting that the rest of the station data or the period considered in this study may be limited in capturing significant precipitation trends due to its inherent wide variability (WMO, 2017). This concurs with most previous findings for Central America (Alfaro-Córdoba et al., 2020; Durán-Quesada et al., 2017; Hannah et al., 2017; Hidalgo et al., 2013, 2017; Maldonado et al., 2021), which have suggested that precipitation trends are not always homogeneous for Central America and depend on the database used in the assessment. However, the investigation of trends in this study was extended through the integration of results based on the reconstructed homogenized data and different trend methods, such as Sen's slope, climate normals, and the occurrence of dry years.

Before homogenization, the trend analysis using the raw data yielded a mixture of trends over the study period, with 55% of the stations exhibiting positive trends and 45% showing negative trends, and a low magnitude of change, as indicated by the Sen's slope values (−0.51 to 0.26 mm·year^{-1}). The difference between the 30-year normals (−6.1 to +4.8%) and the change in dry years (−2 to +5) in 1959–1989 to 1989–2018 did not show a general pattern (Figure 10). However, after homogenization of the station series, the Mann–Kendall test showed a concentration of significant ($p \leq 0.05$) negative trends in the central-western region of the URB, which was identified as the area with the most pronounced drought condition within the URB. The remaining stations of the URB also exhibited a general negative trend; however, these trends did not reach the statistical significance threshold. The negative value of the Sen's slope confirmed declining precipitation in most of the meteorological stations, with

high magnitudes of change (−4 to −6 mm·year^{-1}) (Figure 10). The evidence indicating a trend towards drier conditions was reinforced by strong negative values in the difference of 30-year normals (−22 to −5%), indicating lower mean precipitation in 1989–2018 compared to 1959–1988, and an observable increase in the occurrence of dry years during the second 30-year period (+6 to +11) across the majority of stations.

Applying homogenized data for analysing precipitation trends enhanced spatial and temporal coherence compared to nonhomogenized data (Figures 5 and 11). When executed correctly and with meticulous control of parameters, the improved coherence within long-term trend data series is a consistent and expected result of the homogenization process (Aguilar et al., 2003), widely observed in studies employing climatol methodology on hydroclimatic datasets (e.g., Abahous et al., 2020; Javanshiri et al., 2021; Kessabi et al., 2022; Kuya et al., 2022; Meseguer-Ruiz et al., 2018; Yosef et al., 2019). The validation of the data density and reliability of the homogenization process within the URB (in section 4.1) confirmed the accuracy of trends derived from the homogenized dataset, and it also ensured that the heightened coherence within series directly resulted from effectively eliminating nonclimatic noise while preserving natural climatic data variability and information.

The comparison of results obtained before and after the homogenization process (Figure 11) through the Mann–Kendall test evidenced a transition from significant positive trends to significant negative trends in precipitation records from two of the meteorological stations, as well as a shift from significant to nonsignificant trends in the records of another five stations. Previous studies elsewhere that used homogenization of precipitation data have also reported such trend variations (e.g., Abahous et al., 2020; Kessabi et al., 2022; Kuya et al., 2022) that were attributed as a positive outcome of the homogenization process itself. Indeed, this process is designed to identify and rectify trend inconsistencies introduced by nonclimatic factors and to isolate the precipitation trend driven by true climatic factors (Aguilar et al., 2003). In this study, the absence of spatial coherence in precipitation trends before homogenization could have resulted from the sensor misalignment, station relocations, alterations in observational practices, or the progressive land use change around the station (Ribeiro et al., 2016). This lack of coherence was likely a consequence of the reconfiguration of the meteorological station network in Mexico during the period from the 1980s to the 2020s and resulted in the emergence of artificial trends superimposed upon the true climate trends in URB stations.

Across the scale of precipitation regions represented by the clusters, a noticeable transition towards drier precipitation conditions was evident throughout the study period (Figure 10 and Table 1). Stations experiencing the highest levels of precipitation (C1) were particularly affected, suggesting that the consequences of this shift may be more pronounced in this specific region and at intermediate altitudes. The observed rise in drought conditions over the past few decades aligns with previous studies that have documented warming trends in the Mexican part of the URB (Montero-Martínez et al., 2018) and in Central America across interdecadal scales (Alfaro-Córdoba et al., 2020; Durán-Quesada et al., 2017; Hannah et al., 2017; Hidalgo et al., 2013, 2017; Maldonado et al., 2021). Such temperature trends can have substantial implications for the regional hydrological cycle and water resources, as the concurrent increase in evaporation and evapotranspiration may lead to shifts in atmospheric circulation patterns, altering the distribution and intensity of rainfall, and a significant reduction in water availability and runoff. Additionally, warmer temperatures can increase the capacity of the atmosphere to hold moisture, potentially leading to more intense rainfall events but also longer periods of drought. However, it is important to note that the relationship between warming trends and precipitation variability is complex, and further improvements in the study could be achieved by considering longer time-series data, for example, using paleo-precipitation records, or by incorporating reanalysis data calibrated with local rain gauge data. These additional sources of information, as demonstrated in previous studies (e.g., Hidalgo et al., 2017), can provide valuable insights for a more comprehensive understanding of precipitation trends.

The escalating aridity in the URB region holds significant importance for stakeholders, particularly because the socio-economic development of the area relies mainly on crop and livestock production. These crucial sectors are exceedingly susceptible to fluctuations in water availability and extreme weather events like droughts. Hence, it becomes imperative to take these changing drying conditions into thoughtful consideration.

5 | CONCLUSIONS

This study made a significant contribution by creating a complete and homogenized precipitation dataset for the Usumacinta River Basin, spanning 1959–2018 and including meteorological stations from Guatemala. The climatol imputation and homogenization process demonstrated high reliability through strong Spearman correlations and low absolute differences and bias percentages between raw and homogenized data. The homogenization process corrected abrupt shifts and artificial trends in 13 time series primarily observed between 1980 and 2000. The resulting temporal evolution showed improved spatial consistency, enhancing temporal and spatial

coherence while preserving the overall distribution of raw data. The 60 meteorological stations were grouped into three clusters based on distinct annual accumulated precipitation ranges, mainly related to the orographic effect of altitude. Interannual variability in cluster time series was associated with El Niño Southern Oscillation. Although the Mann–Kendall test did not show statistical significance for most stations, combining it with Sen's slope analysis and comparing 30-year precipitation normals and dry year occurrences revealed a discernible decreasing trend in homogenized precipitation data. This trend was particularly evident in the cluster characterized by the highest precipitation levels in the Usumacinta River Basin (C1), suggesting a higher risk of intensifying droughts in this region, corresponding to the intermediate altitudes of Chiapas. Understanding how local and global factors (e.g., topography and ocean–atmosphere interactions) influence precipitation in the region is crucial. The Usumacinta River Basin is an exceptionally diverse region with high economic potential, and extreme events in the context of future climate change may affect key aspects of essential sectors such as health, agriculture, environmental science, and water and disaster risk management.

AUTHOR CONTRIBUTIONS

Johanna L. J. Jupin: Conceptualization; formal analysis; investigation; methodology; validation; data curation; writing – original draft. **Alan A. Garcia-López:** Conceptualization; investigation; methodology; data curation; validation; formal analysis; writing – review and editing. **Francisco J. Briceño-Zuluaga:** Conceptualization; methodology; formal analysis; writing – review and editing. **Abdelfettah Sifeddine:** Conceptualization; supervision; funding acquisition; writing – review and editing; resources. **Ana Carolina Ruiz-Fernández:** Conceptualization; supervision; funding acquisition; resources; writing – review and editing. **Joan-Albert Sanchez-Cabeza:** Conceptualization; writing – review and editing. **José Gilberto Cardoso-Mohedano:** Conceptualization; writing – review and editing.

ACKNOWLEDGEMENTS

Support by Posgrado en Ciencias del Mar y Limnologia-UNAM and a PhD fellowship from Consejo Nacional de Ciencia y Tecnología-Mexico (CONACYT, CVU 1102000) is acknowledged by Johanna L. J. Jupin. Financial support was provided by Universidad Nacional Autónoma de México (project DGAPA PAPIIT-IN102821), and by the Institut de Recherche pour le Developpement (IRD) through the international network Groupement de Recherche Sud "Dynamics of extreme events and their impacts on the ecology of coastal resources in the Eastern Tropical Pacific" (DEXICOTROP). The participation of Francisco J. Briceño-Zuluaga was supported by the CHARISMA project (JEAI-IRD/UMNG-Colombia), derived from the research project EXT-CIAS-3638 (validity 2021-1) financed by the vice-rectorate for research of the Nueva Granada University and IRD-France. The authors are grateful for the technical support of L. H. Pérez-Bernal, M. A. Gómez-Ponce, J. G. Flores-Trujillo, L. F., Álvarez-Sánchez, H. Álvarez-Guillén, A. Reda Deara, and H. Bojórquez-Leyva, and the comments and suggestions of E. J. Alfaro and the English edition of the manuscript by A. Grant.

CONFLICT OF INTEREST STATEMENT

The authors declare no conflicts of interest.

DATA AVAILABILITY STATEMENT

The original datasets used for this study were retrieved from the national weather services of Mexico and Guatemala. The data from Servicio Meteorológico Nacional (SMN-CONAGUA, Mexico) are available in open access at the website https://smn.conagua.gob.mx/es/climatologia/informacion-climatologica/informacion-estadistica-climatologica. The datasets from Instituto Nacional de Sismología, Vulcanología, Meteorología e Hidrología (INSIVUMEH, Guatemala) are to be requested via email to the Climatology Section of the Meteorology Department (seccion.climatologia@insivumeh.gob.gt). The datasets generated during the current study are available from the corresponding author upon reasonable request.

ORCID

Ana Carolina Ruiz-Fernández https://orcid.org/0000-0002-2515-1249

REFERENCES

Abahous, H., Guijarro, J.A., Sifeddine, A., Chehbouni, A., Ouazar, D. & Bouchaou, L. (2020) Monthly precipitations over semi-arid basins in northern Africa: homogenization and trends. *International Journal of Climatology*, 40(14), 6095–6105. Available from: https://doi.org/10.1002/joc.6569

Abahous, H., Sifeddine, A., Bouchaou, L., Ronchail, J., El Morjani, Z.E.A., Ait Brahim, Y.K. et al. (2018) Inter-annual variability of precipitation in the Souss Massa region and linkage of the North Atlantic Oscillation. *Journal of Materials and Environmental Science*, 9(7), 2023–2031.

Aditya, F., Gusmayanti, E. & Sudrajat, J. (2021) Rainfall trend analysis using Mann–Kendall and Sen's slope estimator test in West Kalimantan. In: *IOP conference series: earth and environmental science*, Vol. 893. Bristol, UK: IOP Publishing Ltd. Available from: https://doi.org/10.1088/1755-1315/893/1/012006

Aguilar, E., Auer, I., Brunet, M., Peterson, T.C. & Wieringa, J. (2003) *Guidance on metadata and homogenization*. Geneva: WMO. WMO-TD No. 1186, p. 53.

Aguilar, E., Peterson, T.C., Obando, P.R., Frutos, R., Retana, J.A., Solera, M. et al. (2005) Changes in precipitation and temperature extremes in Central America and northern South America, 1961–2003. *Journal of Geophysical Research:*

Atmospheres, 110(23), 1–15. Available from: https://doi.org/10.1029/2005JD006119

Alexandersson, H. (1986) A homogeneity test applied to precipitation data. *Journal of Climatology*, 6(6), 661–675. Available from: https://doi.org/10.1002/joc.3370060607

Alfaro, E. (2002) Some characteristics of the precipitation annual cycle in Central America and their relationships with its surrounding tropical oceans. *Tópicos Meteorológicos y Oceanográficos*, 7(2), 99–115.

Alfaro-Córdoba, M., Hidalgo, H.G. & Alfaro, E.J. (2020) Aridity trends in Central America: a spatial correlation analysis. *Atmosphere*, 11(4), 1–13. Available from: https://doi.org/10.3390/ATMOS11040427

Andrade-Velázquez, M. & Medrano-Pérez, O.R. (2020) Precipitation patterns in Usumacinta and Grijalva basins (southern Mexico) under a changing climate Patrones de precipitación en las cuencas Usumacinta y Grijalva (sur de México) bajo un clima cambiante. *Revista Bio Ciencias*, 7, 1–22. Available from: https://doi.org/10.15741/revbio.07.e905

Aswad, F., Yousif, A. & Ibrahim, S. (2020) Trend analysis using Mann–Kendall and Sen's slope estimator test for annual and monthly rainfall for Sinjar District, Iraq. *Journal of the University of Duhok*, 23(2), 501–508. Available from: https://doi.org/10.26682/csjuod.2020.23.2.41

Azorin-Molina, C., Guijarro, J.A., McVicar, T.R., Trewin, B.C., Frost, A.J. & Chen, D. (2019) An approach to homogenize daily peak wind gusts: an application to the Australian series. *International Journal of Climatology*, 39(4), 2260–2277. Available from: https://doi.org/10.1002/joc.5949

Beguería, S. & Vicente-Serrano, S.M. (2017) Package "SPEI." R-package, 16.

Cai, W., Ng, B., Wang, G., Santoso, A., Wu, L. & Yang, K. (2022) Increased ENSO sea surface temperature variability under four IPCC emission scenarios. *Nature Climate Change*, 12(3), 228–231. Available from: https://doi.org/10.1038/s41558-022-01282-z

Chacón, R.E. & Fernandez, W. (1985) Temporal and spatial rainfall variability in the mountainous region of the reventazón river basin, Costa Rica. *Journal of Climatology*, 5(2), 175–188. Available from: https://doi.org/10.1002/joc.3370050205

Coll, J., Domonkos, P., Guijarro, J., Curley, M., Rustemeier, E., Aguilar, E. et al. (2020) Application of homogenization methods for Ireland's monthly precipitation records: comparison of break detection results. *International Journal of Climatology*, 40(14), 6169–6188. Available from: https://doi.org/10.1002/joc.6575

CONAGUA. (2012) *Servicio Meteorológico Nacional: 135 años de historia en México*. Ciudad de México: Climatología Comisión Nacional del Agua.

CONAGUA. (2018) *Estadisticas del agua en México*. Ciudad de México: Comisión Nacional del Agua.

Cotler-Ávalos, H. (2010) Las cuencas hidrograficas de México. In: *Diagnostico y priorizacion*. Mexico, DF: Secretaría de Medio Ambiente y Recursos Naturales. Instituto Nacional de Ecología. Pluralia Ediciones e Impresiones.

CPC. (2021) *Historical El Niño/La Niña episodes (1950–present). Cold & warm episodes by season*. Climate Prediction Center. Available from: https://origin.cpc.ncep.noaa.gov/products/analysis_monitoring/ensostuff/ONI_v5.php [Accessed 10th May 2022].

Daly, C., Neilson, R.P. & Phillips, D.L. (1994) A statistical-topographic model for mapping climatological precipitation over mountainous terrain. *Journal of Applied Meteorology*, 33(2), 140–158. Available from: https://doi.org/10.1175/1520-0450(1994)033<0140:ASTMFM>2.0.CO;2

De la Barreda, B., Metcalfe, S.E. & Boyd, D.S. (2020) Precipitation regionalization, anomalies and drought occurrence in the Yucatan Peninsula, Mexico. *International Journal of Climatology*, 40(10), 4541–4555. Available from: https://doi.org/10.1002/joc.6474

Domonkos, P., Coll, J., Guijarro, J., Curley, M., Rustemeier, E., Aguilar, E. et al. (2020) Precipitation trends in the Island of Ireland using a dense, homogenized, observational dataset. *International Journal of Climatology*, 40(15), 6458–6472. Available from: https://doi.org/10.1002/joc.6592

Durán-Quesada, M.A., Gimeno, L. & Amador, J. (2017) Role of moisture transport for Central American precipitation. *Earth System Dynamics*, 8(1), 147–161. Available from: https://doi.org/10.5194/esd-8-147-2017

Easterling, D.R. (2013) Global data sets for analysis of climate extremes, Extremes in a changing climate. In: AghaKouchak, A., Easterling, D., Hsu, K., Schubert, S. & Sorooshian, S. (Eds.) *Detection, analysis and uncertainty*. Dordrecht: Springer, pp. 347–361.

Fernández, W., Chacón, R.E. & Melgarejo, J.W. (1996) On the rainfall distribution with altitude over Costa Rica. *Revista Geofisica*, 44, 56–72.

Fuentes, H. (2021) Análisis del Control de Calidad de Base de Datos Climática. Unidad de Cambio Climático Instituto Nacional de Sismología, Vulcanología, Meteorología e Hidrología. Available from: https://insivumeh.gob.gt/wp-content/uploads/2022/03/AnalisisControlCalidad.pdf [Accessed 13th November 2021]

Gan, T.Y. & Kwong, Y.T. (1992) Identification of warming trends in northern Alberta and southern Northwest Territories by the non-parametric Kendall's test. In: Kite, G. & Harvey, K. (Eds.) *Using hydrometric data to detect and monitor climatic change. Proceedings of NHRI workshop*. Saskatoon: Environment Canada, National Hydrology Research Institute, pp. 43–56.

García, E. (1973) *Modificaciones al sistema de clasificación climática de Köppen: para adaptarlo a las condiciones de la república mexicana*. Mexico: Universidad Nacional Autónoma de México.

García, E. (1998) Comisión Nacional para el Conocimiento y Uso de la Biodiversidad (CONABIO). "Climas" (clasificación de Koppen, modificado por García). Escala 1:1000000.

Giannini, A., Kushnir, Y. & Cane, M.A. (2000) Interannual variability of Caribbean rainfall, ENSO, and the Atlantic Ocean. *Journal of Climate*, 13(2), 297–311. Available from: https://doi.org/10.1175/1520-0442(2000)013<0297:IVOCRE>2.0.CO;2

Gocic, M. & Trajkovic, S. (2013) Analysis of changes in meteorological variables using Mann–Kendall and Sen's slope estimator statistical tests in Serbia. *Global and Planetary Change*, 100, 172–182. Available from: https://doi.org/10.1016/j.gloplacha.2012.10.014

Grigorieva, E.A. & de Freitas, C.R. (2014) Temporal dynamics of precipitation in an extreme mid-latitude monsoonal climate. *Theoretical and Applied Climatology*, 116(1–2), 1–9. Available from: https://doi.org/10.1007/s00704-013-0925-x

Gubler, S., Hunziker, S., Begert, M., Croci-Maspoli, M., Konzelmann, T., Brönnimann, S. et al. (2017) The influence of station density on climate data homogenization. *International*

Journal of Climatology, 37(13), 4670–4683. Available from: https://doi.org/10.1002/joc.5114

Guijarro, J.A. (2018) Homogenization of climatological series with Climatol Version 3.1.1.

Guijarro, J.A. (2019) Climatol: climate tools (series homogenization and derived products). R package version 3.1.2., pp. 1–35.

Guijarro, J.A., López, J.A., Aguilar, E., Domonkos, P., Venema, V.K.C., Sigró, J. et al. (2023) Homogenization of monthly series of temperature and precipitation: benchmarking results of the MULTITEST project. *International Journal of Climatology*, 43, 3994–4012. Available from: https://doi.org/10.1002/joc.8069

Guimarães Santos, C.A., Brasil Neto, R.M., da Silva, R.M. & dos Santos, D.C. (2019) Innovative approach for geospatial drought severity classification: a case study of Paraíba state, Brazil. *Stochastic Environmental Research and Risk Assessment*, 33(2), 545–562. Available from: https://doi.org/10.1007/s00477-018-1619-9

Hannah, L., Donatti, C.I., Harvey, C.A., Alfaro, E., Rodriguez, D.A., Bouroncle, C. et al. (2017) Regional modeling of climate change impacts on smallholder agriculture and ecosystems in Central America. *Climatic Change*, 141(1), 29–45. Available from: https://doi.org/10.1007/s10584-016-1867-y

Hastenrath, S.L. (1967) Rainfall distribution and regime in Central America. *Archiv für Meteorologie, Geophysik und Bioklimatologie Serie B*, 15(3), 201–241. Available from: https://doi.org/10.1007/BF02243853

Hidalgo, H.G., Alfaro, E.J. & Quesada-Montano, B. (2017) Observed (1970–1999) climate variability in Central America using a high-resolution meteorological dataset with implication to climate change studies. *Climatic Change*, 141(1), 13–28. Available from: https://doi.org/10.1007/s10584-016-1786-y

Hidalgo, H.G., Amador, J.A., Alfaro, E.J. & Quesada, B. (2013) Hydrological climate change projections for Central America. *Journal of Hydrology*, 495, 94–112. Available from: https://doi.org/10.1016/j.jhydrol.2013.05.004

Hirsch, R.M., Slack, J.R. & Smith, R.A. (1982) Techniques of trend analysis for monthly water quality data. *Water Resources Research*, 18(1), 107–121. Available from: https://doi.org/10.1029/WR018i001p00107

Houghton, J.G. (1979) A model for orographic precipitation in the north-central Great Basin. *Monthly Weather Review*, 107(11), 1462–1475. Available from: https://doi.org/10.1175/1520-0493(1979)107<1462:AMFOPI>2.0.CO;2

INSIVUMEH. (2016) Variabilidad y cambio climático en Guatemala, 165. Ciudad de Guatemala. Available from: https://insivumeh.gob.gt/wp-content/uploads/2021/02/Variabilidad_y_cambio_climatico.pdf [Accessed 12th December 2021]

INSIVUMEH. (2021) Meteorología. Instituto Nacional de Sismología, Vulcanologia, Meteorologia e Hidrología. Ciudad de Guatemala. Data are available on request from the Climatology Section of the Meteorology Department via email to seccion.climatologia@insivumeh.gob.gt.

IPCC. (2022) *Climate change 2022: impacts, adaptation, and vulnerability. Contribution of working group II to the sixth assessment report of the Intergovernmental Panel on Climate Change*. Cambridge: Cambridge University Press.

Izadi, N., Karakani, E.G., Saadatabadi, A.R., Shamsipour, A., Fattahi, E. & Habibi, M. (2021) Evaluation of ERA5 precipitation accuracy based on various time scales over Iran during 2000–2018. *Water*, 13, 2538. Available from: https://doi.org/10.3390/w13182538

James, A.L., Yao, H., McConnell, C., Field, T. & Yang, Y. (2022) The DESC catchments: long-term monitoring of inland Precambrian shield catchment streamflow and water chemistry in Central Ontario, Canada. *Hydrological Processes*, 36(2), 1–9. Available from: https://doi.org/10.1002/hyp.14491

Javanshiri, Z., Pakdaman, M. & Falamarzi, Y. (2021) Homogenization and trend detection of temperature in Iran for the period 1960–2018. *Meteorology and Atmospheric Physics*, 133(4), 1233–1250. Available from: https://doi.org/10.1007/s00703-021-00805-1

Jiang, Q., Li, W., Fan, Z., He, X., Sun, W., Chen, S. et al. (2021) Evaluation of the ERA5 reanalysis precipitation dataset over Chinese Mainland. *Journal of Hydrology*, 595, 125660. Available from: https://doi.org/10.1016/j.jhydrol.2020.125660

Kendall, M.G. (1975) *Rank correlation methods*, 4th edition. London: Griffin-Charles.

Kessabi, R., Hanchane, M., Guijarro, J.A., Krakauer, N.Y., Addou, R., Sadiki, A. et al. (2022) Homogenization and trends analysis of monthly precipitation series in the Fez-Meknes region, Morocco. *Climate*, 10(5), 64. Available from: https://doi.org/10.3390/cli10050064

Kolde, R. (2019) Package "pheatmap": Pretty heatmap. R package version 1.0.12., pp. 1–8.

Kotz, M., Levermann, A. & Wenz, L. (2022) The effect of rainfall changes on economic production. *Nature*, 601(7892), 223–227. Available from: https://doi.org/10.1038/s41586-021-04283-8

Kuya, E.K., Gjelten, H.M. & Tveito, O.E. (2022) Homogenization of Norwegian monthly precipitation series for the period 1961–2018. *Advances in Science and Research*, 19, 73–80.

Magaña, V.O., Vázquez, J.L., Pérez, J.L. & Pérez, J.B. (2003) Impact of El Niño on precipitation in Mexico. *Geofisica Internacional*, 42(3), 313–330.

Maldonado, T., Alfaro, E., Rutgersson, A. & Amador, J.A. (2017) The early rainy season in Central America: the role of the tropical North Atlantic SSTs. *International Journal of Climatology*, 37(9), 3731–3742. Available from: https://doi.org/10.1002/joc.4958

Maldonado, T., Alfaro, E.J. & Hidalgo, H.G. (2018) A review of the main drivers and variability of Central America's climate and seasonal forecast systems. *Revista de Biologia Tropical*, 66, S153–S175. Available from: https://doi.org/10.15517/rbt.v66i1.33294

Maldonado, T., Alfaro, E.J. & Hidalgo, J.G. (2021) Análisis de los conglomerados de precipitación y sus cambios estacionales sobre América Central para el período 1976–2015. *Revista de Matemática: Teoría y Aplicaciones*, 28(2), 337–362. Available from: https://doi.org/10.15517/rmta.v28i2.42322

Mann, H.B. (1945) Nonparametric tests against trend. *Econometrica*, 13(3), 245–259.

March-Mifsut, I. & Castro, M. (2010) Cuenca del rio Usumacinta: Perfil y perspectivas para su conservacion y desarrollo sustentable. In: *Las cuencas hidrográficas de México. Diagnostico y priorización*. Mexico City: SEMARNAT, INE, Fundación Gonzalo Río Arronte I.A.P., pp. 194–197.

McKee, T.B., Doeske, N.J. & Kleist, J. (1993) The relationship of drought frequency and duration to time scale. In: *Proceedings of the eighth conference on applied climatology*. Anaheim: American Meteorological Society, pp. 179–184.

Meseguer-Ruiz, O., Ponce-Philimon, P.I., Quispe-Jofré, A.S., Guijarro, J.A. & Sarricolea, P. (2018) Spatial behaviour of daily observed extreme temperatures in northern Chile (1966–2015): data quality, warming trends, and its orographic and latitudinal effects. *Stochastic Environmental Research and Risk Assessment*,

32(12), 3503–3523. Available from: https://doi.org/10.1007/s00477-018-1557-6

Montero-Martínez, M.J., Santana-Sepúlveda, J.S., Pérez-Ortiz, N.I., Pita-Díaz, O. & Castillo-Liñan, S. (2018) Comparing climate change indices between a northern (arid) and a southern (humid) basin in Mexico during the last decades. *Advances in Science and Research*, 15(2014), 231–237. Available from: https://doi.org/10.5194/asr-15-231-2018

Morales-Velazquez, M.I., del Socorro, H.G., Aparicio, J., Rafieeinasab, A. & Lobato-Sanchez, R. (2021) Evaluating reanalysis and satellite-based precipitation at regional scale: a case study in southern Mexico. *Atmosfera*, 34(2), 189–206. Available from: https://doi.org/10.20937/ATM.52789

Murray-Tortarolo, G.N. (2021) Seven decades of climate change across Mexico. *Atmosfera*, 34(2), 217–226. Available from: https://doi.org/10.20937/ATM.52803

Naresh Kumar, M., Murthy, C.S., Sesha Sai, M.V.R. & Roy, P.S. (2009) On the use of Standardized Precipitation Index (SPI) for drought intensity assessment. *Meteorological Applications*, 16(3), 381–389. Available from: https://doi.org/10.1002/met.136

NOAA. (2022) *Tropical cyclone climatology*. Miami, FL: National Hurricane Center and Central Pacific Hurricane Center. National Oceanic and Atmospheric Administration. Available from: https://www.nhc.noaa.gov/climo/ [Accessed 12th February 2022]

Parker, W. S. (2016). Reanalyses and observations: What's the difference? Bulletin of the American Meteorological Society, 97(9), 1565–1572. Available from: https://doi.org/10.1175/bams-d-14-00226.1

Peterson, T.C., Easterling, D.R., Karl, T.R., Groisman, P., Nicholls, N., Plummer, N. et al. (1998) Homogeneity adjustments of in situ atmospheric climate data: a review. *International Journal of Climatology*, 18(13), 1493–1517. Available from: https://doi.org/10.1002/(SICI)1097-0088(19981115)18:13<1493::AID-JOC329>3.0.CO;2-T

Puvaneswaran, K.M. & Smithson, P.A. (1991) Precipitation–elevation relationships over Sri Lanka. *Theoretical and Applied Climatology*, 43(3), 113–122. Available from: https://doi.org/10.1007/BF00867468

Ribeiro, S., Caineta, J. & Costa, A.C. (2016) Review and discussion of homogenisation methods for climate data. *Physics and Chemistry of the Earth, Parts A/B/C*, 94, 167–179. Available from: https://doi.org/10.1016/j.pce.2015.08.007

Saada, N. & Abu-Romman, A. (2017) Multi-site modeling and simulation of the Standardized Precipitation Index (SPI) in Jordan. *Journal of Hydrology: Regional Studies*, 14, 83–91. Available from: https://doi.org/10.1016/j.ejrh.2017.11.002

Salas-Flores, M.A., Hernández-Cerda, M.E., Villicaña-Cruz, J., Azpra-Romero, E. & Lomas Barrié, C.T. (2014) The influence of strong El Niño phases on the rainfall over the Yucatan Peninsula, Mexico. *Scientific Annals of the Alexandru Ioan Cuza University of Iasi: Geography Series*, 60(1), 15–28.

Salas-Flores, M.A. & Jones, P.D. (2014) The ENSO influence in the Mexican regional precipitation during the instrumental period. *Scientific Annals of the Alexandru Ioan Cuza University of Iasi: Geography Series*, 60(1), 29–65.

Sen, K.P. (1968) Estimates of the regression coefficient based on Kendall's tau. *Journal of the American Statistical Association*, 63(324), 1370–1389. Available from: https://doi.org/10.1080/01621459.1968.10480934

Serra, Y.L., Kiladis, G.N. & Hodges, K.I. (2010) Tracking and mean structure of easterly waves over the Intra-Americas Sea. *Journal of Climate*, 23(18), 4823–4840. Available from: https://doi.org/10.1175/2010JCLI3223.1

SMN-CONAGUA. (2022) *Información de estación climatológicas*. Gobierno de México: Servicio Meteorológico Nacional, Comisión Nacional del Agua. Available from: https://smn.conagua.gob.mx/es/climatologia/informacion-climatologica/informacion-estadistica-climatologica [Accessed 2nd February 2022].

Soasores, D. & Garcia-Garcia, A. (2017) *Visión climática de la precipitación en la cuenca del río Usumacinta. La cuenca del río Usumacinta desde la perspectiva del cambio climático*. Mexico: Instituto Mexicano de Tecnología del Agua.

Solorza-Gómez, Á. (2017) *Cuenca Hidrográfica del Río Usumacinta*. Laboratorio de Análisis Geoespacial CRUZMI. Available from: https://idegeo.centrogeo.org.mx/maps/1563 [Accessed 6th May 2022].

Stefanidis, S. & Stathis, D. (2018) Spatial and temporal rainfall variability over the mountainous central Pindus (Greece). *Climate*, 6(3), 75. Available from: https://doi.org/10.3390/cli6030075

Taylor, M.A. & Alfaro, E.J. (2021) Central America and the Caribbean. In: Oliver, J.E. (Ed.) *Encyclopedia of world climatology. Encyclopedia of earth sciences series*. Dordrecht: Springer, pp. 183–189.

Tibshirani, R., Walther, G. & Hastie, T. (2001) Estimating the number of clusters in a data set via the gap statistic. *Journal of the Royal Statistical Society: Series B*, 63(2), 411–423. Available from: https://doi.org/10.1111/1467-9868.00293

Wang, B., Luo, X., Yang, Y.M., Sun, W., Cane, M.A., Cai, W. et al. (2019) Historical change of El Niño properties sheds light on future changes of extreme El Niño. *Proceedings of the National Academy of Sciences of the United States of America*, 116(45), 22512–22517. Available from: https://doi.org/10.1073/pnas.1911130116

WMO. (2012) *Standardized precipitation index. user guide*. Geneva: WMO. OMM No. 1090, pp. 1–23.

WMO. (2017) *Guidelines on the calculation of climate normals*. Geneva: WMO. WMO No. 1203, pp. 1–29.

Yosef, Y., Aguilar, E. & Alpert, P. (2019) Changes in extreme temperature and precipitation indices: using an innovative daily homogenized database in Israel. *International Journal of Climatology*, 39(13), 5022–5045. Available from: https://doi.org/10.1002/joc.6125

Zárate-Hernández, E. (2013) Climatología de masas invernales de aire frío que alcanzan Centroamérica y el Caribe y su relación con algunos índices árticos. *Tópicos Meteorológicos y Oceanográficos*, 12(1), 35–55.

SUPPORTING INFORMATION

Additional supporting information can be found online in the Supporting Information section at the end of this article.

How to cite this article: Jupin, J. L. J., Garcia-López, A. A., Briceño-Zuluaga, F. J., Sifeddine, A., Ruiz-Fernández, A. C., Sanchez-Cabeza, J.-A., & Cardoso-Mohedano, J. G. (2023). Precipitation homogenization and trends in the Usumacinta River Basin (Mexico-Guatemala) over the period 1959–2018. *International Journal of Climatology*, 1–18. https://doi.org/10.1002/joc.8318

1.2. A CASE STUDY OF THE CANDELARIA AND QUELITE RIVER BASINS

1. Introduction

Climate change and land-use change have the potential to alter hydrological regimes and freshwater availability worldwide (Osland et al., 2018). In Mexico, climate change is expected to manifest as changes in the duration of rainy seasons, a decrease in precipitation in southern regions, and an increase in the frequency of extreme precipitation events, significantly influencing socioeconomic activities such as agriculture (Hidalgo et al., 2013, 2017; Hannah et al., 2017). Precipitation can exhibit high variability across regions, and the assessment of its trend may be influenced by the choice of databases and models used, complicating their study (Maldonado et al., 2018). Therefore, accurately assessing local-scale precipitation trends requires complete time series with high spatial and temporal resolution (Easterling, 2013).

Analyzing time series of meteorological observations can contribute to understanding precipitation variability and trends over decades and centuries; however, series are often incomplete and can contain suspicious values, behaviors, or trends. These anomalies, called inhomogeneities, are not a result of climatic factors but rather arise during the measurement process, data digitization, or changes in instrument, calibration, and station location (Guijarro, 2024). To correct these alterations, which can lead to erroneous interpretations, homogeneity tests are used to ensure that the variations observed in meteorological observation series are solely attributable to climatic processes.

In a previous study, precipitation variability and trends in the Usumacinta River basin (URB) were investigated using the data homogenization model 'climatol' (Jupin et al., 2024). This model, developed in the R language by Guijarro (2018), is notable for its accessibility, flexibility to adapt to any climatic variable, high tolerance of missing data, and the possibility

of using different temporal resolution (e.g., days, months, or years). It allows for data quality control, series homogenization, and imputation of missing data by comparing an original series with a reference one derived from an average of nearby stations.

In this additional section of chapter 1, the same methodology were applied to the Candelaria and Quelite river basins, which flow into the CP and EV systems, respectively. The Candelaria River basin holds significant economic importance for the state of Campeche, Mexico, as it hosts a variety of productive activities, including agriculture, livestock farming, industry, fishing, and forestry (Kauffer-Michel, 2010). El Quelite River basin, in the municipality of Mazatlán in Sinaloa, encompasses a smaller surface area but holds ecological significance, as it flows into the protected area Playa Tortuguera El Verde Camacho, which has been designated as a reserve zone and refuge site for the protection, conservation, repopulation, and control of various species of marine turtles in October 1986. Designated as a sanctuary in July 2002, it was later recognized as a Ramsar site, denoting its international significance as a wetland of importance (registration 1349, February 2004) (Briseño-Dueñas, 2003).

Precipitation variability and trends in the Candelaria and EV basins have not been previously studied through the use of observed data and homogenized precipitation series. This work aims to collect observed precipitation data in the Candelaria and Quelite river basins and employ a process of quality control, homogenization, and imputation of missing data to determine precipitation trends over the past decades.

2. Methods

Study sites

The Candelaria River basin covers an area of 7,160 km^2, including a portion in Mexico (84%) and another in Guatemala (16%). The river originates in the Petén region of Guatemala and flows into the CP system, located in the eastern part of TL. It has an annual discharge of 1.6

billion m^3 yr^{-1}, contributing 20% of the total freshwater flowing into TL (Ramos-Miranda and Villalobos-Zapata, 2015). The river flows over limestone and karstic soil, resulting in greater underground drainage than surface drainage (Ayala-Pérez et al., 2015; Ramos-Miranda and Villalobos-Zapata, 2015). Annual precipitation ranges from 1,000 to 1,500 mm yr^{-1} (Fig. 2), with a clearly defined rainy season from June to October, during which approximately 70% of the total precipitation is recorded (Benítez, 2010). During the months of November to February, invasions of polar masses known as "nortes" occur, which can contribute up to 25% of the annual precipitation. Of the approximately 45,000 estimated inhabitants in the basin, 23% of the population resides in the municipality of Candelaria, located in the center of the basin (Benítez, 2010).

The Quelite River covers an area of 835 km^2 and discharges 107 million m^3 yr^{-1} into EV, Sinaloa, on the Mexican Pacific coast. For most of the year, the Quelite River remains dry, with a flow period occurring mainly during the rainy season from June to October (Flores-Verdugo et al., 1995), during which most of the precipitation accumulates. The precipitation in this region has an annual average of 750 mm yr^{-1} (Fig. 2). In the Quelite River basin, a total of 6,000 inhabitants were recorded for the year 2000, including the communities of El Quelite (1,758 inhabitants), Mármol (862), El Quemado (674), and El Recreo (555) (CONAGUA, 2015).

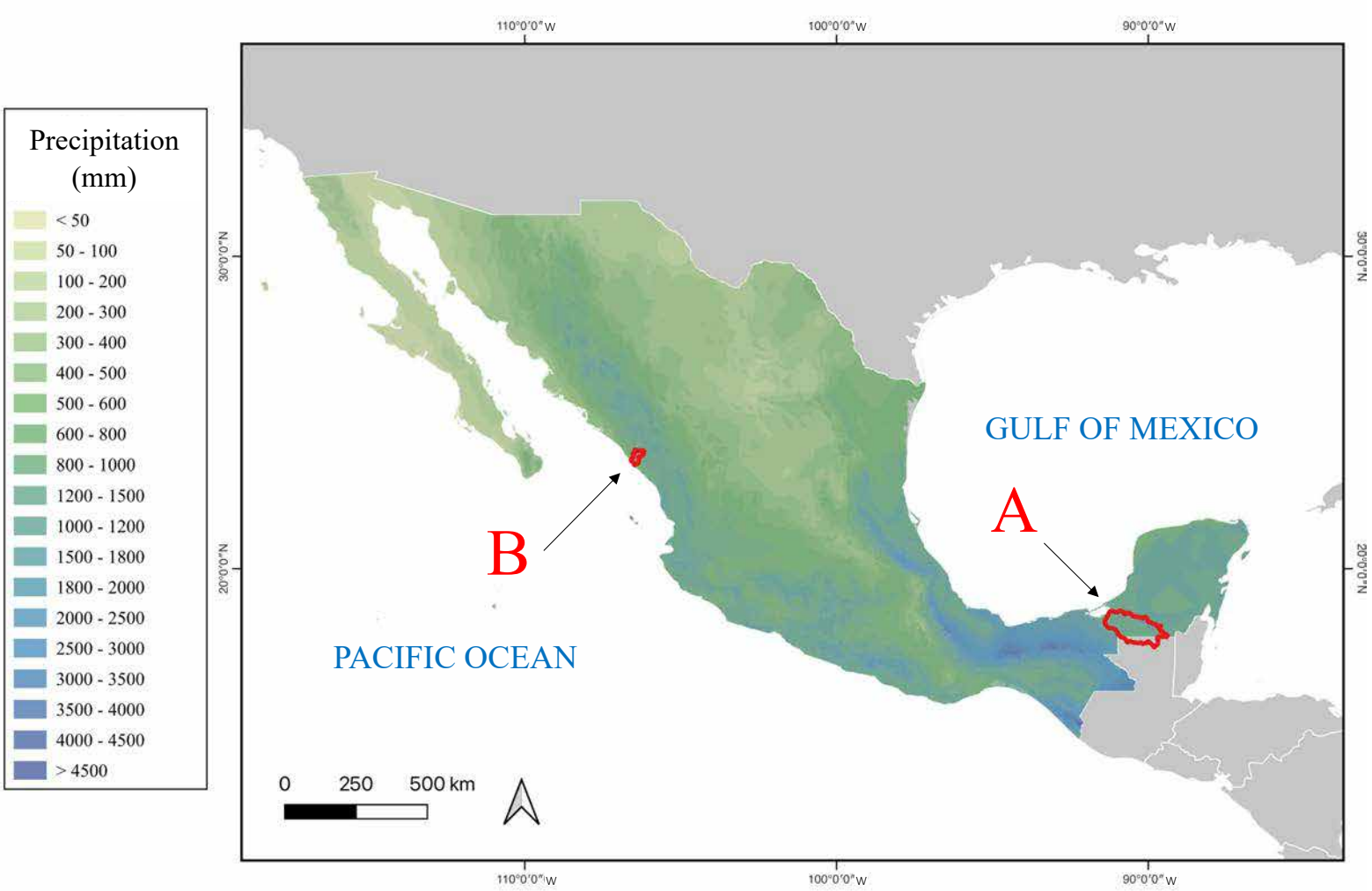

Figure 2. Annual precipitation in Mexico calculated from data recorded between 1910 and 2009. A: Candelaria River basin; B: Quelite River basin. Created using the database provided by Cuervo-Robayo (2014) and river basin data from INEGI-INE-CONAGUA (2007).

Database

The data on accumulated daily precipitation for the Candelaria and Quelite river basins were obtained from databases provided by the Servicio Meteorológico Nacional and Comisión Nacional del Agua (SMN-CONAGUA) for the states of Campeche and Sinaloa, respectively. Additionally, for the Guatemalan part of the Candelaria River basin, a search was conducted in the databases of the Instituto Nacional de Sismología, Vulcanología, Meteorología e Hidrología (INSIVUMEH) of Guatemala.

Data selection

Data selection involved geographically delineating the hydrographic basins of the two rivers using data from INEGI-INE-CONAGUA (2007), and subsequently selecting meteorological stations within each basin. In total, 9 stations were identified in the Candelaria River basin and only 2 stations were found in the Quelite River basin, covering the period from 1944 to 2016 (Fig. 3 and Table 1). No precipitation data were found in the Guatemalan portion of the Candelaria River basin. Monthly accumulated precipitation was calculated from daily data, following the criteria established by the World Meteorological Organization (WMO, 2017), which included the following criteria: 1) there cannot be more than ten days with missing data in a month, and 2) there cannot be more than four consecutive days with missing data in a month.

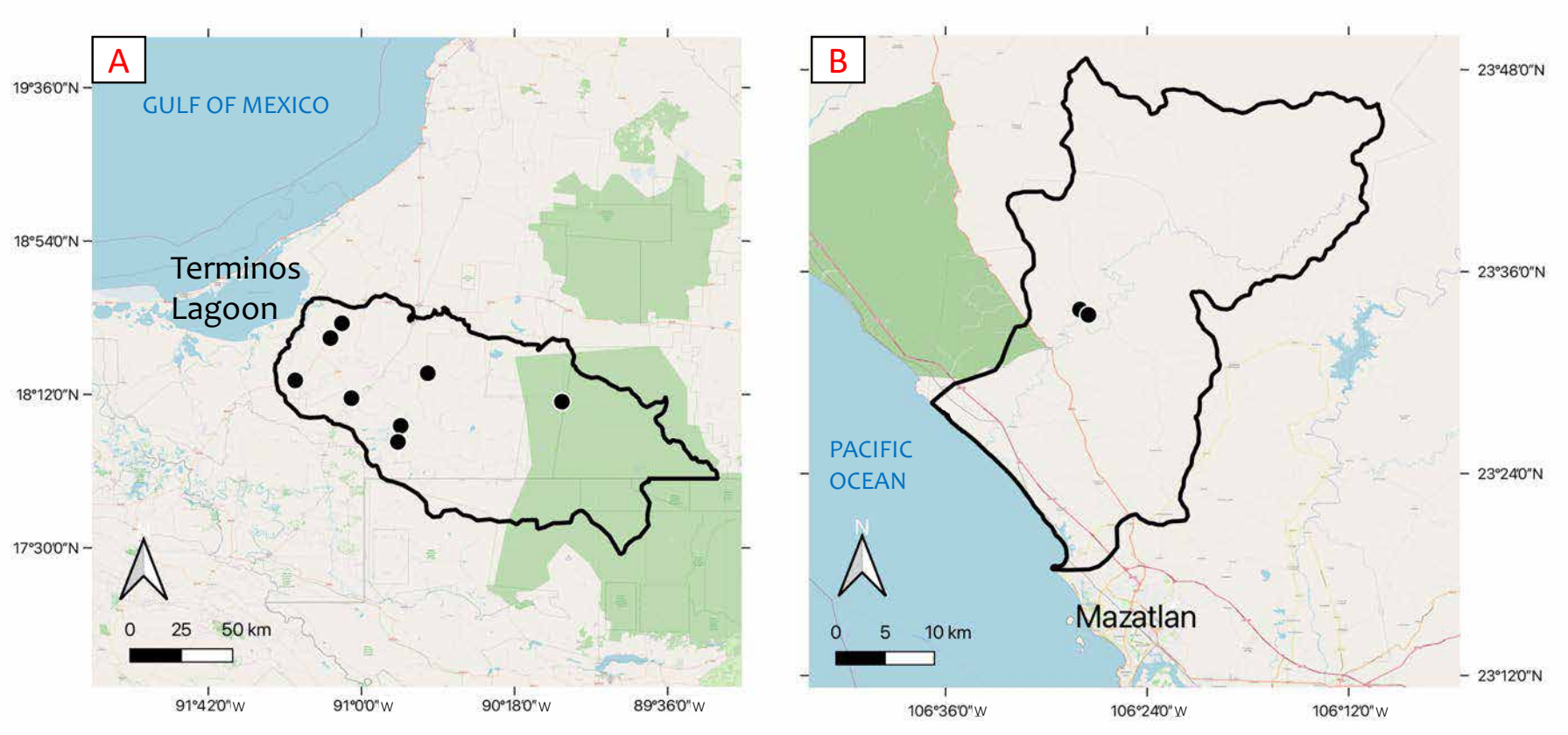

Figure 3. Meteorological stations (●) located in the Candelaria River basin in Campeche, Mexico, and southern Guatemala (A) and in the Quelite River basin in Sinaloa, Mexico (B).

Table 1. Characteristics of the meteorological stations in the Candelaria River basin in Campeche, Mexico, and southern Guatemala, and in the Quelite River basin in Sinaloa, Mexico.

ID	Station	Operation status	Latitude (°)	Longitude (°)	Altitude (m)*	Start	End
Candelaria River							
4004	CANDELARIA (SMN)	OPERATING	18.184	-91.046	40	01/06/1944	31/12/2018
4021	MONCLOVA	OPERATING	18.057	-90.821	100	01/09/1944	31/12/2018
4057	MAMANTEL	OPERATING	18.525	-91.089	12	01/01/1978	31/12/2018
4082	PABLO T. BURGOS	OPERATING	18.297	-90.697	50	01/01/1998	31/12/2018
4083	ENTRE HERMANOS	OPERATING	18.457	-91.142	40	01/01/1998	31/12/2018
4018	LA ESPERANZA	SUSPENDED	18.167	-90.083	290	01/01/1965	31/08/1981
4019	NANZAL	SUSPENDED	18.264	-91.303	10	01/01/1965	31/08/1976
4020	MIGUEL HIDALGO	SUSPENDED	17.983	-90.833	67	01/10/1964	31/12/1989
4039	CANDELARIA (DGE)	SUSPENDED	18.183	-91.046	50	01/01/1961	31/12/1985
Quelite River							
25031	EL QUELITE (CFE)	SUSPENDED	-106.458	23.557	49	01/01/1961	28/02/2001
25176	EL QUEMADO	OPERATING	-106.467	23.563	50	01/08/1979	31/12/2018

Data Availability

The precipitation series in the Quelite River basin, consisting of only 2 stations in total, were insufficient for conducting a process of homogenization and imputation of missing data, as climatol requires a minimum of 3 data points per time step (i.e., month) for its execution.

For the Candelaria River basin, precipitation data collected from the nine stations were organized into two input files, following the procedure detailed by Guijarro (2018). One file contained station metadata, such as coordinates, altitude, code, and name, whereas the other contained monthly accumulated precipitation data for each station for the period between 1970 and 2018. The period 1970-2018 was selected due to inherent limitations of the dataset, as only two stations had monthly prior to the selected period.

In an initial stage, climatol was executed in preliminary mode to assess data availability and quality. It was verified that the set of stations met the requirement of five data points per month, which is the threshold to generate theoretically reliable imputed series. Additionally, parameter values were reported to determine data quality, including the percentage of original data used in the model and the correlation coefficient between precipitation series.

3. Results

In the Candelaria River basin, data availability was observed to fall below the threshold of five data points per month (Fig. 4). Although the climatol model could theoretically complete the series in preliminary mode (Fig. 5), the resulting series could not be considered reliable due to the scarcity of data required to create a reference series for imputing missing data. On average, less than 46% of the percentage of original data was used in the model, and the correlation coefficient between precipitation series was 0.27.

4. Discussion

To calculate precipitation trends accurately, it is recommended to perform data quality control and homogenization, ensuring that the dataset is complete and free from missing or erroneous values (WMO, 2017). However, in the studied sites, the limited data availability from meteorological stations prevented proper execution of climatol and the imputation of missing data in the series. No precipitation data were found in the Guatemalan portion of the Candelaria River basin, which can be attributed to the limited spatial and temporal availability of data in northern Guatemala, resulting from deficient infrastructure of the meteorological station network, affected by access difficulties such as low population density, lack of roads, and the presence of jungle (Fuentes, 2021). Without series homogenization, it was not possible to determine whether the observed trends in the series would have been attributable to climatic or non-climatic factors.

To address the objective of this study, previous research examining precipitation variability at regional, national, and Central American levels was consulted. Studies have been conducted at the scale of the Yucatan Peninsula (e.g., De la Barreda et al., 2020; Márdero et al., 2012), the state of Sinaloa (Llanes-Cárdenas et al., 2022, 2016), Mexico (Murray-Tortarolo, 2021) and Central America (e.g., Aguilar et al., 2005; Alfaro-Córdoba et al., 2020; Karmalkar et al., 2011). However, it is important to note that those studies have not specifically addressed precipitation variability in the Candelaria and Quelite river basins, nor have they employed a series homogenization method to analyze precipitation trends. Given the high variability in precipitation patterns, trends in those studies should be interpreted with caution and findings from regional studies should be preferred over large-scale studies.

De la Barreda et al. (2020) conducted a study on the regionalization of precipitation and the occurrence of dry events on the Yucatan Peninsula. Their findings indicated that precipitation trends were not homogeneous and were distributed by subregions, which aligned with earlier studies (e.g., Hidalgo et al., 2013, 2017; Hannah et al., 2017) suggesting that precipitation trends

vary across Central America and depend on the database and time scale used for assessment. An increase in the occurrence and duration of dry years was observed in certain meteorological stations across the eastern part of the Yucatan Peninsula from 1953 to 2007 (Márdero et al., 2012). In the region where the Candelaria River is situated, significantly negative trends were observed through Mann-Kendall analysis and Sen's slope of observed precipitation data series for the period 1980–2011 (De la Barreda et al., 2020). This trend towards lower precipitation in the Candelaria River basin was consistent with observations in the Usumacinta River basin during the period 1959–2018 (Jupin et al., 2024). In Sinaloa, the occurrence of extreme drought events between 1963 and 2014 was examined using indices to describe their frequency, duration, and intensity (Llanes-Cárdenas et al., 2022). Meteorological stations in southern Sinaloa recorded some of the highest index values compared to those in northern Sinaloa, suggesting a particularly high vulnerability to drought events in south. This trend towards increased drought vulnerability was also observed in northern Sinaloa (Llanes-Cárdenas et al., 2016).

In Mexico, significant relationships have been evidenced between drought events and the El Niño-Southern Oscillation (ENSO) phenomenon (Magaña et al., 2003; Salas-Flores et al., 2014; Salas-Flores and Jones, 2014). Additionally, significant negative correlations have been observed between precipitation series in the URB and the El Niño 3.4 index, which is used to monitor and forecast El Niño events (Jupin et al., 2024). During El Niño events, drier conditions typically prevail in southern Mexico, whereas wetter conditions are more commonly observed in northern Mexico (Magaña et al., 2003). The anticipated increases in the frequency and intensity of extreme El Niño events, attributed to anthropogenic climate change (Cai et al., 2022; Wang et al., 2019), may have varying effects on the northern and southern regions in Mexico; however gaining a deeper understanding and projecting the future behavior of the

ENSO phenomenon under the influence of climate change necessitates further research into its controlling parameters (Cai et al., 2022).

The potential escalating occurrence of drought events in the Candelaria and Quelite river basins raises significant concerns, particularly considering the population's dependence in these regions on agriculture and water supply from precipitation (e.g., De la Barreda et al., 2020). Consequently, changes in precipitation patterns and the increasing frequency of droughts could exacerbate food insecurity and the vulnerability of local population within these areas. Stakeholders should develop strategies to conserve water resources and enhance irrigation efficiency to mitigate the impacts of declining precipitation and ensure agricultural sustainability in the face of increasing drought occurrences.

5. Conclusions

The insufficient observed data in the studied regions represent a barrier to analyzing precipitation variability at a local and long-term scale, making it difficult to project precipitation trends and understand their impacts. Additional studies are required, along with the collection of reliable data, to achieve a more comprehensive understanding of precipitation trends and patterns in these areas. For example, in regions where scarce or no observed data is available, satellite data could be utilized to investigate changes in precipitation since the 1980s, combined with paleoprecipitation records and reanalysis data to create longer time series. However, it is important to consider the limitations of these datasets, such as the possible lack of calibration with local rain gauge data in Mexico for global satellite and reanalysis data, as well as potential low spatial resolution and bias in precipitation estimation in mountainous regions. Comparing multiple models and datasets would facilitate the conduct of more robust studies and interpretation of precipitation trends, subsequently enabling more effective planning by policymakers and stakeholders to address water scarcity challenges in the context of climate change and mitigate the impacts of droughts on the population.

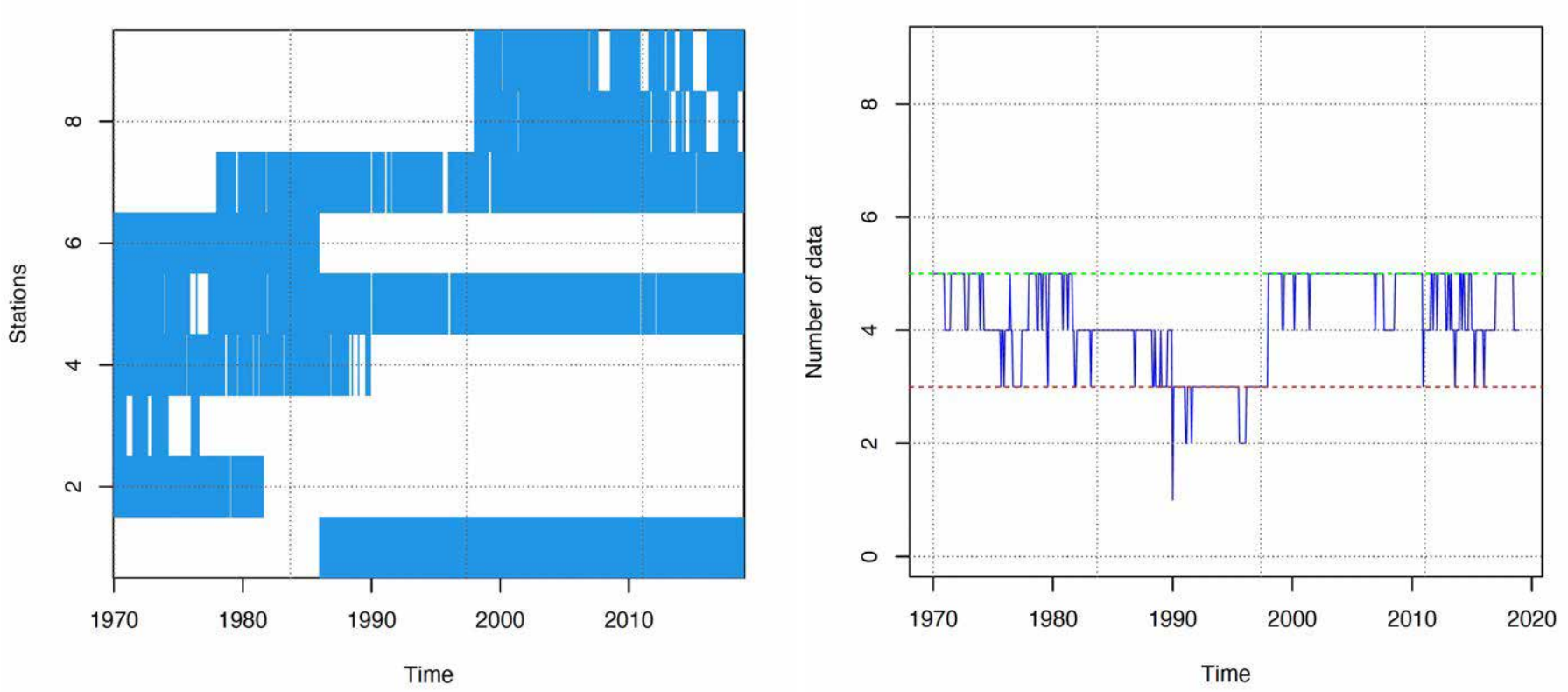

Figure 4. Availability of monthly data at meteorological stations in the Candelaria River basin between 1970 and 2018. Left: available monthly data (in blue) at the nine stations over time. Right: number of monthly data over time. Dashed green line: desirable minimum of 5 data per month for generating reliable imputed series; dashed red line: minimum of 3 data per month for climatol operation.

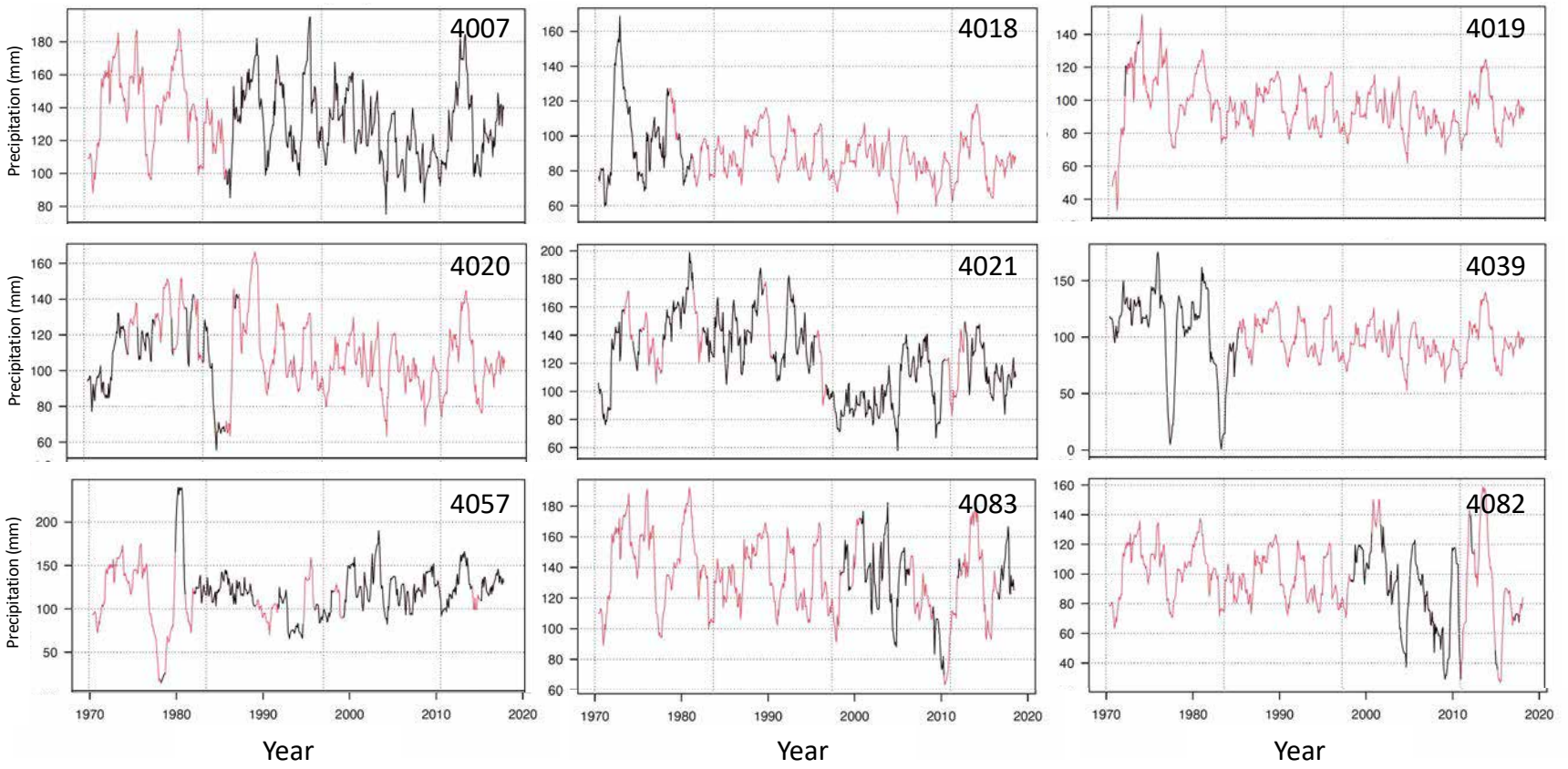

Figure 5. Monthly precipitation series including original (black) and imputed (red) data by climatol over the period 1970-2018 at the nine meteorological stations in the Candelaria River basin.

CHAPTER 2

AGE MODEL AND SEDIMENT ACCUMULATION RATES IN SEDIMENT CORES USING THE LEAD-210 METHOD

The second chapter focuses on estimating age models (i.e., associating sediment depth with its age) and sediment accumulation rates (i.e., the rate at which sediment accumulates) in seven sediment cores from LT and EV. The objective is to understand the temporal variation of sediment accumulation in mangrove ecosystems and relate it to anthropogenic activities (e.g., land use change) and elements of climate change (e.g., sea-level rise). Age models were established based on the activity of ^{210}Pb measured in the sediment cores. The Constant Flux Model and the Bayesian model Plum were used to evaluate variations in the mass accumulation rates (MAR) and sediment accumulation rates (SAR) over the dated period. The ^{210}Pb dating was corroborated by identifying the peak value of ^{137}Cs activities, which is an artificial radionuclide released into the environment by the detonation of thermonuclear weapons in the atmosphere between 1945 and 1980, and/or the records of known meteorological events (e.g., hurricanes and tropical storms) in the sediment cores.

This work sought to answer the following research questions: (1) What are the ranges of MAR and SAR in the study sites over the past 100 years?; (2) How have MAR and SAR changed at the study sites (~100 years)?; and (3) Are these changes in sediment accumulation related to anthropogenic activities such as deforestation and land use change? Based on the fact that mean annual precipitation and freshwater discharge are higher, and the mangrove area is larger in LT than in EV, it was hypothesized that these distinct characteristics would be reflected in significant differences in sedimentation rates between the study sites.

This study represents the first reconstruction of the temporal variability of sediment accumulation rates over the past century, through the analysis of ^{210}Pb-dated sediment cores, in the mangrove ecosystems of LT and EV. It contributes to filling the information gap on MAR in mangrove areas worldwide. It offers an original perspective on how processes related to global change, such as increased continental erosion and sea-level rise, influence MAR variability on a global scale. MAR is an important parameter due to its impact on the accumulation and preservation of carbon in mangroves, which is crucial for quantifying the magnitude of carbon sinks in mangrove sediments as climate change mitigation strategies. Finally, this study provides an example of how mangroves respond to climate change-induced factors and anthropogenic interventions, a topic that remains surrounded by uncertainty. The results and interpretations of this work were published in the article titled "Anthropogenic drivers of increasing sediment accumulation in contrasting Mexican mangrove ecosystems" in June 2023 in the journal *CATENA*.

Catena 226 (2023) 107037

Contents lists available at ScienceDirect

Catena

journal homepage: www.elsevier.com/locate/catena

Anthropogenic drivers of increasing sediment accumulation in contrasting Mexican mangrove ecosystems

J.L.J. Jupin [a,b], A.C. Ruiz-Fernández [c,*], A. Sifeddine [b,d], J.A. Sanchez-Cabeza [c], L.H. Pérez-Bernal [c], J.G. Cardoso-Mohedano [e], M.A. Gómez-Ponce [e], J.G. Flores-Trujillo [f]

[a] Posgrado en Ciencias del Mar y Limnología, Universidad Nacional Autónoma de México. Av. Universidad 3000, Ciudad Universitaria, Coyoacán, 04510 Ciudad de México, Mexico
[b] Institut de Recherche pour le Développement (LOCEAN-IPSL), Sorbonne Université, 75005 Paris, France
[c] Unidad Académica Mazatlán, Instituto de Ciencias del Mar y Limnología, Universidad Nacional Autónoma de México, 82040 Mazatlán, Sinaloa, Mexico
[d] ERC2- Université de Quisqueya, Port au Prince-Haïti
[e] Estación el Carmen, Instituto de Ciencias del Mar y Limnología, Universidad Nacional Autónoma de México, Carretera Carmen-Puerto Real km 9.5, 24157 Ciudad del Carmen, Campeche, México
[f] Universidad Autónoma del Carmen. Calle 56 No. 4, Col. Benito Juárez, 24180 Cd. del Carmen, Campeche, Mexico

ARTICLE INFO

Keywords:
^{210}Pb radiochronology
Mangroves
Sediments
Coastal lagoon
Sea-level rise
Ramsar

ABSTRACT

Mangrove sediments are valuable records to reconstruct the impacts of human-induced changes on the coastal zone. Seven lead-210 dated sediment cores were used to evaluate temporal trends of sedimentation rates over the past century in Mexican mangrove areas at Términos Lagoon (TL; southern Gulf of Mexico) and El Verde Camacho Lagoon (EV; northern Mexican Pacific coast). We hypothesized that the contrasting characteristics (e.g., meteorological, demographic, and land-use change) would lead to significant differences in sedimentation rates between the study sites. Sediment accumulation rates (SAR) in both sites (TL 0.03–2.1 cm yr^{-1}; EV 0.04–4 cm yr^{-1}) were comparable to the global SAR range for mangrove forests. Mass accumulation rates (MAR) in the TL cores (0.03–0.47 g cm^{-2} yr^{-1}) were consistent with previous studies of the region. Excluding conspicuous MAR maxima, attributed to meteorological events, MAR values in the EV cores (0.04–0.9 g cm^{-2} yr^{-1}) were higher than in other mangrove areas of the Mexican Pacific coast, but comparable to other sites in the world. Similar exponentially increasing MAR values towards present in both sites were attributed to general factors driving sediment accumulation in mangroves, mainly continental erosion promoted by land-use changes, which has accelerated since the 1950s, associated with (i) population growth and the consequent expansion of human activities and (ii) sea-level rise, similar in the studied regions and from which mangrove ecosystems seem to adapt. Intensifying population growth and land-use change are already reducing the extent of mangrove coverage in some parts of the study areas. Adaptation to an accelerating sea-level rise depends on maintaining conditions that allow mangroves to accrete vertically. However, both global change pressures may pose future threats to these ecosystems. Efforts to monitor sediment accretion and adapt the management of mangrove conservation areas are required to understand better mangrove response to global change impacts.

1. Introduction

Sedimentary records allow the reconstruction of recent environmental changes and provide quantitative information on anthropogenic impacts and past climatic conditions. Among coastal ecosystems, mangroves are notable for their rapid sediment accumulation (Alongi, 2008). These shrub- and tree-dominated, intertidal, and saltwater communities, which occur throughout the world on tropical and subtropical coastlines (Alongi, 2009), slow down water currents to speeds that facilitate the deposition of suspended material from both river and tidal waters (Cahoon and Lynch, 1997; Sanders et al., 2008).

Mangrove sediment records have yielded much information: to

* Corresponding author.
E-mail addresses: joh.jupin@gmail.com (J.L.J. Jupin), caro@ola.icmyl.unam.mx (A.C. Ruiz-Fernández), abdel.sifeddine@ird.fr (A. Sifeddine), jasanchez@cmarl.unam.mx (J.A. Sanchez-Cabeza), lbernal@ola.icmyl.unam.mx (L.H. Pérez-Bernal), gcardoso@cmarl.unam.mx (J.G. Cardoso-Mohedano), mgomez@cmarl.unam.mx (M.A. Gómez-Ponce), gflores@pampano.unacar.mx (J.G. Flores-Trujillo).

https://doi.org/10.1016/j.catena.2023.107037
Received 20 October 2022; Received in revised form 29 January 2023; Accepted 20 February 2023

Table 1
Main characteristics of the study sites in the Palizada-del-Este and Candelaria-Panlau systems in Términos Lagoon (southern Gulf of Mexico) and El Verde Camacho system (northern Mexican Pacific coast).

	Characteristics	Palizada-del-Este[1]	Candelaria-Panlau[1]	El Verde Camacho[2]
Location	Latitude (°N)	18°29.22-18°29.06	18°36.00-18°38.50	23°29.33-23°17.82
	Longitude (°W)	91°44.60-91°51.52	91°17.50-91°12.50	106°27.17-106°37.07
Meteorology	Mean annual precipitation (mm yr^{-1})	1,750	1,400	750
	Mean annual temperature (° C)	27	27	25
	Mean annual salinity	4	15	14
River	Name	Palizada	Candelaria + Mamantel	Quelite
	Annual mean discharge (10^9 m^3 yr^{-1})	9.1	1.6 + 0.16	0.11
	Basin (km^2)	40,000	7,160 + 520	835
Mangrove	*Laguncularia racemosa*	Present	–	Dominant
	Rhizophora mangle	Dominant	Dominant	Present
	Avicennia germinans	Dominant	Dominant	Present
	Conocarpus erectus	–	–	Present

[1] (Ochoa, 2003);
[2] (Briseño-Dueñas, 2003).

reconstruct sea-level changes during past centuries (Gilman et al., 2006; Sanders et al., 2008) and throughout the Holocene (Woodroffe et al., 2005; Berger et al., 2013); to trace the impacts of extreme events (Smith et al., 2009); to study contamination by trace elements and nutrients (Passos et al., 2022); and to evaluate the temporal variability of blue carbon stocks and accumulation rates as a result of environmental changes caused by anthropogenic impacts (Aldana-Gutiérrez et al., 2021). Sedimentary reconstructions in coastal lagoons have been used to identify the consequences of local land-use change owing to deforestation or to industrial and urban development (Aronson et al., 2014; Ruiz-Fernández et al., 2014, 2012), to detect recent climate impacts on coastal lagoons (Ruiz-Fernández et al., 2016), and to record precipitation variability (Cuellar-Martinez et al., 2017). Sedimentation rates in mangrove areas range from 0.1 to 10.0 mm yr^{-1} with an average of 5 mm yr^{-1} (Alongi, 2012; Breithaupt et al., 2012).

The method most widely used within the past ~100 years for dating recent sediment records is based on the study of lead-210 (^{210}Pb) profiles ($T_{½}$ = 22.23 ± 0.12 years; DDEP, 2012). ^{210}Pb is a natural radionuclide that accumulates in sediments mainly through atmospheric deposition (excess ^{210}Pb, $^{210}Pb_{ex}$) and *in situ* production (supported ^{210}Pb, $^{210}Pb_{sup}$) from the decay of ^{222}Rn, assumed to be in equilibrium with ^{226}Ra. The Constant Flux (CF) model (Appleby and Oldfield, 1978; Robbins et al., 1978) is one of the most robust ^{210}Pb dating models; it is based on the main hypothesis that the flux of $^{210}Pb_{ex}$ to the sediments is constant over time and allows assessment of the variations in the mass accumulation rate (MAR) and the sediment accumulation rate (SAR) throughout the dated period (Sanchez-Cabeza and Ruiz-Fernández, 2012). ^{210}Pb-chronologies should be validated either by comparing the ^{210}Pb-derived ages with independent stratigraphic markers (e.g., artificial radionuclides released from nuclear weapon tests) or by testing the consistency of the age models against those obtained from independent dating models (Appleby, 2001). ^{210}Pb dating is often corroborated with ^{137}Cs ($T_{½}$ = 30.05 ± 0.08 years; DDEP, 2007), an artificial radionuclide released into the environment by the detonation of thermonuclear weapons in the atmosphere between 1945 and 1980 (UNSCEAR, 2000). ^{137}Cs is used as a stratigraphic marker that, in areas where post-depositional processes (e.g., mixing, erosion, bioturbation, diagenesis) are negligible, would show detectable activities shortly after the onset of the nuclear tests (since ~1952; Robbins et al., 2000) and a maximum activity in 1963 (Sanchez-Cabeza and Ruiz-Fernández, 2012).

Términos Lagoon (TL) in the southern Gulf of Mexico, and El Verde Camacho Lagoon (EV) on the Pacific coast, are two Mexican coastal lagoons that lie within areas of high biodiversity, bird migration, and breeding for many coastal species; both sites have been recognized as wetlands of international importance by the Ramsar Convention since 2004 (TL: site 1356; EV: site 1349; RSIS, 2020). However, mean annual precipitation, temperature, and freshwater discharge are higher in TL than in EV, and the mangrove area is greater (143,045 ha in TL and 1,300 ha in EV) (Table 1). Urban growth is much higher in TL than in EV, due to accelerated demographic growth since the second half of the 19th century. For instance, between 1950 and 1960 and 1970–1980, the average annual population growth rate in Carmen Municipality (which surrounds most TL) ranged between 5.5 % and 6.3 % (INEGI, 2002), whereas in Mazatlán Municipality (where EV is located) it ranged between 3.9 % and 4.2 % (INEGI, 2008).

No previous studies have related the reconstructed temporal variation of MAR in TL and EV mangrove sediments to anthropogenic and natural pressures occurring in these lagoons. This study aimed to understand the temporal variation of sediment accumulation in mangrove ecosystems of two contrasting Mexican Ramsar sites, and to answer the questions: (1) what are the ranges of mass accumulation rates? (2) how have mass accumulation rates changed in the study sites over the last 100 years? and (3) are these sediment accumulation changes related to anthropogenic activities, such as deforestation and land-use change? The central hypothesis was that the contrasting characteristics (e.g., meteorological, demographic, and land-use change) between the study sites would be reflected in significant differences in sedimentation rates. This work provides a retrospective evaluation of temporal changes in sediment mass accumulation rate in contrasted Mexican coastal lagoons over the past century, through a geochemical study of ^{210}Pb-dated sediment records.

2. Study sites

2.1. Términos Lagoon

Lying in the southeastern part of the Gulf of Mexico, Términos Lagoon (TL) is the largest coastal lagoon of Mexico, with a surface area of 1,936 km^2 (70 km long and 30 km wide at its widest point) and an average depth of 3.5 m (Yáñez-Arancibia and Day, 1982; Contreras-Ruiz-Esparza et al., 2014) (Fig. 1). TL is surrounded by the Carmen Municipality, in Campeche State; it is permanently connected to the Gulf of Mexico through two inlets at the extremities of Carmen Island, and receives discharges of two main river systems (Palizada and Candelaria), that represent 90% of the freshwater supply. Since TL extends across a wide area, the study has been separated into two subsystems (Fig. 1; Table 1): (1) Palizada-del-Este belongs to the western TL zone, which receives ~ 75% of the total freshwater input into the lagoon through discharge from the Palizada River (9.08×10^9 m^3 yr^{-1}) and is characterized by well-mixed, low-salinity waters, fine sediments (clay and silt), and a warm humid climate (type Am(f)) with abundant summer rains (mean annual precipitation of 1800 mm yr^{-1}) and a mean annual

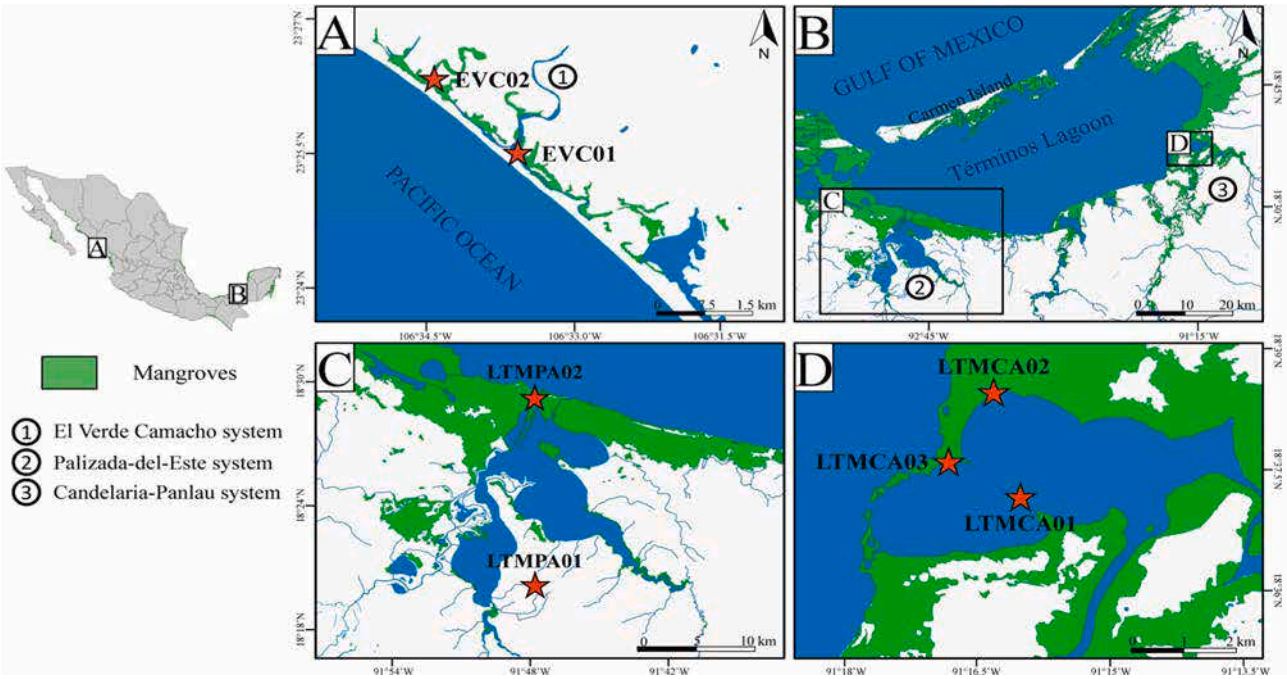

Fig. 1. Sampling location map of the seven sediment cores (★) collected in El Verde Camacho Lagoon (inset A, Mexican Pacific) and Términos Lagoon (inset B, southern Gulf of Mexico). Insets C and D depict the collection sites of cores in Palizada-del-Este and Candelaria-Panlau systems, respectively.

temperature of 27 °C; and (2) Candelaria-Panlau belongs to the central and eastern TL zones, which receive only ~ 15% of the total freshwater input into the lagoon, mainly through the Candelaria River (1.6×10^9 m^3 yr^{-1}); these are shallow and characterized by the presence of calcareous sediments and a warm sub-humid climate (Aw2(w), with a mean annual temperature of 27 °C and precipitation of 1400 mm yr^{-1}) (García, 1973; Ochoa, 2003; Ramos-Miranda and Villalobos-Zapata, 2015) (Table 1).

TL has been affected by human activities, in particular, those associated with the shrimp industry (starting in the 1950s) and the oil industry (starting in the 1970s), for which networks of roads, pipelines, and canals have been built in wetlands, mostly crossing the Palizada-del-Este system (Ochoa, 2003). Forest cover was reduced by 31% between 1974 and 2001 in TL (Soto-Galera 2010); throughout the 1970–2005 period, the degradation of wetlands and primary forests was observed in the basins of the three main rivers discharging into the TL (Palizada, Candelaria, and Chumpan rivers) while urban and agricultural areas increased (Cotler-Avalos, 2010). The mangrove species in TL are *Laguncularia racemosa*, *Avicennia germinans,* and *Rhizophora mangle*. In TL, sediment accumulation rates (SAR) have been reported for mangrove areas near the Palizada River mouth (Lynch et al., 1989) and on the lagoon side of Carmen Island (Gonneea et al., 2004). SAR and MAR have been determined in seagrass meadows in the surroundings of Carmen Island (Ruiz-Fernández et al., 2020a).

2.2. El Verde Camacho Lagoon

El Verde Camacho Lagoon (EV) is on the Mexican Pacific Coast and belongs to the Municipality of Mazatlán, Sinaloa State (Table 1; Fig. 1). It is an internal coastal barrier lagoon with 47 ha, 7 km long, and an average depth of 1 m (Flores-Verdugo et al., 1995). EV is fed by the seasonal flow of the Quelite River, which drains a basin of 835 km^2 and discharges 0.11×10^9 m^3 yr^{-1}. Although EV is closed throughout most of the year, free communication with the sea occurs during the rainy season (June to October) due to the breaking of the sandbar by the combined effects of the Quelite River water flow and the tides that reach their highest levels at this time of year, as well as the impact of occasional tropical storms and hurricanes (Flores-Verdugo et al., 1995). The climate of this region is subhumid tropical, with a mean annual temperature of 25 °C and contrasting seasons (García, 1973). The average salinity is 14 psu, ranging from 10 to 30 psu, depending on whether the sandbar is open or closed. The average annual precipitation is 750 mm yr^{-1}, which falls mainly during the rainy season (CONAGUA, 2015). The dominant mangrove species is *Laguncularia racemosa*, but *Rhizophora mangle*, *Avicennia germinans*, and *Conocarpus erectus* can also be found. The beach and wetlands in this area are relatively well preserved, although in recent years the extent of native vegetation has been reduced by land-use changes (tourism developments, construction of intensive aquaculture ponds, and growth of population settlements; Briseño-Dueñas, 2003). No previous reports on sediment accumulation were available.

3. Methods

3.1. Sampling

Sampling sites were chosen based on the analysis of mangrove distribution in the study areas from aerial pictures and satellite images available at CONABIO (2013, 2021). By comparing mangrove coverage changes between 1970 and 2020, we identified mangrove areas that have remained stable within the past 50 years and have not direct influence of river discharges. Seven sediment push cores were manually collected by inserting PVC tubes (10 cm internal diameter, 1 m length) in the substrate of fringe mangrove communities. All sampling sites were within 15 m of the tidal creek, except for the core LTMCA02, which was collected within 30 m of the creek (Table 2, Fig. 1). The cores were extruded and sectioned at 1 cm intervals; samples were weighed before and after being freeze-dried. Dry bulk density was measured as the weight of the dry mass per the unit volume, expressed as g cm^{-3}, and used to identify compaction. All analyses (except grain size analysis) were carried out on samples ground to a powder with porcelain mortar and pestle. Analytical results are expressed on a dry weight basis.

Table 2
Sediment cores sampled in Términos Lagoon (southern Gulf of Mexico) and El Verde Camacho Lagoon (Mexican Pacific coast).

Core name	System	Date[1]	Coordinates (latitude N; longitude W)	Length (cm)	Mangrove species	Distance[2] (m)
LTMPA01	PDE	2021–02-11	18°20.3319; 91°47.7541	69	*Rhyzophora mangle*	*5*
LTMPA02	PDE	2021–02-11	18°29.0131; 91°47.7362	47	*Rhyzophora mangle; Avicennia germinans; Laguncularia racemosa*	*10*
LTMCA01	CP	2021–02-12	18°37.1903; 91°16.0722	66	*Rhyzophora mangle; Avicennia germinans; Laguncularia racemosa*	*10*
LTMCA02	CP	2021–02-12	18°38.4186; 91°16.3408	64	*Peat sediments surrounded by Rhyzophora mangle and Laguncularia racemosa*	*30*
LTMCA03	CP	2021–02-12	18°37.6450; 91°16.7640	76	*Rhyzophora mangle; Laguncularia racemosa*	*10*
EVC01	EV	2021–07-06	23°42.384; 106°55.820	65	*Rhyzophora mangle; Laguncularia racemosa*	*15*
EVC02	EV	2021–07-06	23°43.893; 106°57.387	69	*Rhyzophora mangle*	*10*

PDE: Palizada-del-Este; CP: Candelaria-Panlau; EV: El Verde Camacho. [1]Date format: yyyy-mm-dd. [2]Estimated distance from the closest tide creek.

3.2. Laboratory analysis

3.2.1. ^{210}Pb dating

Gamma-ray spectrometry (well-type HPGe detectors, GWL-Ortec-Ametek) was used to determine the activities of ^{210}Pb (46.5 keV; $^{210}Pb_{tot}$) and ^{226}Ra (through ^{214}Pb, 351.9 keV, to estimate $^{210}Pb_{sup}$), as well as activities of the bomb fallout radionuclide ^{137}Cs (661.7 keV) to corroborate the ^{210}Pb-derived chronology. Briefly, ~5.0 g of dried and ground samples were packed into standardized geometries (4 mL plastic tubes), sealed with Teflon tape, and stored for three weeks to achieve secular equilibrium between ^{226}Ra and its progeny (Díaz-Asencio et al., 2020). $^{210}Pb_{ex}$ was calculated as the difference between $^{210}Pb_{tot}$ and $^{210}Pb_{sup}$.

3.2.2. Sediment characteristics and composition

Grain size distribution was analyzed to identify hydrodynamic changes, and magnetic susceptibility (MS) to infer changes in sediment provenance, e.g., related to changes in erosion, deposition, and vegetation (Stoner and St-Onge, 2007).

The percentages of sand, silt, and clay fractions were determined by laser diffraction with a Malvern Mastersizer 2000E®. Magnetic susceptibility (in $x10^{-5}$ SI) was measured with a Bartington MS2 magnetic susceptibility meter coupled to an MSG2 frequency sensor. Since meagre sample was available for core LTMCA02, analyses of grain size distribution and magnetic susceptibility could not be performed.

The accuracy of the analytical results was evaluated through the analysis of reference materials (CRM IAEA 300 for gamma spectrometry, Malvern QAS3002 for grain size distribution, and Bartington-G039 for magnetic susceptibility); results were within the reported range of certified values. The precision of the analyses was assessed through the coefficient of variation (CV (%) = standard deviation/mean value × 100) from replicate analysis of a single sample (n = 6): <1% for magnetic susceptibility, <10% for ^{210}Pb and ^{137}Cs, and < 10% for grain size.

3.3. Data treatment

3.3.1. ^{210}Pb dating

The ^{210}Pb chronologies were calculated with the constant flux (CF) model (Robbins et al., 1978; Sanchez-Cabeza and Ruiz-Fernández, 2012). Dating uncertainties were estimated with a Monte Carlo method in which, assuming that the variables included in the CF model follow normal distributions, measured variables are randomized and used to calculate the distribution of derived variables (e.g., section age, MAR, and SAR); and the final uncertainty of each derived variable is the standard deviation of its resulting distribution (Sanchez-Cabeza et al., 2014). To strengthen the confidence and accuracy of the ^{210}Pb chronologies, the age models must be validated using independent dating models and stratigraphic markers (Appleby, 2001). The CF-derived ages were compared with those obtained from a Bayesian ^{210}Pb age-depth modelling (Aquino-López et al., 2018, 2020) implemented through the package rPlum (Blaauw et al., 2021). ^{210}Pb dating was supported by identifying the peak value of the ^{137}Cs activities and/or the records of known meteorological events (e.g., hurricanes or tropical storms).

3.3.2. Statistical analysis

Significant differences in the mean values of the variables among cores were assessed through one-way analysis of variance (ANOVA) and post-hoc Tukey test. In addition, Pearson correlation followed by Student's *t*-test was used to assess associations between variables. These analyses were performed at a 95% confidence level, and significant differences are reported as *p*-values < 0.05.

Exponential regression models for mass accumulation rates (MAR) *versus* time were calculated for each sediment core following the equation:

$$MAR = MAR_0 + a \times e^{b(t-t_0)}$$

where MAR corresponds to the mass accumulation rates; MAR_0 is the initial MAR computed from lowermost sections; t is the time, and t_0 is the time reference (set to 1800); a and b are the fitted model coefficients. Significant peaks were removed to improve the model fit, and a 95% confidence interval was calculated.

4. Results

4.1. ^{210}Pb dating

Total ^{210}Pb ($^{210}Pb_{tot}$) activities ranged from 16 ± 4 to 202 ± 12 Bq kg^{-1} (Table 3) and were comparable among most cores, except for core LTMCA02, which had the highest ($p < 0.05$) activities (Table 3). $^{210}Pb_{ex}$ activities decreased with depth (Fig. 2), but those in the cores from EV displayed irregular profiles. According to ^{210}Pb chronologies, sediment records spanned from 90 to > 100 years.^{137}Cs activities were comparable among cores from TL, except for LTMCA01 which had significantly ($p < 0.05$) lower activities than the rest of the cores.

4.2. Mass and sediment accumulation rates

The values of MAR and SAR were comparable among TL cores, except for LTMCA02, which in recent decades showed significantly ($p < 0.05$) higher values of SAR than the other cores (Table 3; Fig. 3). MAR, and SAR values were comparable ($p < 0.05$) in the EV cores. Notably, high MAR values were found in the years 1956 ± 6 (LTMPA01); 1985 ± 9 and 2014 ± 3 (EVC01); 1944 ± 6, 1950 ± 6, 1987 ± 3 ± 2 and 1997 ± 2 (EVC02) (Fig. 3), and these were removed to compare MAR trends among cores.

MAR is a more reliable variable than SAR because it is independent of compaction. The MAR profiles of all the cores followed a significant ($0.72 \leq r \leq 0.99$; $p < 0.05$) exponential growth from the beginning of the 20th century to 2020 (Fig. 4, Table 4), mostly accelerating since the 1950s. The exponential growth was comparable among the cores from a

Table 3
Radionuclide activities and sediment properties in cores of mangrove areas from Términos Lagoon (southern Gulf of Mexico) and El Verde Camacho Lagoon (Mexican Pac

Core	Statistics	$^{210}Pb_{tot}$ (Bq kg^{-1})	$^{210}Pb_{sup}$ (Bq kg^{-1})	$^{210}Pb_{ex}$ flux (Bq m^{-2} yr^{-1})	Max age and period of the record	^{137}Cs (Bq kg^{-1})	MAR (g cm^{-2} yr^{-1})	SAR (cm yr^{-1})	Sand (%)	Silt (%)
Términos	*Lagoon*									
LTMPA01	Min	18 ± 9	30 ± 2	–	102	1.4 ± 0.1	0.06 ± 0.03	0.07 ± 0.04	4.4 ± 0.2	62 ± 1
	Max	90 ± 7	39 ± 2	–	(1918–2020)	13 ± 1	0.41 ± 0.02	1.3 ± 0.5	17.0 ± 0.7	69 ± 1
	Mean	53 ± 5	34 ± 1	218 ± 13		5.4 ± 0.4	0.25 ± 0.01	0.46 ± 0.05	9.4 ± 0.3	65 ± 1
LTMPA02	Min	30 ± 8	28 ± 2	–	120	0.8 ± 0.1	0.03 ± 0.01	0.02 ± 0.01	2.6 ± 0.1	59 ± 1
	Max	83 ± 7	50 ± 2	–	(1900–2020)	9.8 ± 1	0.47 ± 0.07	0.73 ± 0.1	15.9 ± 0.7	70 ± 1
	Mean	52 ± 5	35 ± 1	245 ± 13		4.7 ± 0.7	0.27 ± 0.05	0.31 ± 0.02	8.9 ± 0.3	65 ± 1
LTMCA01	Min	14 ± 4	12 ± 1	–	118	0.5 ± 0.1	0.07 ± 0.04	0.07 ± 0.03	2.3 ± 0.1	49.7 ± 0.8
	Max	100 ± 8	24 ± 2	–	(1902–2020)	6.5 ± 0.7	0.40 ± 0.06	0.71 ± 0.09	23 ± 1	71 ± 1
	Mean	47 ± 3	20 ± 1	260 ± 12		2.7 ± 0.3	0.24 ± 0.01	0.34 ± 0.02	8.1 ± 0.3	63 ± 1
LTMCA02	Min	16 ± 4	4 ± 1	–	117	1.0 ± 0.1	0.034 ± 0.003	0.11 ± 0.02	NA	NA
	Max	202 ± 12	26 ± 4	–	(1903–2020)	9 ± 1	0.26 ± 0.02	2.1 ± 0.3	NA	NA
	Mean	117 ± 7	9 ± 2	444 ± 6		6 ± 1	0.15 ± 0.01	0.81 ± 0.02	NA	NA
LTMCA03	Min	23 ± 4	16 ± 1	–	112	0.4 ± 0.1	0.06 ± 0.03	0.06 ± 0.03	1.76 ± 0.08	54.7 ± 0.9
	Max	137 ± 9	25 ± 2	–	(1908–2020)	12 ± 1	0.31 ± 0.04	0.8 ± 0.2	11.4 ± 0.5	72 ± 1
	Mean	61 ± 4	21 ± 1	260 ± 9		5.6 ± 0.4	0.20 ± 0.03	0.38 ± 0.02	7.2 ± 0.2	65 ± 1
El Verde	*Camacho*	*Lagoon*								
EVC01	Min	23 ± 9	22 ± 2	–	90	1.0 ± 0.4	0.09 ± 0.09	0.07 ± 0.07	6.7 ± 0.4	28.6 ± 0.8
	Max	47 ± 11	33 ± 2	–	(1931–2021)	4.9 ± 0.8	0.7 ± 0.6*	0.8 ± 0.5*	62 ± 4	64 ± 2
	Mean	33 ± 6	28 ± 1	114 ± 21		2.8 ± 0.5	0.43 ± 0.20*	0.4 ± 0.1*	28 ± 1	49 ± 2
EVC02	Min	21 ± 5	17 ± 1	–	118	0.3 ± 0.1	0.06 ± 0.03	0.06 ± 0.04	0.95 ± 0.05	49 ± 1
	Max	63 ± 9	26 ± 2	–	(1903–2021)	4.6 ± 0.7	0.9 ± 0.3*	1.4 ± 0.4*	8.6 ± 0.5	62 ± 2
	Mean	37 ± 6	22 ± 1	284 ± 17		2.3 ± 0.6	0.43 ± 0.08*	0.6 ± 0.1*	4.4 ± 0.2	53 ± 2

$^{210}Pb_{tot}$: total ^{210}Pb; $^{210}Pb_{sup}$: supported ^{210}Pb (^{226}Ra); MAR: mass accumulation rate; SAR: sediment accumulation rate; DBD: dry bulk density; MS: magnetic susceptibil
available.

* Excluding MAR maxima attributed to meteorological events. See the text for explanation.

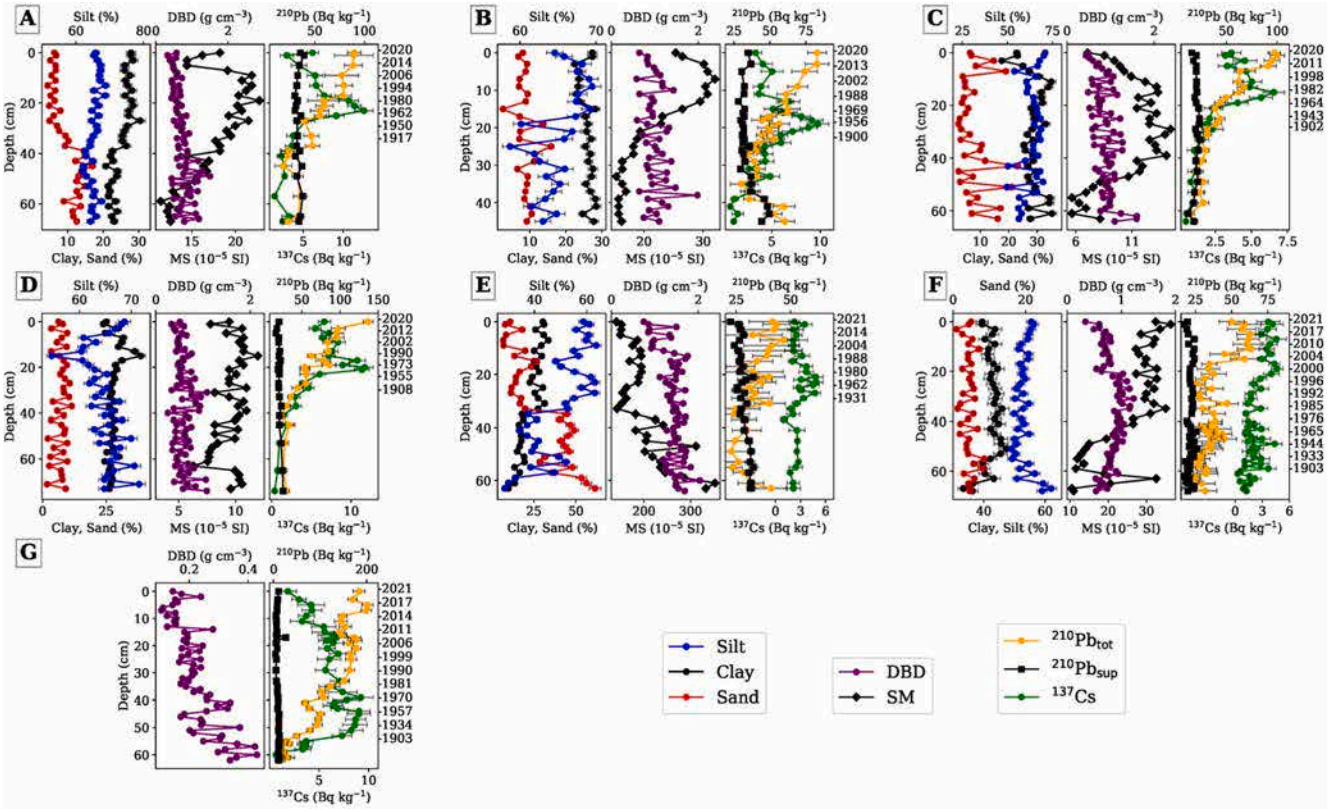

Fig. 2. Grain size distribution, dry bulk density (DBD), magnetic susceptibility (MS), and ^{210}Pb and ^{137}Cs activities in sediment cores from mangrove ecosystems in Términos Lagoon (southern Gulf of Mexico) and El Verde Camacho Lagoon (Mexican Pacific coast). A: LTMPA01; B: LTMPA02; C: LTMCA01; D: LTMCA03; E: EVC01; F: EVC02, G: LTMCA02.

single study site; this was indicated by the model coefficient values of a and b, which were comparable within their uncertainty in the TL system (a: 0.002 ± 0.001 – 0.003 ± 0.001; b: 0.020 ± 0.002 – 0.024 ± 0.002) except for core LTMPA02 (a: 0.0001 ± 0.0001; b: 0.034 ± 0.002), and in the EV system (a: 0.03 ± 0.02; b: 0.013 ± 0.003) (Table 4).

4.3. Sediment characteristics and composition

The TL cores were mainly composed of silt (50–71%) and clay (18–38%), with lower contents of sand (2–23%) (Table 3). In the EV system, EVC01 had significantly ($p < 0.05$) higher proportions of sand and silt, and lower proportions of clay than EVC02. In TL, the profiles of the different grain size fractions showed little variation with depth (Fig. 2), although particular features were observed in some profiles. Those included the following: (1) in LTMCA01, a recent increase of clay percentages (between the surface and 12 cm depth, corresponding to 1993–2020) and fluctuations of sand and silt percentages between 40 cm and the core bottom, occurring during a period earlier than 1900; (2) in LTMPA01, a decrease of sand percentages (between the surface and 42 cm depth, from before 1900 to 2020); (3) in LTMPA02, fluctuations in sand and silt percentages (between 18 and 25 cm depth, from before 1900 to 1961). In the EV system, core EVC01 showed a progressive increase in silts and clays, and a decrease in the sand fraction towards the surface. On the contrary, core EVC02 had an almost homogeneous distribution, except in segment 54–69 cm (<1900 to 1936), where increasing clays and decreasing silts were observed.

Based on the DBD profiles, compaction increased slightly with depth. In general terms, the MS profiles (Fig. 2) shared similar characteristics, with increasing values from deep sections reaching subsurface maxima and decreasing values towards the surface, except in EVC01, where MS decreased steadily from the bottom to the surface.

5. Discussion

5.1. ^{210}Pb dating and sedimentary events

$^{210}Pb_{ex}$ flux ranges in TL cores (218–444 Bq m^{-2} yr^{-1}) were higher than those reported for mangrove sediments (70–169 Bq m^{-2} yr^{-1}; Lynch et al., 1989) and seagrass meadows (46–80 Bq m^{-2} yr^{-1}; Ruiz-Fernández et al., 2020a) in nearby areas. Similarly, the $^{210}Pb_{ex}$ flux ranges in EV cores (111–284 Bq m^{-2} yr^{-1}) were higher than those reported 30 km south of the EV in Urias Lagoon (69–83 Bq m^{-2} yr^{-1}; Ruiz-Fernández et al., 2016) and 150 km to the north in Culiacan River estuary (82 Bq m^{-2} yr^{-1}; Ruiz-Fernández et al., 2002). The magnitude of ^{210}Pb fluxes is directly proportional to factors such as the ^{210}Pb transport from the catchment, water residence time, the fraction of the radionuclide adsorbed onto particles, the mean particle deposition velocity, and the influence of post-depositional transport processes (mixing) (Appleby, 2008). In this study, higher $^{210}Pb_{ex}$ fluxes were likely caused by a preferential accumulation of sediments (i.e., sediment focusing; Likens and Davis, 1975) since the mangroves are effective sediment traps (Cahoon and Lynch, 1997; Sanders et al., 2008).

The departures from the exponential decay function in all ^{210}Pb activity profiles were attributed to variations (i.e., dilution or enhancement) in the sediment supply since $^{210}Pb_{ex}$ activities depend on the balance between the $^{210}Pb_{ex}$ flux (considered constant in the CF model) and MAR (Krishnaswamy et al., 1971; Sanchez-Cabeza and Ruiz-Fernández 2012). The MAR maxima in the EV system (Fig. 3) were likely caused by isolated changes in sediment supply, related to the specific hydrodynamic and morphology of the lagoon. EV is a coastal lagoon with an ephemeral inlet, and most sediment input is provided during the rainy season from the combination of Quelite River water flow and tides, and during occasional high-energy events, such as tropical storms and hurricanes (Flores-Verdugo et al., 1995). The MAR maxima (Fig. 3) can

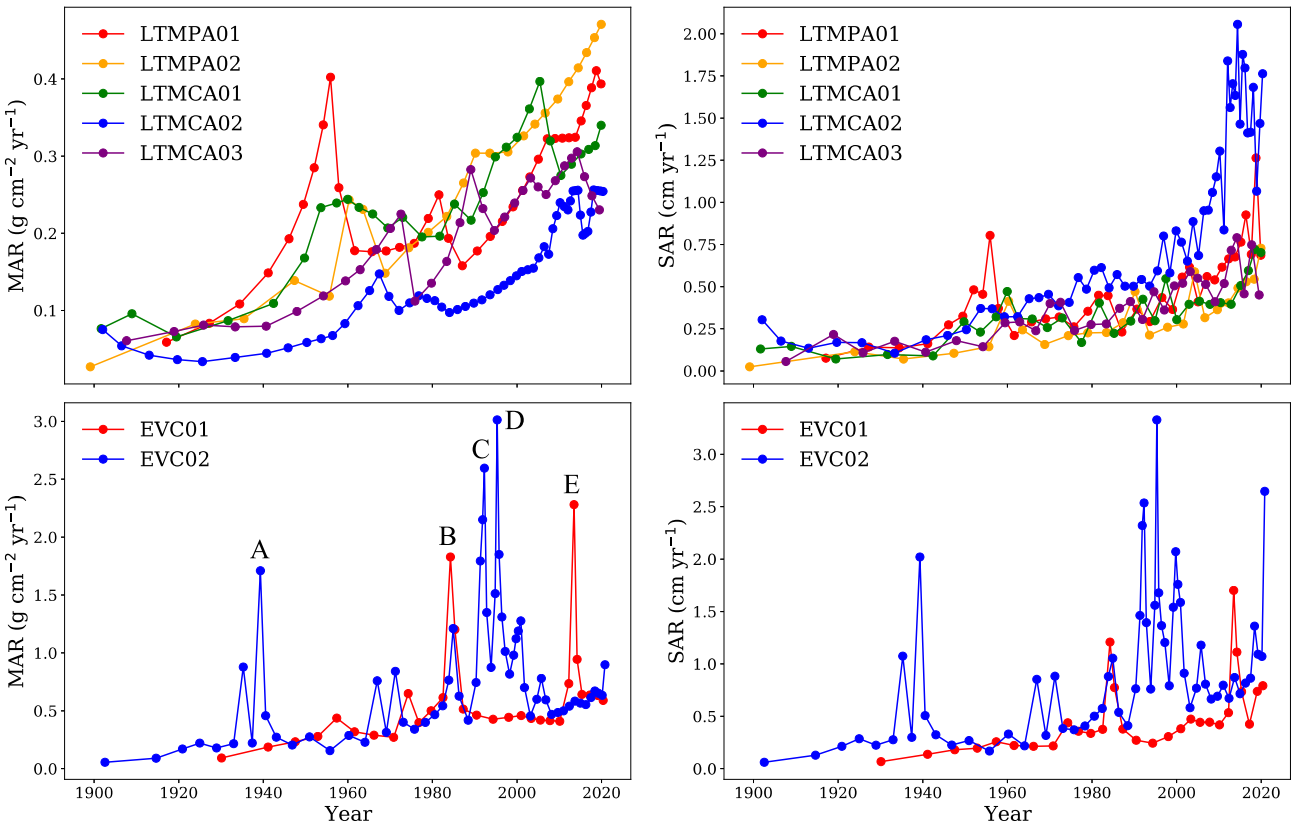

Fig. 3. Mass accumulation rates (MAR) and sediment accumulation rates (SAR) in mangrove sediment cores from Términos Lagoon (above) and El Verde Camacho Lagoon (below). Letters indicate the hurricanes that occurred in the surroundings of the EV system (A = Mazatlán, 1943; B = Tico, 1983; C = Ismael, 1995; D = Isis, 1998; E = Manuel, 2013).

be related to the impact of hurricanes, documented in local newspapers and climatological reports, and these MAR maxima might also serve to corroborate the ^{210}Pb age-models. In core EVC02, MAR maxima (>1.5 g cm^{-2} yr^{-1}) were associated with meteorological events with trajectories over the EV system (Blake et al., 2009) that have had significant human and economic impacts on Mazatlán: 1940 ± 7 associated with hurricane Mazatlán (Oct 9, 1943; Sumner, 1943); 1985 ± 3 with hurricane Tico (Oct 11–24, 1983; Gunther and Cross, 1984); 1993 ± 3 with hurricane Ismael (Sept 12–15, 1995; Mayfield, 1995); and 1996 ± 2 with hurricane Isis (Sep 1–3, 1998; La Jornada, 1998; Pasch, 1999). Core EVC01 recorded two main exceptional events: 1985 ± 9, which that could be associated with hurricane Tico, and 2014 ± 3 with hurricane Manuel (Sept. 13–20, 2013; Pasch and Zelinsky, 2013).

The records of meteorological events in coastal sediments are usually heterogeneous (Cuellar-Martinez et al., 2017 and references therein), because they are influenced by inherent characteristics of those events (e.g., intensity, trajectory, wind speed) and coastal morphology (e.g., presence of wetlands, coast orientation and vulnerability to overwash). In EV, EVC01 is near the mouth of the Quelite river, where the sandbar breaks during the rainy season, and so it receives mainly coarser-grain sediments (significantly higher values of sand and SM were found in EVC01 than in EVC02). EVC02 is farther from the influence of the river, where only enhanced sediment deposition (observed as MAR peaks) is likely provided during exceptional precipitation and storm surge events.

The irregularity of the profiles complicated the corroboration by ^{137}Cs in the EV cores. A ^{137}Cs maximum activity can only be observed in a specific and defined section of the core when sediment accumulation is constant and with a small ^{137}Cs catchment supply (Appleby et al., 2019), a condition that was not observed in the EV system.

Chronologies in the TL cores were corroborated through the depth profiles of the artificial radionuclide ^{137}Cs since the range of highest values at each core (assumed to correspond to the maximum ^{137}Cs fallout occurred in the mid-1960s) agreed with the corresponding ^{210}Pb-derived dates. Maximum ^{137}Cs activities were found in sections 22–24 cm (LTMPA01; 1969 ± 5 – 1973 ± 4), 18–20 cm (LTMPA02; 1956 ± 5 – 1961 ± 5), 15–19 cm (LTMCA01; 1966 ± 4 – 1982 ± 2), 40–46 cm (LTMCA02; 1957 + 1 – 1970 + 1), and 20–23 cm (LTMCA03; 1967 ± 3 – 1973 ± 3), which included the period of maximum ^{137}Cs fallout (1962–1964; Fig. 2). At 40–46 cm, where the ^{137}Cs maximum was expected, ^{137}Cs and ^{210}Pb$_{ex}$ minima and high values of DBD were observed (Fig. 2). As ^{210}Pb$_{ex}$ activities are the balance between the ^{210}Pb$_{ex}$ flux and MAR (Krishnaswamy et al., 1971b), ^{210}Pb$_{ex}$ activities can be enhanced or diluted by changes in sediment inputs; thus, the ^{210}Pb$_{ex}$ minimum could be a result of dilution, owing to a relatively higher sediment input, as observed in the MAR record (Fig. 3), which also caused a low ^{137}Cs activity. The highest ^{137}Cs activities were found for EVC01 in the segment 22 (4.8 ± 0.9 Bq kg^{-1}) to 24 cm (4.9 ± 0.8 Bq kg^{-1}) (period from 1971 ± 11 to 1977 ± 10), and for EVC02 in the segment 48 (3.0 ± 0.9 Bq kg^{-1}) to 50 cm (4.3 ± 0.9 Bq kg^{-1}) (1947 ± 6 to 1956 ± 6), which included the ^{137}Cs fallout maximum, within the uncertainty. However, identifying meteorological events in these sediment records improved the dating validation, especially for ages before the initial onset of ^{137}Cs deposition in the early 1950 s and the maximum ^{137}Cs fallout in 1963.

5.2. *Mass and sediment accumulation rates and sea-level rise*

The MAR ranges in TL cores (0.03–0.47 g cm^{-2} yr^{-1}) were consistent with values reported in seagrass meadows of Carmen Island in TL (MAR: 0.03–0.39 g cm^{-1} yr^{-1}; Ruiz-Fernández et al., 2020a) and mangroves of the Gulf of Mexico and Yucatan Peninsula (Table 5). Excluding the MAR maxima in EV cores, the MAR values (0.04–0.9 g cm^{-2} yr^{-1}) were higher

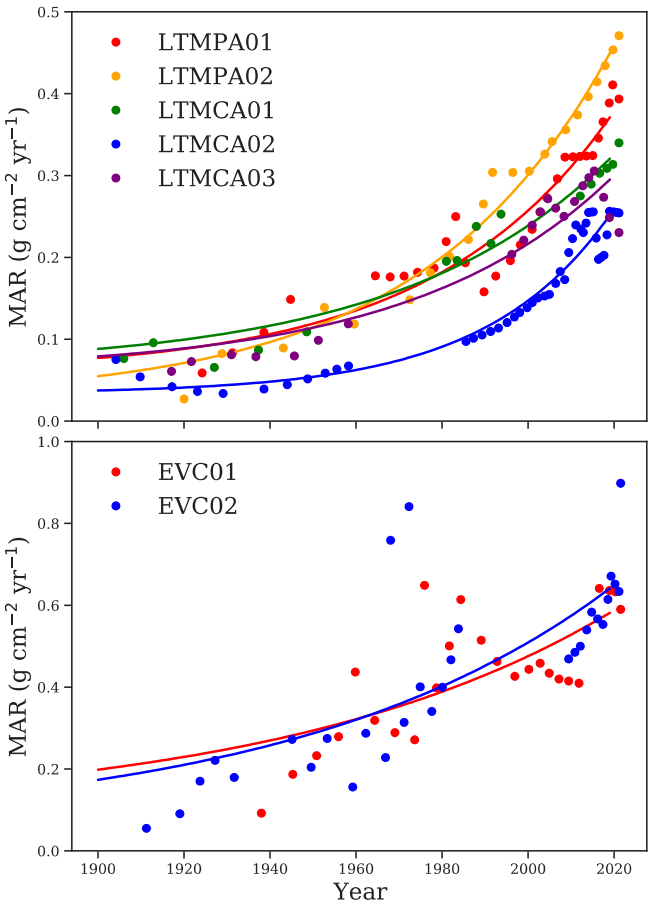

Fig. 4. Exponential regression of mass accumulation rates (MAR) with a 95% confidence interval in mangrove sediment cores from Términos Lagoon (above) and El Verde Camacho Lagoon (below).

than in other mangrove areas of the Mexican Pacific coast but were comparable to other sites in the world (e.g., Brunskill et al., 2002, 2004; Table 5). Excluding the SAR maxima of core LTMCA02 after 2000 and peaks from the EV profiles, SAR values of all the cores (0.02–1.4 cm yr^{-1}) were comparable to the range of values recorded for mangrove forests worldwide (0.01–1 cm yr^{-1} with an average of 0.5 cm yr^{-1}; Alongi, 2012).

The general trend of increasing values of DBD with depth was related to gravitational compaction that affects sediment porosity and water content along the sediment column (Mobilian and Craft, 2022). Changes in sediment MS can indicate variations in the mineralogy, quantity and grain size of the magnetic particles (Thompson and Oldfield, 1986). Except in EVC01, increasing MS values in all sediment cores (Fig. 2) were associated with a progressive change in the amount of magnetic grains present in the sediments transported to the mangroves, and thus a modification in the proportion of sediment sources to the ecosystems (Hilton, 1987; Eriksson and Sandgren, 1999). The lower MS values found in the last 10–20 years in all cores could be caused by a change in sedimentary sources, causing the dilution of magnetic mineral concentrations by paramagnetic or diamagnetic minerals (Hilton, 1987), such as the precipitation of calcium carbonate and diatom silica (Thompson and Oldfield, 1986) or the increase in organic matter inputs (e.g., the deposition of mangrove detritus) (Mohamed et al., 2017). Although grain size distribution changes can also cause the recent decreasing MS values, MS increased with clay in the Palizada cores (LTMPA01 and LTMPA02) and with silt in the Candelaria cores (LTMCA01 and LTMCA03).

In EVC01, increasing content of silt and clay, and decreasing content of sand and MS towards the surface before the 20th century (Fig. 2) likely indicated a shift from a higher- to a lower- energy environment. Unfortunately, no information was available on the hydrodynamic variability of the lagoon or the Quelite River discharge over the past century. However, these changes in grain size and MS could be explained by one or more of the following factors: (1) a change in morphology (for example, the formation of a sandbar, which reduces the energy of water currents, allowing deposition of finer sediments); (2) the growth of the mangroves that progressively attenuate the wave energy and promote the deposition of finer sediments in the lower reaches of the intertidal zone; or (3) a change of sedimentary sources from the Quelite River.

The regression slope of MAR *versus* time depends on the type of environment of deposition, inundation frequency, plant type and productivity, sediment input, and sea-level rise (SLR) (Breithaupt et al., 2014; Sadler, 1981). Despite the different characteristics of the two TL estuaries, MAR values in all cores followed a comparable exponential growth over the last century (Fig. 4). Results suggest that the MAR exponential growth does not depend on specific characteristics of each study site, but on other factors with a widespread impact on mangrove sedimentation.

Mangroves are notable for having high sediment accumulation owing to their ability to reduce water current speed, facilitate suspended material trapping and deposition, and stabilize the shoreline against coastal erosion (Cahoon and Lynch, 1997; Mazda et al., 2006; Sanders et al., 2008), owing to their vegetation structure (e.g., aerial and belowground roots, pneumatophores, seedlings). As the sea-level rises, tidal flooding occurs for more extended periods, prolonging the time for the deposition of suspended particles and reducing soil compaction and organic matter decomposition (Rogers et al., 2005; Gilman et al., 2006; Alongi, 2009). Mangroves can also increase surface elevation through biotic processes, such as generating roots, forming microbial mats, and accumulating leaf litter and vegetation detritus (Mckee et al., 2007; McKee, 2011). Because of their unique intertidal location, mangroves tend to maintain an equilibrium between sedimentary accretion and

Table 4
Exponential regression models for mass accumulation rate (MAR) *versus* time in sediment cores from mangrove ecosystems in Términos Lagoon (southern Gulf of Mexico) and El Verde Camacho Lagoon (Mexican Pacific coast).

Core	n	MAR_0	a	b	r*	p*
LTMPA01	30	0.059	0.002 + 0.001	0.024 ± 0.002	0.96	2.5e^{-16}
LTMPA02	22	0.027	0.003 ± 0.001	0.023 ± 0.001	0.99	4.1e^{-12}
LTMCA01	16	0.065	0.003 ± 0.001	0.020 ± 0.002	0.97	3.9e^{-19}
LTMCA02	45	0.034	0.0001 ± 0.0001	0.034 ± 0.002	0.95	2.2e^{-14}
LTMCA03	21	0.061	0.002 ± 0.001	0.021 ± 0.003	0.94	3.9e^{-15}
EVC01	25	0.092	0.03 ± 0.02	0.013 ± 0.003	0.72	5.1e^{-21}
EVC02	31	0.055	0.03 ± 0.02	0.013 ± 0.003	0.77	1.2e^{-22}

n: number of MAR values per core used in the model; MAR: mass accumulation rates (g cm^{-2} yr^{-1}); MAR_0: initial MAR computed from lowermost sections; t_0: time reference set up to 1800; a, b: fitted coefficient values.

* Correlation coefficient (r) and *p*-value (*p*) obtained from the relationship ln MAR *versus* time.

Table 5
Mass accumulation rates (MAR) in mangrove sites in Mexico and around the world.

Study area	MAR ($g\ cm^{-2}\ yr^{-1}$)	Reference
Gulf of Mexico and Yucatan Peninsula		
Everglades National Park, USA	0.01–0.6	Breithaupt et al. (2014)
Sian'Ka'an Biosphere Reserve, Mexico	0.05–0.28	Carnero-Bravo et al. (2016)
Cancún-Riviera Maya, Mexico	0.02–0.08	Cuéllar-Martínez et al. (2020)
Términos Lagoon, Mexico	0.03–0.47	This study
Mexican Pacific Coast		
Marismas Nacionales, Mexico	0.07–0.41	Cuellar-Martinez et al. (2020); Ruiz-Fernández et al. (2018a)
Estero de Urías Lagoon, Mexico	0.01–0.37	Aldana-Gutiérrez et al. (2021); Cuellar-Martinez et al. (2020)
El Verde Camacho Lagoon, Mexico	0.04–0.9*	This study
Other sites in the world		
Herbert River region, Qld, Australia	0.04–1.2	Brunskill et al., (2002)
Irian Jaya, Indonesia	0.45–1.3	Brunskill et al., (2004)
Ba Lat Estuary, Vietnam	0.22–0.36	Van Santen et al., (2007)
Western Arabian Gulf, Saudi Arabia	0.18–0.50	Cusack et al., (2018)

* Excluding MAR maxima attributed to meteorological events. See the text for explanation.

SLR, facilitating coastal adaptation to a rising sea-level (Lynch et al., 1989; Nyman et al., 2006; Krauss et al., 2014). For this reason, SARs from mangrove sediments have been used to estimate local SLR during the past century (Lynch et al., 1989; Parkinson et al., 1994; Sanders et al., 2010).

Regional SLR depends on factors such as ocean hydrodynamics (e.g., currents, upwelling, and wind-forced ocean circulation), ocean surface properties (e.g., salinity and temperature related to water exchanges between the ocean, atmosphere, and land), local/regional vertical motion of the Earth's crust and glacial isostatic adjustment (Stammer et al., 2013; Zavala-Hidalgo et al., 2015). A relationship between the present SLR and increasing mangrove sediment accumulation rates has been observed in other Mexican coastal lagoons (e.g., Carnero-Bravo et al., 2016, 2018; Ruiz-Fernández et al., 2018b).

SAR depends on compaction along the sediment column (Robbins, 1978). Therefore, to relate mangrove sediment accumulation to SLR, depth is corrected for compaction by normalizing each value by the average bulk density of the bottom sections (e. g., Lynch et al., 1989; Carnero-Bravo et al., 2016, 2018; Ruiz-Fernández et al., 2020a). Corrected SAR values, calculated from the linear regression of age *versus* corrected depth series over significant periods, were 0.48–2.0 mm yr^{-1} before the 1950 s, 1.8–3.6 mm yr^{-1} from 1950 to 2000, and 3.4–6.7 mm yr^{-1} during the 2000–2021 period (Fig. 5, Table 6). The irregularity of the core EVC02 SAR profile, showing various peaks, precluded the detection of a relationship with SLR in the EV system.

Within its uncertainty, the corrected SAR ranges from TL cores (Table 6) were compatible with the SLR rates reported for Carmen City over the period 1956–1992 (3.4 ± 1.0 mm yr^{-1}; Zavala-Hidalgo et al., 2015). Increasingly marine conditions have been reported from the analysis of seagrass meadow sediment records of Carmen Island (Ruiz-Fernández et al., 2020b) and through direct salinity observations in the lagoon between the 1980s and late 1990s (Villéger et al., 2010), because

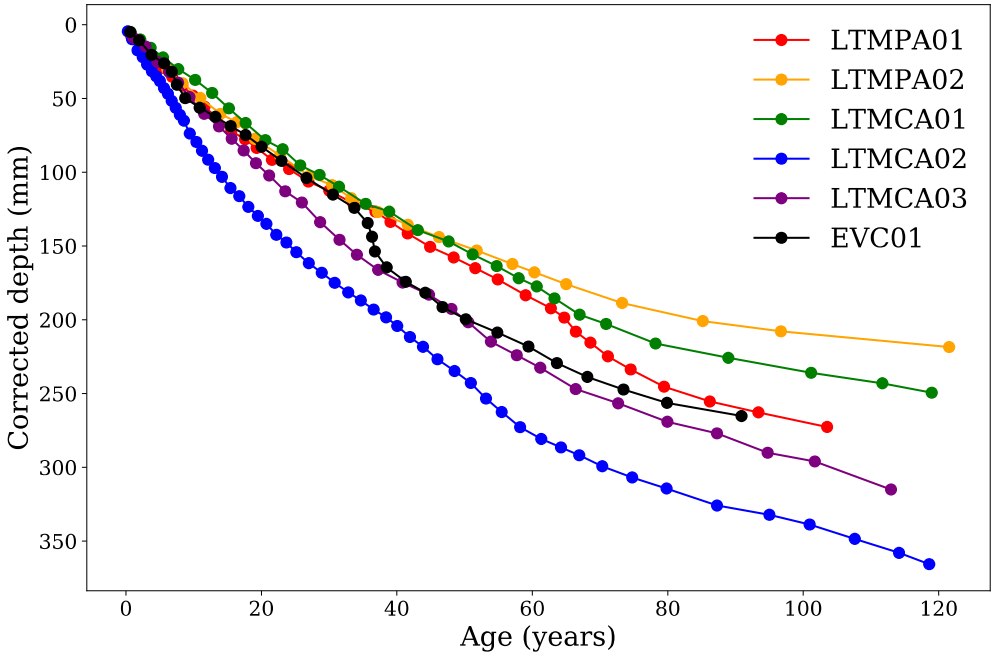

Fig. 5. Age *versus* compaction-corrected depth in sediment cores from mangrove ecosystems in Términos Lagoon (southern Gulf of Mexico) and El Verde Camacho Lagoon (Mexican Pacific coast). Core EVC02 was not considered here because of its irregular profile.

Table 6
Corrected sediment accumulation rate (SAR) calculated from the linear regression of age *versus* compaction-corrected depth series for selected periods.

Core	Start	End	Corrected SAR (mm yr^{-1})	Determination coefficient (r^2)
LTMCA01	1993	2020	3.6 ± 0.5	0.998
	1943	1993	2.3 ± 0.4	0.998
	1902	1943	0.8 ± 0.1	0.998
LTMCA02	2002	2020	6.7 ± 2.3	0.994
	1960	2002	3.6 ± 0.5	0.999
	1903	1960	1.4 ± 0.4	0.992
LTMCA03	1993	2020	4.6 ± 0.8	0.998
	1943	1993	3.1 ± 0.9	0.992
	1902	1943	1.5 ± 0.4	0.990
LTMPA01	2000	2020	4.1 ± 0.9	0.996
	1955	2000	2.5 ± 0.4	0.998
	1947	1955	3.2 ± 0.3	0.994
	1918	1947	1.5 ± 0.4	0.967
LTMPA02	1988	2020	3.4 ± 1.0	0.992
	1948	1988	1.8 ± 0.2	0.997
	1900	1948	0.48 ± 0.04	0.992
EVC01	2013	2021	5.2 ± 2.0	0.971
	1988	2013	3.0 ± 0.2	0.999
	1983	1988	8.9 ± 3.7	0.944
	1931	1983	2.0 ± 1.1	0.968

of rising sea-level. Evidence of progressive SLR-induced erosion along the Campeche state coastline has been reported from 1974 to 2008, particularly along the coast in the northwest of the TL system, where a reduction in mangrove coverage has also been reported (Torres-Rodríguez et al., 2010). Eroded materials could be transported and redistributed by tide currents into the lagoon and would support TL's mangroves to adjust to SLR by increasing MAR, as seen in other studies around the world (e.g., Thampanya et al., 2006; Hayden and Granek, 2015).

Core EVC01 from the EV system showed corrected SAR values of 2.0 ± 1.1 mm yr^{-1} (1931–1983) and 3.0 ± 0.2 mm yr^{-1} (1988–2013). These values were also in agreement with the rates of SLR reported for Estero de Urías Lagoon, 30 km south of EV (1.9 ± 3.3 mm yr^{-1} between 1953 and 1992, Zavala-Hidalgo et al., 2010; 3.87 ± 0.12 mm yr^{-1}, between 1990 and 2012; Ruiz-Fernández et al., 2016). EV has a temporary connection to the ocean during the rainy season (Flores-Verdugo et al., 1995), during which SLR could cause an increase in mangrove sedimentation by increasing the frequency and intensity of the inundations caused by the tides and meteorological events (e.g., hurricanes and tropical storms).

The removal or disturbance of mangroves, whether naturally or anthropogenically caused, leads to a reduction in sediment accretion and a loss of stability against coastline erosion (e.g., Mckee et al., 2007; McKee, 2011; Hayden and Granek, 2015). The ability of a mangrove ecosystem to adapt to SLR depends on factors such as river and marine sediment inputs, the type and conditions of the mangrove communities, and hydrogeomorphic conditions (Krauss et al., 2014). The findings of this study indicate a link between increasing accretion rates at the lowest level of a mangrove transect, the first to be impacted by an increase in the frequency and duration of tidal flooding, such as that caused by sea level rise, and suggest that the sedimentary and

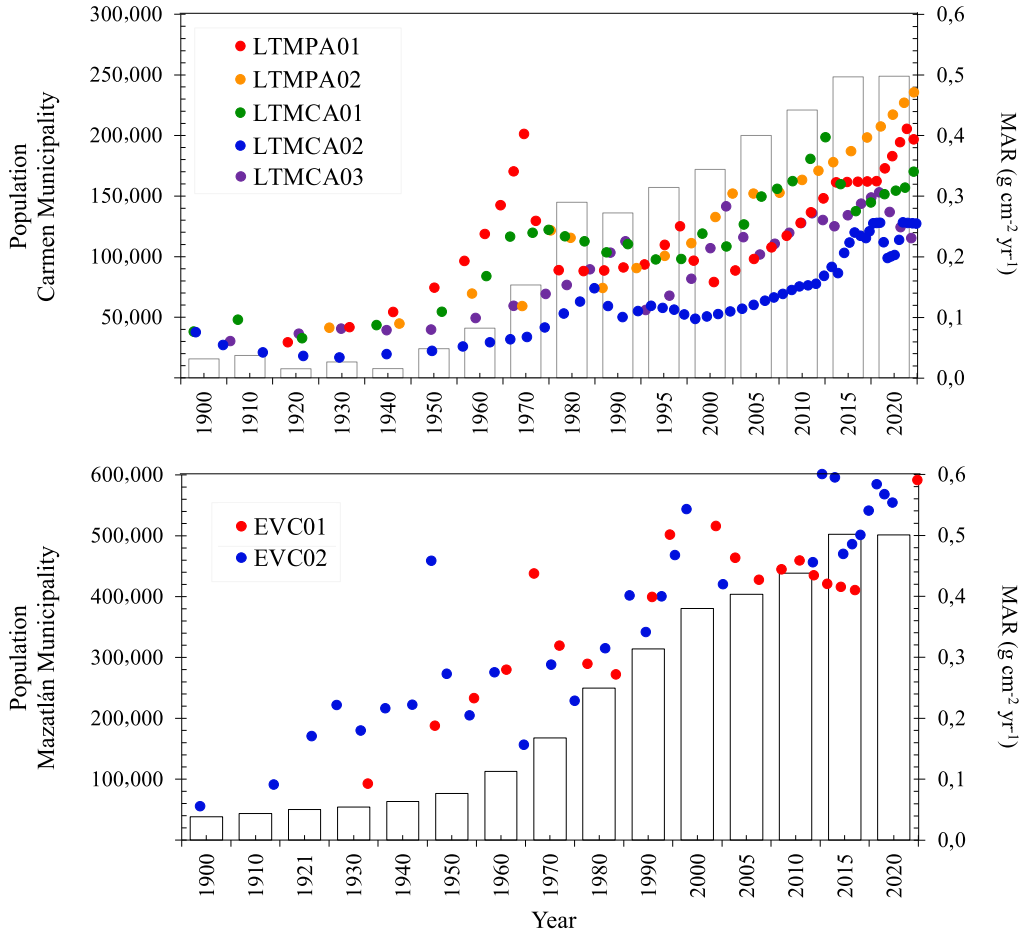

Fig. 6. Population growth in Carmen and Mazatlán municipalities (retrieved from INEGI 2022; bars) *versus* mass accumulation rates (MAR; points) in mangrove sediment cores from Términos Lagoon (above) and El Verde Camacho Lagoon (below) over the period 1900–2021 (INEGI, 2022).

hydrological conditions in the TL and EV areas, as well as the states of the studied mangroves, are favorable for sediment accretion at a rate consistent with current local SLR and coastline stabilization.

5.3. Anthropogenic influences on MAR

MAR in sediment cores showed an exponential increase, mainly accelerated since the 1950s, that was interpreted as the consequence of increased continental erosion led by land-use change and a growing population (e.g., Ruiz-Fernández et al., 2009). The Carmen (including Palizada-del-Este and Candelaria-Panlau systems) and Mazatlán (including the EV system) municipalities doubled their population between 1900 and 1950. Over 1950–2020, the acceleration (x7 and x10 increase in Carmen and Mazatlán municipalities, respectively) was matched by exponential MAR increases (Fig. 6).

The main land-use changes in the surroundings of TL started with the development of the shrimp industry in 1947, induced by an agreement between Mexico and US vessels to support the most intensive commercial shrimp exploitation in the southern Gulf of Mexico; however, this declined in the 1990s when various species of shrimps were close to extinction (Ramos-Miranda and Villalobos-Zapata, 2015). The oil industry started in the 1970s, with the installation of administrative offices of the Mexican state-owned petroleum company (PEMEX, Petróleos Mexicanos) on Carmen Island to identify potential hydrocarbon reserves in TL (Bach et al., 2005). Further oil exploration and exploitation required destroying thousands of hectares of wetlands, especially in the Palizada-del-Este system, where the main roads, pipelines, and canals were installed (Ochoa, 2003). These two industries contributed to the intensification of population growth on Carmen Island (Bach et al., 2005). Other factors may have contributed to increasing continental erosion in the lagoon and its surrounding areas, such as the development of intensive agriculture and urban settlements, each of which increased by 30% throughout the 1974–2001 period, while mangrove, tropical forests, and aquatic vegetation progressively lost 31% of their original cover during the same period (Soto-Galera et al., 2010).

For the EV lagoon, no quantitative studies are available on the consequences of land-use changes on local vegetation; however, in recent decades there has been a reduction in the extent of mangroves as a result of land-use changes, mainly in terms of the development of population settlements and productive activities such as tourism and aquaculture (Briseño-Dueñas, 2003). The annual deforestation rate in the Mazatlán municipality was estimated at 0.36% from 1993 to 2011 (Monjardín-Armenta et al., 2017). Moreover, the EV system has been affected by the recent urban expansion of Mazatlán City, a popular tourist destination lying 30 km south of EV, which hosts one of the largest tuna processing facilities in the world, the main tuna fishing fleet of Latin America and the second largest fishing fleet of Mexico. Harbor and tourism development caused substantial city growth, starting from the 1960s and accelerating since the 1980s, following a direction parallel to the coast toward the north (Beraud-Lozano et al., 2009). In particular, to the north of the city and along the main road leading through the Quelite River Basin to the state capital Culiacán, there has been informal urbanization, construction of intensive aquaculture ponds and agricultural areas, and unregulated population settlements; all these have contributed to the spatial transformation of the Mazatlán municipality (Padilla and De Sicilia, 2020).

This study showed that, although the study areas have endured several anthropogenic disturbances, sediment cores from these mangroves recorded similar MAR growth patterns; these reflected an increasing erosion trend in coastal areas and upper watersheds related to land-use change. Efforts to monitor sediment accretion and improve coastal zone management will allow a better understanding of the mangrove responses to anthropogenic land-based activity and verifying that the environmental services of mangroves, such as reducing the impacts of waves, coastal erosion, storm and SLR-derived flooding (Krauss et al., 2014) are preserved.

6. Conclusions

Retrospective reconstruction of sediment accumulation over the past century from Términos Lagoon and El Verde Camacho Lagoon, two Mexican coastal lagoons with contrasting environmental characteristics, was achieved through ^{210}Pb-dating of mangrove sediment cores, corroborated by the use of ^{137}Cs and MAR maxima (attributed to meteorological events) observed in the sediment records. Both areas' sediment accumulation rates (SAR) were comparable to the global range recorded for mangrove forests worldwide. Furthermore, all cores showed exponential trends in the mass accumulation rate (MAR) towards the present, accelerating since the 1950 s and matching the reported population growth. Contrary to the study hypothesis, MAR increases over the past century were similar, despite differences in meteorological and demographic characteristics between the study sites. This suggested that MAR increases are mainly affected by general factors such as continental soil erosion promoted by land-use changes associated with the regional economic development, and sea-level rise related to climate change, similar in the two study areas. In addition, the density-corrected SAR values were comparable to those recorded in previous studies in these regions, indicating that the fringe mangrove sites of this study are currently under conditions favorable to sediment accumulation at a rate comparable to local sea-level rise.

Declaration of Competing Interest

The authors declare that they have no known competing financial interests or personal relationships that could have appeared to influence the work reported in this paper.

Data availability

Data will be made available on request.

Acknowledgments

This work was supported by Universidad Nacional Autónoma de México (UNAM) through the projects PAPIIT-DGAPA IN102821 and IA101821, and ICML-Antropopausa Laguna de Términos, as well as by the Institut de Recherche pour le Développement (IRD) through the international network DEXICOTROP. The support of Posgrado en Ciencias del Mar y Limnologia - UNAM, and a Ph.D. fellowship from Consejo Nacional de Ciencia y Tecnología-Mexico (CONACYT, CVU 1102000) are acknowledged by Jupin J.L.J. The authors are grateful for the support received from the staff of the APFF Meseta de Cacaxtla (CONANP-SEMARNAT), and the assistance provided by J. A. Martinez-Trejo (sampling), L.F. Álvarez-Sánchez (data curation), C. Súarez-Gutiérrez (informatics), A.A. García-López and C.L. Aybar-Camacho (statistics), and A. Grant (English edition of the manuscript).

References

Aldana-Gutiérrez, G., Ruiz-Fernández, A.C., Pérez-Bernal, L.H., Flores-Verdugo, F., Cuellar-Martinez, T., Sánchez-Cabeza, J.A., 2021. Flujos e inventarios de Carbono Azul en manglares asociados a una laguna costera antropizada. Geofís Int 1, 13–30.

Alongi, D.M., 2008. Mangrove forests: Resilience, protection from tsunamis, and responses to global climate change. Estuar Coast Shelf Sci 76, 1–13. https://doi.org/10.1016/j.ecss.2007.08.024.

Alongi, D.M., 2012. Carbon sequestration in mangrove forests. Carbon Manag 3, 313–322. https://doi.org/10.4155/cmt.12.20.

Alongi, D.M., 2009. The energetics of mangrove forests. Springer Science & Business Media. Springer SBM, Dordrecht, p. 216.

Appleby, P.G., 2001. Chronostratigraphic techniques in recent sediments. In: Last, W.M., Smol, J.P (Eds.), Tracking Environmental Change Using Lake Sediments volume 1: basin analysis, coring, and chronological techniques. Kluwer Academic, Dordrecht, pp. 171–203.

Appleby, P.G., 2008. Three decades of dating recent sediments by fallout radionuclides: A review. Holocene 18, 83–93. https://doi.org/10.1177/0959683607085598.

Appleby, P.G., Oldfield, F., 1978. The calculation of lead-210 dates assuming a constant rate of supply of unsupported ^{210}Pb to the sediment. Catena (Amst) 5, 1–8. https://doi.org/10.1016/S0341-8162(78)80002-2.

Appleby, P.G., Semertzidou, P., Piliposian, G.T., Chiverrell, R.C., Schillereff, D.N., Warburton, J., 2019. The transport and mass balance of fallout radionuclides in Brotherswater, Cumbria (UK). J Paleolimnol 62, 389–407. https://doi.org/10.1007/s10933-019-00095-z.

Aquino-López, M.A., Blaauw, M., Christen, J.A., Sanderson, N.K., 2018. Bayesian Analysis of ^{210}Pb Dating. J Agric Biol Environ Stat 23, 317–333. https://doi.org/10.1007/s13253-018-0328-7.

Aquino-López, M.A., Ruiz-Fernández, A.C., Blaauw, M., Sanchez-Cabeza, J.A., 2020. Comparing classical and Bayesian ^{210}Pb dating models in human-impacted aquatic environments. Quat Geochronol 60, 101106. https://doi.org/10.1016/j.quageo.2020.101106.

Bach, L., Calderon, R., Cepeda, M.F., Oczkowski, A., Olsen, S.B., Robadue, D., 2005.. Resumen del Perfil de Primer Nivel del Sitio Laguna de Términos y su Cuenca, México. Coastal Resources Center, University of Rhode Island, Narragansett, p. 30.

Beraud-Lozano, J.L., Covantes-Rodríguez, C., Beraud-Martínez, I.P., 2009. Vulnerabilidad socioambiental en Mazatlan, Mexico. In: Sánchez González, D., Egea Jiménez, C. (Eds.), Vulnerabilidad Sociodemográfica y Ambiental, Viejos y Nuevos Riesgos. Cuadernos Geográficos (49). Universidad de Granada, Granada, pp. 31–62.

Berger, J.F., Charpentier, V., Crassard, R., Martin, C., Davtian, G., López-Sáez, J.A., 2013. The dynamics of mangrove ecosystems, changes in sea level and the strategies of Neolithic settlements along the coast of Oman (6000–3000cal.BC). J Archaeol Sci 40, 3087–3104. https://doi.org/10.1016/j.jas.2013.03.004.

Blaauw, M., Christen, J.A., Aquino-López, M.A., Esquivel-Vazquez, J., Gonzalez, O.M., Belding, T., Theiler, J., Gough, B., Karney, C., 2021. rplum: Bayesian Age-Depth Modelling of Cores Dated by Pb-210. *R package version* 0.1.4. URL https://cran.r-project.org/web/packages/rplum/index.html (accessed 1.2.23).

Blake, E.S., Gibney, E.J., Brown, D.P., Mainelli, M., Franklin, J.L., Kimberlain, T.B., Hammer, G.R., 2009. Tropical cyclones of the eastern North Pacific Basin, 1949-2006. National Climatic Data Center, Historical climatology series; 6-5.

Breithaupt, J.L., Smoak, J.M., Smith, T.J., Sanders, C.J., Hoare, A., 2012. Organic carbon burial rates in mangrove sediments: Strengthening the global budget. Global Biogeochem Cycles 26, 1–11. https://doi.org/10.1029/2012GB004375.

Breithaupt, J.L., Smoak, J.M., Smith, T.J., Sanders, C.J., 2014. Temporal variability of carbon and nutrient burial, sediment accretion, and mass accumulation over the past century in a carbonate platform mangrove forest of the Florida Everglades. J Geophys Res Biogeosci 119, 2032–2048. https://doi.org/10.1002/2014JG002715.

Briseño-Dueñas, R., 2003. Ficha Informativa de los Humedales de Ramsar (FIR). "Playa Tortuguera El Verde Camacho". URL: https://rsis.ramsar.org/RISapp/files/RISrep/MX1349RIS.pdf (accessed 2.1.22).

Brunskill, G.J., Zagorskis, I., Pfitzner, J., 2002. Carbon Burial Rates in Sediments and a Carbon Mass Balance for the Herbert River Region of the Great Barrier Reef Continental Shelf, North Queensland, Australia. Estuar Coast Shelf Sci 54, 677–700. https://doi.org/10.1006/ecss.2001.0852.

Brunskill, G.J., Zagorskis, I., Pfitzner, J., Ellison, J., 2004. Sediment and trace element depositional history from the Ajkwa River estuarine mangroves of Irian Jaya (West Papua), Indonesia. Cont Shelf Res 24, 2535–2551. https://doi.org/10.1016/j.csr.2004.07.024.

Cahoon, D., Lynch, J., 1997. Vertical accretion and shallow subsidence in a mangrove forest of southwestern Florida, U.S.A. Mangroves and Salt Marshes 3, 173–186. https://doi.org/10.1023/A:1009904816246.

Carnero-Bravo, V., Sanchez-Cabeza, J.A., Ruiz-Fernández, A.C., Merino-Ibarra, M., Hillaire-Marcel, C., Corcho-Alvarado, J.A., Röllin, S., Diaz-Asencio, M., Cardoso-Mohedano, J.G., Zavala-Hidalgo, J., 2016. Sedimentary records of recent sea level rise and acceleration in the Yucatan Peninsula. Sci Total Environ 573, 1063–1069. https://doi.org/10.1016/j.scitotenv.2016.08.142.

Carnero-Bravo, V., Sanchez-Cabeza, J.A., Ruiz-Fernández, A.C., Merino-Ibarra, M., Corcho-Alvarado, J.A., Sahli, H., Hélie, J.-F., Preda, M., Zavala-Hidalgo, J., Díaz-Asencio, M., Hillaire-Marcel, C., 2018. Sea level rise sedimentary record and organic carbon fluxes in a low-lying tropical coastal ecosystem. Catena (Amst) 162, 421–430. https://doi.org/10.1016/j.catena.2017.09.016.

CONABIO, 2013. "Distribución de los manglares en México en 1970-1981", escala: 1: 50000. edición: 1. Comisión Nacional para el Conocimiento y Uso de la Biodiversidad. Proyecto: GQ004, Los manglares de México: Estado actual y establecimiento de un programa de monitoreo. URL http://geoportal.conabio.gob.mx/metadatos/doc/html/mexman70gw.html (accessed 1.1.23).

CONABIO, 2021. "Distribución de los manglares en México en 2020", escala: 1:50000. edición: 1. Comisión Nacional para el Conocimiento y Uso de la Biodiversidad. Sistema de Monitoreo de los Manglares de México (SMMM). URL http://geoportal.conabio.gob.mx/metadatos/doc/html/mx_man20gw.html (accessed 1.1.23).

CONAGUA, 2015. Determinación de la Disponibilidad de Agua en el acuífero Río Quelite (2508), estado de Sinaloa.

Contreras-Ruiz-Esparza, A., Douillet, P., Zavala-Hidalgo, J., 2014. Tidal dynamics of the Terminos Lagoon, Mexico: Observations and 3D numerical modelling. Ocean Dyn 64, 1349–1371. https://doi.org/10.1007/s10236-014-0752-3.

Cuellar-Martinez, T., Ruiz-Fernández, A.C., Sánchez-Cabeza, J.A., Alonso-Rodríguez, R., 2017. Sedimentary record of recent climate impacts on an insular coastal lagoon in the Gulf of California. Quat Sci Rev 160, 138–149. https://doi.org/10.1016/j.quascirev.2017.01.002.

Cuellar-Martinez, T., Ruiz-Fernández, A.C., Sánchez-Cabeza, J.A., Pérez-Bernal, L., López-Mendoza, P.G., Carnero-Bravo, V., Agraz-Hernández, C.M., van Tussenbroek, B.I., Sandoval-Gil, J., Cardoso-Mohedano, J.G., Vázquez-Molina, Y., Aldana-Gutiérrez, G., 2020. Temporal records of organic carbon stocks and burial rates in Mexican blue carbon coastal ecosystems throughout the Anthropocene. Glob Planet Change 192, 103215. https://doi.org/10.1016/j.gloplacha.2020.103215.

Cusack, M., Saderne, V., Arias-Ortiz, A., Masqué, P., Krishnakumar, P.K., Rabaoui, L., Qurban, M.A., Qasem, A.M., Prihartato, P., Loughland, R.A., Elyas, A.A., Duarte, C. M., 2018. Organic carbon sequestration and storage in vegetated coastal habitats along the western coast of the Arabian Gulf. Environ Res Lett 13, 074007. https://doi.org/10.1088/1748-9326/aac899.

DDEP, 2007. Table de radionucleides ^{137}Cs. LNE-LNHB/CEA. URL http://www.nucleide.org/DDEP_WG/Nuclides/Cs-137_tables.pdf (accessed 10.10.21).

DDEP, 2012. Table de radionucleides ^{210}Pb. LNE-LNHB/CEA. URL http://www.nucleide.org/DDEP_WG/DDEPdata.htm. (accessed 1.30.22).

Díaz-Asencio, M., Sanchez-Cabeza, J.A., Ruiz-Fernández, A.C., Corcho-Alvarado, J.A., Pérez-Bernal, L.H., 2020. Calibration and use of well-type germanium detectors for low-level gamma-ray spectrometry of sediments using a semi-empirical method. J Environ Radioact 225. https://doi.org/10.1016/j.jenvrad.2020.106385.

Eriksson, M.G., Sandgren, P., 1999. Mineral magnetic analyses of sediment cores recording recent soil erosion history in central Tanzania. Palaeogeogr Palaeoclimatol Palaeoecol 152, 365–383. https://doi.org/10.1016/S0031-0182(99)00043-7.

Flores-Verdugo, F.J., Briseño-Dueñas, R., González-Farías, F., Calvario-Martínez, O., 1995. Balance de carbono en un ecosistema lagunar estuarino de boca efímera de la costa noroccidental de México (Estero El Verde, Sinaloa). In: González-Farias, F., de la Rosa Vélez, J. (Eds.), Temas de oceanografía biológica en México II. Universidad Autónoma de Baja California, Ensenada, pp. 137–160.

García, E., 1973. Modificaciones al sistema de clasificación climática de Köppen: para adaptarlo a las condiciones de la república mexicana, 6th ed. Universidad Nacional Autónoma de México, México, D.F., p. 246

Gilman, E.L., Ellison, J.C., Jungblut, V., van Lavieren, H., Wilson, L., Areki, F., Brighouse, G., Bungitak, J., Dus, E., Henry, M., Kilman, M., Matthews, E., Sauni, I., Teariki-Ruatu, N., Tukia, S., Yuknavage, K., 2006. Adapting to Pacific Island mangrove responses to sea level rise and climate change. Clim Res 32, 161–176. https://doi.org/10.3354/cr032161.

Gonneea, M.E., Paytan, A., Herrera-Silveira, J.A., 2004. Tracing organic matter sources and carbon burial in mangrove sediments over the past 160 years. Estuar Coast Shelf Sci 61, 211–227. https://doi.org/10.1016/j.ecss.2004.04.015.

Gunther, E.B., Cross, R.L., 1984. Eastern North Pacific Tropical Cyclones of 1983. Mon Weather Rev 112, 1419–1440.

Hayden, H.L., Granek, E.F., 2015. Coastal sediment elevation change following anthropogenic mangrove clearing. Estuar Coast Shelf Sci 165, 70–74. https://doi.org/10.1016/j.ecss.2015.09.004.

Hilton, J., 1987. A Simple Model for the Interpretation of Magnetic Records in Lacustrine and Ocean Sediments. Quat Res 27, 160–166. https://doi.org/10.1016/0033-5894(87)90074-3.

INEGI, 2002. Cuaderno Estadistico Municipal: Municipio Carmen, Estado de Campeche. Instituto Nacional de Estadística, Geografía e Informática. URL http://internet.contenidos.inegi.org.mx/contenidos/productos/prod_serv/contenidos/espanol/bvinegi/productos/historicos/181/702825934392/702825934392.pdf (accessed 2.9.22).

INEGI, 2008. Mazatlán estado de Sinaloa. Cuaderno estadístico municipal. Edición 2008. Instituto Nacional de Estadística, Geografía e Informática. URL https://www.inegi.org.mx/app/biblioteca/ficha.html?upc=702825937904 (accessed 5.9.22).

INEGI, 2022. Serie histórica censal e intercensal (1990-2010). URL https://www.inegi.org.mx/programas/ccpv/cpvsh/ (accessed 4.1.22).

La Jornada, 1998. Impacto de Isis en costas sinaloenses; los Cabos: zona de desastre. URL https://www.jornada.com.mx/1998/09/03/impacto.html (accessed 2.1.21).

Krauss, K.W., McKee, K.L., Lovelock, C.E., Cahoon, D.R., Saintilan, N., Reef, R., Chen, L., 2014. How mangrove forests adjust to rising sea level. New Phytologist 202, 19–34. https://doi.org/10.1111/nph.12605.

Krishnaswamy, S., Lal, D., Martin, J.M., Meybeck, M., 1971. Geochronology of lake sediments. Earth Planet Sci Lett 11, 407–414. https://doi.org/10.1016/0012-821X(71)90202-0.

Likens, G.E., Davis, M.B., 1975. Post-glacial history of Mirror Lake and its watershed in New Hampshire, U. S. A.: an initial report. SIL Proceedings, 1922-2010 19, 982–993. https://doi.org/10.1080/03680770.1974.11896148.

Lynch, J.C., Meriwether, J.R., Mckee, B.A., Vera-Herrera, F., Twilley, R.R., 1989. Recent accretion in mangrove ecosystems based on ^{137}Cs and ^{210}Pb. Estuaries 12, 284–299.

Mayfield, M., 1995. Preliminary Report. Hurricane Ismael. 12-15 September 1995. National Hurricane Center. URL https://web.archive.org/web/20090831170642/http://www.nhc.noaa.gov/1995ismael.html (accessed 3.28.22).

Mazda, Y., Magi, M., Ikeda, Y., Kurokawa, T., Asano, T., 2006. Wave reduction in a mangrove forest dominated by Sonneratia sp. Wetl Ecol Manag 14, 365–378. https://doi.org/10.1007/s11273-005-5388-0.

McKee, K.L., 2011. Biophysical controls on accretion and elevation change in Caribbean mangrove ecosystems. Estuar Coast Shelf Sci 91, 475–483. https://doi.org/10.1016/j.ecss.2010.05.001.

Mckee, K.L., Cahoon, D.R., Feller, I.C., 2007. Caribbean mangroves adjust to rising sea level through biotic controls on change in soil elevation. Glob Ecol Biogeogr 16, 545–556. https://doi.org/10.1111/j.1466-8238.2007.00317.x.

Mobilian, C., Craft, C.B., 2022. Wetland Soils: Physical and Chemical Properties and Biogeochemical Processes. In: Mehner, T., Tockner, K. (Eds.), Encyclopedia of Inland Waters, Second ed. Elsevier, Oxford, pp. 157–168. https://doi.org/10.1016/B978-0-12-819166-8.00049-9.

Mohamed, K.J., Andrade, A., Rey, D., Rubio, B., Bernabeu, A.M., 2017. A kinetic model to explain the grain size and organic matter content dependence of magnetic susceptibility in transitional marine environments: A case study in Ria de Muros (NW Iberia). Geochem. Geophys. Geosyst. 18 (6), 2200–2215.

Monjardín-Armenta, S.A., Pacheco-Angulo, C.E., Plata-Rocha, W., Corrales-Barraza, G., 2017. La deforestación and sus factores causales en el estado de Sinaloa, México. Madera Bosques 23, 7–22. https://doi.org/10.21829/myb.2017.2311482.

Nyman, J.A., Walters, R.J., Delaune, R.D., Patrick, W.H., 2006. Marsh vertical accretion via vegetative growth. Estuar Coast Shelf Sci 69, 370–380. https://doi.org/10.1016/j.ecss.2006.05.041.

Ochoa, E.P., 2003. Ficha Informativa de los Humedales de Ramsar (FIR) 1–17. URL https://rsis.ramsar.org/RISapp/files/RISrep/MX1355RIS.pdf (accessed 2.12.22).

Padilla, L.S., De Sicilia, R.A., 2020. Transformaciones espaciales de la ciudad puerto de Mazatlán, México: 1980–2010. Boletín geográfico 42, 59–81.

Parkinson, R.W., DeLaune, R.D., White, J.R., 1994. Holocene sea-level rise and the fate of mangrove forests within the wider Caribbean region. J Coast Res 10, 1077–1086.

Pasch, R.J., Zelinsky, D.A., 2013. Hurricane Manuel. National Hurricane Center. Tropical Cyclone Report. EP132013, 1–23.

Pasch, R.J., 1999. Preliminary Report. Hurricane Isis. 1 - 3 September, 1998. URL https://web.archive.org/web/20060710223936/http://www.nhc.noaa.gov/1998isis.html (accessed 8.12.21).

Passos, T., Sanders, C.J., Barcellos, R., Penny, D., 2022. Assessment of the temporal retention of mercury and nutrient records within the mangrove sediments of a highly impacted estuary. Environ Res 206, 112569. https://doi.org/10.1016/j.envres.2021.112569.

Ramos-Miranda, J., Villalobos-Zapata, G.J., 2015. Aspectos socioambientales de la región de la laguna de Términos. Universidad Autónoma de Campeche, Campeche, p. 210.

Robbins, J.A., 1978. Geochemical and geophysical applications of radioactive lead. Biogeochemistry of Lead in the Environment 285–393.

Robbins, J.A., Edgington, D.N., Kemp, A.L.W., 1978. Comparative ^{210}Pb, ^{137}Cs, and Pollen Geochronologies of Sediments from Lakes Ontario and Erie. Quat Res 10, 256–278. https://doi.org/10.1016/0033-5894(78)90105-9.

Robbins, J.A., Holmes, C., Halley, R., Bothner, M., Shinn, E., Graney, J., Keeler, G., TenBrink, M., Orlandini, K.A., Rudnick, D., 2000. Time-averaged fluxes of lead and fallout radionuclides to sediments in Florida Bay. J Geophys Res Oceans 105, 28805–28821. https://doi.org/10.1029/1999jc000271.

Rogers, K., Saintilan, N., Heijnis, H., 2005. Mangrove encroachment of salt marsh in Western Port Bay, Victoria: The role of sedimentation, subsidence, and sea level rise. Estuaries 28, 551–559. https://doi.org/10.1007/BF02696066.

RSIS, 2020. Ramsar Sites Information Service. Playa Tortuguera El Verde Camacho. URL: https://rsis.ramsar.org/ris/1349 (accessed 25.5.22).

Ruiz-Fernández, A.C., Hillaire-Marcel, C., Ghaleb, B., Soto-Jiménez, M., Páez-Osuna, F., 2002. Recent sedimentary history of anthropogenic impacts on the Culiacan River Estuary, northwestern Mexico: geochemical evidence from organic matter and nutrients. Environ Pollut 118, 365–377. https://doi.org/10.1016/S0269-7491(01)00287-1.

Ruiz-Fernández, A.C., Hillaire-Marcel, C., de Vernal, A., Machain-Castillo, M.L., Vásquez, L., Ghaleb, B., Aspiazu-Fabián, J.A., Páez-Osuna, F., 2009. Changes of coastal sedimentation in the Gulf of Tehuantepec, South Pacific Mexico, over the last 100 years from short-lived radionuclide measurements. Estuar Coast Shelf Sci 82, 525–536. https://doi.org/10.1016/j.ecss.2009.02.019.

Ruiz-Fernández, A.C., Sánchez-Cabeza, J.A., Serrato de la Peña, J.L., Perez-Bernal, L.H., Cearreta, A., Flores-Verdugo, F.J., Machain-Castillo, M.L., Chamizo, E., García-Tenorio, R., Queralt, I., Dunbar, R.B., Mucciarone, D., Diaz-Asencio, M., 2016. Accretion rates in coastal wetlands of the southeastern Gulf of California and their relationship with sea-level rise. Holocene 26, 1126–1137. https://doi.org/10.1177/0959683616632882.

Ruiz-Fernández, A.C., Carnero-Bravo, V., Sánchez-Cabeza, J.A., Pérez-Bernal, L.H., Amaya-Monterrosa, O.A., Bojórquez-Sánchez, S., López-Mendoza, P.G., Cardoso-Mohedano, J.G., Dunbar, R.B., Mucciarone, D.A., Marmolejo-Rodríguez, A.J., 2018b. Carbon burial and storage in tropical salt marshes under the influence of sea level rise. Science of the Total Environment 630, 1628–1640. https://doi.org/10.1016/j.scitotenv.2018.02.246.

Ruiz-Fernández, A.C., Agraz-Hernández, C.M., Sanchez-Cabeza, J.A., Díaz-Asencio, M., Pérez-Bernal, L.H., Chan Keb, C.A., López-Mendoza, P.G., Blanco y Correa, J.M., Ontiveros-Cuadras, J.F., Osti Saenz, J., Reyes Castellanos, J.E., 2018a. Sediment Geochemistry, Accumulation Rates and Forest Structure in a Large Tropical Mangrove Ecosystem. Wetlands 38, 307–325. https://doi.org/10.1007/s13157-017-0969-2.

Ruiz-Fernández, A.C., Sánchez-Cabeza, J.A., Cuéllar-Martínez, T., Pérez-Bernal, L.H., Carnero-Bravo, V., Ávila, E., Cardoso-mohedano, J.G., 2020a. Increasing salinization and organic carbon burial rates in seagrass meadows from an anthropogenically-modified coastal lagoon in southern Gulf of Mexico. Estuar Coast Shelf Sci 242, 106843. https://doi.org/10.1016/j.ecss.2020.106843.

Ruiz-Fernández, A.C., Sánchez-Cabeza, J.A., Cuéllar-Martínez, T., Pérez-Bernal, L.H., Carnero-Bravo, V., Ávila, E., Cardoso-mohedano, J.G., Sanchez-Cabeza, J.A., Cuéllar-Martínez, T., Pérez-Bernal, L.H., Carnero-Bravo, V., Ávila, E., Cardoso-mohedano, J.G., 2020b. Increasing salinization and organic carbon burial rates in seagrass meadows from an anthropogenically-modified coastal lagoon in southern Gulf of Mexico. Estuar Coast Shelf Sci 242, 106843. https://doi.org/10.1016/j.ecss.2020.106843.

Sanchez-Cabeza, J.A., Ruiz-Fernández, A.C., 2012. ^{210}Pb sediment radiochronology: An integrated formulation and classification of dating models. Geochim Cosmochim Acta 82, 183–200. https://doi.org/10.1016/j.gca.2010.12.024.

Sanders, C.J., Smoak, J.M., Sathy-Naidu, A., Patchineelam, S.R., 2008. Recent sediment accumulation in a mangrove forest and its relevance to local sea-level rise (Ilha Grande, Brazil). J Coast Res 24, 533–536. https://doi.org/10.2112/07-0872.1.

Sanchez-Cabeza, J.A., Ruiz-Fernández, A.C., Ontiveros Cuadras, J.F., Pérez Bernal, L.H., Olid, C., 2014. Monte Carlo uncertainty calculation of ^{210}Pb chronologies and accumulation rates of sediments and peat bogs. Quat Geochronol 23, 80–93.

Sanders, C.J., Smoak, J.M., Naidu, A.S., Araripe, D.R., Sanders, L.M., Patchineelam, S.R., 2010. Mangrove forest sedimentation and its reference to sea level rise, Cananeia, Brazil. Environ Earth Sci 60, 1291–1301. https://doi.org/10.1007/s12665-009-0269-0.

Smith, T.J., Anderson, G.H., Balentine, K., Tiling, G., Ward, G.A., Whelan, K.R.T., 2009. Cumulative impacts of hurricanes on Florida mangrove ecosystems: Sediment deposition, storm surges and vegetation. Wetlands 29, 24–34. https://doi.org/10.1672/08-40.1.

Soto-Galera, E., Piera, J., López, P., 2010. Spatial and temporal land cover changes in Terminos Lagoon Reserve, Mexico. Rev Biol Trop 58, 565–575. https://doi.org/10.15517/rbt.v58i2.5229.

Stammer, D., Cazenave, A., Ponte, R.M., Tamisiea, M.E., 2013. Causes for Contemporary Regional Sea Level Changes. Ann Rev Mar Sci 5, 21–46. https://doi.org/10.1146/annurev-marine-121211-172406.

Stoner, J.S., St-Onge, G., 2007. Chapter Three Magnetic Stratigraphy in Paleoceanography: Reversals, Excursions, Paleointensity, and Secular Variation. Dev Mar Geol 1, 99–138. https://doi.org/10.1016/S1572-5480(07)01008-1.

Sumner, H.C., 1943. North Atlantic hurricanes and tropical disturbances of 1943. Monthly Weather Review.sumn. U.S. Weather Bureau. 71, 5.

Thampanya, U., Vermaat, J.E., Sinsakul, S., Panapitukkul, N., 2006. Coastal erosion and mangrove progradation of Southern Thailand. Estuar Coast Shelf Sci 68, 75–85. https://doi.org/10.1016/j.ecss.2006.01.011.

Thompson, R., Oldfield, F., 1986. Environmental Magnetism, Allen & Unwin. Springer, Netherlands, Dordrecht. https://doi.org/10.1007/978-94-011-8036-8.

Torres-Rodríguez, V., Márquez-García, A., Bolongaro-Crevenna, A., Chavarria-Hernández, J., Expósito-Díaz, G., Márquez-García, E., 2010. Tasa de erosión y vulnerabilidad costera en el estado de Campeche debidos a efectos del cambio climático. In: Botello, A.V., Villanueva-Fragoso, S., Gutiérrez, J., Rojas Galaviz, J.L. (Eds.), Vulnerabilidad de Las Zonas Costeras Mexicanas Ante El Cambio Climático. SEMARNAT-INE, UNAM-ICMyL. Universidad Autónoma de Campeche, Campeche, pp. 325–344.

Unscear, 2000. Sources and effects of ionizing radiation., in: United Nations Scientific Committee on the Effects of Atomic Radiation. Report to the General Assembly, with Scientific Annexes, 1, Annex C. United Nations, New York, p. 654.

van Santen, P., Augustinus, P.G.E.F., Janssen-Stelder, B.M., Quartel, S., Tri, N.H., 2007. Sedimentation in an estuarine mangrove system. J Asian Earth Sci 29, 566–575. https://doi.org/10.1016/j.jseaes.2006.05.011.

Villéger, S., Ramos-Miranda, J., Flores-Hernández, D., Mouillot, D., 2010. Contrasting changes in taxonomic vs. functional diversity of tropical fish communities after habitat degradation. Ecol Appl 20, 1512–1522. https://doi.org/10.1890/09-1310.1.

Woodroffe, S.A., Horton, B.P., Larcombe, P., Whittaker, J.E., 2005. Intertidal mangrove foraminifera from the central Great Barrier Reef Shelf, Australia: Implications for sea-level reconstruction. J Foraminifer Res 35, 259–270. https://doi.org/10.2113/35.3.259.

Yáñez-Arancibia, A., Day, J.W., 1982. Ecological characterization of Terminos Lagoon, a tropical lagoon-estuarine system in the southern Gulf of Mexico. Oceanol Acta 5, 431–440.

Zavala-Hidalgo, J., de Buen-Kalman, R., Romero-Centeno, R., Hernández-Maguey, F., 2010. Tendencias del nivel del mar en las costas mexicanas. In: Botello, A.V., Villanueva-Fragoso, S., Guitiérrez, J., Rojas Galaviz, J.L. (Eds.), Vulnerabilidad de la zonas costeras mexicanas ante el cambio climático. Semarnat-INE, UNAM-ICMyL, Universidad Autónoma de Campeche, Campeche, pp. 249–268.

Zavala-Hidalgo, J., Ochoa de la Torre, J.L., Sánchez-Cabeza, J.L., Machain-Castillo, M.L., Ruiz-Fernández, A.C., Hernández-Maguey, F., Santiago-Santiago, J.A., Gómez-Ramos, O., Zarza-Alvarado, M.A., Gutiérrez-Quijada, S.V., Kostoglodov, V., Ortiz-Figueroa, M., Blanchon, P.A., 2015. Cambios en el nivel del mar. In: Reporte Mexicano de Cambio Climático, Grupo I Bases Científicas. Mexicano de Cambio Climático, Grupo I Bases Científicas. Modelos y Modelación. Universidad Nacional Autónoma de México/Programa de Investigación en Cambio Climático, Cuidad de México, p. 57.

CHAPTER 3

SPATIAL AND TEMPORAL VARIABILITY OF ORGANIC CARBON SOURCE, BURIAL RATES, AND STOCKS

The third chapter focuses on evaluating the temporal variability of different aspects of C_{org} dynamics, such as provenance, concentration, burial rates, and stocks in the seven sediment cores from the LT and EV systems. To assess the contribution of C_{org} sources, the Bayesian mixing model MixSIAR (Stock and Semmens, 2016; Stock et al., 2018) was applied, incorporating the δ^{13} C_{org} and $\delta^{15}N$ values measured in the seven cores studied (mixing values) and the reference δ^{13} C_{org} and $\delta^{15}N$ data obtained from previous studies conducted at the study sites or their surroundings (source values). The main sources of C_{org} included: i) mangrove detritus, considered the primary source of in situ C_{org}; ii) terrestrial particulate organic matter transported by rivers; and iii) phytoplankton, as an indicator of marine-origin C_{org} (in the case of EV) or lagoon-origin C_{org} (in the case of PDE and CP). By integrating the mixing and source values, the MixSIAR model provided box plots of posterior density distributions, i.e., mean, standard deviation, and Bayesian credible intervals (5-95%) for each core and each decadal period (e.g., 0-10 years). To evaluate the capacity of mangroves as atmospheric CO_2 sinks and their role in climate change mitigation, C_{org} burial rates were calculated, representing the accumulation rate of C_{org}, as well as C_{org} stocks, which quantify the amount of C_{org} stored within the sediment that could be released as CO_2 emissions if mangrove sediments were disturbed. Equivalent CO_2 emissions were also calculated in the case of significant loss of the sedimentary C_{org} stock.

The main questions addressed were: (1) What are the primary sources of C_{org} accumulated in the sediment cores?; (2) How do the ranges of C_{org} burial rates and stocks compare between the study areas and other mangrove ecosystems around the world?; (3) Have changes in sediment and C_{org} sources influenced the temporal trends (~100 years) of C_{org} burial rates and stocks in the study sites? The research hypothesis proposed a general decrease in C_{org} concentration, burial rates, and stocks over the last century as a result of increased sediment inputs, land-use changes, and mangrove cover loss, which would favor the accumulation of allochthonous C_{org} over autochthonous C_{org}.

The novel contribution of this study is the use of one of the most recent Bayesian mixing models, MixSIAR, to evaluate the temporal variation of C_{org} sources (e.g., autochthonous vs. allochthonous) in sediment cores. This model provides more realistic predictions of the variability in source proportions compared to previous models and has not yet been fully utilized in blue carbon research. This work also explores the influence of local conditions (e.g., hydrology, precipitation, land-use change) on C_{org} fluxes in mangrove ecosystems and highlights the difficulty of considering global patterns to explain these flux dynamics on a regional or local scale. Finally, it emphasizes the importance of using reliable dating methods (e.g., ^{210}Pb) and comparable study periods (e.g., 1900-2000) to facilitate comparisons between sites around the world. The results and interpretations of this work were compiled into the article titled "Terrestrial inputs boost organic carbon accumulation in Mexican mangroves", which was published in open access in *Science of the Total Environment* in March 2024.

Science of the Total Environment 940 (2024) 173440

Contents lists available at ScienceDirect

Science of the Total Environment

journal homepage: www.elsevier.com/locate/scitotenv

Terrestrial inputs boost organic carbon accumulation in Mexican mangroves

J.L.J. Jupin [a,b], A.C. Ruiz-Fernández [c,*], A. Sifeddine [b], M. Mendez-Millan [b], J.A. Sanchez-Cabeza [c], L.H. Pérez-Bernal [c], J.G. Cardoso-Mohedano [d], M.A. Gómez-Ponce [d], J.G. Flores-Trujillo [e]

[a] Posgrado en Ciencias del Mar y Limnología, Universidad Nacional Autónoma de México, Av. Universidad 3000, Ciudad Universitaria, Coyoacán, 04510 Ciudad de México, Mexico
[b] IRD, CNRS, SU, MNHN, IPSL, LOCEAN, Laboratoire d'Océanographie et du Climat: Expérimentation et Approches Numériques Centre IRD France Nord, 93143 Bondy, France
[c] Unidad Académica Mazatlán, Instituto de Ciencias del Mar y Limnología, Universidad Nacional Autónoma de México, 82040 Mazatlán, Sin., Mexico
[d] Estación el Carmen, Instituto de Ciencias del Mar y Limnología, Universidad Nacional Autónoma de México, Carretera Carmen-Puerto Real km 9.5, 24157 Ciudad del Carmen, Campeche, Mexico
[e] Universidad Autónoma del Carmen, Calle 56 No. 4, Col. Benito Juárez, 24180 Cd. del Carmen, Camp., Mexico

HIGHLIGHTS

- Burial rates and stocks of mangrove sediment organic carbon (C_{org}) are reported.
- Highest C_{org} stocks was observed in sites with autochthonous-dominated C_{org}.
- Global C_{org} patterns do not fully explain the local C_{org} variability in study sites.
- Long-term rise in terrestrial C_{org} inputs led to higher C_{org} burial rates and stocks.
- Despite cover loss, mangroves areas remained effective C_{org} producers and sinks.

GRAPHICAL ABSTRACT

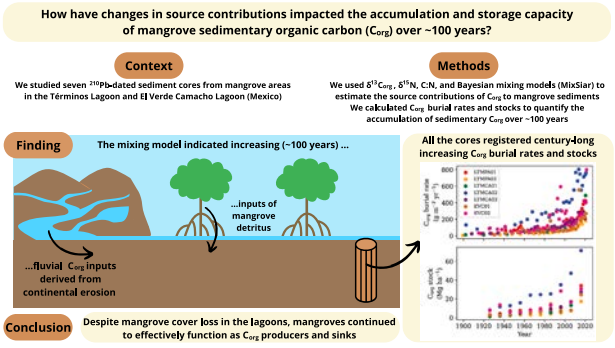

ARTICLE INFO

Editor: Jan Vymazal

Keywords:
Blue carbon
Burial rate
Stock
Mangroves

ABSTRACT

Despite their ability to mitigate climate change by efficiently absorbing atmospheric carbon dioxide (CO_2) and acting as natural long-term carbon sinks, mangrove ecosystems have faced several anthropogenic threats over the past century, resulting in a decline in the global mangrove cover. By using standardized methods and the most recent Bayesian tracer mixing models MixSIAR, this study aimed to quantify source contributions, burial rates, and stocks of organic carbon (C_{org}) and explore their temporal changes (~100 years) in seven lead-210 dated sediment cores collected from three contrasting Mexican mangrove areas. The spatial variation in C_{org} burial rates and stocks in these blue carbon ecosystems primarily depended on the influence of local rivers, which

* Corresponding author.
E-mail addresses: caro@ola.icmyl.unam.mx (A.C. Ruiz-Fernández), abdel.sifeddine@ird.fr (A. Sifeddine), mercedes.mendez@ird.fr (M. Mendez-Millan), jasanchez@cmarl.unam.mx (J.A. Sanchez-Cabeza), lbernal@ola.icmyl.unam.mx (L.H. Pérez-Bernal), gcardoso@cmarl.unam.mx (J.G. Cardoso-Mohedano), mgomez@cmarl.unam.mx (M.A. Gómez-Ponce), gflores@pampano.unacar.mx (J.G. Flores-Trujillo).

https://doi.org/10.1016/j.scitotenv.2024.173440
Received 26 February 2024; Received in revised form 29 April 2024; Accepted 20 May 2024
Available online 25 May 2024

^{210}Pb radiochronology
MixSIAR

controlled C_{org} sources and fluxes within the mangrove areas. The C_{org} burial rates in the cores ranged from 66 ± 16 to 400 ± 40 g m^{-2} yr^{-1}. The C_{org} stocks ranged from 84.9 ± 0.7 to 255 ± 2 Mg ha^{-1} at 50 cm depth and from 137 ± 2 to 241 ± 4 Mg ha^{-1} at 1 m depth. The highest C_{org} burial rates and stocks were observed in cores from the carbonate platform of Yucatan and in cores with reduced river influence and high mangrove detritus inputs, in contrast to patterns identified from global databases. Over the past century, the rising trends in C_{org} burial rates and stocks in the study sites were primarily driven by enhanced inputs of fluvial-derived C_{org} and, in some cores, mangrove-derived C_{org}. Despite their decreasing extension, mangrove areas remained highly effective producers and sinks of C_{org}. Ongoing efforts to enhance the global database should continue, including mangrove area characteristics and reliable timescales to facilitate cross-comparison among studies.

1. Introduction

Despite the multiple benefits provided by mangroves (Blankespoor et al., 2017; Primavera et al., 2019b), the world's mangrove cover has declined due to land-use changes, particularly the conversion of mangroves to aquaculture and agriculture areas (Goldberg et al., 2020; Valiela et al., 2001). Thanks to the implementation of conservation policies, the worldwide rate of mangrove cover loss is now lower than in the past (i.e., >2 % in 1980–2005, FAO, 2007; 0.16–0.39 % in 2000–2012, Hamilton and Casey, 2016). Nevertheless, the loss rates vary among countries (e.g., 0.7 % in Myanmar, 0.08 % in Mexico, and 0.03 % in Australia between 2000 and 2012; Hamilton and Casey, 2016) due to differences in mangrove management policies and regulations, economic conditions, and demography (Primavera et al., 2019a). In addition, the loss rates do not provide information about the conservation status of the remaining forests nor the magnitude of potential loss in ecosystem services and carbon storage.

The extent of ecosystem service loss resulting from mangrove cover loss varies depending on the type of mangrove and the hydrologic and biogeographic characteristics of the region. Furthermore, a large fraction of sedimentary organic carbon (C_{org}) stocks in degraded mangrove ecosystems may be oxidized to carbon dioxide (CO_2) and released into the atmosphere, contributing to global warming (Hamilton and Friess, 2018; Kauffman et al., 2014). Therefore, the conservation and restoration of mangroves are significant and low-cost strategies for climate change mitigation to reduce atmospheric CO_2 (Murdiyarso et al., 2015; Pendleton et al., 2012), needed to keep global warming under 2 °C by 2050 (UN, 2015).

The study of C_{org} burial rates and stocks is essential for conducting comprehensive assessments of actual and past C_{org} storage in mangroves. The wide ranges of C_{org} stocks (72–936 Mg ha^{-1}; Atwood et al., 2017) and C_{org} burial rates (2.3–1750 g m^{-2} yr^{-1}; Breithaupt and Steinmuller, 2022) in mangrove ecosystems worldwide result from the strong spatial and temporal heterogeneity of processes (e.g., climate,

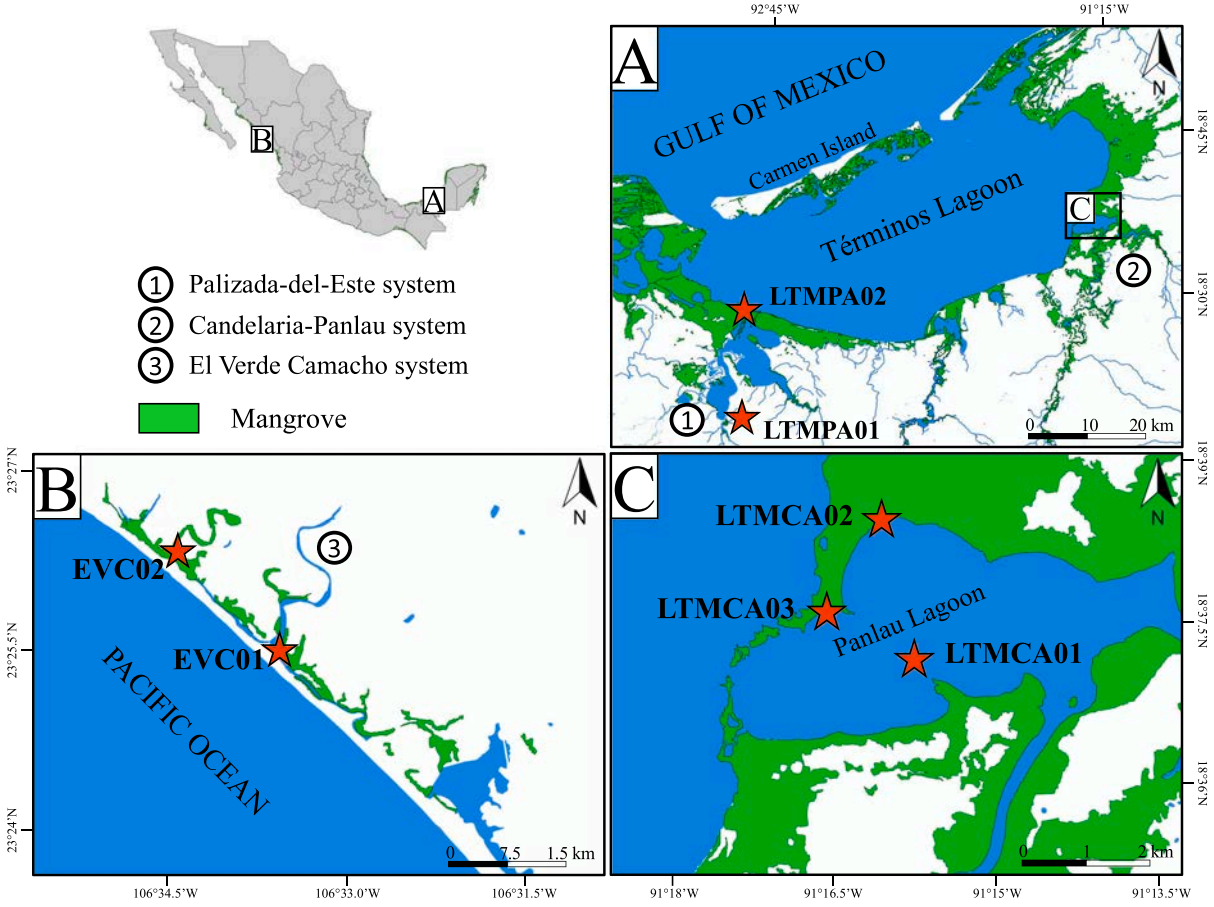

Fig. 1. Location of the seven sediment cores (★) collected in Términos Lagoon (southern Gulf of Mexico) and El Verde Camacho Lagoon (entrance of the Gulf of California).

hydrology, sedimentary and geomorphic settings) that influence C_{org} accumulation and degradation, and therefore complicate the understanding of C_{org} dynamics and their implications at regional and global scales (Breithaupt and Steinmuller, 2022; Rosentreter et al., 2018). Uncertainty persists regarding mangrove responses to climate-induced factors (e.g., droughts, floods, hurricanes) and anthropogenic interventions (e.g., land-use changes, deforestation), with impacts spatially nonuniform worldwide (Macreadie et al., 2019).

The stable isotopic composition of carbon ($\delta^{13}C$) and nitrogen ($\delta^{15}N$) and the C:N ratio are valuable indicators for discerning the origin of C_{org} stored in mangrove sediments (e.g., Bouillon et al., 2003, 2008; Kusumaningtyas et al., 2019), which enable the interpretation of the variability of C_{org} accumulation and the effectiveness of C_{org} storage. Unlike linear mixing models, which use a fixed isotopic composition for each source, Bayesian tracer mixing models account for the potential variability within isotopic composition data (i.e., mixtures and sources) and effectively propagates the associated uncertainties, resulting in more realistic predictions within the estimated likelihood (Stock and Semmens, 2016a). The Bayesian mixing model MixSIAR is the most recent advancement among mixing models. It builds upon years of investigation on mixing models, incorporating features from previous models, such as MixSIR (Moore and Semmens, 2008) and SIAR (Parnell et al., 2013, 2010), and introducing novel user-specified parameters (e.g., a priori information, categorical and continuous covariates) to improve accuracy and reliability in estimating source-to-mixture proportions (Stock et al., 2018). It has been successfully employed to investigate food webs and trophic structures (e.g., Soria-Barreto et al., 2021) and carbon sourcing in river catchments (e.g., Menges et al., 2020). In mangrove sediments, carbon sources may exhibit notable spatial and temporal variations (e.g., Gonneea et al., 2004), however the flexibility and repeatability of MixSIAR enables the exploration of most realistic predictions by creating a framework of different Bayesian mixing models and incorporating customizable options.

In a previous study, Jupin et al. (2023) assessed the temporal trends of sediment accumulation rates over the past century in seven lead-210 (^{210}Pb) dated sediment cores collected in mangrove areas in two contrasting coastal lagoons of Términos Lagoon (TL) in the southern Gulf of Mexico and El Verde Camacho Lagoon (EV) in the entrance of the Gulf of California. The study lagoons exhibited contrasting characteristics, as TL experienced higher rainfall rates, river discharges, and economic development than EV. Consistent exponential trends in mass accumulation rates (MAR) toward the present were observed across all cores, with an acceleration noted since the 1950s. These trends were attributed to continental soil erosion induced by land-use change and sea-level rise.

The present study, based on the ^{210}Pb-derived chronology previously established for the seven sediment cores from TL and EV mangroves, provides new insights on changes in source contributions, burial rates, and stocks of sedimentary C_{org} over the past century, by using Bayesian tracer mixing model MixSIAR and standardized methods. The main questions addressed in this study were: i) how do the ranges of C_{org} burial rates and stocks in the study areas compare to each other and with other mangrove ecosystems worldwide? ii) have changes in sediment and C_{org} sources influenced the temporal trends (~100 years) of C_{org} burial rates and stocks in the study sites? Over the past century, an overall decline in C_{org} concentration, burial rates, and stocks was hypothesized as a result of increasing land-use changes, mangrove cover loss, and sediment inputs, which would favor the accumulation of allochthonous C_{org}.

2. Study sites

2.1. Términos Lagoon

Términos Lagoon (TL), in the southern Gulf of Mexico, is Mexico's most extensive coastal lagoon (Yáñez-Arancibia and Day, 1982;

Table 1
Main characteristics of the study sites in the southern Gulf of Mexico and the entrance of the Gulf of California.

Characteristics	Palizada-del-Este	Candelaria-Panlau	El Verde Camacho	Reference
Sedimentary setting[a]	Terrigenous	Carbonate	Terrigenous	Ortiz-Pérez and de la Lanza-Espino (2006); Rendón-Von Osten et al. (2006); Medina-Gómez et al. (2015)
Geomorphic class	Fluvial-Lagoon	Fluvial-Lagoon	Lagoon	
Climate regime (type)	Warm, humid (Am (f))	Warm, sub-humid (Aw2 (w))	Very warm, semiarid (BW(h')w (e))	García (1973); Briseño-Dueñas (2003); Ochoa (2003); CONAGUA (2015); Ramos-Miranda and Villalobos-Zapata (2015)
Mean annual precipitation (mm yr^{-1})	1750	1400	750	
Mean annual temperature (°C)	27	27	25	
Mean annual salinity	4	15	14	
River name	Palizada	Candelaria + Mamantel	Quelite	Bach et al. (2005); Fichez et al. (2017)
Annual mean discharge (10^9 m^3 yr^{-1})	9.1	1.6 + 0.16	0.11	
Basin (km^2)	40,000	7160 + 520	835	
Annual mangrove loss (ha yr^{-1})[b]	60	16	1	CONABIO (2013, 2021)
Total mangrove loss (%)[b]	21	9	27	

[a] Sedimentary settings were defined based on Breithaupt and Steinmuller (2022). Terrigenous settings indicate externally sourced sediments; carbonate settings indicate locally formed sediments through calcareous processes.
[b] Mangrove loss was estimated over the 1970–2020 period based on CONABIO (2013, 2021).

Contreras-Ruiz-Esparza et al., 2014). It is characterized by a permanent water exchange with the Gulf of Mexico via the inlets on opposite sides of Carmen Island (Fig. 1). The Palizada-del-Este (PDE) in the western zone and the Candelaria-Panlau (CP) in the eastern zone of TL were previously defined as fluvial-lagoon subsystems (e.g., Rendón-Von Osten et al., 2006; Medina-Gómez et al., 2015). Details regarding the main geological, climatic, and hydrologic characteristics of PDE and CP are detailed in Table 1. TL has experienced significant land-use changes due to the population growth of El Carmen Municipality, mainly driven by shrimp and oil industries since the 1950s and 1970s, respectively. The construction of canal networks, pipelines, and roads has negatively impacted wetland areas, particularly the PDE system (Ochoa, 2003). In the basins of the main rivers that discharge into TL, the gradual conversion of wetlands and primary forests into urban and agricultural zones accounted for a forest cover loss of ~31 % between 1974 and 2001 (Cotler-Ávalos, 2010; Soto-Galera et al., 2010).

Previous studies about C_{org} accumulation in TL mangrove sediments include C_{org} burial rates in channels at southeastern Carmen Island (53 and 65 g m^{-2} yr^{-1}, Gonneea et al., 2004) and C_{org} stocks in the southeast of Carmen Island (12–222 Mg ha^{-1}, Cerón-Bretón et al., 2011) and in the Pom-Atasta System northwest of TL (80–236 Mg ha^{-1}, Guerra-Santos et al., 2014). However, C_{org} stocks were obtained from undated sediment cores (30 or 60 cm long), so they were likely not formed during comparable periods. Presently, studies examining C_{org} sources, burial rates, and stocks in mangrove areas of TL and its subsystems are scarce, especially using ^{210}Pb-dated sediment cores.

2.2. El Verde Camacho Lagoon

El Verde Camacho Lagoon (EV) is a 47 ha internal coastal barrier lagoon (Fig. 1, Table 1). It receives marine water inputs during the rainy season (June to October) when the sandbar breaks due to the higher elevation of tides, the larger Quelite River discharge, and occasional tropical storms and hurricanes (Flores-Verdugo et al., 1995). The beach and wetlands in EV are relatively well preserved; however, native vegetation loss has been promoted by the development of tourism, aquaculture facilities, and human settlements in the Mazatlán municipality (Briseño-Dueñas, 2003). The mean annual deforestation rate in Mazatlán was estimated at 0.36 % between 1993 and 2011 (Monjardín-Armenta et al., 2017). During the dry season, ~90 % of C_{org} inputs to the EV come from mangrove leaf defoliation, whereas during the rainy season, C_{org} is exported to the ocean through the Quelite River and tidal currents (Flores-Verdugo et al., 1995, 1987; González-Farías and Mee, 1988). To our knowledge, there are no previous investigations on sedimentary C_{org} burial rates and stocks in EV mangroves.

3. Methods

3.1. Sampling, dating, and analysis

3.1.1. Core sampling and sediment dating

Sampling and ^{210}Pb dating of the cores are detailed in Jupin et al. (2023). Briefly, sampling sites were selected by analyzing mangrove distribution in the study areas using aerial photographs and satellite images (CONABIO, 2021, 2013) to identify unchanged mangrove areas over the past 50 years. Two sediment cores were to be retrieved at each study site to guarantee duplicate samples and high-quality data. However, the presence of fine roots at one sampling site within the CP system prompted the collection of an additional core from a third sample site to ensure accurate ^{210}Pb dating of the cores. Ultimately, a total of seven sediment push cores (PVC tubes of 10 cm internal diameter, 1 m length) were collected in 2021 in undisturbed flat areas within fringe mangrove communities with similar topographic features and species composition for site comparison (Table 2). All cores yielded positive results upon processing, enabling the valuable reconstruction of local variations in C_{org} burial rates and stocks, especially in regions where data are notably scarce and absent from the global database. The cores were extruded and sectioned at 1 cm intervals, and the samples were lyophilized and ground to powder with porcelain mortar and pestle (except those for grain size analysis). Analytical results are expressed on a dry weight basis.

For core dating, ^{210}Pb, ^{226}Ra, and ^{137}Cs activities were determined by low background gamma-spectrometry as described in Díaz-Asencio et al. (2020). The Constant Flux (CF) model, which assumed a constant flux of atmospheric ^{210}Pb to the sediment surface, was used to obtain the age models and the mass accumulation rates (MAR; g cm^{-2} yr^{-1}) of the cores (Sanchez-Cabeza and Ruiz-Fernández, 2012). Dating uncertainties were estimated using Monte Carlo simulation with 30,000 iterations (Sanchez-Cabeza et al., 2014). To strengthen confidence in the ^{210}Pb chronologies, ages derived from CF model were cross-compared to those generated by Bayesian ^{210}Pb age-depth using the package rPlum (Blaauw et al., 2021). The maximum of ^{137}Cs activities and the identification of meteorological events were used to corroborate the ^{210}Pb chronologies in the sediment cores.

3.1.2. Element and isotopic composition

Concentrations of organic carbon (C_{org}) and total nitrogen (N) and isotopic composition of C ($\delta^{13}C$) and N ($\delta^{15}N$) were measured with an Elemental Analyzer Flash 2000 HT coupled to an Isotope Ratio Mass Spectrometer Delta V Advantage (EA-IRMS) from Thermo Fisher Scientific. For C_{org} and $\delta^{13}C$ determination, carbonates were removed from bulk sediment using HCl (10 %) before analyses. N and $\delta^{15}N$ were determined on bulk sediments. Isotope ratios were reported in the conventional delta (δ in ‰) notation relative to Pee Dee Belemnite (PDB) carbonate standard and atmospheric N_2 (air), respectively.

Table 2
Sampling data of mangrove sediment cores from Términos Lagoon (southern Gulf of Mexico) and El Verde Camacho Lagoon (entrance of the Gulf of California).

System	Core collection date	Core name	Length (cm)	Coordinates (latitude N; longitude W)	Dominant mangrove species	Age (dated period)	MAR (g cm^{-2} yr^{-1})
Términos Lagoon							
PDE	2021-02-11	LTMPA01	69	18°20.3319; 91°47.7541	Rm	102 (1918–2020)	0.25 ± 0.03
		LTMPA02	47	18°29.0131; 91°47.7362	Rm; Ag; Lr	120 (1900–2020)	0.27 ± 0.01
CP	2021-02-12	LTMCA01	66	18°37.1903; 91°16.0722	Rm; Ag; Lr	118 (1902–2020)	0.24 ± 0.01
		LTMCA02	64	18°38.4186; 91°16.3408	Rm; Lr	117 (1903–2020)	0.14 ± 0.01
		LTMCA03	76	18°37.6450; 91°16.7640	Rm; Lr	112 (1908–2020)	0.20 ± 0.07
El Verde Camacho Lagoon							
EV	2021-07-06	EVC01	65	23°42.384; 106°55.820	Rm; Lr	90 (1931–2021)	0.43 ± 0.20[a]
		EVC02	69	23°43.893; 106°57.387	Rm	118 (1903–2021)	0.43 ± 0.08[a]

PDE: Palizada-del-Este; CP: Candelaria-Panlau; EV: El Verde Camacho.
Rm: *Rhyzophora mangle*; Lr: *Laguncularia racemose*; Ag: *Avicennia germinans*.
[a] Mass accumulation rates (MAR) were calculated excluding maxima attributed to meteorological events. See the text for an explanation.

Element composition (Al, Ca, Ti, Na) was determined using an Inductively Coupled Plasma – Mass Spectrometer (ICP-MS) Agilent 7500 cx, for which aliquots of ~25 mg of sediments were previously acid-digested (2 mL HF 40 % Normapure, 1 mL $HClO_4$ 70–72 % Merck, 2 mL HNO_3 65 % Normapure) on a hot-plate (150 °C for six days) (Carter et al., 2015). The annual fluxes of Al and Ca were calculated by multiplying their respective element concentrations by ^{210}Pb-derived MAR. They served as indicators of terrestrial inputs originating from river basins with terrigenous (PDE and EV) and carbonate (CP) settings (Table 1). The Al/Ti ratios were used to discern variations in mineralogical composition or input sources within the sediment cores and the Na/Al ratios were used as a proxy for assessing marine influence and paleosalinity (Croudace and Rothwell, 2015).

3.1.3. Quality control and quality assurance

Analysis of certified reference materials provided results within the reported range of the recommended values, including IAEA-384 for gamma-ray spectrometry, MESS-3 for trace elemental analysis, and HOS for EA-IRMS. The analytical precision was determined through the coefficient of variation (CV (%) = standard deviation/mean value × 100) from replicate analysis of a single sample ($n = 6$); CVs were <5 % for ^{210}Pb, ^{137}Cs, and elemental determination, and <0.35 % for δ^{13}C and δ^{15}N.

3.2. Data treatment

3.2.1. Mixing model setup for organic carbon sources

The fractions of different sources contributing to sedimentary C_{org} in the cores were estimated using the Bayesian isotope mixing model MixSIAR (Stock and Semmens, 2016a; Stock et al., 2018). The mixture data were the δ^{13}C and δ^{15}N values ($n = 327$) from the seven study cores (Fig. 2). Reference δ^{13}C and δ^{15}N values for the main sources were obtained from previous studies (Table S1, in Supplementary Material) in the study sites or their vicinity. The reference source values were averaged, and the means, along with their standard deviations (mean ± SD), were utilized in the mixing model (Stock and Semmens, 2016b). Primary sources included: i) mangrove detritus, mainly composed of mangrove leaves, and considered the primary in situ C_{org} source; ii) particulate organic matter of terrestrial origin transported by rivers; and iii) phytoplankton, as an indicator of marine-derived C_{org} for EV and C_{org} originating from the TL for PDE and CP.

Assumptions of the model included that all sources were known and quantified, mixture data were conserved through the mixing process and mixture and source values were fixed (Stock and Semmens, 2016b; Stock et al., 2018). The MixSIAR parameters can include a discrimination factor to address variation between values found in the mixture and those from the sources. In this study, this factor was considered as negligible and defined as '0' in the models, on the assumptions that diagenesis had a limited impact on the stable isotope composition of carbon and nitrogen (Cifuentes et al., 1996; Kusumaningtyas et al., 2019; Meyers, 1997) and mixing values found in sediments cores, representing different ages, were comparable to contemporary published source values (Douglas et al., 2022; Menges et al., 2020). Those assumptions were supported by the minimal differences observed in δ^{13}C and δ^{15}N values between preserved mangrove leaves and detritus from published values (Gonneea et al., 2004; Medina-Contreras et al., 2023; Sepúlveda-Lozada et al., 2017, 2015). The model setup included as categorical factors the core name per site and decadal periods (e.g., 0–10 years). Sections older than 100 years were categorized as ">100 years". The prior was defined as an "uninformative" prior with $\alpha = c(1,1,1)$ to indicate equal weighting for each source without any prior information influencing the model. MixSIAR models were executed using Markov Chain Monte Carlo (MCMC). Results were summarized as boxplots of the posterior density distributions, i.e., mean, standard deviation, and Bayesian 5–95 % credible intervals of each categorical factor.

C_{org} sources in mangrove sediments may vary spatially and temporally (Adame and Fry, 2016; Gonneea et al., 2004). A comprehensive literature review was conducted to identify studies providing source values that best represented the study sites and addressed minor uncertainty. The utilization of local or regional reference values from published data, while occasionally limited for certain sites, proved effective in minimizing uncertainty and enhancing consistency in mixing models compared to global means. To guarantee accurate estimation of the posterior distributions, a MCMC run (selected as "long" within the software) consisting of 300,000 iterations was executed. The model convergence was assessed through the Gelman-Rubin and Geweke tests (for more detail, see Stock and Semmens, 2016b). Changes in C_{org} sources were further associated with temporal variability of additional indicators, such as the C:N ratio, elemental composition, and environmental data (e.g., precipitation, river discharge, and land-use change).

3.2.2. Organic carbon burial rates and stocks

C_{org} burial rates (g m^{-2} yr^{-1}) were calculated as the product of C_{org} concentrations and ^{210}Pb-derived MAR at each core section (Ruiz-Fernández et al., 2018b). MAR maxima in EV cores were attributed to meteorological events (Jupin et al., 2023) and excluded from the calculations. C_{org} stocks (Mg ha^{-1}), which represent the current amount of C_{org} stored within the sediment that might be released as CO_2 emissions if mangrove sediments were disturbed, were calculated as the sum, from the core surface to the bottom, of the product of the concentration of C_{org}, the dry bulk density, and the thickness of each section (Howard et al., 2014). For comparison purposes, C_{org} stocks in all cores were calculated up to 50 cm depth (C_{org} $stock_{-50cm}$). For sediment cores displaying constant C_{org} concentrations in their bottom sections (i.e., LTMPA02, LTMCA03, EVC01, Fig. 3), suggesting negligible C_{org} degradation over time, C_{org} stocks were extrapolated to 1 m depth (C_{org} $stock_{-1m}$) by extending the known average C_{org} stock from the bottom sections up to the depth of 1 m, assuming uniformity of C_{org} stocks in the intervening layers (Ruiz-Fernández et al., 2018a). The resulting values of C_{org} $stock_{-1m}$ were compared with the global database (Atwood et al., 2017), exclusively considering information from countries with available field data (i.e., excluding country estimations derived from calculations based on the global mean C_{org} $stock_{-1m}$). The temporal variation of C_{org} stocks was calculated per decade ($stock_{-10yr}$), century (C_{org} $stock_{-100yr}$), as well as for the periods 1900–1950 (C_{org} $stock_{-1900\text{-}1950}$) and 1950 to sampling date (C_{org} $stock_{-1950\text{-}2021}$).

The CO_2 equivalent (CO_{2eq}, in Mg ha^{-1}) emissions, in case of significant C_{org} stock loss, were calculated by multiplying the C_{org} stocks (at 50 cm or 1 m) by the conversion factor 3.67 (i.e., the ratio of C to CO_2 molecular weights) (Howard et al., 2014). Potential annual CO_{2eq} emissions from mangrove losses were estimated by multiplying the mean CO_{2eq} per site by the mean yearly mangrove habitat loss calculated for 1970–2020 (CONABIO, 2013, 2021). The uncertainties of C_{org} stocks, burial rates, and CO_{2eq} emissions were estimated by quadratic uncertainty propagation (Cuellar-Martinez et al., 2019). The uncertainties of C_{org} stocks by depth (1–6 %) were low owing to the precision of the C_{org} measurements, whereas the larger uncertainties in 10 years-C_{org} stocks (7–32 %) were primarily caused by the MAR uncertainties, associated with the dating computation.

3.3. Statistical analysis

The Shapiro-Wilk test confirmed that the variables in the dataset were not normally distributed. The distribution of variable ranks among cores was compared using the non-parametric Kruskal-Wallis one-way analysis of variance (ANOVA) and the post-hoc Dunn test. Associations between variables were assessed through a Spearman correlation analysis followed by a Student's *t*-test. All tests were performed at a 95 % confidence level.

Table 3
Elemental concentration and isotopic composition of C and N, C:N ratio, and burial rates in mangrove sediment cores from Términos Lagoon (southern Gulf of Mexico) and El Verde Camacho Lagoon (entrance of the Gulf of California).

Core	Statistics	C_{org} (%)	N (%)	$\delta^{13}C$ (‰)	$\delta^{15}N$ (‰)	C:N ratio	C_{org} burial rate (g m^{-2} yr^{-1})
Términos	Lagoon						
LTMPA01	Min	1.69 ± 0.02	0.112 ± 0.002	−29.94 ± 0.06	3.7 ± 0.1	14.6 ± 0.3	25 ± 13
	Max	10.8 ± 0.1	0.540 ± 0.010	−26.98 ± 0.06	5.1 ± 0.1	29.4 ± 0.9	430 ± 170
	Mean	3.90 ± 0.05	0.222 ± 0.004	−28.09 ± 0.06	4.3 ± 0.1	19.3 ± 0.4	140 ± 65
LTMPA02	Min	0.97 ± 0.03	0.078 ± 0.002	−28.4 ± 0.1	4.3 ± 0.1	12.5 ± 0.4	4 ± 2
	Max	4.66 ± 0.04	0.275 ± 0.003	−26.4 ± 0.1	6.3 ± 0.2	22.9 ± 0.5	210 ± 30
	Mean	1.91 ± 0.03	0.154 ± 0.002	−27.0 ± 0.1	5.2 ± 0.2	15.7 ± 0.5	66 ± 16
LTMCA01	Min	1.50 ± 0.03	0.109 ± 0.001	−27.9 ± 0.1	4.2 ± 0.3	13.6 ± 0.4	11 ± 5
	Max	14.3 ± 0.1	0.531 ± 0.007	−25.9 ± 0.1	6.5 ± 0.3	35.8 ± 0.8	490 ± 50
	Mean	3.13 ± 0.04	0.211 ± 0.004	−26.7 ± 0.1	5.2 ± 0.3	20.0 ± 0.5	110 ± 23
LTMCA02	Min	12.20 ± 0.2	0.386 ± 0.006	−29.6 ± 0.1	1.6 ± 0.3	18.9 ± 0.6	81 ± 16
	Max	32.0 ± 0.5	1.570 ± 0.020	−26.1 ± 0.1	2.7 ± 0.3	69.0 ± 2.0	800 ± 84
	Mean	24.6 ± 0.4	1.090 ± 0.020	−28.5 ± 0.1	2.2 ± 0.3	26.5 ± 0.8	400 ± 40
LTMCA03	Min	2.53 ± 0.04	0.163 ± 0.005	−27.7 ± 0.1	4.03 ± 0.05	8.9 ± 0.3	24 ± 13
	Max	11.7 ± 0.7	0.690 ± 0.020	−25.90 ± 0.06	6.44 ± 0.05	26.0 ± 1.0	290 ± 30
	Mean	4.4 ± 0.3	0.315 ± 0.009	−26.72 ± 0.08	5.0 ± 0.3	14.0 ± 1.0	120 ± 24
El Verde	Camacho	Lagoon					
EVC01	Min	0.65 ± 0.04	0.032 ± 0.001	−26.51 ± 0.03	6.2 ± 0.1	10.9 ± 0.3	12 ± 13
	Max	4.56 ± 0.05	0.244 ± 0.005	−23.94 ± 0.03	9.3 ± 0.2	25.0 ± 2.0	270 ± 160[a]
	Mean	1.53 ± 0.04	0.010 ± 0.002	−24.9 ± 0.1	8.0 ± 0.1	17.5 ± 0.9	86 ± 95[a]
EVC02	Min	1.63 ± 0.07	0.100 ± 0.004	−27.59 ± 0.03	2.9 ± 0.3	14.8 ± 0.6	33 ± 22
	Max	8.90 ± 0.07	0.396 ± 0.007	−24.8 ± 0.2	7.5 ± 0.3	26.0 ± 1.0	800 ± 240[a]
	Mean	3.17 ± 0.05	0.190 ± 0.005	−25.8 ± 0.1	6.0 ± 0.3	19.4 ± 0.8	190 ± 30[a]

C_{org}: organic carbon; N: total nitrogen; Min: minimum; Max: maximum.
[a] C_{org} burial rates were calculated excluding maxima of mass accumulation rates attributed to meteorological events. See the text for an explanation.

4. Results

4.1. Organic carbon and total nitrogen concentration and trends

The C_{org} and N concentrations were highest ($p < 0.05$) in core LTMCA02 and lowest in LTMPA02, but comparable among the rest of the TL cores (LTMCA02 > LTMCA01 = LTMCA03 = LTMPA01 > LTMPA02; Table 3). In EV, EVC02 C_{org} concentrations were higher ($p < 0.05$) than in EVC01. Significant correlations ($p < 0.05$) between C_{org} and N concentrations ($r > 0.90$ in PDE; $r > 0.86$ in CP; $r > 0.90$ in EV) were observed in the sediment cores, indicating that N content in the sediment was predominantly originated from organic sources. C_{org} and N concentrations gradually increased from the oldest sections to the present (Fig. 3).

4.2. Organic carbon sources

4.2.1. C:N ratios and C_{org} and N isotope composition

In TL, C:N ratios and $\delta^{13}C$ and $\delta^{15}N$ values were highest ($p < 0.05$) in LTMCA02 and lowest in LTMPA02, but comparable in the other cores LTMCA01, LTMPA01, and LTMCA03 (Table 3). In EV, the cores EVC02 and EVC01 had comparable C:N ratios but different $\delta^{13}C$ and $\delta^{15}N$ (EVC01 > EVC02). The C:N ratios in all cores generally decreased from the older sections to the last few decades, followed by an increase observed in the period 2000–2021 (Fig. 3). In the TL cores, $\delta^{13}C$ values generally decreased toward the most recent sections, whereas $\delta^{15}N$ profiles showed high variability. In EV cores, $\delta^{13}C$ and $\delta^{15}N$ values increased from older sections to the early 2000s and then decreased to the present time.

Table 4
Storage and source contributions of organic carbon in mangrove sediment cores from Términos Lagoon (southern Gulf of Mexico) and El Verde Camacho Lagoon (entrance of the Gulf of California).

Core	Stock (Mg ha^{-1})						Mean contribution of C_{org} sources (%)		
		Over the 1900–1950 period	Over the 1950–2021 period	Over the past 100 years	To 50 cm depth	Extrapolated to 1 m depth	Mangrove detritus	Fluvial	Phytoplankton
Términos	Lagoon								
LTMPA01	C_{org}	19 ± 3	92 ± 3	105 ± 1	131 ± 1	na	55	32	13
	CO_{2eq}	72 ± 9	337 ± 11	385 ± 4	478 ± 3	na			
LTMPA02	C_{org}	6.4 ± 0.3	43 ± 1	47.8 ± 0.5	85 ± 1	137 ± 2	19	64	17
	CO_{2eq}	24 ± 1	158 ± 2	176 ± 2	311 ± 2	501 ± 6			
LTMCA01	C_{org}	8.0 ± 0.5	69 ± 1	74.2 ± 0.9	106 ± 1	na	14	71	15
	CO_{2eq}	29 ± 2	251 ± 4	272 ± 3	387 ± 3	na			
LTMCA02	C_{org}	50 ± 1	254 ± 1	276.1 ± 0.9	255 ± 2	na	84	3	13
	CO_{2eq}	182 ± 3	899 ± 4	1013 ± 3	935 ± 6	na			
LTMCA03	C_{org}	15.2 ± 0.4	86 ± 1	95.4 ± 0.6	137 ± 2	241 ± 4	24	65	11
	CO_{2eq}	56 ± 1	316 ± 2	350 ± 2	502 ± 6	883 ± 13			
El Verde	Camacho	Lagoon							
EVC01	C_{org}	16 ± 2	70 ± 3	79 ± 3	98 ± 1	182 ± 1	21	78	1
	CO_{2eq}	58 ± 6	258 ± 12	291 ± 10	358 ± 3	666 ± 4			
EVC02	C_{org}	36 ± 1	113 ± 2	139 ± 3	114 ± 1	na	43	41	16
	CO_{2eq}	133 ± 4	414 ± 7	512 ± 10	429 ± 3	na			

C_{org}: organic carbon; CO_{2eq}: carbon dioxide equivalent emissions in case of sediment disturbances in the sampling sites. na = not available. See the text for an explanation.

4.2.2. Mixing models

The relative contribution of the primary sources of C_{org} to the sediments varied both geographically and temporally, with the predominance of autochthonous mangrove detritus in LTMPA01 and LTMCA02, and the predominance of allochthonous fluvial C_{org} in LTMPA02, LTMCA01, and LTMCA03 (Table 4). In EV cores, allochthonous fluvial C_{org} predominated in EVC01, while EVC02 sediments exhibited a combination of mangrove detritus and fluvial C_{org}. Only a minor contribution of phytoplankton-derived C_{org} was observed in the cores (Table 4).

In the sediment cores, both fluvial and mangrove C_{org} sources generally increased by 5–41 % and by 5–32 %, respectively, from before the 1900s to the 2000s (Fig. 4), except in LTMCA02 where fluvial C_{org} remained minimal (1.2–4.4 %). After the 2000s, contributions of mangrove detritus increased by 18–20 % in PDE cores, 5–6 % in CP cores, and 19–27 % in EV cores. Simultaneously, contributions of phytoplankton-derived C_{org} decreased by 12–32 % in all cores, except for EVC01, where contributions remained consistently low (0.5–3.6 %). The Bayesian 5–95 % credible intervals for C_{org} sources in the CP cores during the period 1961–1981 were notably wider compared to other time intervals. In LTMCA01 and LTMCA03, this period revealed an increase of 11–14 % in the contribution of lagoon phytoplankton-derived C_{org}, along with a simultaneous reduction of 21 % in the contribution of fluvial C_{org}, relative to the preceding decade. The core LTMCA02 recorded a 6 % increase in lagoon phytoplankton-derived C_{org}, with no concurrent increase in fluvial C_{org}.

4.2.3. Indicators of terrestrial and marine inputs

In the post-1950s segment, the Al and Ca concentrations and the Al/Ti ratios generally increased in all cores, whereas the Na/Al ratios decreased, particularly in cores LTMPA01, LTMCA01, LTMCA03, and EVC01.

4.3. Organic carbon burial rates and stocks

The order of C_{org} burial rates in TL cores was LTMCA02 > LTMCA01 = LTMCA03 = LTMPA01 > LTMPA02, whereas in EV cores, they were higher ($p < 0.05$) in EVC02 than in EVC01 (Table 3). Both C_{org} stock$_{-10yr}$ and burial rates increased steadily from the early 1900s to the present in all cores, although the pace accelerated from the ~1950s onward (Figs. 4 and 5).

C_{org} stock$_{-50cm}$ values were higher in CP than other systems, whereas those of C_{org} stock$_{-1m}$ (where available) varied considerably (LTMCA03 > LTMPA01 > EVC01) (Table 4). The lowest C_{org} burial rates were observed in the cores LTMPA02 and EVC02 that were collected in mangrove areas closer to river mouths. In contrast, the highest C_{org} burial rates were found in cores LTMCA02 and LTMPA01 collected farther from the direct river influence (Fig. 1). C_{org} stocks$_{-1950\text{-}2021}$ were ~12–32 % higher than C_{org} stocks$_{-1900\text{-}1950}$ (Table 4), contributing to 80–92 % of the total stocks accumulated between 1900 and 2021 in each core. The C_{org} stocks$_{-10yr}$ in core LTMCA02 were the highest, ranging from ~2 to 6-fold higher than in the other cores (Fig. 4). The potential CO_{2eq} emissions in case of sediment disturbances reached 311–935 Mg ha^{-1} at 50 cm depth and 501–883 Mg ha^{-1} at 1-meter depth (where available) (Table 4). Potential annual CO_{2eq} emissions from mangrove losses per site were 30.1 ± 0.4 Tg yr^{-1} in PDE, 14.1 ± 0.2 Tg yr^{-1} in CP, and 0.67 ± 0.01 Tg yr^{-1} in EV.

5. Discussion

5.1. Major sources of organic carbon

The dominant fluvial C_{org} contribution (64–78 %; Table 4) in cores LTMPA02, LTMCA01, LTMCA03, and EVC01 is a common feature in river-influenced mangrove ecosystems, where the allochthonous C_{org} usually represents most of the total contribution (Kusumaningtyas et al., 2019; Sasmito et al., 2020). The relatively minor contribution of phytoplankton-derived C_{org} (1–17 %; Table 4) or seagrass material in all cores suggested a limited influence of the tidal regime onto the C_{org} supply to the sediments, in comparison to the fluvial sources. Seagrass is often considered in the investigation of organic matter sources in mangroves (Gonneea et al., 2004; Sepúlveda-Lozada et al., 2017, 2015) and was initially integrated as a primary source in the mixing models. However, during the preliminary analysis of $\delta^{13}C$ and $\delta^{15}N$ values within the mixing polygon defined by basal sources (Fig. 2; Brett, 2014), the integration of seagrass as a source resulted in mixing data falling outside the polygon, indicating an incorrect or missing source (Stock and Semmens, 2016b), and led to convergence issues in the models. While seagrass may be present in the study sites, it was determined as a minor contributor (<2 %) and therefore was excluded in this study.

The relatively high accumulation of mangrove-derived detritus C_{org} in cores LTMPA01 and LTMCA02 (55 and 84 %, respectively; Table 4) is typical for mangrove ecosystems without significant river or tidal influence, where C_{org} primarily originates from autochthonous sources, such as mangrove leaves and roots (Alongi, 2014). The high contribution of mangrove detritus in the mixing models was aligned with the highest C:N values (29–69; Table 3), corresponding to values generally found in mangroves detritus (20–30 in mangrove leaves and 50–60 in mangrove wood; Lallier-Vergès et al., 1998; Marchand et al., 2005). The uppermost sections of other cores (LTMPA02, EVC01, and EVC02) also showed high C:N values coinciding with lower $\delta^{13}C$ and $\delta^{15}N$ values (Fig. 3) that

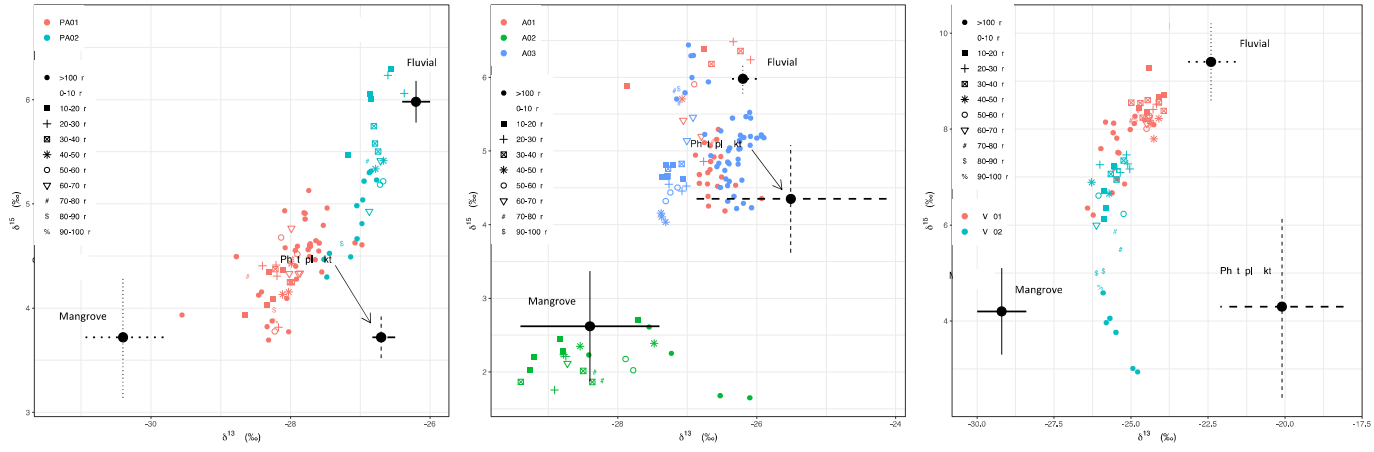

Fig. 2. Values of isotopic composition ($\delta^{13}C$ and $\delta^{15}N$) for mixture (sediment samples) and source data (mangrove: organic matter from mangrove detritus; fluvial: particulate organic matter from river inputs; phytoplankton: lagoon or marine-derived phytoplankton) in sediment cores from Términos Lagoon (southern Gulf of Mexico) and El Verde Camacho Lagoon (entrance of the Gulf of California).

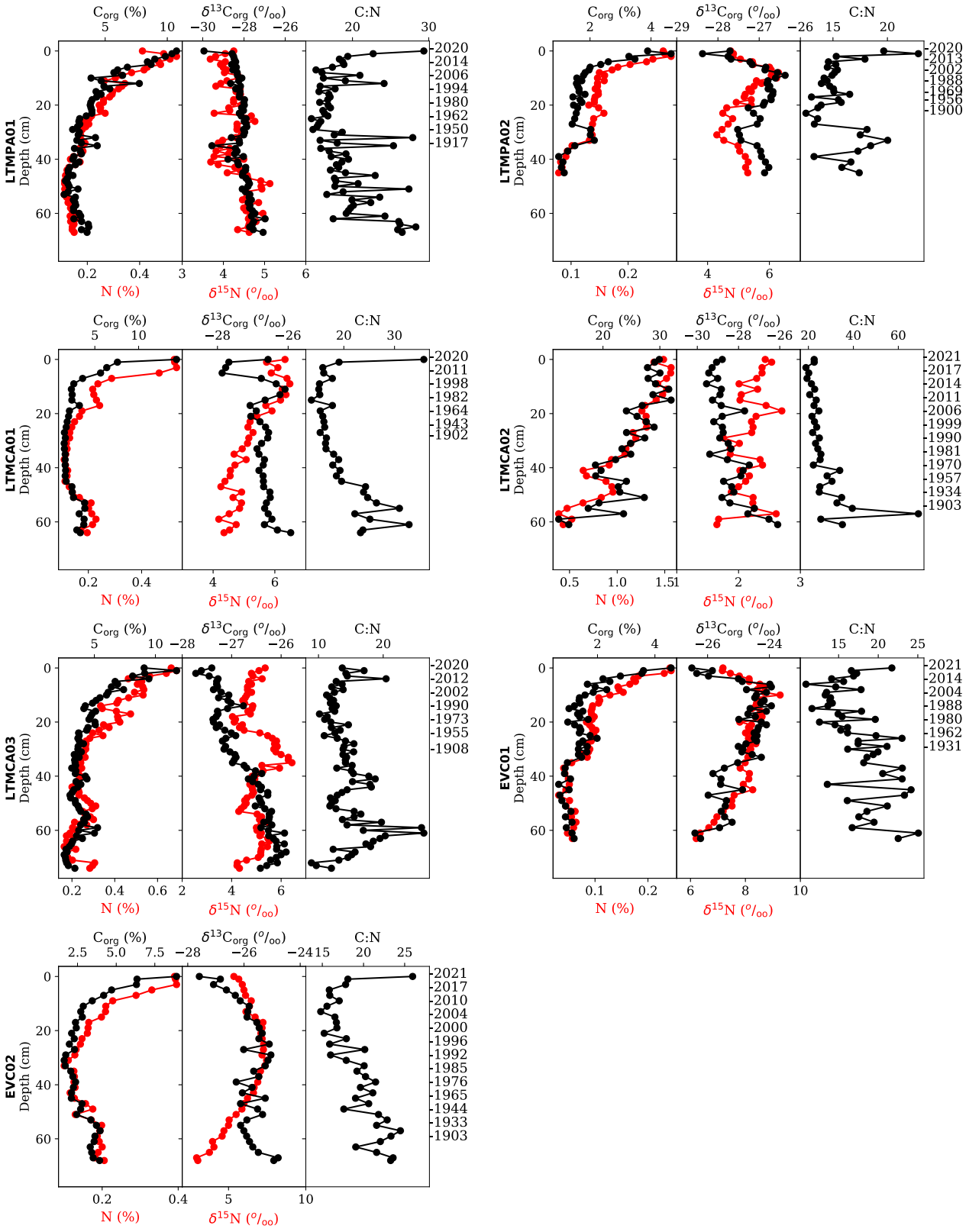

Fig. 3. Elemental concentration and isotopic composition of C and N, and C:N ratios in mangrove sediment cores from Términos Lagoon (southern Gulf of Mexico) and El Verde Camacho Lagoon (entrance of the Gulf of California).

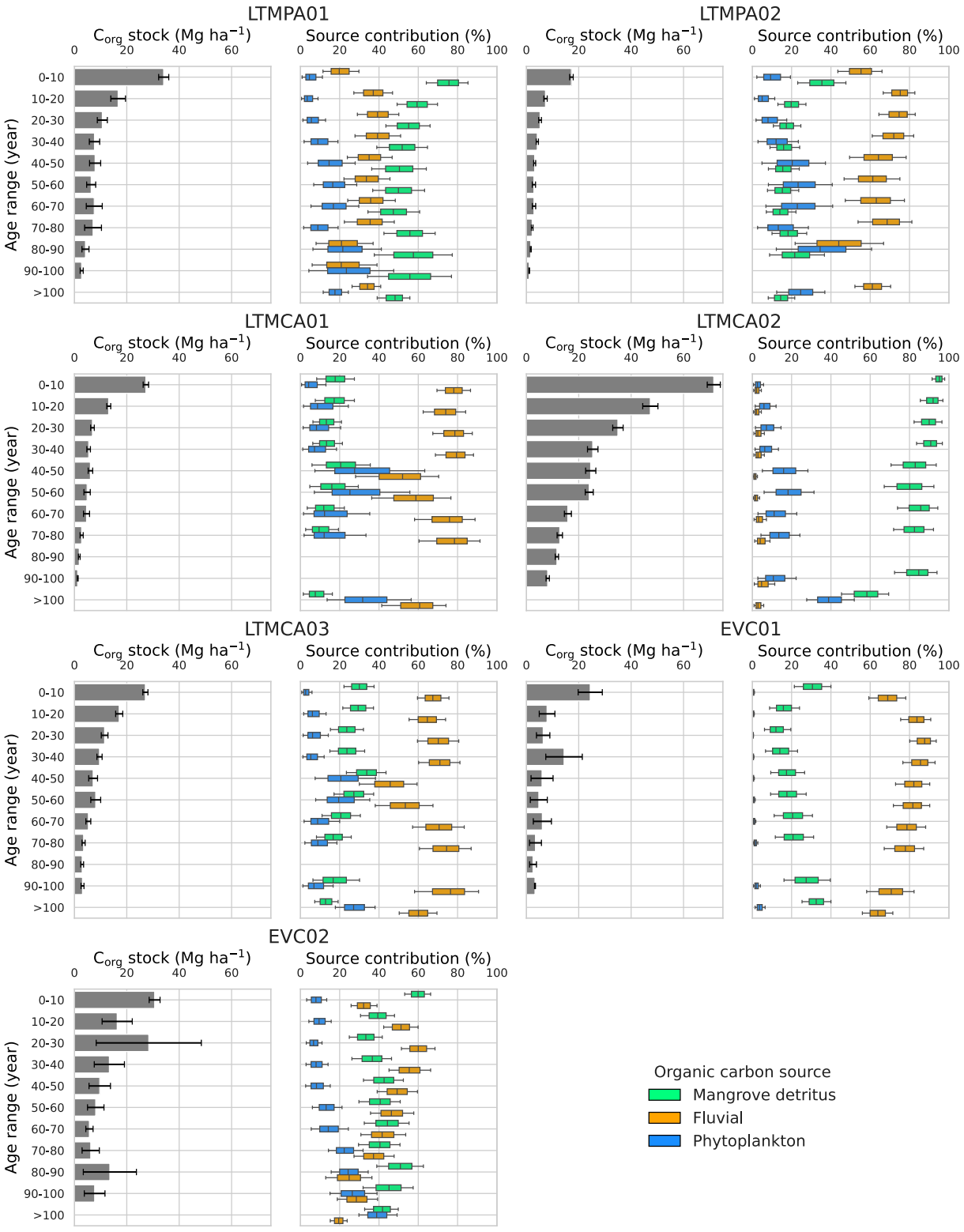

Fig. 4. Temporal variation of organic carbon (C_{org}) stocks and source contribution in mangrove sediment cores from Términos Lagoon (southern Gulf of Mexico) and El Verde Camacho Lagoon (entrance of the Gulf of California).

indicated a higher contribution of mangrove detritus in the most recent period (2021–2011).

The core EVC02 displayed a mixture of fluvial C_{org} and mangrove detritus sources (41 and 43 %, respectively; Table 4), attributed to changes in hydrodynamic conditions influenced by river discharge and storms (Jupin et al., 2023). The impact of storms on C_{org} accumulation can vary considerably, influencing river and tidal currents and sediment dynamics in two ways: i) increasing C_{org} accumulation, facilitated by the trapping of material (e.g., fallen vegetation) derived from storms by mangrove root systems, ultimately resulting in higher sediment accretion and C_{org} accumulation; or ii) causing erosion, C_{org} exportation to the ocean, or mangrove degradation leading to a reduction in productivity

(Pérez et al., 2018; Smoak et al., 2013). EVC02 registered a greater influx of C_{org} during these particular events (Fig. 5), suggesting that its location, farther from the influence of the Quelite River, was prone to C_{org} accumulation during storms, in contrast to EVC01.

5.2. Accumulation of organic carbon in contrasting environmental settings

The mean C_{org} burial rates in PDE (103 ± 47 g m^{-2} yr^{-1}) and EV (138 ± 70 g m^{-2} yr^{-1}) fell within the global mean for mangroves of 139 (120–159) g m^{-2} yr^{-1} (Fig. 6; Breithaupt and Steinmuller, 2022), whereas those in the CP system (210 ± 30 g m^{-2} yr^{-1}) were above the global mean. According to observations from global databases (Breithaupt and Steinmuller, 2022; Woodroffe et al., 2016), mangroves in estuaries or terrigenous settings, which usually receive high contributions of allochthonous C_{org}, tend to exhibit higher C_{org} burial rates compared to mangroves in lagoon or carbonate settings. Conversely, in this study, the highest C_{org} burial rates were found in mangrove areas where the input of autochthonous C_{org} prevailed (LTMCA02 and LTMPA01; Fig. 4) and in mangroves in carbonate settings (CP) compared to those in terrigenous settings (PDE and EV). The comparable C_{org} burial rates among cores from the three subsystems (LTMPA01, LTMCA01, LTMCA03, and EVC02; Table 3) and the significant ($p < 0.05$) differences in C_{org} burial rates among cores from the same study site (e.g., LTMPA01 > LTMPA02 in PDE; LTMCA02 > LTMCA01 and LTMCA02 > LTMCA03 in CP; and EVC02 > EVC01 in EV; Table 3) suggested that, irrespective of the sedimentary settings or geomorphic classes, the spatial distribution of C_{org} burial rates in the study sites was somewhat influenced by local conditions, specific to each core surroundings. The disparity between local and global observations can be attributed to the high local-scale variability commonly observed in mangroves (Jennerjahn, 2020; Pérez et al., 2018), which increases data uncertainties and database biases (e.g., interpolation errors, different timescales, and insufficient data; Sidik and Friess, 2021). The complexity of the processes that affect C_{org} accumulation in mangroves, often overlooked in global-scale analyses, is shown by the wide range of reported C_{org} burial rates in mangrove ecosystems worldwide, which tend to broaden as more data are reported (20–1020 g m^{-2} yr^{-1}, Breithaupt et al., 2012; 2–1749 g m^{-2} yr^{-1}, Breithaupt and Steinmuller, 2022).

The lowest observed C_{org} burial rates in cores LTMPA02 and EVC01 were attributed to their proximity to the river discharge (Fig. 1, Table 3). EVC01 showed a significantly ($p < 0.05$) coarser sediment composition than EVC02, suggesting higher hydrodynamic conditions near the Quelite River mouth (Jupin et al., 2023). Increased hydrodynamic can diminish C_{org} accumulation and storage by regulating the sediments, oxygen, and nutrients supply, thus preventing long-term C_{org} deposition through resuspension processes and promoting aerobic decomposition of sedimentary C_{org} (Allais et al., 2024; Kusumaningtyas et al., 2019). In particular, EVC01 was likely influenced by the seasonal export of in situ C_{org} to the ocean by the Quelite River, occurring during the rainy season (Flores-Verdugo et al., 1995), which would explain its lower proportion of mangrove detritus compared to EVC02 (Table 4). Although the TL cores exhibited comparable grain size distributions (Jupin et al., 2023), runoff in the surroundings of LTMPA02 may have promoted the flushing of suspended sedimentary matter out of the lagoon, promoting export rather than accumulation of autochthonous C_{org} (Bouillon et al., 2003).

5.3. Storage of organic carbon in contrasting environmental settings

At a comparable core depth, the C_{org} $stock_{-50cm}$ values for each mangrove area (PDE: 108 ± 1 Mg ha^{-1}; CP: 166 ± 2 Mg ha^{-1}; EV: 106 ± 1 Mg ha^{-1}; Table 4) were similar to the range found in anthropized mangrove ecosystems of South Australia (87–120 Mg ha^{-1}; Lavery et al., 2019) and pristine mangrove ecosystems in Indonesia (62 ± 10 to 180 ± 82 Mg ha^{-1}; Sasmito et al., 2020), but might be lower than values estimated for Mexican mangrove ecosystems from the southern Mexican Pacific (180 Mg ha^{-1}), the Gulf of Mexico (210 Mg ha^{-1}) and Yucatán (360 Mg ha^{-1}) (Herrera-Silveira et al., 2016), although this comparison is limited because the uncertainties of such values are unavailable. Among cores with available C_{org} $stock_{-1m}$ (Table 4), only that of LTMCA03 (241 ± 4 Mg ha^{-1}) was comparable to the global mean estimate of 251 (200–302) Mg ha^{-1} and the mean estimate for Mexico of 370 ± 176 Mg ha^{-1} (Fig. 7; Atwood et al., 2017). The higher C_{org} stocks (Table 4) were found in cores with higher C_{org} burial rates (Table 3) and sourced from mangrove detritus (Fig. 4), suggesting an efficient preservation of the accumulated autochthonous C_{org}. The C_{org} stocks at 50 cm and 1 m depth were highest in CP and were comparable between EV (North Pacific) and PDE (Gulf of Mexico). This contrasted with the regional pattern previously observed in Mexico (Herrera-Silveira et al., 2020), which showed a lower mean C_{org} $stock_{-1m}$ in the North Pacific (270 ± 52 Mg ha^{-1}) compared to the Gulf of Mexico (438 ± 76 Mg ha^{-1}), attributed to regional climates (lower C_{org} $stock_{-1m}$ arid and humid regions) and coastal geomorphology (limited habitat available for mangroves in the North Pacific).

The high variability in C_{org} $stock_{-1m}$ around the world is reflected in the wide range of values among countries (72–936 Mg ha^{-1}; Fig. 7; Atwood et al., 2017) and regions in Mexico (10–1952 Mg ha^{-1}; Herrera-Silveira et al., 2020), adds complexity to the general understanding of factors driving C_{org} accumulation and preservation in mangroves. The inclusion of data from diverse periods in databases (1985–2017, Atwood et al., 2017; 1996–2016, Herrera-Silveira et al., 2020) may introduce a potential limitation for stock comparison since this study (Fig. 4) and other publications employing dated sediment cores (e.g., Cuellar-Martinez et al., 2020; López-Mendoza et al., 2020) have demonstrated that C_{org} stocks vary over time. The present study proposes the establishment of C_{org} stock databases over comparable timeframes, such as 100 years (e.g., 1900–2000 or 1920–2020), employing reliable dating methods (e.g., ^{210}Pb). It also emphasizes the significance of standardizing measurement techniques and adopting best practices in sediment sampling and measurement to ensure consistency and comparability across assessments of C_{org} burial rates and stocks.

The CO_2 emission rates per ha resulting from sediment disturbance were higher in LTMCA03 than in other cores (Table 4). However, when accounting for the annual rate of mangrove loss, the PDE system has been releasing a larger volume of yearly CO_2 emissions (30.1 ± 0.4 Tg yr^{-1}) due to ongoing deforestation (Table 1). Although the overall range of potential CO_2 emissions in the study sites (501–883 Mg ha^{-1}) was lower than mean values estimated for mangroves worldwide (1415 Mg ha^{-1}; Howard et al., 2014), the conversion or degradation of these ecosystems could result in a higher amount of CO_2 emissions, considering potential disturbances extending beyond 1 m (Kauffman et al., 2020; Lovelock et al., 2017) and the exclusion of other possible greenhouse gas emissions such as CH_4 and N_2O (Macreadie et al., 2019). Mangrove protection and restoration efforts are crucial to mitigate these emissions and capitalize on this natural climate solution.

5.4. Temporal evolution of sources and its impact on burial rates and stocks

In all sediment cores, the increase by 5–41 % of the fluvial C_{org} contribution over the last century (Fig. 4) is associated with a rising flux of terrestrial elements (Al, Ca) and a shift in detrital sources shown by increasing values of the Al/Ti ratio (Fig. 5), indicating an increasing influence of river inputs across all the studied mangroves. This was consistent with the river discharge data (Fig. 5; data not available for the Quelite River) and previous studies that reported increasing discharges in the Usumacinta and Candelaria rivers since the 1950s, attributed to deforestation and land-use changes (Benítez et al., 2005; Fichez et al., 2017; Soto-Galera et al., 2010). Decreasing values of C:N ratios (except for 2021–2011 in specific cores; see Section 5.1) and variations in $\delta^{13}C$ and $\delta^{15}N$ values (Fig. 3) suggested progressive alterations in C_{org} inputs

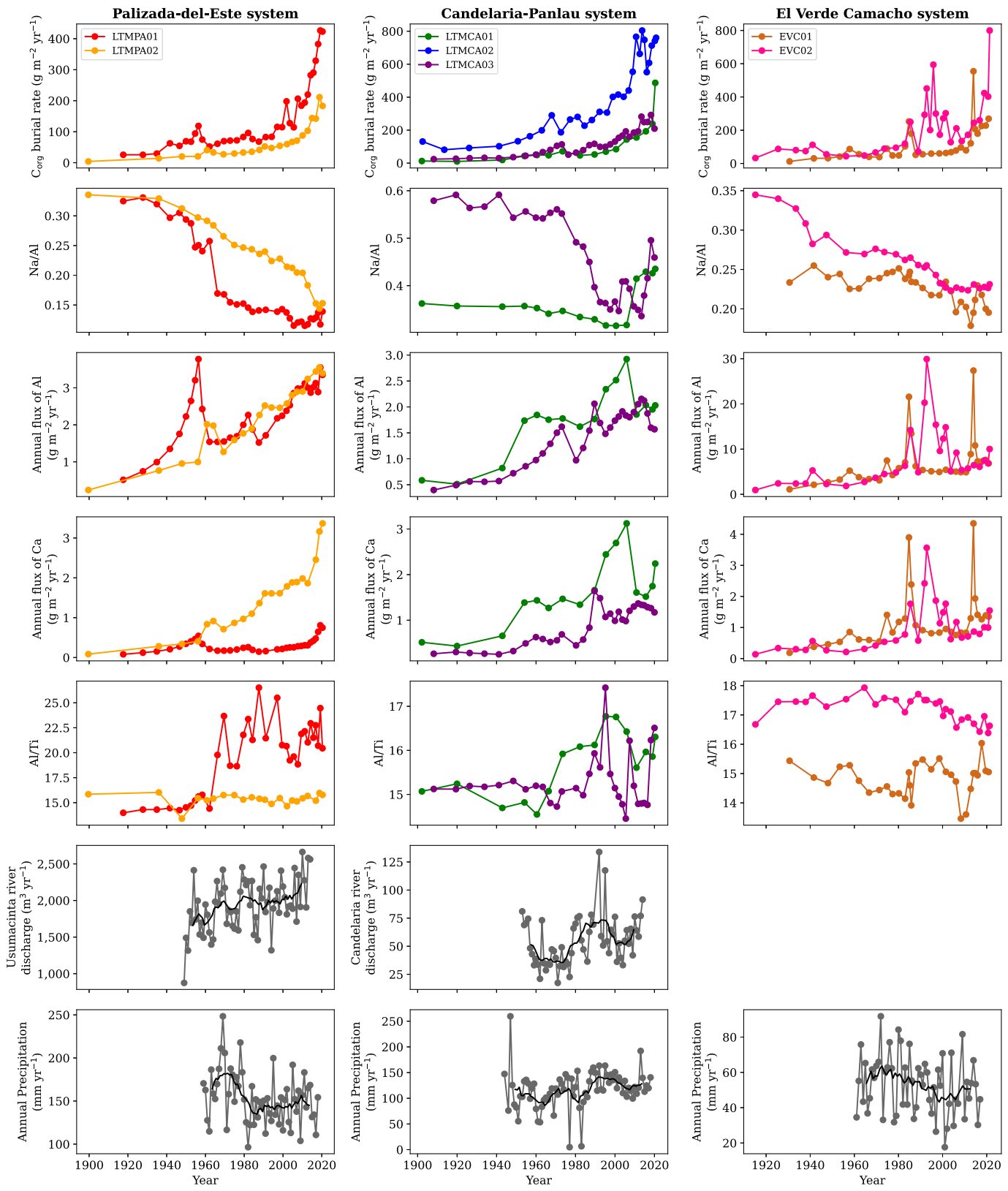

Fig. 5. Temporal variations in organic carbon and elemental accumulation in mangrove sediment cores from Términos Lagoon (southern Gulf of Mexico) and El Verde Camacho Lagoon (entrance of the Gulf of California). Annual river discharge and precipitation are shown in Table S1 in Supplementary Material.

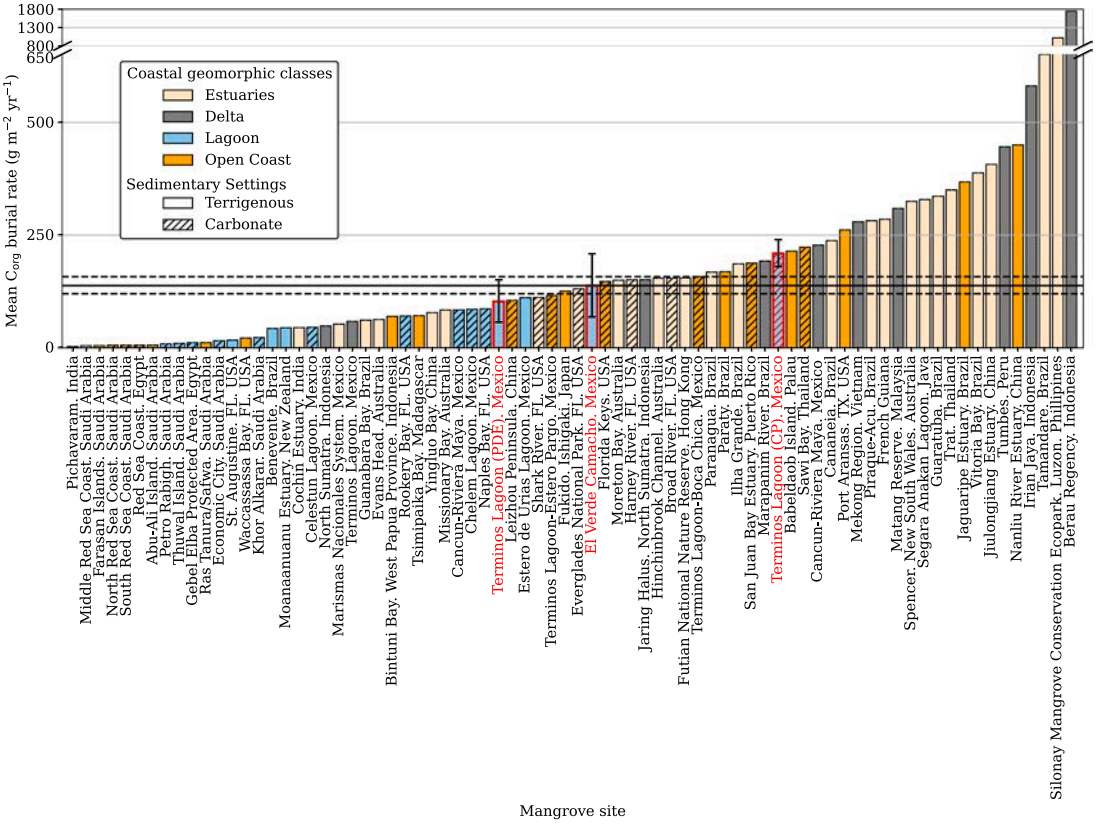

Fig. 6. Cross-comparison of organic carbon (C_{org}) burial rates in mangrove ecosystems worldwide. The sites from this study are represented with red bars. Horizontal black solid and dashed lines indicate the mean and 95 % confidence interval. PDE: Palizada-del-Este; CP: Candelaria-Panlau. The database was sourced from Breithaupt and Steinmuller (2022).

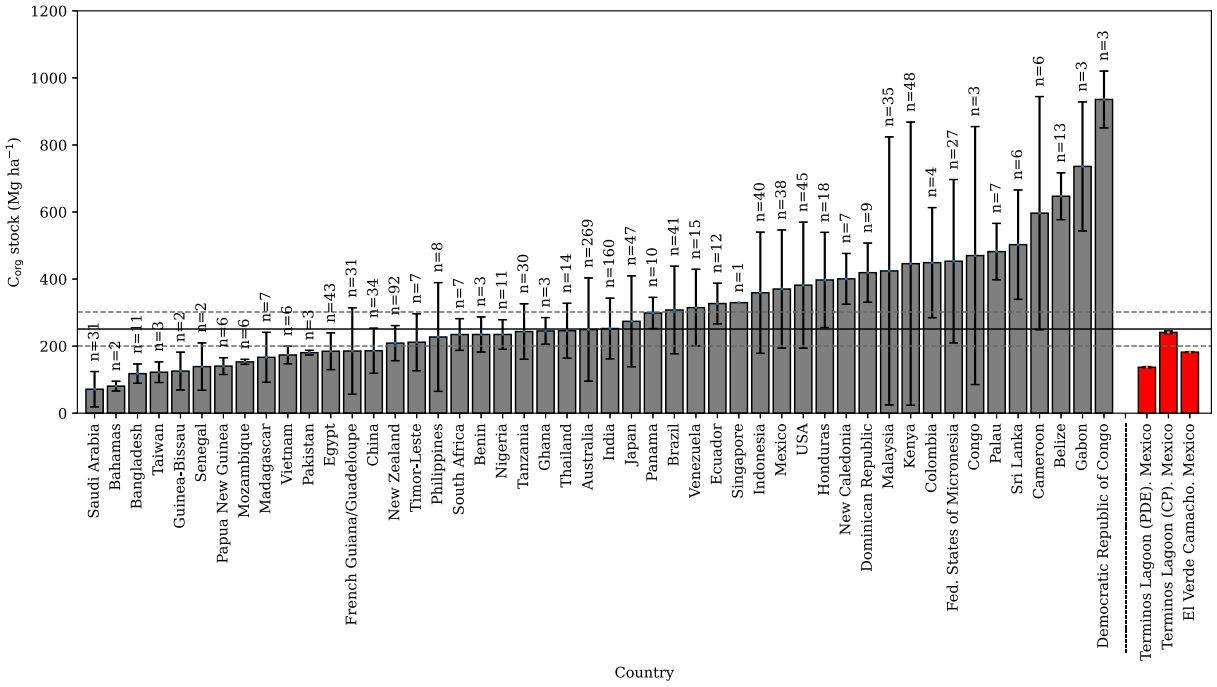

Fig. 7. Cross-comparison of organic carbon (C_{org}) stocks at 1 m depth in mangrove ecosystems worldwide. The sites from this study are represented with red bars. Horizontal black solid and dashed lines indicate the mean and 95 % confidence interval. PDE: Palizada-del-Este; CP: Candelaria-Panlau. The database was sourced from Atwood et al. (2017).

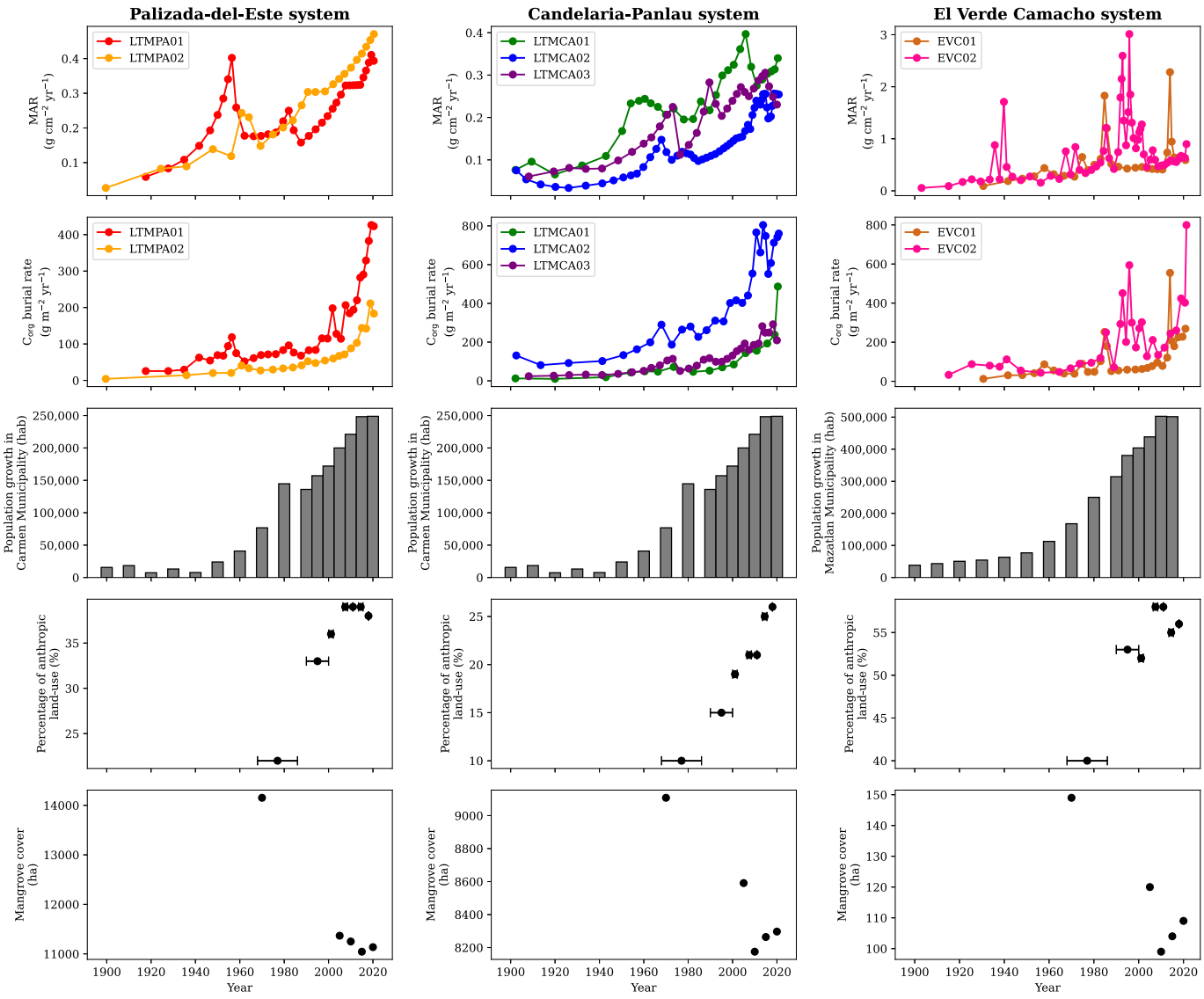

Fig. 8. Environmental factors affecting sediment and organic carbon (C_{org}) accumulation in Términos Lagoon (southern Gulf of Mexico) and El Verde Camacho Lagoon (entrance of the Gulf of California). MAR: Mass accumulation rate. References can be found in Table S2 in Supplementary Material.

or composition.

The rising trends in fluvial inputs and C_{org} burial rates coincided with the consistently increasing MAR trend and its acceleration after the 1950s (Fig. 8; Jupin et al., 2023). The determination coefficients of the regression between C_{org} burial rates and MAR indicated that MAR explained between 72 and 99 % of the increasing C_{org} burial rates in the study sites. The rise of MAR was attributed to a progressive change in sediment sources in the mangrove ecosystems. It was interpreted as an outcome of global factors (i.e., continental erosion and sea-level rise) influencing the temporal variability of sediment accumulation in the study sites (Jupin et al., 2023). Over the last century, the increase in continental erosion was driven by population growth and the consequential land-use changes within the river basins (Fig. 8). Within the study sites, it resulted in a progressive increase in C_{org} concentrations, burial rates, and stock$_{\text{-10yr}}$ (Figs. 3, 4, and 5) over the past century, with a majority of C_{org} stock$_{\text{-100yr}}$ (80–92 %) accumulated in the post-1950 period (Table 4), contradicting the research hypothesis. This phenomenon, documented in coastal areas worldwide (e.g., Ruiz-Fernández et al., 2009), has been previously associated with a consistent increase in C_{org} burial rates and stocks in some mangrove (e.g., Cuellar-Martinez et al., 2020) and seagrass meadow ecosystems (e.g., López-Mendoza et al., 2020; Ruiz-Fernández et al., 2020).

In the CP cores, the wider Bayesian credible intervals (5–95 %) during 1961–1981 than other time intervals were associated with a higher contribution of lagoon-derived C_{org} and a diminished contribution of fluvial C_{org} (Fig. 4). This was attributed to the occurrence of low precipitation conditions and reduced river discharge magnitudes (Fig. 5), potentially favoring marine intrusion during this period. In the subsequent decades (1980–2000) characterized by high river discharges and precipitation, there was a concurrent increase in the accumulation of Al and Ca and values of Al/Ti ratios observed in the cores LTMCA01 and LTMCA03 (Fig. 5), suggesting a substantial influx of terrigenous and carbonate sediment inputs, with a distinct mineralogical composition. The lowest Na/Al ratios were found during the same period, confirming a minor marine influence. In core EVC02, the observed increase in MAR and C_{org} burial rate (Fig. 8) from 1995 to 2005 coincided with the highest contributions of fluvial C_{org} in this core (Fig. 4), likely due to an intensified influence of the Quelite River.

Mangrove areas accumulated sediments in equilibrium with local sea-level rise in the TL and EV systems (Jupin et al., 2023). However, the decline in the contribution of marine or lagoon phytoplankton-derived C_{org} in the cores over the past century (Fig. 4), along with reducing

trends of the Na/Ti ratio (Fig. 5), suggested that the increasing dominance of fluvial C_{org} contribution has been outpacing the potential rise in C_{org} contributions associated with sea-level rise in the study sites. The decreasing contribution of phytoplankton-derived C_{org} was also evident in LTMCA02, characterized by a minor river influence, and was attributed to a progressive increase in the contribution of mangrove detritus during the study period (Fig. 4).

Besides LTMCA02, a growing mangrove contribution over the last century was also observed in several cores (LTMPA01, LTMCA01, and LTMCA03) and attributed to a combination of factors that could include i) a potential increase in mangrove aboveground productivity over time driven by rising nutrient inputs from the river (Morris et al., 2016), ii) a rise in surface elevation through biotic processes (root generation, microbial mat formation, and detritus accumulation) to compensate sea-level rise (McKee, 2011; Mckee et al., 2007), and iii) enhanced preservation of autochthonous C_{org}, facilitated by heightened sediment deposition and water flooding, effectively relocating C_{org} away from the surface and aerobic conditions (Burdige, 2007). These observations indicated that, although the mangrove cover was reduced in the study sites (Fig. 8), primarily resulting from deforestation for the development of intensive agriculture and urban settlements (Monjardín-Armenta et al., 2017; Soto-Galera et al., 2010), the remaining mangroves continue to play a crucial role as significant producers and sinks of in situ C_{org} in these sites, by adapting to the changing environmental conditions.

6. Conclusions

This research quantified source contributions and accumulation and storage capacity of sedimentary organic carbon over ~100 years by using geochemical data from seven ^{210}Pb-dated sediment cores collected in mangrove areas in the Términos Lagoon and El Verde Camacho Lagoon (Mexico). The distinction between cores with dominant fluvial contributions and those with dominant autochthonous contributions (mangrove detritus) was determined using the mixing model MixSIAR and attributed to the influence of local rivers on the origin, importation, and exportation of organic carbon within the sites. The highest burial rates and stocks were observed in mangrove areas with limited river influence and dominated by autochthonous inputs of organic carbon. The carbonate system Candelaria-Panlau, in Términos Lagoon, showed the highest accumulation and storage of sedimentary organic carbon, constituting the most effective sinks among sites. While general patterns based on coastal morphology and regional climate regimes have been identified globally, these patterns did not accurately apply to the local-scale variability observed in study sites. Burial rates and stocks generally increased over the past century, contradicting the initial hypothesis. This upward trend was mainly associated with the rising prevalence of organic material supplied by river systems, driven by continental erosion, and enhanced production and preservation of mangrove detritus. Despite the reported reduction in their cover within river basins, this study highlighted i) that mangroves continue to serve as influential producers and sinks of organic carbon and ii) the need for sustained efforts to improve databases, aiming to bolster their protection and facilitate restoration initiatives.

CRediT authorship contribution statement

J.L.J. Jupin: Conceptualization, Formal analysis, Investigation, Validation, Writing – original draft. **A.C. Ruiz-Fernández:** Writing – review & editing, Writing – original draft, Supervision, Resources, Project administration, Methodology, Investigation, Funding acquisition, Formal analysis, Data curation, Conceptualization. **A. Sifeddine:** Writing – review & editing, Funding acquisition, Conceptualization. **M. Mendez-Millan:** Writing – review & editing, Formal analysis, Data curation, Conceptualization. **J.A. Sanchez-Cabeza:** Conceptualization, Investigation, Methodology, Writing – review & editing. **L.H. Pérez-Bernal:** Data curation, Formal analysis, Methodology, Writing – review & editing. **J.G. Cardoso-Mohedano:** Formal analysis, Investigation, Methodology, Writing – review & editing. **M.A. Gómez-Ponce:** Formal analysis, Methodology, Writing – review & editing. **J.G. Flores-Trujillo:** Formal analysis, Investigation, Writing – review & editing.

Declaration of competing interest

The authors declare that they have no known competing financial interests or personal relationships that could have appeared to influence the work reported in this paper.

Data availability

Data will be made available on request.

Acknowledgments

This work was possible due to the support of the Universidad Nacional Autónoma de México (UNAM) through the project PAPIIT-DGAPA IN102821, and of the Institut de Recherche pour le Développement (IRD) through the international network DEXICOTROP and the Alysés platform facilities for geochemical and isotopic analyses. A Ph.D. fellowship provided by Consejo Nacional de Ciencia y Tecnología-Mexico (CONACYT, CVU 1102000) and the support of the Posgrado en Ciencias del Mar y Limnologia, UNAM, is acknowledged by Jupin J. L. J. Authors are grateful for the support received from M. Amador-Medina and J. C. Gonzalez-Palacios (Comisión Nacional de Áreas Naturales Protegidas del Santuario Plata El Verde Camacho), E. Ramírez-Tirado (El Recreo Community), J. A. Martinez-Trejo (sampling), L. F. Álvarez-Sánchez (data curation), I. Djouraev (data analysis), and C. Súarez-Gutiérrez (informatics).

Appendix A. Supplementary data

Supplementary data to this article can be found online at https://doi.org/10.1016/j.scitotenv.2024.173440.

References

Adame, M.F., Fry, B., 2016. Source and stability of soil carbon in mangrove and freshwater wetlands of the Mexican Pacific coast. Wetl. Ecol. Manag. 24, 129–137. https://doi.org/10.1007/s11273-015-9475-6.

Allais, L., Thibodeau, B., Khan, N.S., Crowe, S.A., Cannicci, S., Not, C., 2024. Salinity, mineralogy, porosity, and hydrodynamics as drivers of carbon burial in urban mangroves from a megacity. Sci. Total Environ. 912, 168955 https://doi.org/10.1016/j.scitotenv.2023.168955.

Alongi, D.M., 2014. Carbon cycling and storage in mangrove forests. Ann. Rev. Mar. Sci. 6, 195–219. https://doi.org/10.1146/annurev-marine-010213-135020.

Atwood, T.B., Connolly, R.M., Almahasheer, H., Carnell, P.E., Duarte, C.M., Lewis, C.J.E., Irigoien, X., Kelleway, J.J., Lavery, P.S., Macreadie, P.I., Serrano, O., Sanders, C.J., Santos, I.R., Steven, A.D.L., Lovelock, C.E., 2017. Global patterns in mangrove soil carbon stocks and losses. Nat. Clim. Chang. 7, 523–528. https://doi.org/10.1038/nclimate3326.

Bach, L., Calderon, R., Cepeda, M.F., Oczkowski, A., Olsen, S.B., Robadue, D., 2005. Resumen del Perfil de Primer Nivel del Sitio Laguna de Términos y su Cuenca, México, Coastal Resources Center. University of Rhode Island. Coastal Resources Center, University of Rhode Island, Narragansett.

Benítez, J.A., Sanvicente Sánchez, H., Lafragua Contreras, J., Zamora Crescencio, P., Morales Manilla, L.M., Mas Caussel, J.F., García Gil, G., Couturier, S.A., Zetina Tapia, R., Calan Yam, R.A., Amabilis Sánchez, L., Acuña, C., Mejenes, M., 2005. Sistemas de información geográfica de la cuenca del río Candelaria: reconstrucción histórica de los cambios de cobertura forestal y su efecto sobre la hidrología y calidad del agua-marco teórico y resultados iniciales. In: Edith, F., Kauffer, M. (Eds.), El Agua En La Frontera México-Guatemala-Belice. Ecosur/tnc/unach, Tuxtla Gutiérrez, Chiapas, pp. 19–32.

Blaauw, M., Christen, J.A., Aquino-López, M.A., Esquivel-Vazquez, J., Gonzalez, O.M., Belding, T., Theiler, J., Gough, B., Karney, C., 2021. Bayesian age-depth modelling of cores dated by Pb-210. https://cran.r-project.org/web/packages/rplum/rplum.pdf.

Blankespoor, B., Dasgupta, S., Lange, G.-M., 2017. Mangroves as a protection from storm surges in a changing climate. Ambio 46, 478–491. https://doi.org/10.1007/s13280-016-0838-x.

Bouillon, S., Dahdouh-Guebas, F., Rao, A.V.V.S., Koedam, N., Dehairs, F., 2003. Sources of organic carbon in mangrove sediments: variability and possible ecological

implications. Hydrobiologia 495, 33–39. https://doi.org/10.1023/A:1025411506526.
Bouillon, S., Connolly, R.M., Lee, S.Y., 2008. Organic matter exchange and cycling in mangrove ecosystems: recent insights from stable isotope studies. J. Sea Res. 59, 44–58. https://doi.org/10.1016/j.seares.2007.05.001.
Breithaupt, J.L., Steinmuller, H.E., 2022. Refining the global estimate of mangrove carbon burial rates using sedimentary and geomorphic settings. Geophys. Res. Lett. 49 https://doi.org/10.1029/2022GL100177.
Breithaupt, J.L., Smoak, J.M., Smith, T.J., Sanders, C.J., Hoare, A., 2012. Organic carbon burial rates in mangrove sediments: strengthening the global budget. Global Biogeochem. Cycles 26, 1–11. https://doi.org/10.1029/2012GB004375.
Brett, M.T., 2014. Resource polygon geometry predicts Bayesian stable isotope mixing model bias. Mar. Ecol. Prog. Ser. Inter-Research 514, 1–12. https://doi.org/10.3354/meps11017.
Briseño-Dueñas, R., 2003. Ficha Informativa de los Humedales de Ramsar (FIR). "Playa Tortuguera El Verde Camacho" [WWW Document]. URL. https://rsis.ramsar.org/RISapp/files/RISrep/MX1349RIS.pdf.
Burdige, D.J., 2007. Linking sediment organic geochemistry and sediment diagenesis. In: Geochemistry of Marine Sediments. Princeton University Press, Princeton, pp. 237–270. https://doi.org/10.1515/9780691216096-013.
Carter, S., Fisher, A., Garcia, R., Gibson, B., Lancaster, S., Marshall, J., Whiteside, I., 2015. Atomic spectrometry update. Review of advances in the analysis of metals, chemicals and functional materials. J. Anal. At. Spectrom 30, 2249–2294. https://doi.org/10.1039/C5JA90045J.
Cerón-Bretón, J.G., Cerón-Bretón, R.M., Rangel-marrón, M.M., Muriel-García, M., Cordova-Quiroz, A.V., Estrella-Cahuich, A., 2011. Determination of carbon sequestration rate in soil of a mangrove forest in Campeche, Mexico. WSEAS Trans. Environ. Dev. 7, 54–64.
Cifuentes, L.A., Coffin, R.B., Solorzano, L., Cardenas, W., Espinoza, J., Twilley, R.R., 1996. Isotopic and elemental variations of carbon and nitrogen in a mangrove estuary. Estuar. Coast. Shelf Sci. 43, 781–800. https://doi.org/10.1006/ecss.1996.0103.
CONABIO, 2013. Distribución de los manglares en México en 1970-1981, escala: 1: 50000. edición: 1. Proyecto: GQ004, Los manglares de México: Estado actual y establecimiento de un programa de monitoreo a largo [WWW Document]. Comisión Nacional para el Conocimiento y Uso de la Biodiversidad. URL. http://geoportal.conabio.gob.mx/metadatos/doc/html/mexman70gw.html (accessed 1.2.23).
CONABIO, 2021. Distribución de los manglares en México en 2020, escala: 1:50000. edición: 1. Sistema de Monitoreo de los Manglares de México (SMMM). [WWW Document]. Comisión Nacional para el Conocimiento y Uso de la Biodiversidad. URL. http://geoportal.conabio.gob.mx/metadatos/doc/html/mx_man20gw.html (accessed 1.2.23).
CONAGUA, 2015. Determinación de la Disponibilidad de Agua en el acuífero Río Quelite, estado de Sinaloa. Comisión Nacional del Agua CONAGUA.
Contreras-Ruiz-Esparza, A., Douillet, P., Zavala-Hidalgo, J., 2014. Tidal dynamics of the Terminos Lagoon, Mexico: observations and 3D numerical modelling. Ocean Dyn. 64, 1349–1371. https://doi.org/10.1007/s10236-014-0752-3.
Cotler-Ávalos, H., 2010. Las cuencas hidrograficas de México. Diagnostico y Priorizacion, Secretaría de Medio Ambiente y Recursos Naturales. Instituto Nacional de Ecología. Pluralia Ediciones e Impresiones, México, D.F.
Croudace, I.W., Rothwell, R.G., 2015. Micro-XRF Studies of Sediment Cores, Developments in Paleoenvironmental Research. Springer, Netherlands, Dordrecht. https://doi.org/10.1007/978-94-017-9849-5.
Cuellar-Martinez, T., Ruiz-Fernández, A.C., Sanchez-Cabeza, J.A., Pérez-Bernal, L.H., Sandoval-Gil, J., 2019. Relevance of carbon burial and storage in two contrasting blue carbon ecosystems of a north-east Pacific coastal lagoon. Sci. Total Environ. 675, 581–593. https://doi.org/10.1016/j.scitotenv.2019.03.388.
Cuellar-Martinez, T., Ruiz-Fernández, A.C., Sanchez-Cabeza, J.A., Pérez-Bernal, L., López-Mendoza, P.G., Carnero-Bravo, V., Agraz-Hernández, C.M., van Tussenbroek, B.I., Sandoval-Gil, J., Cardoso-Mohedano, J.G., Vázquez-Molina, Y., Aldana-Gutiérrez, G., 2020. Temporal records of organic carbon stocks and burial rates in Mexican blue carbon coastal ecosystems throughout the Anthropocene. Glob. Planet Change 192, 103215. https://doi.org/10.1016/j.gloplacha.2020.103215.
Díaz-Asencio, M., Sanchez-Cabeza, J.A., Ruiz-Fernández, A.C., Corcho-Alvarado, J.A., Pérez-Bernal, L.H., 2020. Calibration and use of well-type germanium detectors for low-level gamma-ray spectrometry of sediments using a semi-empirical method. J. Environ. Radioact. 225 https://doi.org/10.1016/j.jenvrad.2020.106385.
Douglas, P.M.J., Stratigopoulos, E., Park, S., Keenan, B., 2022. Spatial differentiation of sediment organic matter isotopic composition and inferred sources in a temperate forest lake catchment. Chem. Geol. 603 https://doi.org/10.1016/j.chemgeo.2022.120887.
FAO, 2007. The World's Mangroves 1980–2005: A Thematic Study Prepared in the Framework of the Global Forest Resources Assessment 2005. FAO Forestry Paper, Rome.
Fichez, R., Archundia, D., Grenz, C., Douillet, P., Gutiérrez-Mendieta, F., Origel-Moreno, M., Denis, L., Contreras-Ruiz-Esparza, A., Zavala-Hidalgo, J., 2017. Global climate change and local watershed management as potential drivers of salinity variation in a tropical coastal lagoon (Laguna de Terminos, Mexico). Aquat. Sci. 79, 219–230. https://doi.org/10.1007/s00027-016-0492-1.
Flores-Verdugo, F.J., Day, J.W., Briseño-Dueñas, R., 1987. Structure, litter fall, decomposition, and detritus dynamics of mangroves in a Mexican coastal lagoon with an ephemeral inlet. Mar. Ecol. Prog. Ser. 35, 83–90.
Flores-Verdugo, F.J., Briseño-Dueñas, R., González-Farías, F., Calvario-Martínez, O., 1995. Balance de carbono en un ecosistema lagunar estuarino de boca efímera de la costa noroccidental de México (Estero El Verde, Sinaloa). In: Temas de oceanografía biológica en México. Universidad Autónoma de Baja California, Ensenada, 8.C., México. II.
García, E., 1973. Modificaciones al sistema de clasificación climática de Köppen: para adaptarlo a las condiciones de la república mexicana, 6th ed. Universidad Nacional Autónoma de México, México, D. F.
Goldberg, L., Lagomasino, D., Thomas, N., Fatoyinbo, T., 2020. Global declines in human-driven mangrove loss. Glob. Chang. Biol. 26, 5844–5855. https://doi.org/10.1111/gcb.15275.
Gonneea, M.E., Paytan, A., Herrera-Silveira, J.A., 2004. Tracing organic matter sources and carbon burial in mangrove sediments over the past 160 years. Estuar. Coast. Shelf Sci. 61, 211–227. https://doi.org/10.1016/j.ecss.2004.04.015.
González-Farías, F., Mee, L.D., 1988. Effect of mangrove humic-like substances on biodegradation rate of detritus. J. Exp. Mar. Biol. Ecol. 119, 1–13. https://doi.org/10.1016/0022-0981(88)90148-7.
Guerra-Santos, J.J., Cerón-Bretón, R.M., Cerón-Bretón, J.G., Damián-Hernández, D.L., Sánchez-Junco, R.C., Guevara-Carrió, E.C., 2014. Estimation of the carbon pool in soil and above-ground biomass within mangrove forests in Southeast Mexico using allometric equations. J. For. Res. (Harbin) 25, 129–134. https://doi.org/10.1007/s11676-014-0437-2.
Hamilton, S.E., Casey, D., 2016. Creation of a high spatio-temporal resolution global database of continuous mangrove forest cover for the 21st century (CGMFC-21). Glob. Ecol. Biogeogr. 25, 729–738. https://doi.org/10.1111/geb.12449.
Hamilton, S.E., Friess, D.A., 2018. Global carbon stocks and potential emissions due to mangrove deforestation from 2000 to 2012. Nat. Clim. Chang. 8, 240–244. https://doi.org/10.1038/s41558-018-0090-4.
Herrera-Silveira, J.A., Camacho-Rico, A., Pech, E., Pech, M., Ramírez-Ramírez, J., Teutli-Hernández, C., 2016. Carbon dynamics (stocks and fluxes) in mangroves of Mexico. Terra Latinoamericana 34–I, 61–72.
Herrera-Silveira, J.A., Pech-Cardenas, M.A., Morales-Ojeda, S.M., Cinco-Castro, S., Camacho-Rico, A., Caamal-Sosa, J.P., Mendoza-Martinez, J.E., Pech-Poot, E.Y., Montero, J., Teutli-Hernández, C., 2020. Blue carbon of Mexico, carbon stocks and fluxes: a systematic review. PeerJ 8, e8790. https://doi.org/10.7717/peerj.8790.
Coastal blue carbon: methods for assessing carbon stocks and emissions factors in mangroves, tidal salt marshes, and seagrasses. In: Howard, J., Hoyt, S., Isensee, K., Telszewski, M., Pidgeon, E. (Eds.), 2014. Conservational International, Intergovernmental Oceanographic Commission of UNESCO. International Union for Conservation of Nature, Arlington, Virginia, USA.
Jennerjahn, T.C., 2020. Relevance and magnitude of "blue carbon" storage in mangrove sediments: carbon accumulation rates vs. stocks, sources vs. sinks. Estuar. Coast. Shelf Sci. 247, 107027 https://doi.org/10.1016/j.ecss.2020.107027.
Jupin, J.L.J., Ruiz-Fernández, A.C., Sifeddine, A., Sanchez-Cabeza, J.A., Pérez-Bernal, L. H., Cardoso-Mohedano, J.G., Gómez-Ponce, M.A., Flores-Trujillo, J.G., 2023. Anthropogenic drivers of increasing sediment accumulation in contrasting Mexican mangrove ecosystems. Catena (Amst) 226, 107037. https://doi.org/10.1016/j.catena.2023.107037.
Kauffman, J.B., Heider, C., Norfolk, J., Payton, F., 2014. Carbon stocks of intact mangroves and carbon emissions arising from their conversion in the Dominican Republic. Ecol. Appl. 24, 518–527. https://doi.org/10.1890/13-0640.1.
Kauffman, J.B., Adame, M.F., Arifanti, V.B., Schile-Beers, L.M., Bernardino, A.F., Bhomia, R.K., Donato, D.C., Feller, I.C., Ferreira, T.O., Jesus Garcia, M. del C., MacKenzie, R.A., Megonigal, J.P., Murdiyarso, D., Simpson, L., Hernández Trejo, H., 2020. Total ecosystem carbon stocks of mangroves across broad global environmental and physical gradients. Ecological monographs 90. https://doi.org/10.1002/ecm.1405.
Kusumaningtyas, M.A., Hutahaean, A.A., Fischer, H.W., Pérez-Mayo, M., Ransby, D., Jennerjahn, T.C., 2019. Variability in the organic carbon stocks, sources, and accumulation rates of Indonesian mangrove ecosystems. Estuar. Coast. Shelf Sci. 218, 310–323. https://doi.org/10.1016/j.ecss.2018.12.007.
Lallier-Vergès, E., Perrussel, B.P., Disnar, J.R., Baltzer, F., 1998. Relationships between environmental conditions and the diagenetic evolution of organic matter derived from higher plants in a modern mangrove swamp system (Guadeloupe, French West Indies). Org. Geochem. 29, 1663–1686. https://doi.org/10.1016/S0146-6380(98)00179-X.
Lavery, P., Lafratta, A., Serrano, O., Masque, P., Jones, A., Fernandes, M., Gaylard, S., Gillanders, B., 2019. Coastal carbon opportunities: carbon storage and accumulation rates at three case study sites. In: Technical Report Series No. 19/21 (Adelaide).
López-Mendoza, P.G., Ruiz-Fernández, A.C., Sanchez-Cabeza, J.A., van Tussenbroek, B.I., Cuellar-Martinez, T., Pérez-Bernal, L.H., 2020. Temporal trends of organic carbon accumulation in seagrass meadows from the northern Mexican Caribbean. Catena (Amst.) 194, 104645. https://doi.org/10.1016/j.catena.2020.104645.
Lovelock, C.E., Fourqurean, J.W., Morris, J.T., 2017. Modeled CO2 emissions from coastal wetland transitions to other land uses: tidal marshes, mangrove forests, and seagrass beds. Front. Mar. Sci. 4, 1–11. https://doi.org/10.3389/fmars.2017.00143.
Macreadie, P.I., Anton, A., Raven, J.A., Beaumont, N.J., Connolly, R.M., Friess, D.A., Kelleway, J.J., Kennedy, H., Kuwae, T., Lavery, P.S., Lovelock, C.E., Smale, D.A., Apostolaki, E.T., Atwood, T.B., Baldock, J.A., Bianchi, T.S., Chmura, G.L., Eyre, B.D., Fourqurean, J.W., Hall-Spencer, J.M., Huxham, M., Hendriks, I.E., Krause-Jensen, D., Laffoley, D., Luisetti, T., Marbà, N., Masque, P., McGlathery, K.J., Megonigal, J.P., Murdiyarso, D., Russell, B.D., Santos, I.R., Serrano, O., Silliman, B. R., Watanabe, K., Duarte, C.M., 2019. The future of blue carbon science. Nat. Commun. 10, 1–13. https://doi.org/10.1038/s41467-019-11693-w.
Marchand, C., Disnar, J.R., Lallier-Vergès, E., Lottier, N., Lallier-Vergès, E., Lottier, N., 2005. Early diagenesis of carbohydrates and lignin in mangrove sediments subject to variable redox conditions (French Guiana). Geochim. Cosmochim. Acta 69, 131–142. https://doi.org/10.1016/j.gca.2004.06.016.

McKee, K.L., 2011. Biophysical controls on accretion and elevation change in Caribbean mangrove ecosystems. Estuar. Coast. Shelf Sci. 91, 475–483. https://doi.org/10.1016/j.ecss.2010.05.001.

Mckee, K.L., Cahoon, D.R., Feller, I.C., 2007. Caribbean mangroves adjust to rising sea level through biotic controls on change in soil elevation. Glob. Ecol. Biogeogr. 16, 545–556. https://doi.org/10.1111/j.1466-8238.2007.00317.x.

Medina-Contreras, D., Sánchez, A., Arenas, F., 2023. Macroinvertebrates food web and trophic relations of a peri urban mangrove system in a semi-arid region, Gulf of California, México. J. Mar. Syst. 240 https://doi.org/10.1016/j.jmarsys.2023.103864.

Medina-Gómez, I., Villalobos-Zapata, G.J., Herrera-Silveira, J.A., 2015. Spatial and temporal hydrological variations in the inner estuaries of a large coastal lagoon of the Southern Gulf of Mexico. J. Coast. Res. 316, 1429–1438. https://doi.org/10.2112/jcoastres-d-13-00226.1.

Menges, J., Hovius, N., Andermann, C., Lupker, M., Haghipour, N., Märki, L., Sachse, D., 2020. Variations in organic carbon sourcing along a trans-Himalayan river determined by a Bayesian mixing approach. Geochim. Cosmochim. Acta 286, 159–176. https://doi.org/10.1016/j.gca.2020.07.003.

Meyers, P.A., 1997. Organic geochemical proxies of paleoceanographic, paleolimnologic, and paleoclimatic processes. Org. Geochem. 27, 213–250. https://doi.org/10.1016/S0146-6380(97)00049-1.

Monjardín-Armenta, S.A., Pacheco-Angulo, C.E., Plata-Rocha, W., Corrales-Barraza, G., 2017. La deforestación and sus factores causales en el estado de Sinaloa, México. Madera Bosques 23, 7–22. https://doi.org/10.21829/myb.2017.2311482.

Moore, J.W., Semmens, B.X., 2008. Incorporating uncertainty and prior information into stable isotope mixing models. Ecol. Lett. 11, 470–480. https://doi.org/10.1111/j.1461-0248.2008.01163.x.

Morris, J.T., Barber, D.C., Callaway, J.C., Chambers, R., Hagen, S.C., Hopkinson, C.S., Johnson, B.J., Megonigal, P., Neubauer, S.C., Troxler, T., Wigand, C., 2016. Contributions of organic and inorganic matter to sediment volume and accretion in tidal wetlands at steady state. Earths Futur. 4, 110–121. https://doi.org/10.1002/2015EF000334.

Murdiyarso, D., Purbopuspito, J., Kauffman, J.B., Warren, M.W., Sasmito, S.D., Donato, D.C., Manuri, S., Krisnawati, H., Taberima, S., Kurnianto, S., 2015. The potential of Indonesian mangrove forests for global climate change mitigation. Nat. Clim. Chang. 5, 1089–1092. https://doi.org/10.1038/nclimate2734.

Ochoa, E.P., 2003. Ficha Informativa de los Humedales de Ramsar (FIR), pp. 1–17.

Ortiz-Pérez, M.A., de la Lanza-Espino, G., 2006. Diferenciación del espacio costero de México: un inventario regional. Geografía para el Siglo XXI. Universidad Nacional Autónoma de México, Instituto de Geografía, CDMX.

Parnell, A.C., Inger, R., Bearhop, S., Jackson, A.L., 2010. Source partitioning using stable isotopes: coping with too much variation. PloS One 5. https://doi.org/10.1371/journal.pone.0009672.

Parnell, A.C., Phillips, D.L., Bearhop, S., Semmens, B.X., Ward, E.J., Moore, J.W., Jackson, A.L., Grey, J., Kelly, D.J., Inger, R., 2013. Bayesian stable isotope mixing models. Environmetrics 24, 387–399. https://doi.org/10.1002/env.2221.

Pendleton, L., Donato, D.C., Murray, B.C., Crooks, S., Jenkins, W.A., Sifleet, S., Craft, C., Fourqurean, J.W., Kauffman, J.B., Marbà, N., Megonigal, P., Pidgeon, E., Herr, D., Gordon, D., Baldera, A., 2012. Estimating global "blue carbon" emissions from conversion and degradation of vegetated coastal ecosystems. PloS One 7, e43542. https://doi.org/10.1371/journal.pone.0043542.

Pérez, A., Libardoni, B.G., Sanders, C.J., 2018. Factors influencing organic carbon accumulation in mangrove ecosystems. Biol. Lett. 14, 20180237. https://doi.org/10.1098/rsbl.2018.0237.

Primavera, Jurgenne H., Friess, D.A., Van Lavieren, H., Lee, S.Y., 2019a. The mangrove ecosystem. In: Press, Academic (Ed.), World Seas: An Environmental Evaluation. Elsevier, pp. 1–34. https://doi.org/10.1016/B978-0-12-805052-1.00001-2.

Primavera, J.H., Friess, D.A., Van Lavieren, H., Lee, S.Y., 2019b. The mangrove ecosystem. In: World Seas: An Environmental Evaluation Volume III: Ecological Issues and Environmental Impacts, 2nd ed. Elsevier Ltd. https://doi.org/10.1016/B978-0-12-805052-1.00001-2 666p.

Ramos-Miranda, J., Villalobos-Zapata, G.J., 2015. Aspectos socioambientales de la región de la laguna de Términos. Universidad Autónoma de Campeche, Campeche.

Rendón-Von Osten, J., Memije, M.G., Ortiz, A., Soares, A.M.V.M., Guilhermino, L., 2006. An integrated approach to assess water quality and environmental contamination in the fluvial-lagoon system of the Palizada River, Mexico. Environ. Toxicol. Chem. 25, 3024–3034. https://doi.org/10.1897/05-491R.1.

Rosentreter, J.A., Maher, D.T., Erler, D.V., Murray, R.H., Eyre, B.D., 2018. Seasonal and temporal CO2 dynamics in three tropical mangrove creeks – a revision of global mangrove CO2 emissions. Geochim. Cosmochim. Acta 222, 729–745. https://doi.org/10.1016/j.gca.2017.11.026.

Ruiz-Fernández, A.C., Hillaire-Marcel, C., de Vernal, A., Machain-Castillo, M.L., Vásquez, L., Ghaleb, B., Aspiazu-Fabián, J.A., Páez-Osuna, F., 2009. Changes of coastal sedimentation in the Gulf of Tehuantepec, South Pacific Mexico, over the last 100 years from short-lived radionuclide measurements. Estuar. Coast. Shelf Sci. 82, 525–536. https://doi.org/10.1016/j.ecss.2009.02.019.

Ruiz-Fernández, A.C., Agraz-Hernández, C.M., Sanchez-Cabeza, J.A., Díaz-Asencio, M., Pérez-Bernal, L.H., Chan Keb, C.A., López-Mendoza, P.G., Blanco y Correa, J.M., Ontiveros-Cuadras, J.F., Osti Saenz, J., Reyes Castellanos, J.E., 2018a. Sediment geochemistry, accumulation rates and forest structure in a large tropical mangrove ecosystem. Wetlands 38, 307–325. https://doi.org/10.1007/s13157-017-0969-2.

Ruiz-Fernández, A.C., Carnero-Bravo, V., Sánchez-Cabeza, J.A., Pérez-Bernal, L.H., Amaya-Monterrosa, O.A., Bojórquez-Sánchez, S., López-Mendoza, P.G., Cardoso-Mohedano, J.G., Dunbar, R.B., Mucciarone, D.A., Marmolejo-Rodríguez, A.J., 2018b. Carbon burial and storage in tropical salt marshes under the influence of sea level rise. Sci. Total Environ. 630, 1628–1640. https://doi.org/10.1016/j.scitotenv.2018.02.246.

Ruiz-Fernández, A.C., Sanchez-Cabeza, J.A., Cuéllar-Martínez, T., Pérez-Bernal, L.H., Carnero-Bravo, V., Ávila, E., Cardoso-mohedano, J.G., Sanchez-Cabeza, J.A., Cuéllar-Martínez, T., Pérez-Bernal, L.H., Carnero-Bravo, V., Ávila, E., Cardoso-mohedano, J.G., 2020. Increasing salinization and organic carbon burial rates in seagrass meadows from an anthropogenically-modified coastal lagoon in southern Gulf of Mexico. Estuar. Coast. Shelf Sci. 242, 106843 https://doi.org/10.1016/j.ecss.2020.106843.

Sanchez-Cabeza, J.A., Ruiz-Fernández, A.C., 2012. 210Pb sediment radiochronology: an integrated formulation and classification of dating models. Geochim. Cosmochim. Acta 82, 183–200. https://doi.org/10.1016/j.gca.2010.12.024.

Sanchez-Cabeza, J.A., Ruiz-Fernández, A.C., Ontiveros-Cuadras, J.F., Pérez Bernal, L.H., Olid, C., 2014. Monte Carlo uncertainty calculation of 210Pb chronologies and accumulation rates of sediments and peat bogs. Quat. Geochronol. 23, 80–93. https://doi.org/10.1016/j.quageo.2014.06.002.

Sasmito, S.D., Kuzyakov, Y., Lubis, A.A., Murdiyarso, D., Hutley, L.B., Bachri, S., Friess, D.A., Martius, C., Borchard, N., 2020. Organic carbon burial and sources in soils of coastal mudflat and mangrove ecosystems. Catena (Amst.) 187, 104414. https://doi.org/10.1016/j.catena.2019.104414.

Sepúlveda-Lozada, A., Mendoza-Carranza, M., Wolff, M., Saint-Paul, U., Ponce-Mendoza, A., 2015. Differences in food web structure of mangroves and freshwater marshes: evidence from stable isotope studies in the southern Gulf of Mexico. Wetl. Ecol. Manag. 23, 293–314. https://doi.org/10.1007/s11273-014-9382-2.

Sepúlveda-Lozada, A., Saint-Paul, U., Mendoza-Carranza, M., Wolff, M., Yáñez-Arancibia, A., 2017. Flood pulse induced changes in isotopic niche and resource utilization of consumers in a Mexican floodplain system. Aquat. Sci. 79, 597–616. https://doi.org/10.1007/s00027-017-0520-9.

Sidik, F., Friess, D.A., 2021. Dynamic Sedimentary Environments of Mangrove Coasts. Elsevier. https://doi.org/10.1016/C2018-0-00130-9.

Smoak, J.M., Breithaupt, J.L., Smith, T.J., Sanders, C.J., 2013. Sediment accretion and organic carbon burial relative to sea-level rise and storm events in two mangrove forests in Everglades National Park. Catena (Amst.) 104, 58–66. https://doi.org/10.1016/j.catena.2012.10.009.

Soria-Barreto, M., Montaña, C.G., Winemiller, K.O., Castillo, M.M., Rodiles-Hernández, R., 2021. Seasonal variation in basal resources supporting fish biomass in longitudinal zones of the Usumacinta River Basin, southern Mexico. Mar. Freshw. Res. 72, 353–364. https://doi.org/10.1071/MF19341.

Soto-Galera, E., Piera, J., López, P., 2010. Spatial and temporal land cover changes in Terminos Lagoon Reserve, Mexico. Rev. Biol. Trop. 58, 565–575. https://doi.org/10.15517/rbt.v58i2.5229.

Stock, B., Semmens, B., 2016a. Unifying error structures in commonly used biotracer mixing models. Ecology 97, 2562–2569. https://doi.org/10.1002/ecy.1517.

Stock, B., Semmens, B., 2016b. MixSIAR GUI User Manual v3.1 (Version 3.1).

Stock, B.C., Jackson, A.L., Ward, E.J., Parnell, A.C., Phillips, D.L., Semmens, B.X., 2018. Analyzing mixing systems using a new generation of Bayesian tracer mixing models. PeerJ 6, e5096. https://doi.org/10.7717/peerj.5096.

UN, 2015. on Climate Change (21st Session, Paris). United Nations, p. 25. https://unfccc.int/sites/default/files/english_paris_agreement.pdf.

Valiela, I., Bowen, J.L., York, J.K., 2001. Mangrove forests: one of the world's threatened major tropical environments. Bioscience 51, 807–815. https://doi.org/10.1641/0006-3568(2001)051[0807:MFOOTW]2.0.CO;2.

Woodroffe, C.D., Rogers, K., McKee, K.L., Lovelock, C.E., Mendelssohn, I.A., Saintilan, N., 2016. Mangrove sedimentation and response to relative sea-level rise. Ann. Rev. Mar. Sci. 8, 243–266. https://doi.org/10.1146/annurev-marine-122414-034025.

Yáñez-Arancibia, A., Day, J.W., 1982. Ecological characterization of Terminos Lagoon, a tropical lagoon-estuarine system in the southern Gulf of Mexico. Oceanol. Acta 5, 431–440.

CHAPTER 4

SPATIAL AND TEMPORAL VARIABILITY OF ORGANIC CARBON COMPOSITION AND STABILITY

The fourth chapter focuses on evaluating the temporal variability of C_{org} composition and stability over the studied period (<100 years) in four of the seven sediment cores from LT and EV. The determination of the quantity and stability of C_{org} and the composition of organic matter (OM) in mangrove sediments was carried out using Rock-Eval® pyrolysis and palynofacies analysis. Rock-Eval pyrolysis involves a programmed temperature pyrolyzer that quantifies and identifies different C_{org} species released during two successive stages of pyrolysis (heating in the absence of oxygen) and combustion (heating in the presence of oxygen). It has been used as a tool to simulate the natural decomposition of OM in sediment during early diagenesis. Higher resistance to temperature indicates greater stability of the organic material, which reflects its 'refractory,' 'recalcitrant,' or 'resistant' nature. In contrast, labile OM, which degrades at temperatures below 400°C, generally includes easily decomposable organic compounds that can be rapidly eliminated during the early stages of diagenesis. Palynofacies analysis, on the other hand, allows the quantification and identification of organic compounds that can be classified based on their source (i.e., terrestrial or aquatic), their characteristics (i.e., biogenic, anthropogenic, or fossil), and their formation process (i.e., biodegradation, oxidation, or combustion). Based on the combined results of Rock-Eval and palynofacies, the labile and refractory proportions in C_{org} stocks were reported, allowing the determination of whether the mangrove sediments at the study sites were sinks or sources of C_{org}.

The main questions addressed in this study were: (1) Are there differences in the quantity and stability of C_{org}, as well as the origin and composition of OM, between the sites?; (2) What has been the evolution of the quantity and stability of sedimentary C_{org} over the last century?; and (3) Can these mangrove sediments be considered sinks or sources of atmospheric CO_2? The hypothesis suggested that specific site characteristics (e.g., deforestation, land-use change) could reflect differences in the origin, storage, and preservation of C_{org} in mangrove sediments. The previously observed increase in sediment accumulation at the sites could induce a shift in the dominant type of C_{org}, from autochthonous to allochthonous, which in turn could reduce the lability of the C_{org} stored in mangrove sediments over time. This alteration in C_{org} provenance could eventually lead to a reduction in CO_2 emissions derived from the decomposition of the autochthonous labile Corg fraction.

The originality of this study lies in the detailed investigation of aspects such as the origin and composition of OM, and the quantity and stability of C_{org}, which had not been previously addressed in the studied mangrove sites. Establishing the stability of C_{org} stocks is crucial to determining whether these mangroves can be considered long-term C_{org} sinks, allowing us to evaluate whether their conservation constitutes a strategy for contributing to climate change mitigation. The results and interpretations of this work were compiled into the article titled "Predominance of allochthonous and refractory carbon in sediments from two contrasting Mexican mangrove ecosystems", published in open access in August 2024 in *CATENA*.

Catena 245 (2024) 108279

Contents lists available at ScienceDirect

Catena

journal homepage: www.elsevier.com/locate/catena

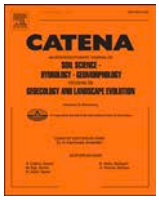

Predominance of allochthonous and refractory carbon in sediments from two contrasting Mexican mangrove ecosystems

J.L.J. Jupin [a,b], M. Boussafir [c], A. Sifeddine [b], A.C. Ruiz-Fernández [d,*], J.A. Sanchez-Cabeza [d], L. H. Pérez-Bernal [d]

[a] Posgrado en Ciencias del Mar y Limnología, Universidad Nacional Autónoma de México. Av. Universidad 3000, Ciudad Universitaria, Coyoacán, 04510, Ciudad de México, Mexico
[b] IRD, CNRS, SU, MNHN, IPSL, LOCEAN, Laboratoire d'Océanographie et du Climat : Expérimentation et Approches Numériques Centre IRD France Nord, 93143 Bondy, France
[c] Université de Tours, UR 6293, Géo-Hydrosystèmes Continentaux, Faculté des Sciences et Techniques, Parc de Grandmont, 37200 Tours, France
[d] Unidad Académica Mazatlán, Instituto de Ciencias del Mar y Limnología, Universidad Nacional Autónoma de México, 82040 Mazatlán, Sin., Mexico

ARTICLE INFO

Keywords:
Blue carbon
Organic carbon
Organic matter
Climate change
Mangroves
Rock-Eval
Palynofacies
Coastal lagoon
Ramsar

ABSTRACT

Mangroves are one of the most Blue Carbon-rich ecosystems worldwide, as they are highly efficient at storing and sequestering a large amount of organic carbon (C_{org}). The degradation of C_{org} inventories in mangrove sediments could cause carbon dioxide (CO_2) emissions, contributing to atmospheric warming. In this study, we used Rock-Eval pyrolysis and palynofacies identification to explore the composition and sources of organic matter (OM) and the quantity and liability of C_{org} in four ^{210}Pb-dated sediment cores from contrasting Mexican mangrove areas. The composition of terrestrial and refractory OM was similar in all cores, with variations attributed to the influence of the local river discharges on OM inputs and preservation. A progressive decrease in C_{org} quantity and lability from 2021 to 1990 in some cores was attributed to early diagenesis. Past precipitation and river discharge events appeared to have influenced carbon accumulation and preservation: increased influx and preservation of labile C_{org} in the sediments occurred during low river discharge and precipitation, whereas larger inputs and oxidation of refractory C_{org} occurred during high river discharge and precipitation. Sedimentary C_{org} stocks, assessed for 1921–2021, were primarily composed of refractory organic components, with degradation of allochthonous and autochthonous C_{org} mainly occurring before sediment burial. Sediments acted as efficient and long-term sinks for the C_{org} supplied to these mangroves, particularly in the context of increasing C_{org} inputs caused by an acceleration since the 1950s in continental erosion.

1. Introduction

Mangroves are considered high-priority ecosystems for large-scale international conservation efforts due to their high efficiency in storing Blue Carbon (i.e., carbon stored in coastal vegetated ecosystems), particularly in the context of climate change (Alongi, 2020; Friess et al., 2020). Those shrub-and-tree-dominated, intertidal, and salt-tolerant communities are important in the carbon cycle at local and global scales, owing to their (i) high primary production enhanced by nutrient trapping and recycling (Holguin et al., 2001); (ii) high organic carbon (C_{org}) accumulation from autochthonous (*in situ* litter and root production) and allochthonous inputs from adjacent habitats (Donato et al., 2011), and (iii) low rates of C_{org} decomposition due to suboxic to anoxic conditions (Alongi, 2005). The accumulation and preservation of C_{org} in mangrove ecosystems can exhibit high spatial and temporal variability, influenced by environmental settings (e.g., tidal, riverine, or wave-dominated), mangrove community structure, source and fluxes of allochthonous and autochthonous C_{org}, efficiency of C_{org} degradation during early diagenesis, and sediment accumulation rates (Woodroffe et al., 2005; Rovai et al., 2018).

While the majority of studies provide evidence that many mangrove forests effectively act as long-term sinks of atmospheric carbon dioxide (CO_2) and mitigate climate change (e.g., Bouillon et al., 2008; Kristensen et al., 2008), they may also be a source of greenhouse gases to the

* Corresponding author
E-mail addresses: johanna.jupin@ird.fr (J.L.J. Jupin), mohammed.boussafir@univ-tours.fr (M. Boussafir), abdel.sifeddine@ird.fr (A. Sifeddine), caro@ola.icmyl.unam.mx (A.C. Ruiz-Fernández), jasanchez@cmarl.unam.mx (J.A. Sanchez-Cabeza), lbernal@ola.icyml.unam.mx (L.H. Pérez-Bernal).

https://doi.org/10.1016/j.catena.2024.108279
Received 9 April 2024; Received in revised form 24 July 2024; Accepted 4 August 2024

atmosphere (e.g., Borges et al., 2003; Rosentreter et al., 2018), in particular CO_2 and methane (CH_4) emissions coming from the surrounding waters (Bouillon et al., 2003; Koné and Borges, 2008). This apparent discrepancy can be attributed to the complex and dynamic nature of C_{org} accumulation and degradation processes (Rosentreter et al., 2018). This must be clarified since the role of mangroves as either sinks or sources of atmospheric CO_2 is fundamental in formulating effective strategies for mitigating climate change (Murdiyarso et al., 2015).

Rock-Eval® pyrolysis is a rapid and cost-effective method for determining the organic matter (OM) content of samples, including both organic and inorganic carbon fractions. The temperature-programmed pyrolyzer identifies OM sources, maturation types, and stages in diverse environments, such as soil (e.g., Sebag et al., 2016; Le Meur et al., 2021), recent lake sediments (e.g., Boussafir et al., 2012; Zhang et al., 2023), marine sediments (e.g., Baudin et al., 2015 and references therein), and mangrove sediments (e.g., Duan et al., 2020; Marchand et al., 2008). Rock-Eval can serve as a simulation of the natural OM decomposition during early diagenesis in sediments (Disnar, 1994; Williams and Rosenheim, 2015) and facilitates the determination of variations in OM stability over depth, time, and across different sites. The stability of OM is revealed through its resistance to thermal cracking during the Rock-Eval pyrolysis (Disnar et al., 2003), with higher temperature resistance indicating greater stability of the organic material and its 'refractory', 'recalcitrant' or 'resistant' character. Conversely, thermally labile OM is generally composed of readily decomposable organic compounds that can be rapidly removed during the earliest stages of diagenesis.

The complex interplay of factors, such as the variability of biological sources and soil environments, can challenge the interpretation of the Rock-Eval results (Disnar et al., 2003; Baudin et al., 2015). To address this, palynofacies analysis has commonly been used to complement Rock-Eval analyses of soil and sediment samples from continental, marine, and coastal environments (e.g., Sebag et al., 2006 and references therein), as it identifies and quantifies OM particles according to their source (terrestrial or aquatic), characteristics (biogenic, anthropogenic, or fossil), and formation process (biodegradation, oxidation, or combustion) (Combaz, 1964; Tyson, 1995).

Rock-Eval parameters and palynofacies analysis were used to determine C_{org} quantity and stability, and OM origin and composition in mangrove sediments from Términos Lagoon (TL) in the southern Gulf of Mexico and the El Verde Camacho Lagoon (EV) in the entrance of the Gulf of California. The Ramsar Convention recognizes TL and EV as wetlands of international importance (RSIS, 2024), as they exhibit rich biodiversity and serve as critical breeding grounds for numerous coastal species (Briseño-Dueñas, 2003; Venegas-Pérez, 2003). Despite higher precipitation, freshwater discharge, and land-use changes observed in TL compared to EV, a previous study on seven lead-210 (^{210}Pb) dated cores collected from mangrove sediments in both regions revealed a consistent century-long increase in sediment accumulation rates across all cores (Jupin et al., 2023).

In this study, four cores were re-examined with the hypotheses that site-specific characteristics would reflect differences in C_{org} origin, storage, and preservation within the mangrove ecosystems and that increasing sediment accumulation in the study sites may have induced a shift from autochthonous- to allochthonous-dominated C_{org} storage, thereby reducing the lability of sedimentary C_{org} stocks over time. The main questions addressed here were: (1) are the C_{org} quantity and stability and the OM origin and composition different among sites?; (2) what is the evolution of quantity and stability of the sedimentary C_{org} over the past century?; and (3) are these mangrove sediments a sink or a source of atmospheric CO_2?

2. Study sites

Términos Lagoon (TL), in the southern Gulf of Mexico, is Mexico's largest coastal lagoon (Fig. 1A). It is directly connected to the ocean via inlets on either side of Carmen Island, allowing a continuous influx of marine water into the lagoon. Most of the water that enters TL is fresh water from the Palizada River (9.08×10^9 m^3 yr^{-1}) and the Candelaria River discharge (1.6×10^9 m^3 yr^{-1}) (Fichez et al., 2017). The Palizada-del-Este (PDE) system, in the western TL zone, is the eastern part of the Grijalva-Usumacinta fluvial system, the largest river basin in Mexico; it has well-mixed conditions, low-salinity waters, and fine sediments. The climate is warm humid with an average annual temperature of 27 °C and abundant summer rains, averaging 1800 mm yr^{-1} (Bach et al., 2005; Yáñez-Arancibia and Day, 2005). In the eastern TL zone, the Candelaria-Panlau (CP) system has shallow lagoons and calcareous sediments, typical of the Yucatán calcareous peninsula. The climate of this eastern zone is warm sub-humid, with an average annual temperature of 27 °C and precipitation of 1400 mm yr^{-1}.

El Verde Camacho Lagoon (EV) is a 47-hectare internal coastal barrier lagoon (Fig. 1B), closed for most of the year but receiving marine water during the rainy season (June to October) when the sandbar is broken by the combined effects of the Quelite River water flow (0.11×10^9 m^3 yr^{-1}), high tides, and occasional tropical storms and hurricanes (Flores-Verdugo et al., 1995). The climate in the area is sub-humid tropical (García, 1973), with an average temperature of 25 °C and contrasting seasons. Depending on the sandbar status (open or closed) and the quantity of precipitation, averaging 750 mm yr^{-1} and falling mainly during the rainy season, the average salinity varies from 10 to 30 (CONAGUA, 2015).

3. Materials and methods

3.1. Sampling and dating

The four sediment cores were previously used for the evaluation of temporal variations in sediment accumulation in TL and EV, exploring how site characteristics (e.g., climate and anthropic activity) have influenced these trends over the past century; procedures for sampling and ^{210}Pb dating of the cores are detailed in Jupin et al. (2023). Briefly, four sediment push cores were collected by inserting PVC tubes (10 cm internal diameter, 1 m length) into the sediments of fringe mangrove communities (Fig. 1). The cores were extruded and sectioned every 1 cm, and samples were freeze-dried and ground to a powder. Age models and mass accumulation rates (MAR) were determined through the ^{210}Pb dating method using the Constant Flux model (Robbins, 1978; Sanchez-Cabeza and Ruiz-Fernández, 2012) and the radionuclide data (^{210}Pb, ^{226}Ra, and ^{137}Cs) obtained by gamma-ray spectrometry, as described in Díaz-Asencio et al., (2020). Sediment records spanned from 90 to 120 years, and MAR values varied from 0.03 ± 0.01 to 0.7 ± 0.6 g cm^{-2} yr^{-1} (Jupin et al., 2023).

3.2. Rock-Eval analysis

3.2.1. Concept and parameters

The composition and origin of OM and the concentration of C_{org} in the sediment samples were determined using a Rock-Eval 6® analyzer (Vinci Technologies™). About 60 mg of homogenized bulk sediment samples were analyzed by a pyrolysis program adapted for recent sediments, including two successive stages performed with heating rates of 30 °C min^{-1} (Baudin et al., 2015). It started with a sample pyrolysis (200–650 °C) under inert gas (helium), followed by an oxidation of the residual carbon (400–650 °C) under purified air. During the sequential program, the release of hydrocarbons (HC), carbon monoxide (CO), and CO_2 is continuously measured and reported in pyrograms; in particular, the S2 pyrogram corresponds with the quantity of HC compounds produced during the pyrolysis. The method's precision was determined by analyzing 20 sample duplicates; the coefficients of variation were < 4 % across the parameters and sediment cores.

Standard Rock-Eval parameters (Espitalié et al., 1977, 1985a, 1985b;

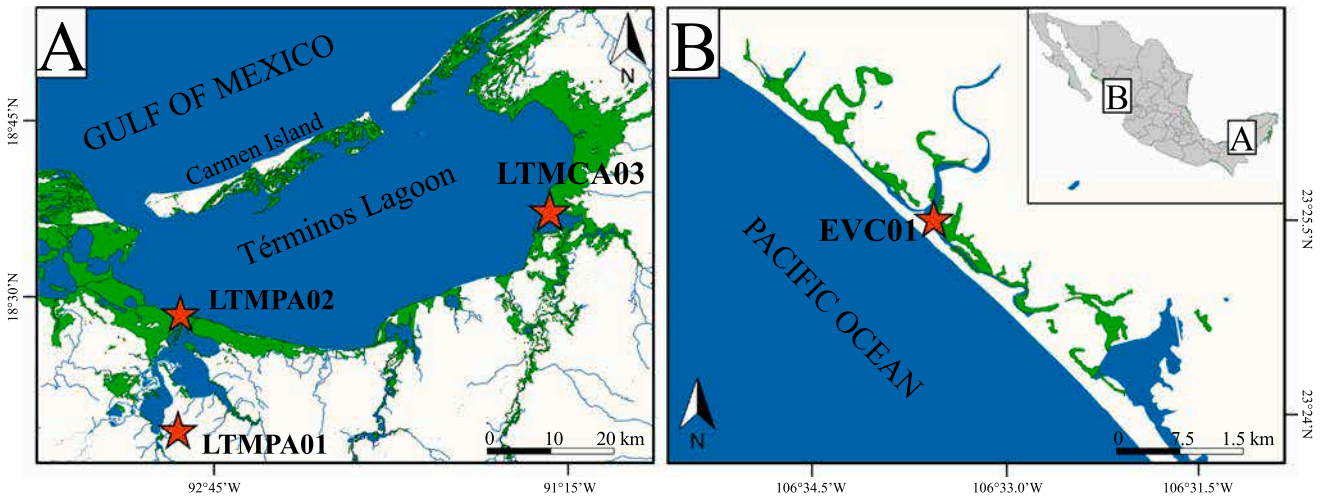

Fig. 1. Location of the sediment cores (★) from (A) Términos Lagoon (southern Gulf of Mexico) and (B) El Verde Camacho Lagoon (entrance of the Gulf of California). Green shading indicate the presence of mangrove areas.

Lafargue et al., 1998) were calculated to assess the C_{org} concentration and stability. The pyrolyzed carbon (PC, in %) corresponds to the carbon species (HC, CO, and CO_2) released during the pyrolysis stage, whereas the residual carbon (RC, %) is the most refractory fraction released as CO and CO_2 during the oxidation phase. The total organic carbon (TOC, %) content is the sum of the PC and RC fractions. The hydrogen index (HI, mg HC g^{-1} TOC) represents the quantity of HC produced during pyrolysis normalized to the TOC, indicating the hydrogen richness of OM, whereas the oxygen index (OI, mg CO_2 g^{-1} TOC) is the amount of oxygen released as CO and CO_2 during the pyrolysis and oxidation phases normalized to the TOC, indicating the oxygen richness and/or oxidation degree of OM.

The parameter R400 (i.e., the fraction of the S2 pyrogram integrated before 400 °C) was used to qualitatively interpret the diagenetic evolution of labile *versus* refractory C_{org} (Disnar et al., 2003). This is based on the concept that pyrolysis for readily labile biological compounds is generally finished at 400 °C, R400 is typically expressed as a percentage of the total integrated S2 curve. A novel parameter, $R400_{PC}$ (mg HC g^{-1}), was defined in this study to facilitate the quantitative interpretation of R400. It was calculated by multiplying R400 (%) by the quantity of PC content in the S2 curve (mg HC g^{-1}).

Three core sections (top, intermediate, and bottom) were defined to investigate distinct depositional conditions and diagenetic processes influencing the C_{org} quantity and stability along the cores based on the variation in Rock-Eval parameters. The non-parametric Kruskal-Wallis one-way analysis of variance and post-hoc Dunn tests were used to evaluate the differences in the rank distribution of Rock-Eval parameter values among cores. Additionally, associations between variables were assessed using Spearman correlation analysis and Student's *t*-test. All analyses were conducted with a confidence level of 95 %.

3.2.2. Analysis of organic matter source and stability

A pseudo van Krevelen diagram (HI *versus* OI) was used to identify OM sources, stability, and diagenetic processes (Baudin et al., 2015). Higher HI and lower OI values indicate thermally labile organic material from lacustrine (Type I) or marine (Type II) phytoplankton sources. Conversely, lower HI and higher OI values (Type III) indicate terrestrial inputs or well-oxidized organic material from Types I and II (Le Meur et al., 2021). The S2 pyrogram often does not follow a Gaussian distribution in immature samples such as mangrove sediments. Instead, it has multiple peaks or shoulders, indicating that the samples consist of a mixture of different fractions or clusters of organic components undergoing thermal degradation at various specific temperatures (e.g., Disnar and Trichet, 1984; Disnar et al., 2003; Sebag et al., 2016). To identify these distinct clusters from the multilobed S2 signal, mathematical deconvolution was used to isolate five elemental Gaussian distributions with peaks at well-defined temperatures of 300 °C, 360 °C, 415 °C, 470 °C, and 560 °C (±15 °C) (Table S1; Figs S1 to S4 in Supplementary Material). A semi-quantitative calculation determined the relative contributions (%) of each organic component pool from the S2 signal (Disnar et al., 2003; Le Meur et al., 2021). This contribution was then multiplied by the PC content (mg HC g^{-1}) in the S2 curve and expressed as a ratio to sediment mass (mg HC g^{-1}).

3.3. Palynofacies analysis

Five to six samples (~1 g) of each sediment core were selected in sections with apparent changes, peaks, or transitions observed in the Rock-Eval parameters TOC, HI, and OI. These changes served as indicators of potential shifts in the C_{org} quantity and stability within the sediment. Carbonates and silicates were eliminated using hydrochloric (50 mL) and hydrofluoric (50 mL) acids (Graz et al., 2010). Remnants were examined with a transmitted light microscope or under UV excitation (ZEISS Axioscope 5 Polarisation coupled to a camera ZEISS Axiocam 305 color) using a 50x magnification objective (Fig. 2).

Morphological and textural criteria allowed us to identify four main categories of components: (1) amorphous organic matter (AOM), lacking any discernible biological structures; (2) algal organic matter (algOM) derived from phytoplankton production, identified under UV light owing to the fluorescence of hydrocarbon-rich fractions (Boussafir et al., 2012); (3) lignocellulosic (LC) particles originating from higher plants characterized by an elongated shape; and (4) other particles with distinct and easily recognizable morphology (e.g., pollen, membrane) (Table 1). According to their characteristics, the particles were categorized as (a) preserved, including preserved or slightly degraded LC, cuticular and mycelial fragments, membranes, spores, pollen grains, and algOM; or (b) degraded, including floccular and gelified AOM, gelified and opaque LC, and opaque detritus.

Mass concentration of the particles was determined using a known pollen standard (10 mg mL^{-1}) incorporated into the samples (Battarbee and Kneen, 1982; de Vernal et al., 1987). *Cupressus* sp. was chosen as the standard because its strong reaction under UV excitation precludes confusion. Study particles and standards were counted per area unit delimited by the microscope's field of view. To ensure variations in relative abundances remained below 5 %, at least 500 area units per sediment sample were counted (Di-Giovanni et al., 1998; Sebag et al., 2006; Graz et al., 2010). The mass concentration of particles (mg g^{-1}) was estimated using the ratio between the areas (%) of studied particles

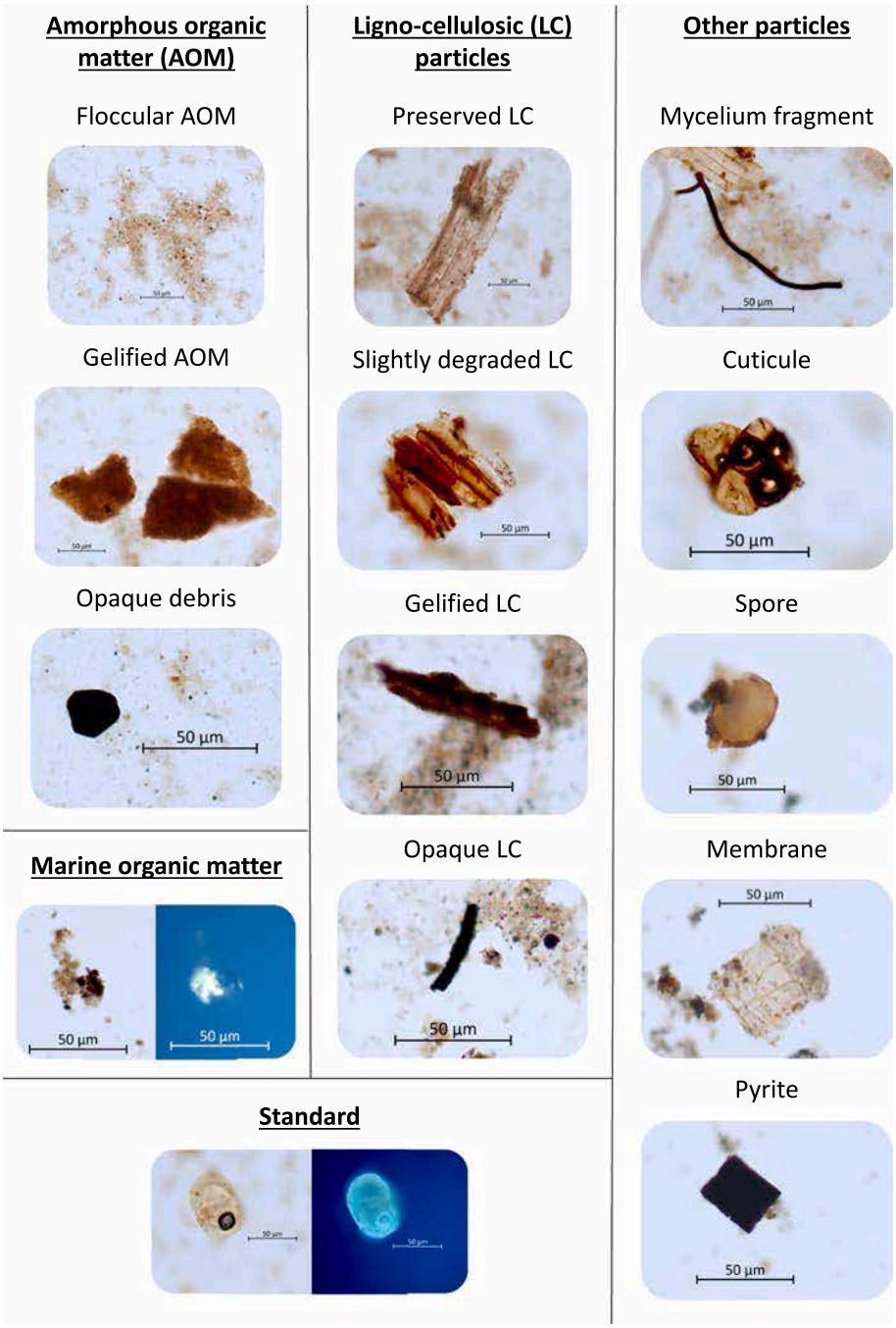

Fig. 2. Palynofacies categories in mangrove sediment cores from Términos Lagoon (southern Gulf of Mexico) and El Verde Camacho Lagoon (entrance of the Gulf of California).

and standards, multiplied by the standard mass concentration (mg mL^{-1}) in the sample (Graz et al., 2010).

3.4. Labile and refractory organic carbon stocks

The Rock-Eval-derived C_{org} stocks (i.e., the quantity of C_{org} stored per unit area, Mg ha^{-1}) were calculated per decade (C_{org} stocks$_{-10yr}$) and for the period from 1921 to 2021 (C_{org} stocks$_{-1921-2021}$) as the product of dry bulk density, section thickness, and C_{org} concentration (Howard et al., 2014). Labile C_{org} stocks included the most labile fraction of the PC (i.e., R400), whereas refractory C_{org} stocks were defined as the sum of the carbon pyrolyzed after 400 °C and the RC. The CO_2 equivalent (CO_{2eq}) emissions in case of significant loss of labile C_{org} fraction were calculated as the product of the labile C_{org} stocks, and the conversion factor of 3.67 (i.e., the ratio of C to CO_2 molecular weights) and were expressed as CO_{2eq} per hectare (Mg ha^{-1}) at decadal scale and over the 1921–2021 period (Howard et al., 2014).

4. Results

4.1. Basic Rock-Eval parameters

TOC in the sediment cores ranged from 0.38 % to 8.81 %, with a median of 2.17 % (Table 2). RC constituted the major fraction of the TOC (71–80 %), with PC at 20–29 %. The HI values ranged from 93 to 354 mg HC g^{-1} TOC, and OI values ranged from 115 to 332 mg CO_2 g^{-1} TOC,

Table 1
Characteristics of the organic particles in mangrove sediment cores form Términos Lagoon (southern Gulf of Mexico) and El Verde Camacho Lagoon (entrance of the Gulf of California).

Class	Abbreviation	Category	Characteristics	Group of preservation state
Amorphous particles	fAOM	Floccular amorphous organic matter	Diffuse edges. Gray to yellow in transmitted light, and opaque or slightly orange in reflected light. Size 10–100 μm.	Degraded
	gAOM	Gelified amorphous organic matter	Entirely gelified, without internal structure. Orange to red in transmitted light and dark orange in reflected light. Size can exceed 100 μm.	Degraded
	OD	Opaque debris	Sharp contours, high reflectance, and appears dark in transmitted light. Size ~ 10 μm.	Degraded
Phytoplankton particles	algOM	Algal OM	Transparent in reflected light. Brilliant yellow particles under fluorescent light.	Preserved
Lignocellulosic particles	PLC	Preserved or slightly degraded lignocellulosic	Elongated particles with visible internal structures, yellow in transmitted light. Size 10–100 μm.	Preserved
	GLC	Gelified lignocellulosic	Elongated particles with visible internal structures, yellow to orange in transmitted light. Size from 10 μm, and up to 100 μm with increased gelification.	Degraded
	OCL	Opaque lignocellulosic	No visible internal structure. Elongated. High reflectance. Size 10–100 μm.	Degraded
Other organic particles	Div	Preserved diverse organic particle	Mycelium fragments elongate, brown.	Preserved
			Cuticular fragments brown and with edges and botanic structures. Size variable and can exceed several hundred μm.	Preserved
			Spores and pollen grains from terrestrial and aquatic flora. Translucent or yellow when fresh, brown-orange when preserved.	Preserved
	Pyr	Pyrite	Opaque with geometrical forms under transmitted light	Degraded

Table 2
Rock-Eval parameters and clusters of organic components (C1 to C5) in mangrove sediment cores from Términos Lagoon (southern Gulf of Mexico) and El Verde Camacho Lagoon (entrance of the Gulf of California).

Variable	Statistics	LTMPA01	LTMPA02	LTMCA03	EVC01
TOC	Min	1.66	0.97	2.19	0.38
(%)	Max	8.14	3.25	8.81	3.91
	Mean	3.02	1.63	3.96	1.27
PC	Min	0.32	0.23	0.54	0.10
(%)	Max	2.18	0.95	3.17	0.87
	Mean	0.68	0.42	1.14	0.25
RC	Min	1.34	0.74	1.65	0.28
(%)	Max	5.96	2.30	5.64	3.04
	Mean	2.34	1.20	2.81	1.01
HI	Min	129	131	204	93
(mg HC g^{-1}	Max	218	251	354	195
TOC)	Mean	162	179	255	130
OI	Min	137	191	115	179
(mg CO_2 g^{-1}	Max	208	332	198	237
TOC)	Mean	182	255	154	211
R400	Min	0.36	0.30	0.27	0.23
(%)	Max	0.45	0.44	0.35	0.44
	Mean	0.40	0.36	0.29	0.34
$R400_{PC}$*	Min	3.54	2.40	2.96	1.84
(mg HC g^{-1} sed.)	Max	7.81	4.04	5.25	3.75
	Mean	4.40	3.12	3.78	2.67
C1*	Min	1.22	1.30	0.09	0.72
(mg HC g^{-1} sed.)	Max	3.41	4.43	1.23	3.03
	Mean	2.14	2.80	0.66	1.79
C2*	Min	0.64	1.68	3.38	2.04
(mg HC g^{-1} sed.)	Max	3.78	6.55	6.82	5.94
	Mean	2.38	2.93	4.87	3.92
C3*	Min	3.53	0.36	1.21	2.23
(mg HC g^{-1} sed.)	Max	8.75	4.61	3.58	5.51
	Mean	5.09	3.41	2.72	3.33
C4*	Min	5.22	6.23	7.18	6.16
(mg HC g^{-1} sed.)	Max	8.59	8.69	9.88	10.87
	Mean	7.08	7.47	8.84	7.95
C5*	Min	0.22	0.60	0.19	0.00
(mg HC g^{-1} sed.)	Max	1.36	1.28	0.80	0.96
	Mean	0.89	0.98	0.49	0.58

TOC, total organic carbon; PC, pyrolyzed carbon; RC, residual carbon; HI, hydrogen index; OI, oxygen index; R400 and $R400_{PC}$, hydrocarbons produced during pyrolysis before 400 °C with respect to the PC; C1-C5, clusters of organic components.

* Calculated as a ratio to sediment mass (see Methods).

indicating a general prevalence of terrestrial type (III) OM in the Van Krevelen pseudo-diagram (Fig. 3) across sediment cores. However, TOC, PC and HI values were significantly higher in LTMCA03 compared to other cores (LTMCA03 > LTMPA01 > LTMPA02 > EVC01), suggesting a higher proportion or better preservation of algal or mangrove-derived OM in this specific core. The OI values were significantly higher in LTMPA02 (>250 mg CO_2 g^{-1} TOC) than in the other cores (LTMPA02 > EVC01 > LTMPA01 > LTMCA03). R400 accounted for 29 % to 40 % of the S2 peak, and $R400_{PC}$ ranged from 1.84 to 7.81 mg HC g^{-1}.

The parameters TOC, PC, and RC exhibited strong correlations across all cores ($0.92 \leq r \leq 0.99$; $p < 0.05$). With increasing depth, TOC, PC, and RC values generally decreased in the top sections, showed low variability in intermediate sections, and increased by 1.12–1.24 % in LTMPA01 and LTMCA03, or remained unchanged in LTMPA02 and EVC01 in the bottom sections (Fig. 4). However, at 28–36 cm in LTMPA02 and 49–67 cm in LTMCA03, TOC, PC, and RC tended to increase with depth. In each core, TOC, R400, and $R400_{PC}$ increased from the 1950s to the 1960s, then accelerated towards the end of the century (Fig. 5).

HI and OI were significantly negatively correlated throughout the depth profile of LTMPA02 ($r = -0.75$, $p < 0.05$); no significant correlation was observed in the other cores. In the top sections of cores LTMPA02 and LTMCA03, trends of decreasing HI and increasing OI with depth were observed (Fig. 4). Contrasting changes in HI and OI were noted in the bottom sections of all cores. During the dating period, cores LTMPA01, LTMPA02, and LTMCA03 had a significant correlation between TOC and HI ($0.75 \leq r \leq 0.98$; $p < 0.05$), with both parameters showing increasing trends over time (Fig. 5). TOC and OI were negatively correlated in LTMPA02 ($r = -0.75$, $p < 0.05$) and positively correlated in LTMPA01 and EVC01 ($0.70 \leq r \leq 0.84$; $p < 0.05$).

4.2. Clusters of organic components

The dominant cluster was C4 (470 ± 15 °C), constituting 42–51 % of the total S2 peak, with concentrations ranging from 5.22 to 10.87 mg HC g^{-1} sed. (Table 1). On average, the second dominant clusters were C2 (360 ± 15 °C) in LTMCA03 (29 %) and EVC01 (25 %), and C3 (415 ± 15 °C) in the PDE system cores (LTMPA01: 27 %; LTMPA02: 19 %). C1 at 300 ± 15 °C (4–14 %) and C5 at 560 ± 15 °C (3–5 %) were minor clusters.

Generally, there was a trend of increasing C1 and decreasing C2 over depth (Figs. 4 and 5). A significant negative correlation between C1 and

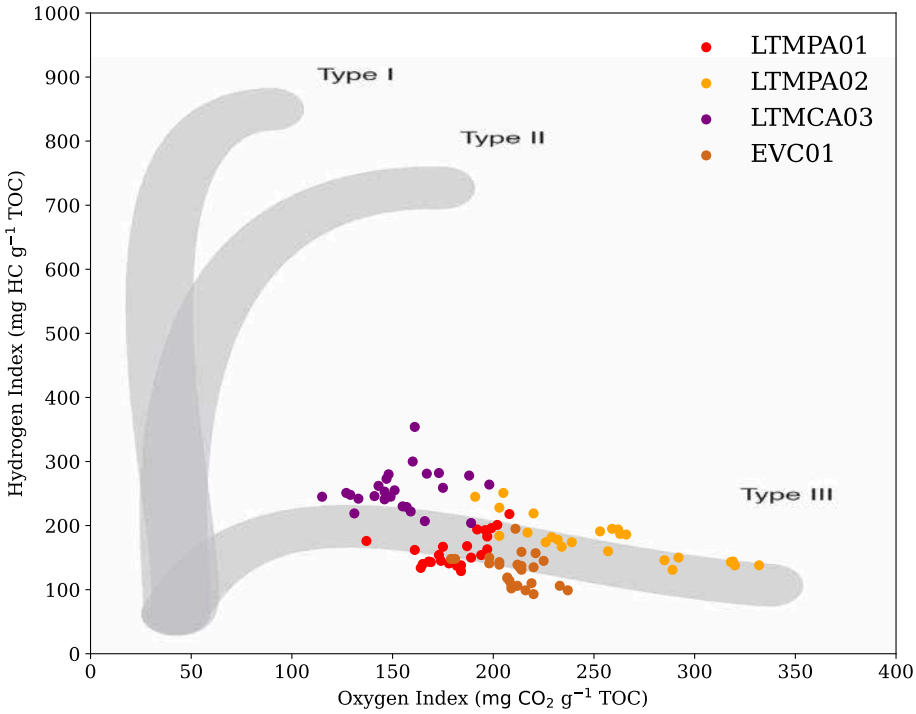

Fig. 3. Van Krevelen pseudo-diagram (Hydrogen Index *vs* Oxygen Index) for mangrove sediment cores from Términos Lagoon (southern Gulf of Mexico: LTM cores) and El Verde Camacho Lagoon (entrance of the Gulf of California: EVC core). TOC, total organic carbon; HC, hydrocarbons. Type of organic carbon: I, lacustrine; II, marine; III, terrestrial.

C2 was observed throughout all core depths of LTMCA03 ($r = -0.90$, $p < 0.05$). When considering only the dating period from 1918 to 2021, a significant negative correlation between C1 and C2 was also observed in LTMPA02 ($r = -0.79$, $p < 0.05$). C1 and C2 were not significantly correlated in cores LTMPA02 and EVC01. Clusters C3 and C4 showed little variations in the top and intermediate sections and were inversely related to each other in the bottom sections of the cores. No notable change was observed for cluster C5.

In sections 31–32 cm of LTMPA02, the S2 peak was unusual, showing two dominant peaks (Fig. S2 in Supplementary Material). As a consequence, these peaks, designated C2′ and C3′, were pyrolyzed at higher temperatures than the other depth sections, i.e., C2′ at 380 °C instead of the usual 360 °C for C2; C3′ at 430 °C instead of the usual 415 °C for C3.

4.3. Palynofacies identification

AOM was predominant among the palynofacies groups, comprising 70 % to 94 % of the total organic components in the cores (Fig. 6). Within this category, floccular AOM accounted for 49–92 %, whereas gelified AOM accounted for 1–38 %. LC particles accounted for only 5.6 % of the organic components among the cores, mostly in a gelified form (2.4 %). Preserved terrestrial organic particles (cuticular and mycelial fragments, membranes, spores, and pollen grains) constituted less than 1 % of all particles. The algOM accounted for 0.25 % in LTMPA01 and 1.02 % in the PDE cores but reached 3.80 % and 3.73 % in the top sections of cores LTMCA03 and EVC01. Degraded particles were dominant, constituting on average 92 % of the total particles in the samples from all cores (Fig. 6). Preserved particles were mainly concentrated in the top sections, with specific exceptions at 30–31 cm in LTMPA01, 31–32 cm in LTMPA02, and 47–48 cm in EVC01.

4.4. Organic carbon stocks

In the sediment cores, C_{org} stocks$_{\text{-10yr}}$ varied from 1.06–3.02 Mg ha^{-1} for 1921–1931 and 14.68–30.66 Mg ha^{-1} for 2011–2021. C_{org} stocks$_{\text{-10yr}}$ were highest (2.02–30.66 Mg ha^{-1}) in LTMPA01 and lowest (1.06–14.67 Mg ha^{-1}) in LTMPA02. The C_{org} stocks$_{\text{-1921-2021}}$ reached 42–89 Mg ha^{-1} among cores. Across all cores, C_{org} stocks$_{\text{-10yr}}$ increased from the early 1900 s to 2021, with noticeable acceleration after the 1950s (Fig. 7).

Throughout the period studied, the labile fraction represented 6–11 % of the total C_{org} stocks$_{\text{-10yr}}$, whereas refractory C_{org} stocks reached up to 89–94 % (Fig. 7). These proportions remained relatively constant over the last century, with a maximum difference of 0.3–2.1 % across all cores. The CO_{2eq} emissions that could be expected from the decomposition of the labile C_{org} stocks$_{\text{-10yr}}$ ranged from 0.35 to 12.10 Mg ha^{-1} across all cores, whereas those from the decomposition of the labile C_{org} stocks$_{\text{-1921-2021}}$ ranged from 13.8 to 31.2 Mg ha^{-1}.

5. Discussion

5.1. Sources and composition of organic matter

In all sediment cores, the restriction of OM to Type III on the Van Krevelen pseudo-diagram indicated that it was poor in hydrogenated compounds (hydrocarbons-rich OM) and rich in oxygenated ones (lignocellulosic-rich OM) (Fig. 3). The values of HI (93–354 mg HC g^{-1} TOC) and OI (115–332 mg CO_2 g^{-1} TOC) indicated a high proportion of terrestrial detritus compared to other sources (e.g., mangrove- or marine-derived OM); land-derived debris is usually lignocellulosic with low HI values (<250 mg HC g^{-1} TOC) associated with high OI values (>100 mg CO_2 g^{-1} TOC) (Meyers and Lallier-Vergès, 1999). Results suggested minor contribution of fresh mangrove detritus (420–556 mg HC g^{-1} TOC in mangrove leaf; 323–480 mg HC g^{-1} TOC in mangrove wood; Marchand et al., 2008), and marine-derived OM (HI>400 mg HC g^{-1} TOC; OI<100 mg CO_2 g^{-1} TOC; Meyers and Lallier-Vergès, 1999) that typically comprise hydrogen-rich compounds. However, low HI and high OI values may also suggest the oxidation of OM from mangrove or marine sources, as oxidation typically results in a decrease in HI, a slight increase in OI, and a modification of OM stability (Meyers and Lallier-

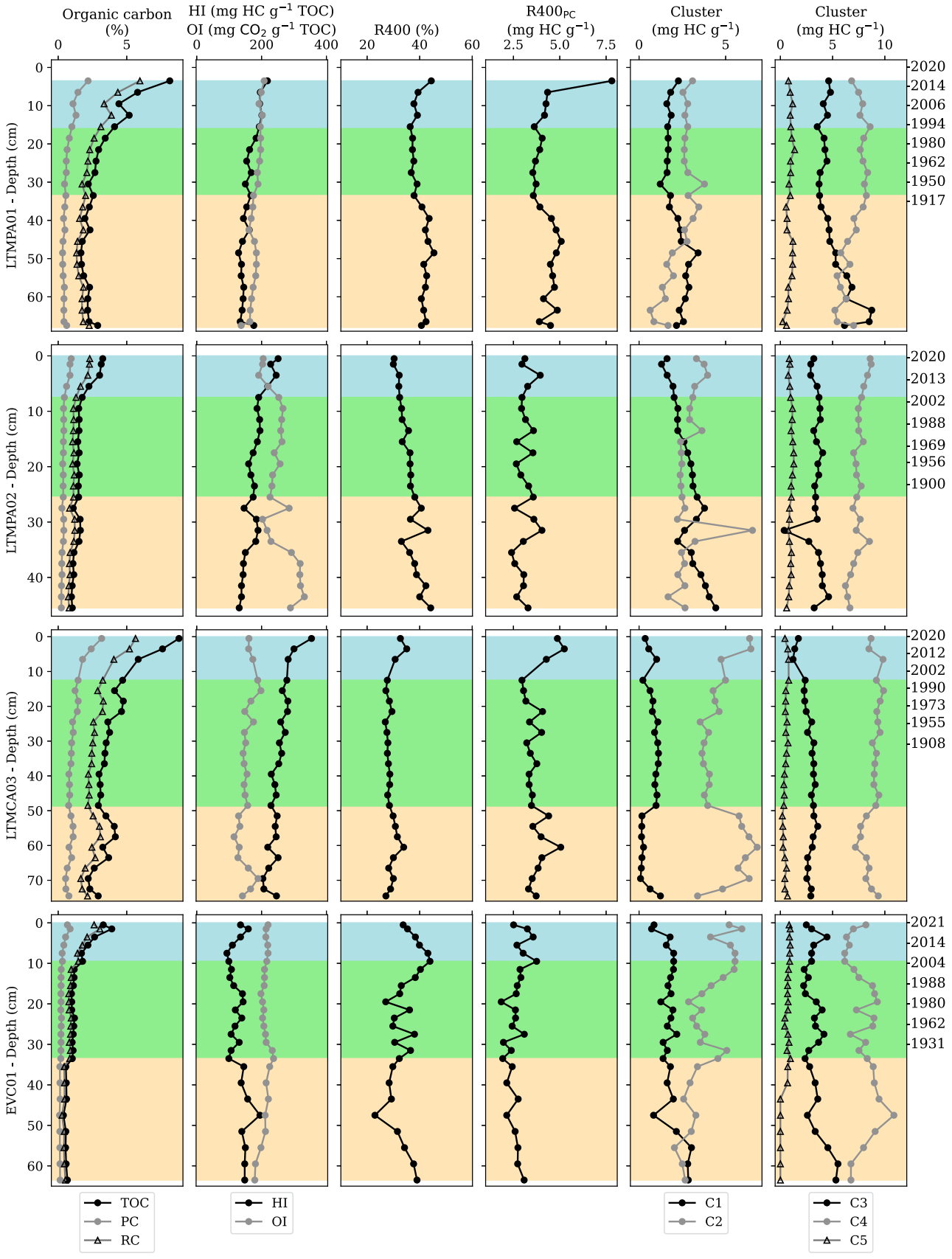

Fig. 4. Rock-Eval parameters (TOC, HI, OI, R400, and R400$_{PC}$) and clusters of organic components (C1 to C5) in mangrove sediment cores from Términos Lagoon (southern Gulf of Mexico) and El Verde Camacho Lagoon (entrance of the Gulf of California). Core sections: blue, bottom; green, intermediate; and yellow, bottom.

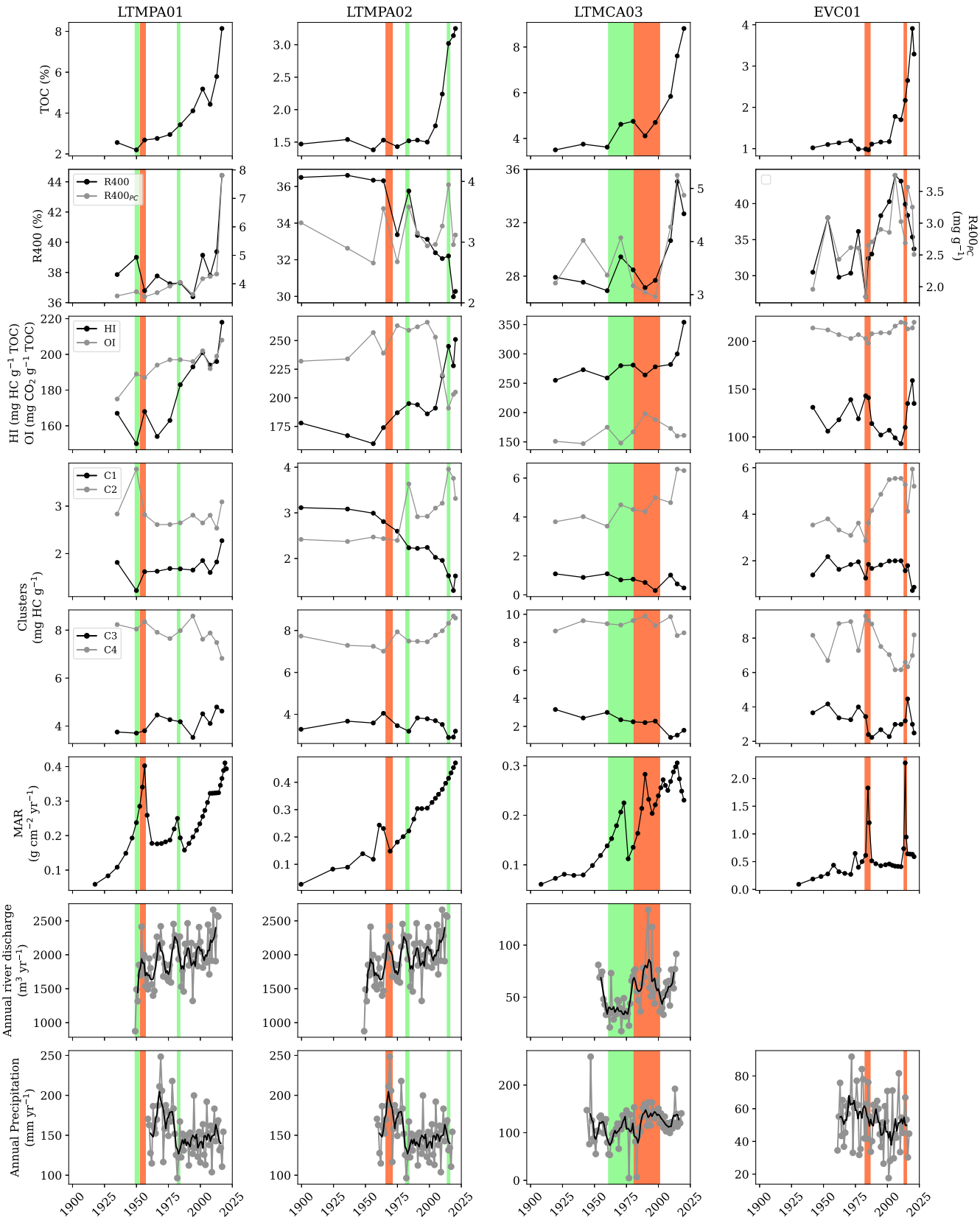

Fig. 5. Temporal variation of Rock-Eval parameters (TOC, HI, OI, R400, and R400$_{PC}$) and clusters of organic components (C1 to C5) in mangrove sediment cores from Términos Lagoon (southern Gulf of Mexico) and El Verde Camacho Lagoon (entrance of the Gulf of California). Time sections: green, events of enhanced organic carbon liability; red, events of decreased organic carbon liability. For mass accumulation rates (MAR), river discharges (when available), and precipitation data see Supplementary Material.

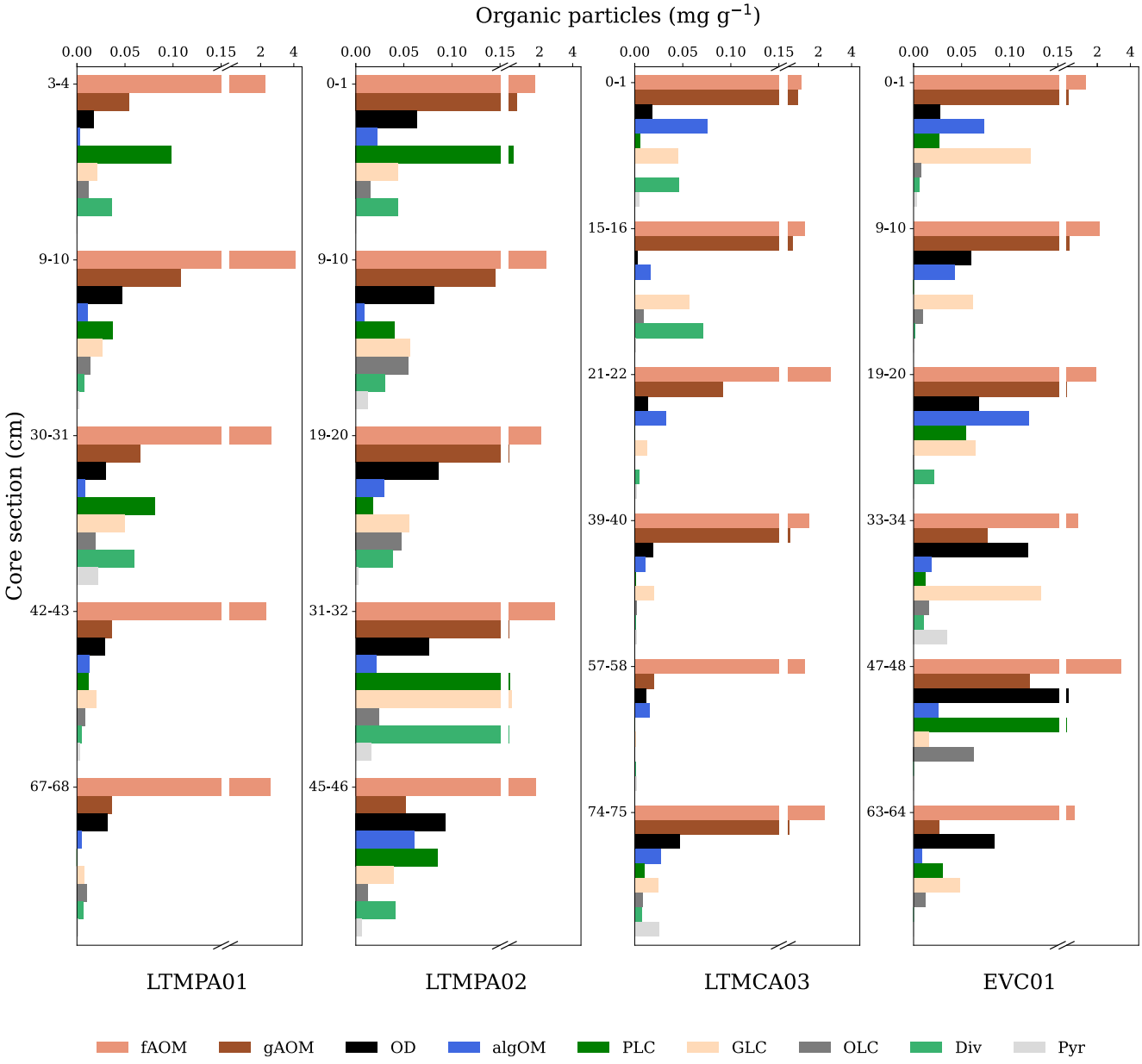

Fig. 6. Concentration of palynofacies in mangrove sediment cores from Términos Lagoon (southern Gulf of Mexico) and El Verde Camacho Lagoon (entrance of the Gulf of California). For palynofacies abbreviations see Table 1.

Vergès, 1999).

Although the Van Krevelen pseudo-diagram interpretation can provide insights into both the OM origin and liability, it may not directly pinpoint the specific contributions of each process (i.e., source and diagenetic state). However, the predominance of the palynofacies group AOM and the cluster C4 throughout the cores confirmed that most OM was in a refractory state when deposited in mangrove sediments. The AOM group indicated the presence of a mixture of plant, bacterial, algal, and planktonic fragments that have already undergone degradation (Batten and Stead, 2006; Sebag et al., 2006). The thermal breakdown of this mixture, observed at 470 ± 15 °C (C4), indicated high thermal stability and suggested resistance to microbial-driven decomposition. Low proportions of gelified AOM and LC suggested anoxic conditions during sequestration (Boussafir et al., 2012). Gelified LC typically originates from vascular plant tissues, likely mangrove leaves or wood, during the early stage of diagenesis under anoxic conditions (Lallier-Vergès et al., 1998).

The median C_{org} value of 2.17 % in these sites aligned with the global median of 2.2 % for mangrove ecosystems (Kristensen et al., 2008a). Consistent clusters of organic components and palynofacies across the cores indicated similarities in OM composition and sources among the mangrove sites. However, spatial variations in C_{org} concentrations were attributed to geomorphological, sedimentary, and local hydrological conditions specific to each site or core surroundings, influencing OM influx and preservation (Jupin et al., 2024b). The algal OM is more prone to decomposition than OM from higher plants and mangrove debris (Patience, 1996; Marchand et al., 2003; Ranjan et al., 2011), which may explain its relatively infrequent presence in the sediment cores. AlgOM contribution was higher in cores LTMCA03 and EVC01 from the smaller river systems (CP and EV), whereas the presence of algOM was less obvious in cores LTMPA02 and LTMPA01 from the PDE system, where the Palizada River dominates freshwater inputs to the Términos Lagoon (Contreras-Ruiz-Esparza et al., 2014).

Core LTMCA03 predominantly exhibited terrestrial characteristics with minor contribution of other OM sources, similar to cores LTMPA01, LTMPA02, and EVC01 (Fig. 3). However, significant higher values of

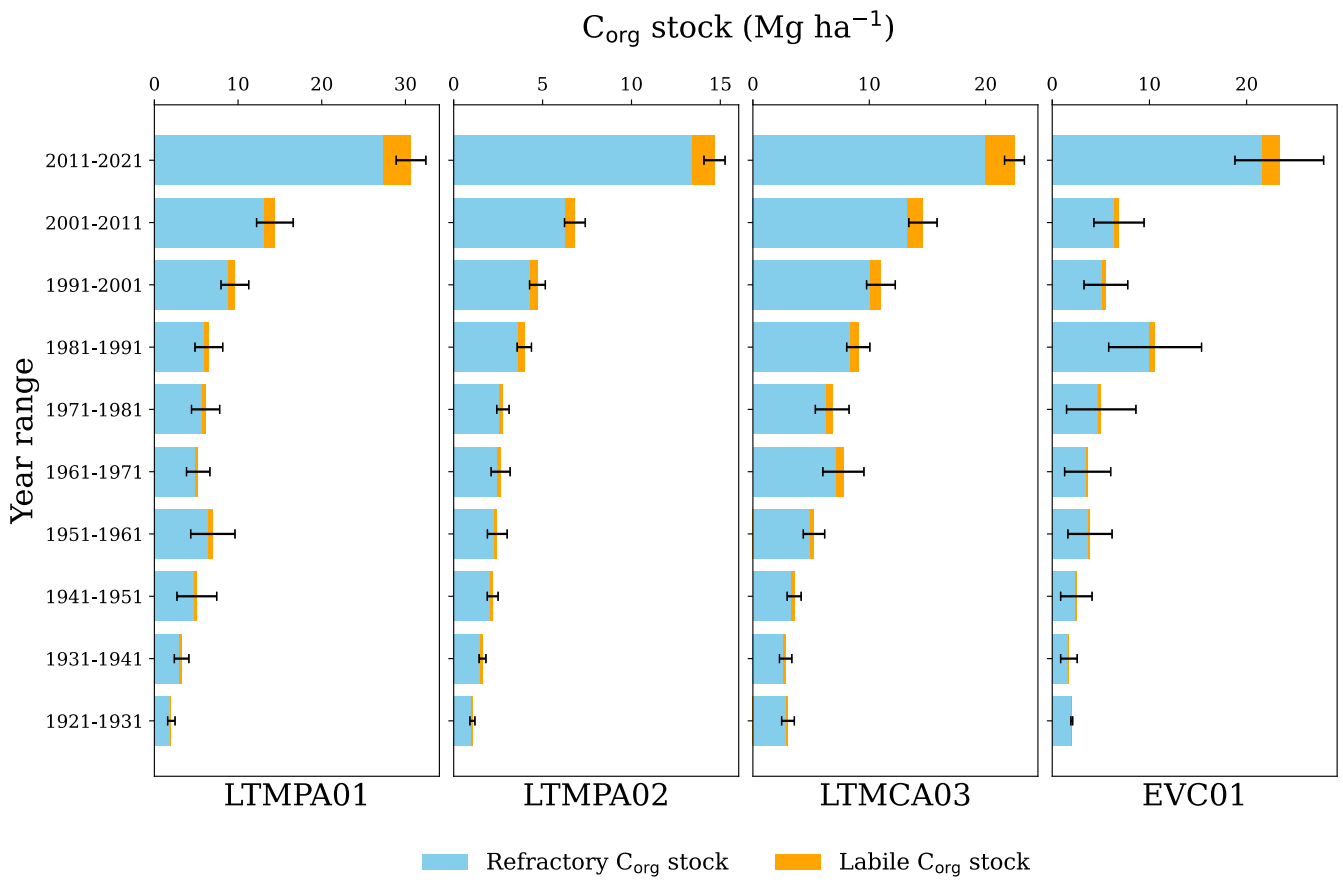

Fig. 7. Organic carbon stocks over 100 years in mangrove sediment cores from Términos Lagoon (southern Gulf of Mexico) and El Verde Camacho Lagoon (entrance of the Gulf of California).

TOC, PC, and HI, and lower values of OI in LTMCA03 suggested a greater influx of hydrogen-rich and labile or better-preserved OM in the CP system compared to other sites. Carbonate mangroves, such as those in the CP system, typically receive more autochthonous and labile OM inputs compared to terrigenous mangroves, such as the PDE and EV systems. This difference arises because carbonate mangroves have minimal allochthonous inputs of OM and sediments, minimizing dilution of deposited autochthonous OM (Jennerjahn, 2020; Twilley et al., 2018). The higher autochthonous OM contribution in LTMCA03 was supported by the highest concentrations of C2, associated with LC compounds (Disnar et al., 2003), such as mangrove tree wood and roots (Marchand et al., 2008). A better preservation of labile OM at this site could also be attributed to anoxic depositional conditions that inhibit microbial decomposition (Meyers, 1994). Evidence of recurrent anoxic conditions is supported by the higher proportion of gelified particles in LTMCA03 compared to other cores. These anoxic conditions may result from karstic water inputs characteristics of the CP system. Karstic waters typically exhibit temporary sub-anoxic to anoxic conditions (Bao et al., 2023) and were reported during the dry season in the CP system (Martínez-Trejo et al., 2024).

The high OI values in LTMPA02, particularly in sections from 25 to 26 cm and from 35 cm to the core bottom, indicated a high degree of oxidation or degradation of the OM (Boussafir et al., 2012) during specific periods. The presence of amorphized and gelified LC particles, along with high concentrations of C5 and opaque LC particles, aligned with prolonged oxidation phases (Boussafir et al., 2012). These periods may correspond to variations in the dynamics of the Palizada River, which influences the LTMPA02 area, as river discharge can promote sedimentary OM's resuspension, export, and aerobic decomposition (Kusumaningtyas et al., 2019; Allais et al., 2024). In contrast, LTMPA01, collected from an upstream mangrove creek within the PDE system, experienced higher autochthonous OM inputs and lability than LTMPA02, due to the lack of direct influence from the Palizada River.

5.2. *Temporal variability in quantity and liability of sedimentary organic carbon*

In the top sections of the cores LTMPA02 (2000–2021) and LTMCA03 (1990–2021), the decrease in HI values with depth indicated the dehydrogenation of organic compounds and the loss of hydrogen bonds, whereas the increase in OI values with depth was associated with mineralization and carbon loss, reflecting an oxidation profile (Meyers, 1997). This progressive shift was associated with a decline in TOC and $R400_{PC}$, indicating reduced C_{org} quantity and lability with increasing depth. Additionally, decreasing C2 values and increasing C1 values with depth were attributed to the progressive degradation of C2 organic components into smaller C1 compounds (Disnar et al., 2003). The gradual decrease in well-preserved particles, particularly LC, in the top sections coincided with the decline in C2 associated with mangrove detritus.

In the top section of core EVC01, decreasing HI values and stable OI values with depth may indicated an initial stage of decomposition of higher plant debris, mainly affecting the easily degradable hydrogen bounds (Marchand et al., 2003); however, the isolated peak in $R400_{PC}$ and C3 in 2014 ± 3 suggested a recent C_{org} supply. In the top section of LTMPA01, increasing values of HI, OI, and labile clusters (C1 and C2) towards the surface, associated with increasing values of TOC, PC, RC, and $R400_{PC}$, indicated a recent increase in labile C_{org} inputs to sediments. The increase in C_{org} quantity and lability in recent times in cores EVC01 and LTMPA01 may also be attributed to enhanced C_{org}

preservation owing to increased sediment accumulation rates (Jupin et al., 2023). Higher sediment deposition accelerates C_{org} burial, reducing exposure to aerobic conditions and promoting preservation (Burdige, 2007; Morris et al., 2016; Cuellar-Martinez et al., 2020).

River discharge, influenced by precipitation, regulates sediment, C_{org}, and nutrient transport in the TL and EV basins. Increased river discharge can promote sediment resuspension and C_{org} aerobic decomposition, preventing long-term C_{org} accumulation (Kusumaningtyas et al., 2019). In these cores, decreasing values of TOC, $R400_{PC}$, HI, and C2, alongside increasing OI and C4 values, were associated with high river discharge and precipitation (Fig. 5), such as in 1964 ± 4 in LTMPA02 and 1980–2000 in LTMCA03, indicating increased fluvial refractory C_{org} inputs to mangrove sediments. On the contrary, rising values of TOC, HI, $R400_{PC}$, and contributions of C2 and well-preserved particles, along with reduced OI and C3 values, indicated enhanced C_{org} quantity and lability in LTMPA01 at 31–32 cm (1947 ± 7), in LTMPA02 at 3–4 cm (2015.0 ± 0.6), at 13–14 cm (1984 ± 3) and 31–32 cm (>100 yr), in LTMCA03 at 18–25 cm (1961–1981), and in EVC01 at 19–21 cm (1977–1983). When data on river discharge and precipitation were available for comparison with the palynofacies data, such as in 1947 ± 7 for LTMPA01 and in 1976 ± 3 for LTMCA03, the increasing C_{org} quantity and lability were associated with a substantial proportion of preserved LC and other preserved organic particles (mycelial and cuticular fragments, spores, and pollen grains), and low river discharge and precipitation. This indicated that reduced riparian influence allowed a more significant contribution of autochthonous and well-preserved mangrove detritus to the total C_{org} accumulated.

The presence of two dominant peaks in the S2 spectrum at 31–32 cm in LMPA02 indicated two OM types with distinct preservation states during similar periods. Palynofacies analysis revealed a predominance of degraded particles (floccular AOM, gelified AOM, opaque debris, and gelified LC) in that core, along with high proportions of preserved LC and cuticular fragments derived from vascular plants compared to the proportions in the bottom sections of other cores. This suggests a reduction in Palizada River influence more than 100 years ago, although no river discharge data confirm this. In EVC01, MAR peaks in 1985 ± 9 and 2014 ± 3, previously linked to hurricanes (Jupin et al., 2023), were associated with increased TOC, $R400_{PC}$, HI, and C3, likely resulting from high-energy events facilitating material trapping by mangrove roots and higher C_{org} deposition (Smoak et al., 2013). Palynofacies data indicate increased preserved LC and algOM in 1985 ± 9, suggesting rapid accumulation and preservation of mangrove and marine-derived C_{org}. As the Gulf of California experienced higher rainfall and major hurricanes during El Niño conditions (Farfán *et al.*, 2013), this event was possibly related to the intense El Niño event of 1982–1983 and hurricane Tico on 11–24 October 1983 (Gunther and Cross, 1984). The MAR peak in 2014 ± 3, with similar variations in Rock-Eval parameters, may relate to the intense El Niño event of 2014–2016.

5.3. Are the studied mangroves a sink or source of atmospheric CO_2?

For C_{org} stocks to play a significant role in climate mitigation and blue carbon management, it is important to determine whether C_{org} stocks are prone to remineralization or stable over time (Howard et al., 2021). The relative proportions of labile and refractory material would be expected to change during the early stage of diagenesis because the degradation of OM by microbial activity is generally selective, with labile organic materials typically degrading more easily than refractory ones (Benner et al., 1990; Meyers, 1997; Southward et al., 2005). The most labile part of the pyrolyzed carbon (R400) is particularly susceptible to decomposition in the sediment column (Disnar et al., 2003), potentially leading to CO_2 emissions during the early diagenesis in mangrove sediments. In contrast, the refractory C_{org} stocks, such as woody material or organic compounds highly resistant to pyrolysis, require temperatures exceeding 400 °C for breakdown (Disnar et al., 2003). Although evidence of decomposition of recalcitrant organic components has been found in mangrove sediments, which depends on the stage of evolution of the mangrove forest and the redox conditions, low decomposition rates were reported under anoxic conditions (Marchand et al., 2003, 2005, 2008; Lallier-Vergès et al., 2008). The low proportion of highly labile C_{org} stocks and minimal change in the proportions between labile and refractory C_{org} stocks along the cores, including the top sections, confirmed that most C_{org} degradation occurred before burial and indicated limited potential for CO_{2eq} emissions from labile C_{org} decomposition. The predominance of refractory C_{org} stocks, as confirmed by palynofacies analysis, indicated the potential of these mangrove ecosystems as long-term C_{org} sinks.

The upward trends in C_{org} concentrations and $stocks_{\text{-}10yr}$ were partly due to increased river discharge since the 1950 s in the TL (Benítez et al., 2005; Soto-Galera et al., 2010; Fichez et al., 2017; no available data for EV), and the consequent increase in sediment inputs from rivers to these mangrove areas (Fig. 5; Jupin et al., 2023). Previous studies have shown that the increasing discharge from Usumacinta and Candelaria rivers was unrelated to precipitation (Benítez et al., 2005; Fichez et al., 2017); indeed, precipitation tended to decrease from 1959 to 2018 in the Usumacinta River Basin (Jupin et al., 2024a). The increasing sediment discharge by rivers has been attributed to exacerbated continental erosion caused by population growth and changes in land use and land cover (Benítez et al., 2005; Fichez et al., 2017; Jupin et al., 2023).

The observation of C_{org} decomposition, inferred from the relative proportions of labile and refractory C_{org} $stocks_{\text{-}10yr}$, may be underestimated, as decomposition in anoxic and saturated mangrove sediments is generally slow (Lallier-Vergès et al., 2008) compared to the recent and rapid accumulation of refractory C_{org} in these sites. Moreover, variations in Rock-Eval parameters showed sporadic changes in OM lability and nature, as a result of OM provenance changes, potentially complicating oxidation profiles and accurate assessments of C_{org} degradation rates. Despite C_{org} originating mainly from external sources and being refractory rather than newly formed from *in situ* capture of atmospheric CO_2, these mangroves have significantly contributed to accumulating allochthonous C_{org} in their sediments. Over time, mangroves have adapted to new sediment and C_{org} deposition patterns, resulting in greater C_{org} stocks. Typically, up to 90 % of total C_{org} stocks in mangrove ecosystems is stored in sediments (e.g., Phang et al., 2015; Ezcurra et al., 2016; Cooray et al., 2021). This may indicate that, overall, the C_{org} stocks in the studied mangroves can be considered stable and efficient C_{org} sinks over time; hence, the conservation of these ecosystems contributes significantly to mitigating climate change.

6. Conclusions

Rock-Eval pyrolysis and palynofacies analyses of mangrove sediment cores from two Mexican Ramsar sites showed similar provenance and composition of organic matter (OM) across the sampling sites, with specific differences among cores attributed to the influence of local sedimentary and hydrological conditions. Most of the observed sedimentary organic carbon (C_{org}) in this study was refractory and proceeds from terrestrial detritus. The high proportions of refractory C_{org} stocks and degraded organic particles in the cores indicated that the C_{org} degradation processes mainly occurred before its burial in the sediment column. A trend towards decreasing C_{org} concentration from 1990 to 2021 in some cores was attributed to early oxidative diagenesis of C_{org}, in agreement with decreasing hydrogen-rich and preserved compounds with depth. The increase in C_{org} concentrations and stocks over 1921–2021 was attributed to the increasing supply of refractory and riverine C_{org}, resulting from a century of deforestation and land-use change in the regions surrounding these mangroves, rather than the mangrove ecosystems themselves. However, mangroves efficiently served as long-term sinks for the external supply of refractory C_{org}. The Ramsar status of the studied ecosystems is appropriate in the face of the deleterious effects of global change; however, local mangrove conservation and management strategies should be improved to favor the

expansion and restoration of these ecosystems with high Blue Carbon sequestration potential.

CRediT authorship contribution statement

J.L.J. Jupin: Writing – original draft, Validation, Investigation, Formal analysis, Data curation. **M. Boussafir:** Writing – review & editing, Validation, Resources, Methodology, Investigation, Formal analysis. **A. Sifeddine:** Writing – review & editing, Supervision, Resources, Funding acquisition, Conceptualization. **A.C. Ruiz-Fernández:** Writing – review & editing, Validation, Supervision, Resources, Project administration, Methodology, Investigation, Funding acquisition, Formal analysis, Conceptualization. **J.A. Sanchez-Cabeza:** Writing – review & editing, Investigation, Conceptualization. **L.H. Pérez-Bernal:** Writing – review & editing, Methodology, Formal analysis, Data curation.

Declaration of competing interest

The authors declare that they have no known competing financial interests or personal relationships that could have appeared to influence the work reported in this paper.

Data availability

Data will be made available on request.

Acknowledgments

This study was developed with the support of Universidad Nacional Autónoma de México (UNAM) through the research grant IN102821 from PAPIIT-DGAPA and the mobility grants for JL Jupin from the Instituto de Ciencias del Mar y Limnología, the Centro de Estudios Mexicanos UNAM-Francia, and the Institut de Recherche pour le Développement (IRD) through the international network DEXICOTROP. J. L. Jupin acknowledges a Ph.D. fellowship provided by Consejo Nacional de Ciencia y Tecnología-Mexico (CONACYT, CVU 1102000) and expresses gratitude for the support received from the Posgrado en Ciencias del Mar y Limnologia, UNAM and the Laboratoire GéoHydrosystèmes COntinentaux from the Université de Tours. The authors thanks J. G. Cardoso-Mohedano., M. A. Gómez-Ponce, J. G. Flores-Trujillo, and J. A. Martinez-Trejo (sampling); L. F. Álvarez-Sánchez (data curation), C. Súarez-Gutiérrez (informatics); and A. Grant (English edition of the manuscript) for their valuable support. C. Le-Milbeau and R. Boscardin from the Institut des Sciences de la Terre d'Orléans, France, are acknowledged for their technical support in Rock-Eval analyses.

Appendix A. Supplementary data

Supplementary data to this article can be found online at https://doi.org/10.1016/j.catena.2024.108279.

References

Allais, L., Thibodeau, B., Khan, N.S., Crowe, S.A., Cannicci, S., Not, C., 2024. Salinity, mineralogy, porosity, and hydrodynamics as drivers of carbon burial in urban mangroves from a megacity. *Science of the Total Environment*. Elsevier b.v. 912, 168955 https://doi.org/10.1016/j.scitotenv.2023.168955.

Alongi, D.M., 2005. Mangrove-microbe-soil relations. In: Kristensen, E., Haese, R.R., Kostka, J.E. (Eds.), Interactions between Macro-and Microorganisms in Marine Sediments. American Geophysical Union, Washington, pp. 85–103.

Alongi, D.M., 2020. Global Significance of Mangrove Blue Carbon in Climate Change Mitigation (Version 1). *Sci.* MDPI AG 2 (3), 57. https://doi.org/10.3390/sci2030057.

Bach L, Calderon R, Cepeda MF, Oczkowski A, Olsen SB, Robadue D. 2005. *Resumen del Perfil de Primer Nivel del Sitio Laguna de Términos y su Cuenca, México. Coastal Resources Center, University of Rhode Island*. Coastal Resources Center, University of Rhode Island: Narragansett.

Bao, J., Wu, X., Zhang, Q., Yuan, D., Guo, F., Liu, F., 2023. Unveiling the nitrogen transport and transformation in different karst aquifers media. *Journal of Hydrology*. Elsevier b.v. 620 https://doi.org/10.1016/j.jhydrol.2023.129335.

Battarbee, R.W., Kneen, M.J., 1982. The use of electronically counted microspheres in absolute diatom analysis. Limnology and Oceanography 27 (1), 184–188. https://doi.org/10.4319/lo.1982.27.1.0184.

Batten, D.J., Stead, D.T., 2006. Palynofacies Analysis and its Stratigraphic Application. Applied Stratigraphy. Springer, Netherlands, pp. 203–226.

Baudin, F., Disnar, J.-R., Aboussou, A., Savignac, F., 2015. Guidelines for Rock-Eval analysis of recent marine sediments. *Organic Geochemistry*. Elsevier Ltd 86, 71–80. https://doi.org/10.1016/j.orggeochem.2015.06.009.

Benítez JA, Sanvicente Sánchez H, Lafragua Contreras J, Zamora Crescencio P, Morales Manilla LM, Mas Caussel JF, García Gil G, Couturier SA, Zetina Tapia R, Calan Yam RA, Amabilis Sánchez L, Acuña C, Mejenes M. 2005. Sistemas de información geográfica de la cuenca del río Candelaria: reconstrucción histórica de los cambios de cobertura forestal y su efecto sobre la hidrología y calidad del agua-marco teórico y resultados iniciales. In: Edith F and Kauffer M (eds) *El agua en la frontera México-Guatemala- Belice*. Ecosur/tnc/unach: Tuxtla Gutiérrez, Chiapas, 19–32.

Benner, R., Hatcher, P.G., Hedges, J.I., 1990. Early diagenesis of mangrove leaves in a tropical estuary: Bulk chemical characterization using solid-state 13C NMR and elemental analyses. Geochimica et Cosmochimica Acta 54 (7), 2003–2013. https://doi.org/10.1016/0016-7037(90)90268-P.

Borges, A.V., Djenidi, S., Lacroix, G., Théate, J., Delille, B., Frankignoulle, M., 2003. Atmospheric CO2 flux from mangrove surrounding waters. Geophysical Research Letters 30 (11), 12–15. https://doi.org/10.1029/2003GL017143.

Bouillon, S., Dahdouh-Guebas, F., Rao, A.V.V.S., Koedam, N., Dehairs, F., 2003. Sources of organic carbon in mangrove sediments: Variability and possible ecological implications. Hydrobiologia 495, 33–39. https://doi.org/10.1023/A:1025411506526.

Bouillon, S., Borges, A.V., Castañeda-Moya, E., Diele, K., Dittmar, T., Duke, N.C., Kristensen, E., Lee, S.Y., Marchand, C., Middelburg, J.J., Rivera-Monroy, V.H., Smith, T.J., Twilley, R.R., 2008. Mangrove production and carbon sinks: A revision of global budget estimates. Global Biogeochemical Cycles 22 (2), 1–12. https://doi.org/10.1029/2007GB003052.

Boussafir, M., Sifeddine, A., Jacob, J., Foudi, M., Cordeiro, R.C., Albuquerque, A.L.S., Abrao, J.J., Turcq, B., 2012. Petrographical and geochemical study of modern lacustrine sedimentary organic matter (Lagoa do Caçò, Maranão, Brazil): Relationship between early diagenesis, organic sedimentation and lacustrine filling. Organic Geochemistry 47, 88–98. https://doi.org/10.1016/j.orggeochem.2012.03.013.

Briseño-Dueñas, R., 2003. Ficha Informativa de los Humedales de Ramsar. (FIR). "Playa Tortuguera El Verde Camacho".

Burdige, D.J., 2007. The Controls on Organic Carbon Preservation in Marine Sediments. Geochemistry of Marine Sediments. Princeton University Press, Princeton, pp. 408–441.

Combaz, A., 1964. Les palynofaciès. Revue De Micropaléontologie 7 (3), 205–218.

Conagua, 2015. Determinación de la Disponibilidad de Agua en el acuífero Río Quelite (2508), estado de Sinaloa. Comisión Nacional Del Agua 25.

Contreras-Ruiz-Esparza, A., Douillet, P., Zavala-Hidalgo, J., 2014. Tidal dynamics of the Terminos Lagoon, Mexico: Observations and 3D numerical modelling. Ocean Dynamics 64 (9), 1349–1371. https://doi.org/10.1007/s10236-014-0752-3.

Cooray, P.L.I.G.M., Kodikara, A.S.K., Kumara, M.P., Jayasinghe, U.I., Madarasinghe, S.K., Dahdouh-Guebas, F., Gorman, D., Huxham, M., Jayatissa, L.P., 2021. Climate and intertidal zonation drive variability in the carbon stocks of Sri Lankan mangrove forests. *Geoderma*. Elsevier b.v. 389 https://doi.org/10.1016/j.geoderma.2021.114929.

Cuellar-Martinez, T., Ruiz-Fernández, A.C., Sanchez-Cabeza, J.A., Pérez-Bernal, L., López-Mendoza, P.G., Carnero-Bravo, V., Agraz-Hernández, C.M., van Tussenbroek, B.I., Sandoval-Gil, J., Cardoso-Mohedano, J.G., Vázquez-Molina, Y., Aldana-Gutiérrez, G., 2020. Temporal records of organic carbon stocks and burial rates in Mexican blue carbon coastal ecosystems throughout the Anthropocene. Global and Planetary Change, 192. Elsevier B.V, p. 103215. https://doi.org/10.1016/j.gloplacha.2020.103215.

de Vernal, A., Larouche, A., Richard, P.J.H., 1987. Evaluation of palynomorph concentrations: Do the aliquot and the marker-grain methods yield comparable results? Pollen et Spores XXIX(2–3), 291–304.

Díaz-Asencio, M., Sanchez-Cabeza, J.A., Ruiz-Fernández, A.C., Corcho-Alvarado, J.A., Pérez-Bernal, L.H., 2020. Calibration and use of well-type germanium detectors for low-level gamma-ray spectrometry of sediments using a semi-empirical method. Journal of Environmental Radioactivity 225 (June). https://doi.org/10.1016/j.jenvrad.2020.106385.

Di-Giovanni, C., Disnar, J.R., Bichet, V., Campy, M., Guillet, B., 1998. Geochemical characterization of soil organic matter and variability of a postglacial detrital organic supply (Chaillexon Lake, France). Earth Surface Processes and Landforms 23 (12), 1057–1069. https://doi.org/10.1002/(SICI)1096-9837(199812)23:12<1057::AID-ESP921>3.0.CO;2-H.

Disnar, J.R., 1994. Determination of maximum paleotemperatures of burial (MPTB) of sedimentary rocks from pyrolysis data on the associated organic matter: basic principles and practical application. Chemical Geology 118 (1–4), 289–299. https://doi.org/10.1016/0009-2541(94)90182-1.

Disnar, J.R., Guillet, B., Keravis, D., Di-Giovanni, C., Sebag, D., 2003. Soil organic matter (SOM) characterization by Rock-Eval pyrolysis: scope and limitations. Organic Geochemistry 34 (3), 327–343. https://doi.org/10.1016/S0146-6380(02)00239-5.

Disnar, J.-R., Trichet, J., 1984. The influence of various divalent cations (UO22+, Cu2+, Pb2+, Co2+, Ni2+, Zn2+, Mn2+) on the thermally induced evolution of organic

matter isolated from an algal mat. Organic Geochemistry 6, 865–874. https://doi.org/10.1016/0146-6380(84)90109-8.
Donato, D.C., Kauffman, J.B., Murdiyarso, D., Kurnianto, S., Stidham, M., Kanninen, M., 2011. Mangroves among the most carbon-rich forests in the tropics. *Nature Geoscience*. Nature Publishing Group 4 (5), 293–297. https://doi.org/10.1038/ngeo1123.
Duan, D., Lan, W., Chen, F., Lei, P., Zhang, H., Ma, J., Wei, Y., Pan, K., 2020. Neutral monosaccharides and their relationship to metal contamination in mangrove sediments. *Chemosphere*. Elsevier Ltd 251. https://doi.org/10.1016/j.chemosphere.2020.126368.
Espitalié, J., Laporte, J.L., Madec, M., Marquis, F., Leplat, P., Paulet, J., Boutefeu, A., 1977. Méthode rapide de caractérisation des roches mètres, de leur potentiel pétrolier et de leur degré d'évolution. Revue De L'institut Français Du Pétrole 32 (1), 23–42. https://doi.org/10.2516/ogst:1977002.
Espitalié, J., Deroo, G., Marquis, F., 1985a. La pyrolyse Rock-Eval et ses applications. Deuxième partie. *Revue de l'Institut français du Pétrole*. EDP. Sciences 40 (6), 755–784.
Espitalié, J., Deroo, G., Marquis, F., 1985b. Rock-Eval pyrolysis and its applications (part one). Oil & Gas Science and Technology-Revue d'IFPEN. EDP. Sciences 40 (5), 563–579.
Ezcurra, P., Ezcurra, E., Garcillán, P.P., Costa, M.T., Aburto-Oropeza, O., 2016. Coastal landforms and accumulation of mangrove peat increase carbon sequestration and storage. Proceedings of the National Academy of Sciences 113 (16), 4404–4409. https://doi.org/10.1073/pnas.1519774113.
Fichez, R., Archundia, D., Grenz, C., Douillet, P., Gutiérrez-Mendieta, F., Origel-Moreno, M., Denis, L., Contreras-Ruiz-Esparza, A., Zavala-Hidalgo, J., 2017. Global climate change and local watershed management as potential drivers of salinity variation in a tropical coastal lagoon (Laguna de Terminos, Mexico). *Aquatic Sciences*. Research across Boundaries, Springer Verlag 79 (2), 219–230. https://doi.org/10.1007/s00027-016-0492-1.
Flores-Verdugo FJ, Briseño-Dueñas R, González-Farías F, Calvario-Martínez O. 1995. Balance de carbono en un ecosistema lagunar estuarino de boca efímera de la costa noroccidental de México (Estero El Verde, Sinaloa). *Temas de oceanografía biológica en México. Universidad Autónoma de Baja California. Ensenada, 8.C., México.*, II.
Friess, D.A., Yando, E.S., Abuchahla, G.M.O., Adams, J.B., Cannicci, S., Canty, S.W.J., Cavanaugh, K.C., Connolly, R.M., Cormier, N., Dahdouh-Guebas, F., Diele, K., Feller, I.C., Fratini, S., Jennerjahn, T.C., Lee, S.Y., Ogurcak, D.E., Ouyang, X., Rogers, K., Rowntree, J.K., Sharma, S., Sloey, T.M., Wee, A.K.S., 2020. Mangroves give cause for conservation optimism, for now. *Current Biology*. Elsevier 30 (4), R153–R154. https://doi.org/10.1016/j.cub.2019.12.054.
García, E., 1973. Modificaciones al sistema de clasificación climática de Köppen: para adaptarlo a las condiciones de la república mexicana. Universidad Nacional Autónoma de México, México, D. F.
Graz, Y., Di-Giovanni, C., Copard, Y., Laggoun-Défarge, F., Boussafir, M., Lallier-Vergès, E., Baillif, P., Perdereau, L., Simonneau, A., 2010. Quantitative palynofacies analysis as a new tool to study transfers of fossil organic matter in recent terrestrial environments. International Journal of Coal Geology 84 (1), 49–62. https://doi.org/10.1016/j.coal.2010.08.006.
Gunther, E.B., Cross, R.L., 1984. Eastern North Pacific Tropical Cyclones of 1983. Monthly Weather Review 112, 1419–1440.
Holguin, G., Vazquez, P., Bashan, Y., 2001. The role of sediment microorganisms in the productivity, conservation, and rehabilitation of mangrove ecosystems: an overview. Biology and Fertility of Soils 33 (4), 265–278. https://doi.org/10.1007/s003740000319.
Howard J, Hoyt S, Isensee K, Telszewski M, Pidgeon E, (eds). 2014. *Coastal blue carbon: methods for assessing carbon stocks and emissions factors in mangroves, tidal salt marshes, and seagrasses*. Conservational International, Intergovernmental Oceanographic Commission of UNESCO, International Union for Conservation of Nature.: Arlington, Virginia, USA.
Howard JL, Lopes CC, Wilson SS, McGee-Absten V, Carrión CI, Fourqurean JW. 2021. Decomposition Rates of Surficial and Buried Organic Matter and the Lability of Soil Carbon Stocks Across a Large Tropical Seagrass Landscape. *Estuaries and Coasts*. Springer, 44(3): 846–866. Doi: 10.1007/s12237-020-00817-x.
Jennerjahn, T.C., 2020. Relevance and magnitude of "Blue Carbon" storage in mangrove sediments: Carbon accumulation rates vs. stocks, sources vs. sinks. *Estuarine, Coastal and Shelf Science*. Elsevier Ltd 247 (January), 107027. https://doi.org/10.1016/j.ecss.2020.107027.
Jupin, J.L.J., Ruiz-Fernández, A.C., Sifeddine, A., Sanchez-Cabeza, J.A., Pérez-Bernal, L. H., Cardoso-Mohedano, J.G., Gómez-Ponce, M.A., Flores-Trujillo, J.G., 2023. Anthropogenic drivers of increasing sediment accumulation in contrasting Mexican mangrove ecosystems. CATENA 226, 107037. https://doi.org/10.1016/j.catena.2023.107037.
Jupin, J.L.J., Garcia-López, A.A., Briceño-Zuluaga, F.J., Sifeddine, A., Ruiz-Fernández, A. C., Sanchez-Cabeza, J., Cardoso-Mohedano, J.G., 2024a. Precipitation homogenization and trends in the Usumacinta River Basin (Mexico-Guatemala) over the period 1959–2018. *International Journal of Climatology*. John Wiley and Sons Ltd 44 (1), 108–125. https://doi.org/10.1002/joc.8318.
Jupin, J.L.J., Ruiz-Fernández, A.C., Sifeddine, A., Mendez-Millan, M., Sanchez-Cabeza, J. A., Pérez-Bernal, L.H., Cardoso-Mohedano, J.G., Gómez-Ponce, M.A., Flores-Trujillo, J.G., 2024b. Terrestrial inputs boost organic carbon accumulation in Mexican mangroves. *Science of the Total Environment*. Elsevier b.v. 940 https://doi.org/10.1016/j.scitotenv.2024.173440.
Koné, Y.J.M., Borges, A.V., 2008. Dissolved inorganic carbon dynamics in the waters surrounding forested mangroves of the Ca Mau Province (Vietnam). Estuarine, Coastal and Shelf Science 77 (3), 409–421. https://doi.org/10.1016/j.ecss.2007.10.001.
Kristensen, E., Bouillon, S., Dittmar, T., Marchand, C., 2008a. Organic carbon dynamics in mangrove ecosystems: A review. Aquatic Botany 201–219.
Kristensen, E., Flindt, M.R., Ulomi, S., Borges, A.V., Abril, G., Bouillon, S., 2008b. Emission of CO2 and CH4 to the atmosphere by sediments and open waters in two Tanzanian mangrove forests. Marine Ecology Progress Series 370, 53–67. https://doi.org/10.3354/meps07642.
Kusumaningtyas, M.A., Hutahaean, A.A., Fischer, H.W., Pérez-Mayo, M., Ransby, D., Jennerjahn, T.C., 2019. Variability in the organic carbon stocks, sources, and accumulation rates of Indonesian mangrove ecosystems. *Estuarine, Coastal and Shelf Science*. Elsevier 218 (December 2018), 310–323. https://doi.org/10.1016/j.ecss.2018.12.007.
Lafargue, E., Marquis, F., Pillot, D., 1998. Rock-Eval 6 applications in hydrocarbon exploration, production, and soil contamination studies. Revue De L'institut Francais Du Petrole 53 (4), 421–437. https://doi.org/10.2516/ogst:1998036.
Lallier-Vergès, E., Perrussel, B.P., Disnar, J.R., Baltzer, F., 1998. Relationships between environmental conditions and the diagenetic evolution of organic matter derived from higher plants in a modern mangrove swamp system (Guadeloupe, French West Indies). Organic Geochemistry 29 (5–7–7 pt 2), 1663–1686. https://doi.org/10.1016/S0146-6380(98)00179-X.
Lallier-Vergès, E., Marchand, C., Disnar, J.R., Lottier, N., 2008. Origin and diagenesis of lignin and carbohydrates in mangrove sediments of Guadeloupe (French West Indies): Evidence for a two-step evolution of organic deposits. *Chemical Geology*. Elsevier b.v. 255 (3–4), 388–398. https://doi.org/10.1016/j.chemgeo.2008.07.009.
Le Meur, M., Boussafir, M., Le Milbeau, C., Debure, M., Claret, F., Robinet, J.-C., Lerouge, C., 2021. Organic matter oxidation of the Tégulines Clay formation, (Paris Basin, France): Spatial Heterogeneities. *Applied Geochemistry*. Elsevier Ltd 134, 105093. https://doi.org/10.1016/j.apgeochem.2021.105093.
Marchand, C., Lallier-Vergès, E., Baltzer, F., 2003. The composition of sedimentary organic matter in relation to the dynamic features of a mangrove-fringed coast in French Guiana. Estuarine, Coastal and Shelf Science 56 (1), 119–130. https://doi.org/10.1016/S0272-7714(02)00134-8.
Marchand, C., Disnar, J.R., Lallier-Vergès, E., Lottier, N., Lallier-Vergès, E., Lottier, N., 2005. Early diagenesis of carbohydrates and lignin in mangrove sediments subject to variable redox conditions (French Guiana). Geochimica et Cosmochimica Acta 69 (1), 131–142. https://doi.org/10.1016/j.gca.2004.06.016.
Marchand, C., Lallier-Vergès, E., Disnar, J.R., Kéravis, D., 2008. Organic carbon sources and transformations in mangrove sediments: A Rock-Eval pyrolysis approach. Organic Geochemistry 39 (4), 408–421. https://doi.org/10.1016/j.orggeochem.2008.01.018.
Martínez-Trejo JA, Cardoso-Mohedano JG, Sanchez-Cabeza JA, Ayón JMH, Ruiz-Fernández AC, Gómez-Ponce MA, Barranco L, Pech D. 2024. Variability of Dissolved Inorganic Carbon in the Most Extensive Karst Estuarine-Lagoon System of the Southern Gulf of Mexico. *Estuaries and Coasts*. Springer. Doi: 10.1007/s12237-024-01384-1.
Meyers, P.A., 1994. Preservation of elemental and isotopic source identification of sedimentary organic matter. Chemical Geology 114 (3–4), 289–302. https://doi.org/10.1016/0009-2541(94)90059-0.
Meyers, P.A., 1997. Organic geochemical proxies of paleoceanographic, paleolimnologic, and paleoclimatic processes. Organic Geochemistry 27 (5–6), 213–250. https://doi.org/10.1016/S0146-6380(97)00049-1.
Meyers, P.A., Lallier-Vergès, E., 1999. Lacustrine sedimentary organic matter records of Late Quaternary paleoclimates. Journal of Paleolimnology 21 (3), 345–372. https://doi.org/10.1023/A:1008073732192.
Morris JT, Barber DC, Callaway JC, Chambers R, Hagen SC, Hopkinson CS, Johnson BJ, Megonigal P, Neubauer SC, Troxler T, Wigand C. 2016. Contributions of organic and inorganic matter to sediment volume and accretion in tidal wetlands at steady state. *Earth's Future*. John Wiley and Sons Inc, 4(4): 110–121. Doi: 10.1002/2015EF000334.
Murdiyarso, D., Purbopuspito, J., Kauffman, J.B., Warren, M.W., Sasmito, S.D., Donato, D.C., Manuri, S., Krisnawati, H., Taberima, S., Kurnianto, S., 2015. The potential of Indonesian mangrove forests for global climate change mitigation. Nature Climate Change 5 (12), 1089–1092. https://doi.org/10.1038/nclimate2734.
Patience, A., 1996. Relationships between organo-mineral supply and early diagenesis in the lacustrine environment: a study of surficial sediments from the Lac du Bouchet (Haute Loire, France). Quaternary Science Reviews 15 (2–3), 213–221. https://doi.org/10.1016/0277-3791(95)00024-0.
Phang, V.X.H., Chou, L.M., Friess, D.A., 2015. Ecosystem carbon stocks across a tropical intertidal habitat mosaic of mangrove forest, seagrass meadow, mudflat and sandbar. *Earth Surface Processes and Landforms*. John Wiley and Sons Ltd 40 (10), 1387–1400. https://doi.org/10.1002/esp.3745.
Ranjan, R.K., Routh, J., Ramanathan, A.L., Klump, J.V., 2011. Elemental and stable isotope records of organic matter input and its fate in the Pichavaram mangrove–estuarine sediments (Tamil Nadu, India). Marine Chemistry 126 (1–4), 163–172. https://doi.org/10.1016/j.marchem.2011.05.005.
Robbins, J.A., 1978. Geochemical and geophysical applications of radioactive lead. *Biogeochemistry of Lead in the Environment*. Elsevier Scientific, pp. 285–393.
Rosentreter, J.A., Maher, D.T., Erler, D.V., Murray, R.H., Eyre, B.D., 2018. Methane emissions partially offset "blue carbon" burial in mangroves. Science Advances 4 (6). https://doi.org/10.1126/sciadv.aao4985.
Rovai, A.S., Twilley, R.R., Castañeda-Moya, E., Riul, P., Cifuentes-Jara, M., Manrow-Villalobos, M., Horta, P.A., Simonassi, J.C., Fonseca, A.L., Pagliosa, P.R., 2018. Global controls on carbon storage in mangrove soils. *Nature Climate Change*. Springer, US 8 (6), 534–538. https://doi.org/10.1038/s41558-018-0162-5.
Rsis, 2024. Área de Protección de Flora y Fauna. Playa Tortuguera El Verde Camacho, Ramsar Sites Information Service.

Sanchez-Cabeza, J.A., Ruiz-Fernández, A.C., 2012. 210Pb sediment radiochronology: An integrated formulation and classification of dating models. Geochimica et Cosmochimica Acta 82, 183–200. https://doi.org/10.1016/j.gca.2010.12.024.

Sebag, D., Copard, Y., Di-Giovanni, C., Durand, A., Laignel, B., Ogier, S., Lallier-Vergès, E., 2006. Palynofacies as useful tool to study origins and transfers of particulate organic matter in recent terrestrial environments: Synopsis and prospects. Earth-Science Reviews 79 (3–4), 241–259. https://doi.org/10.1016/j.earscirev.2006.07.005.

Sebag, D., Verrecchia, E.P., Cécillon, L., Adatte, T., Albrecht, R., Aubert, M., Bureau, F., Cailleau, G., Copard, Y., Decaens, T., Disnar, J.-R., Hetényi, M., Nyilas, T., Trombino, L., 2016. Dynamics of soil organic matter based on new Rock-Eval indices. *Geoderma*. Elsevier b.v. 284, 185–203. https://doi.org/10.1016/j.geoderma.2016.08.025.

Smoak, J.M., Breithaupt, J.L., Smith, T.J., Sanders, C.J., 2013. Sediment accretion and organic carbon burial relative to sea-level rise and storm events in two mangrove forests in Everglades National Park. *Catena*. Elsevier b.v. 104, 58–66. https://doi.org/10.1016/j.catena.2012.10.009.

Soto-Galera, E., Piera, J., López, P., 2010. Spatial and temporal land cover changes in Terminos Lagoon Reserve. Mexico. *Revista De Biologia Tropical* 58 (2), 565–575. https://doi.org/10.15517/rbt.v58i2.5229.

Southward, A.J., Tyler, P.A., Young, C.M., Fuiman, L.A., 2005. Aquatic Geomicrobiology. Elsevier, Amsterdam.

Twilley, R.R., Rovai, A.S., Riul, P., 2018. Coastal morphology explains global blue carbon distributions. Frontiers in Ecology and the Environment 16 (9), 503–508. https://doi.org/10.1002/fee.1937.

Tyson, R.V., 1995. *Sedimentary Organic Matter*. *Sedimentary Organic Matter*. Dordrecht, Springer, Netherlands.

Venegas-Pérez, M.C.Y., 2003. Ficha Informativa de los Humedales de Ramsar (FIR). Laguna de Términos.

Williams, E.K., Rosenheim, B.E., 2015. What happens to soil organic carbon as coastal marsh ecosystems change in response to increasing salinity? An exploration using ramped pyrolysis. *Geochemistry, Geophysics, Geosystems*. Blackwell Publishing Ltd 16 (7), 2322–2335. https://doi.org/10.1002/2015GC005839.

Woodroffe, S.A., Horton, B.P., Larcombe, P., Whittaker, J.E., 2005. Intertidal mangrove foraminifera from the central Great Barrier Reef Shelf, Australia: Implications for sea-level reconstruction. Journal of Foraminiferal Research 35 (3), 259–270. https://doi.org/10.2113/35.3.259.

Yáñez-Arancibia, A., Day, J.W., 2005. Ecosystem functioning: The basis for sustainable management of Terminos Lagoon. Campeche Mexico, Jalapa, Veracruz, Mexico.

Zhang, Y., Fu, H., Yang, X., Liu, Z., 2023. Anthropogenically driven changes to organic matter input in sediments of Lake Chaohu. In: Over the past 166 Years. *Catena*. Elsevier B.V, Eastern China, p. 231. https://doi.org/10.1016/j.catena.2023.107285.

GENERAL DISCUSSION

1. Spatial and temporal variability of precipitation in the study sites

In the URB, the analysis of homogenized and imputed series revealed a distribution pattern of precipitation influenced by altitude as a result of the orographic effect, which occurs because of the combination of cooling and drying of moist air with altitude (Houghton, 1979; Daly et al., 1994; Fernández et al., 1996). The belt of maximum precipitation at intermediate altitudes observed in URB is a common phenomenon in mountainous regions of the tropics and subtropics (Hastenrath, 1967), such as in India (Puvaneswaran and Smithson, 1991), Costa Rica (Chacón and Fernandez, 1985; Fernández et al., 1996), and Morocco (Abahous et al., 2018).

Extreme precipitation events in the URB showed a significant negative correlation with the El Niño 3.4 index (Jupin et al., 2024), owing to the influence of El Niño and La Niña events on the moisture transport in Central America (Durán-Quesada et al., 2017). During El Niño events, drier conditions were observed in the URB and in Campeche, whereas southern Sinaloa experienced increased precipitation (Magaña et al., 2003; Salas-Flores et al., 2014; Salas-Flores and Jones, 2014). With Climate change, the frequency and intensity of extreme El Niño events may increase (Wang et al., 2019; Cai et al., 2022), potentially amplifying extreme precipitation or drought occurrences in Mexico, thereby leading to socioeconomic repercussions in the river basins.

The observed trends toward increased drought in the URB between 1959 and 2018 (Jupin et al., 2024), in the southern Yucatan Peninsula from 1980 to 2011 (De la Barreda et al., 2020), and in southern Sinaloa from 1963 to 2014 (Llanes-Cárdenas et al., 2022, 2016) aligned with warming

trends reported in Mexico (Montero-Martínez et al., 2018) and Central America over interdecadal scales (Hidalgo et al., 2013, 2017; Durán-Quesada et al., 2017; Hannah et al., 2017; Alfaro-Córdoba et al., 2020; Maldonado et al., 2021). Increasing temperatures can alter the distribution and intensity of precipitation, resulting in increased evaporation, evapotranspiration, and atmospheric moisture retention, thereby leading to more intense rainfall events and prolonged drought periods (Aguilar et al., 2005). However, the relationship between warming and precipitation trends is complex. To gain a more comprehensive understanding of precipitation trends and the underlying factors across time scales, it is necessary to consider the use of long-term series, such as paleoprecipitation records or reanalysis data calibrated with local rain gauge measurements (Hidalgo et al., 2017).

The increasing aridity observed in this study within the context of climate change poses a significant threat to critical sectors such as health, agriculture, and water and disaster risk management in the study regions. Since socio-economic development in the study sites relies mainly on agricultural and livestock production, these regions are particularly vulnerable to variations in water availability and extreme events such as droughts (De la Barreda et al., 2020; March-Mifsut and Castro, 2010). Specifically in the URB, areas characterized by higher precipitation levels and intermediate altitudes were identified as more susceptible to drought and should receive priority attention in water planning efforts. This study holds great interest to policymakers and stakeholders, providing them with valuable insights to identify vulnerable regions for planning and implementing adaptive measures to mitigate the potential impacts of droughts on populations, ecosystems, and economic activities within these regions.

2. Spatial and temporal variability in sedimentary accumulation in the study sites

The values of SAR and MAR estimated in the study sites were consistent with global range of values for mangrove forests (Alongi, 2012) and previous studies conducted in the regions (e.g., Cuellar-Martinez et al., 2020; Ruiz-Fernández et al., 2020). In the EV system, the maxima in MAR were attributed to meteorological events that influenced sediment supply during the study period; the identification of these events improved dating validation in the EV cores. Excluding these maxima, MAR in the EV cores were higher than in other mangrove areas on the Mexican Pacific coast but comparable to the MAR observed at other sites worldwide (e.g., Brunskill et al., 2002, 2004).

All sediment cores exhibited a comparable increase in MAR over the past century, contradicting the research hypothesis, which assumed that different meteorological and hydrological characteristics at the study sites would result in variable MAR. The exponential trends in MAR observed in the cores, with an acceleration from the 1950s onwards, coincided with reported population growth in the municipalities of Mazatlán, which includes the EV system, and El Carmen, which includes the PDE and CP systems (INEGI, 2022). The population in these municipalities doubled between 1900 and 1950 and increased by 7 times in the municipality of El Carmen and 10 times in the municipality of Mazatlán between 1950 and 2020. The population growth and associated economic development led to changes in land-use that generated a growing trend of erosion in coastal areas and upper basins (e.g., Ruiz-Fernández et al., 2009).

The SAR values, corrected for compaction effects along the sediment column, were comparable to the reported sea-level rise in the study sites (Zavala-Hidalgo et al., 2010, 2015), suggesting that mangroves accumulated sediments at a rate similar to local sea-level rise over the past century.

These findings suggested that sedimentary and hydrological conditions in the TL and EV areas, along with the state of the mangroves, have facilitated sediment accumulation in equilibrium with changes in sea-level and the coastline. While mangroves have demonstrated adaptation to anthropogenic disturbances over the past century, continuous monitoring of sediment accumulation is crucial to anticipate how these ecosystems will respond to global change and ensure favorable conditions for their long-term conservation.

3. Variability in origin, burial rates, and stocks of organic carbon in the study sites

The LTMPA02, LTMCA01, LTMCA03, and EVC01 cores predominantly showed contributions of C_{org} originating from fluvial inputs, a characteristic commonly observed in mangrove ecosystems influenced by rivers, where allochthonous C_{org} typically constitutes the majority of the total contribution (Kusumaningtyas et al., 2019b; Sasmito et al., 2019; Sidik and Friess, 2021). The LTMPA01 and LTMCA02 cores exhibited predominant contributions of autochthonous C_{org}, a common feature in mangrove ecosystems with minimal influence from rivers or tides, where C_{org} mainly originates from autochthonous sources such as mangrove leaf litter and roots (Alongi, 2014). The EVC02 core displayed a mixture of C_{org} derived from both fluvial and autochthonous sources, attributed to the combined effect of river discharge and storm events, which can lead to variations in deposition and export of allochthonous and autochthonous C_{org} inputs (Smoak et al., 2013; Pérez et al., 2018). The relatively minor contribution of C_{org} derived from phytoplankton or seagrasses in all cores indicated limited influence of tides on C_{org} supply at the study sites.

Over the past century, there was a progressive increase in C_{org} burial rates and stocks, contrary to the initial research hypothesis, which anticipated a decline due to increasing land-use changes

and mangrove cover loss. However, the increase in C_{org} burial rates and stocks was primarily attributed to the greater influx of C_{org} from fluvial systems, driven by continental erosion resulting from land-use change (Jupin et al., 2023). Additionally, the contribution of autochthonous C_{org} increased in most sedimentary records, suggesting that, despite reported reductions in mangrove cover within the basins, this ecosystem has continued to serve as an important producer and efficient sink of autochthonous C_{org}.

Global patterns generally report lower C_{org} burial rates and stocks in carbonate systems with predominantly autochthonous C_{org} inputs compared to terrigenous systems that receive high allochthonous inputs (Atwood et al., 2017; Breithaupt and Steinmuller, 2022), However, in the study sites, higher C_{org} burial rates and stocks were observed in mangrove areas with limited fluvial influence and dominant autochthonous C_{org} inputs. The lack of compatibility between the obtained results and global patterns was attributed to the strong local variability evidenced in this study, as well as possible biases in the databases (e.g., scarce data, variations in sampling methods, potential errors in observations; Sidik and Friess, 2021). Moreover, this study, along with other publications using dated sediment cores (e.g., Cuellar-Martinez et al., 2020; López-Mendoza et al., 2020), have shown that C_{org} stocks vary over time. Using comparable time frames (e.g., centennial, such as 1900–2000 or 1920–2020), employing reliable dating methods (e.g., ^{210}Pb) and standardized measurement techniques (e.g., Howard et al., 2014) could mitigate bias in assessments of C_{org} burial rates and stocks.

4. Spatial and temporal variability in the composition and stability of organic carbon in the study sites

The OM found in the four sediment cores LTMPA01, LTMPA02, LTMCA03 exhibited a low content in hydrogenated compounds and a high content in oxygenated compounds, which was indicative of an OM primarily derived from degraded terrestrial detritus during its transport to the deposition zone (Meyers and Lallier-Vergès, 1999). It is also possible that a portion of the OM found in the cores was originated from local production (e.g., mangrove detritus) and marine or lagoon phytoplankton but had undergone certain degradation before its deposition, which would result in a decrease in the hydrogen index and a slight increase in the oxygen index (Meyers, 1997). The refractory nature of the organic material of the cores was confirmed by the prevalent presence of thermal groups of organic components highly resistant to pyrolysis, which degraded above 400°C, along with degraded and amorphous particles identified in the sediment cores. The similar compositions in thermal groups of organic components and palynofacies in the four sediment cores indicated general similarities in sources and deposition conditions among the sites, whereas the spatial variation in the quantity and stability of C_{org} among the cores was attributed to local hydrological and sedimentary conditions (Twilley et al., 2018; Jennerjahn, 2020).

In the LTMPA02 and LTMCA03 cores, the decrease in the quantity and lability of C_{org} within the first 10 centimeters was partly attributed to early diagenesis, as evidenced by the decrease in the hydrogen index, indicating dehydrogenation of organic compounds and loss of hydrogen bonds, and the increase in the oxygen index due to mineralization and carbon loss (Meyers, 1997). Conversely, in the LTMPA01 and EVC01 cores, the increase in the quantity and lability of C_{org} from 1990 to 2021 was attributed to increasing contributions of labile and autochthonous C_{org} during this period, possibly coupled with better preservation of this material, as indicated by both increasing HI and OI toward the present. With exception of the subsurface, in all cores, changes in the quantity and lability of C_{org} were associated to specific events of precipitation and river

discharge (Kusumaningtyas et al., 2019b). The following pattern was observed: increased flow and preservation of labile C_{org} in sediment cores coincided with low river discharge and precipitation, whereas high contributions of refractory C_{org} and intensified oxidation processes were observed during periods of high river discharge and precipitation.

The increasing trends in C_{org} concentrations and stocks were mainly attributed to the increasing river discharges observed since the 1950s in the TL (Benítez et al., 2005; Soto-Galera et al., 2010; Fichez et al., 2017; no data available for EV) and the consequent increase in sediment transport from rivers to mangrove areas (Jupin et al., 2023). This observation confirmed the research hypothesis that suggested a shift from autochthonous- to allochthonous-dominated C_{org} storage toward recent decades, which would reduce the proportion of labile C_{org} stocks in mangrove sediments. The increase in river flow from the river basins was not related to precipitation, as the latter rather decreased in these regions during comparable periods (Benítez et al., 2005; Fichez et al., 2017; Jupin et al., 2024; Llanes-Cárdenas et al., 2022). This study demonstrated that over time, the studied mangroves have adapted to the increase in fluvial sediment and allochthonous C_{org} inputs, resulting in higher C_{org} stocks in sediments. Although C_{org} mainly originated from external sources and exists in a refractory form rather than being derived from *in situ* capture of atmospheric CO_2 and newly formed C_{org}, sedimentary stocks in those mangrove ecosystems are stable and efficient C_{org} sinks over time; therefore, their conservation can significantly contribute to climate change mitigation.

CONCLUSIONS

This doctoral work is the first reconstruction of the recent temporal variability (~100 years) of the origin, composition, concentration, burial rates, stocks, and stability of organic carbon (C_{org}) in mangrove sediment cores from two coastal Ramsar sites in Mexico (Terminos Lagoon, Campeche, and El Verde Camacho Lagoon, Sinaloa) through the analysis of seven Lead-210-dated sediment cores and the study of environmental variables (e.g., precipitation trends, sediment accumulation rates, and sea-level rise). The study provided new insights into the role of mangroves as efficient and long-term sinks of C_{org} under changing environmental conditions over the past century.

The main advancements of this work are as follows:

(i) A relationship was found between the spatial variability in precipitation in the Usumacinta River basin and the basin topography. The occurrence of extreme precipitation events in the three river basins flowing into TL and EV was influenced by the El Niño-Southern Oscillation phenomenon on an interannual scale. This connection underscores the intricate interplay between large-scale climatic patterns and regional hydrological processes, shaping the frequency and intensity of extreme weather events in the study areas. Since the 1960s, increased aridity was observed in these river basins, attributed to climate change, posing significant challenges for water resource management and ecosystem sustainability in these areas.

(ii) Overall, sediment cores collected at study sites with different climatic, hydrological, and demographic characteristics recorded similar trends in sediment accumulation rates and the composition and origin of C_{org}. However, disparities were observed among cores from the same

site, highlighting marked local variability primarily influenced by sedimentary and hydrological conditions in the lagoons.

(iii) In the study sites, trends in sediment and C_{org} accumulation do not appear to be directly linked to precipitation trends in the region. Instead, increasing sediment and C_{org} accumulation were associated with the rising river discharge resulting from intensified continental erosion driven by population growth and alterations in land use and land cover. However, the occurrence of extreme precipitation events, which can lead to heightened river flows, resulted in increased inputs of refractory C_{org} and oxidation processes affecting C_{org} deposited in mangrove sediments.

(iv) Despite alterations in source and transport of sediment and C_{org} due to anthropogenic activities within the river basins, mangroves showed remarkable resilience in adapting to these changes over the past century, as evidenced by their progressive adjustments in C_{org} accumulation and production. The increase in sediment inputs from rivers also contributed to assisting mangroves to adapt to rising sea-level.

(v) This study illustrated that the study mangroves served as efficient and long-term sinks for C_{org}, suggesting that their conservation could represent a natural and effective strategy to contribute to climate change mitigation.

This study underscores the critical necessity of globally monitoring mangroves to better understand their role in the carbon cycle and their response to both climate change and human intervention over time. This approach will facilitate comparisons across different mangrove areas and countries, enabling the identification of general patterns regulating the sources, accumulation, and preservation of C_{org} in mangrove sediments, while also acknowledging the inherent local variability within these complex ecosystems. The quantitative results obtained in this study can

support mangrove conservation efforts in the study sites and provide valuable insights for future research on mangroves globally. Given the diverse, complex, and dynamic nature of mangrove ecosystems, forest management strategies should be approached from a multi-temporal (short to long-term), multidimensional (local to global), and multidisciplinary (e.g., economic, environmental, and social) perspective.

REFERENCES

Abahous, H., Sifeddine, A., Bouchaou, L., Ronchail, J., El Morjani, Z.E.A., Ait Brahim, Y.K., Kenny, L., 2018. Inter-annual variability of precipitation in the Souss Massa region and linkage of the North Atlantic Oscillation. Journal of Materials and Environmental Science 9, 2023–2031.

Adame, M.F., Wright, S.F., Grinham, A., Lobb, K., Reymond, C.E., Lovelock, C.E., 2012. Terrestrial-marine connectivity: Patterns of terrestrial soil carbon deposition in coastal sediments determined by analysis of glomalin related soil protein. Limnol Oceanogr 57, 1492–1502. https://doi.org/10.4319/lo.2012.57.5.1492

Aguilar, E., Peterson, T.C., Obando, P.R., Frutos, R., Retana, J.A., Solera, M., Soley, J., García, I.G., Araujo, R.M., Santos, A.R., Valle, V.E., Brunet, M., Aguilar, L., Álvarez, L., Bautista, M., Castañón, C., Herrera, L., Ruano, E., Sinay, J.J., Sánchez, E., Hernández-Oviedo, G.I., Obed, F., Salgado, J.E., Vázquez, J.L., Baca, M., Gutiérrez, M., Centella, C., Espinosa, J., Martínez, D., Olmedo, B., Espinoza, C.E., Ojeda-Núñez, R., Haylock, M., Benavides, H., Mayorga, R., 2005. Changes in precipitation and temperature extremes in Central America and northern South America, 1961-2003. Journal of Geophysical Research Atmospheres 110, 1–15. https://doi.org/10.1029/2005JD006119

Aldana-Gutiérrez, G., Ruiz-Fernández, A.C., Pérez-Bernal, L.H., Flores-Verdugo, F., Cuéllar-Martínez, T., Sanchez-Cabeza, J.A., 2021. Flujos e inventarios de carbono azul en manglares asociados a una laguna costera antropizada. Geofísica Internacional 60, 13–30. https://doi.org/10.22201/igeof.00167169p.2021.60.1.2011

Alfaro-Córdoba, M., Hidalgo, H.G., Alfaro, E.J., 2020. Aridity Trends in Central America: A Spatial Correlation Analysis. Atmosphere (Basel) 11, 427. https://doi.org/10.3390/atmos11040427

Alongi, D.M., 2020. Global Significance of Mangrove Blue Carbon in Climate Change Mitigation (Version 1). Sci 2, 57. https://doi.org/10.3390/sci2030057

Alongi, D.M., 2014. Carbon cycling and storage in mangrove forests. Ann Rev Mar Sci 6, 195–219. https://doi.org/10.1146/annurev-marine-010213-135020

Alongi, D.M., 2012. Carbon sequestration in mangrove forests. Carbon Manag 3, 313–322. https://doi.org/10.4155/cmt.12.20

Alongi, D.M., 2009. The energetics of mangrove forests, Springer Science & Business Media. Springer SBM, Dordrecht, Netherlands.

Alongi, D.M., 2008. Mangrove forests: Resilience, protection from tsunamis, and responses to global climate change. Estuar Coast Shelf Sci 76, 1–13. https://doi.org/10.1016/j.ecss.2007.08.024

Alongi, D.M., Murdiyarso, D., Fourqurean, J.W., Kauffman, J.B., Hutahaean, A., Crooks, S., Lovelock, C.E., Howard, J., Herr, D., Fortes, M., Pidgeon, E., Wagey, T., 2016. Indonesia's blue carbon: a globally significant and vulnerable sink for seagrass and mangrove carbon. Wetl Ecol Manag 24, 3–13. https://doi.org/10.1007/s11273-015-9446-y

Alongi, D.M., Pfitzner, J., Trott, L.A., Tirendi, F., Dixon, P., Klumpp, D.W., 2005. Rapid sediment accumulation and microbial mineralization in forests of the mangrove Kandelia candel in the Jiulongjiang Estuary, China. Estuar Coast Shelf Sci 63, 605–618. https://doi.org/10.1016/j.ecss.2005.01.004

Atwood, T.B., Connolly, R.M., Almahasheer, H., Carnell, P.E., Duarte, C.M., Lewis, C.J.E., Irigoien, X., Kelleway, J.J., Lavery, P.S., Macreadie, P.I., Serrano, O., Sanders, C.J., Santos, I.R., Steven, A.D.L., Lovelock, C.E., 2017. Global patterns in mangrove soil carbon stocks and losses. Nat Clim Chang 7, 523–528. https://doi.org/10.1038/nclimate3326

Ayala-Pérez, L.A., Ramos, J., Flores, D., Sosa, A., Martinez, E., 2015. Ictiofauna Marina y Costera de Campeche. Universidad Autónoma de Campeche, Unversidad Autónoma Metropolitana-Xochimilco.

Bao, H., Wu, Y., Unger, D., Du, J., Herbeck, L.S., Zhang, J., 2013. Impact of the conversion of mangroves into aquaculture ponds on the sedimentary organic matter composition in a tidal flat estuary (Hainan Island, China). Cont Shelf Res 57, 82–91. https://doi.org/10.1016/j.csr.2012.06.016

Benítez, J.A., 2010. Situación actual de las cuencas de los ríos Candelaria y Hondo, in: Cotler-Avalos, H. (Ed.), Las Cuencas Hidrográficas de México. Diagnóstico y Priorización. Mexico City, pp. 203–209.

Benítez, J.A., Sanvicente Sánchez, H., Lafragua Contreras, J., Zamora Crescencio, P., Morales Manilla, L.M., Mas Caussel, J.F., García Gil, G., Couturier, S.A., Zetina Tapia, R., Calan Yam, R.A., Amabilis Sánchez, L., Acuña, C., Mejenes, M., 2005. Sistemas de información geográfica de la cuenca del río Candelaria: reconstrucción histórica de los cambios de cobertura forestal y su efecto sobre la hidrología y calidad del agua-marco teórico y resultados iniciales, in: Edith, F., Kauffer, M. (Eds.), El Agua En La Frontera México-Guatemala- Belice. Ecosur/tnc/unach, Tuxtla Gutiérrez, Chiapas, pp. 19–32.

Borges, A. V., Djenidi, S., Lacroix, G., Théate, J., Delille, B., Frankignoulle, M., 2003. Atmospheric CO2 flux from mangrove surrounding waters. Geophys Res Lett 30, 12–15. https://doi.org/10.1029/2003GL017143

Bouillon, S., Borges, A. V., Castañeda-Moya, E., Diele, K., Dittmar, T., Duke, N.C., Kristensen, E., Lee, S.Y., Marchand, C., Middelburg, J.J., Rivera-Monroy, V.H., Smith, T.J., Twilley, R.R., 2008. Mangrove production and carbon sinks: A revision of global budget estimates. Global Biogeochem Cycles 22, 1–12. https://doi.org/10.1029/2007GB003052

Bouillon, S., Dahdouh-Guebas, F., Rao, A.V.V.S., Koedam, N., Dehairs, F., 2003. Sources of organic carbon in mangrove sediments: Variability and possible ecological implications. Hydrobiologia 495, 33–39. https://doi.org/10.1023/A:1025411506526

Bouillon, S., Moens, T., Overmeer, I., Koedam, N., Dehairs, F., 2004. Resource utilization patterns of epifauna from mangrove forests with contrasting inputs of local versus imported organic matter. Mar Ecol Prog Ser 278, 77–88. https://doi.org/10.3354/meps278077

Boysen-Jensen, P., Station, C.D.B., 1915. Studies concerning the organic matter of the sea bottom. Copenhagen Dansk Biologisk.

Breithaupt, J.L., Smoak, J.M., Smith, T.J., Sanders, C.J., Hoare, A., 2012. Organic carbon burial rates in mangrove sediments: Strengthening the global budget. Global Biogeochem Cycles 26, 1–11. https://doi.org/10.1029/2012GB004375

Breithaupt, J.L., Steinmuller, H.E., 2022. Refining the Global Estimate of Mangrove Carbon Burial Rates Using Sedimentary and Geomorphic Settings. Geophys Res Lett 49. https://doi.org/10.1029/2022GL100177

Briseño-Dueñas, R., 2003. Ficha Informativa de los Humedales de Ramsar (FIR). "Playa Tortuguera El Verde Camacho" [WWW Document]. URL https://rsis.ramsar.org/RISapp/files/RISrep/MX1349RIS.pdf (accessed 2.1.22).

Brunskill, G.J., Zagorskis, I., Pfitzner, J., 2002. Carbon Burial Rates in Sediments and a Carbon Mass Balance for the Herbert River Region of the Great Barrier Reef Continental Shelf, North Queensland, Australia. Estuar Coast Shelf Sci 54, 677–700. https://doi.org/10.1006/ecss.2001.0852

Brunskill, G.J., Zagorskis, I., Pfitzner, J., Ellison, J., 2004. Sediment and trace element depositional history from the Ajkwa River estuarine mangroves of Irian Jaya (West Papua), Indonesia. Cont Shelf Res 24, 2535–2551. https://doi.org/10.1016/j.csr.2004.07.024

Cai, W., Ng, B., Wang, G., Santoso, A., Wu, L., Yang, K., 2022. Increased ENSO sea surface temperature variability under four IPCC emission scenarios. Nat Clim Chang 12, 228–231. https://doi.org/10.1038/s41558-022-01282-z

Cerón-Bretón, J.G., Cerón-Bretón, R.M., Rangel-marrón, M.M., Muriel-García, M., Cordova-Quiroz, A. V., Estrella-Cahuich, A., 2011. Determination of carbon sequestration rate in soil of a mangrove forest in Campeche, Mexico. WSEAS Transactions on Environment and Development 7, 54–64.

Chacón, R.E., Fernandez, W., 1985. Temporal and spatial rainfall variability in the mountainous region of the reventazón river basin, costa rica. Journal of Climatology 5, 175–188. https://doi.org/10.1002/joc.3370050205

Chmura, G.L., Anisfeld, S.C., Cahoon, D.R., Lynch, J.C., 2003. Global carbon sequestration in tidal, saline wetland soils. Global Biogeochem Cycles 17, n/a-n/a. https://doi.org/10.1029/2002gb001917

Combaz, A., 1964. Les palynofaciès. Revue de Micropaléontologie 7, 205–218.

CONABIO, 2020. Manglares de México. Actualización y análisis de los datos 2020. Comisión Nacional para el Conocimiento y Uso de la Biodiversidad, México CDMX.

CONABIO, 2017. Enciclovida CONABIO [WWW Document]. URL http://bios.conabio.gob.mx/ (25/05/2020).

CONAGUA, 2015. Determinación de la Disponibilidad de Agua en el acuífero Río Quelite (2508), estado de Sinaloa [WWW Document]. Comisión Nacional del Agua. URL https://www.gob.mx/cms/uploads/attachment/file/103346/DR_2508.pdf (accessed 4.23.24).

Conrad, S., Brown, D.R., Alvarez, P.G., Bates, B., Ibrahim, N., Reid, A., Monteiro, L.S., Silva, D.A., Mamo, L.T., Bowtell, J.R., Lin, H.A., Tolentino, N.L., Sanders, C.J., 2019. Does regional development influence sedimentary blue carbon stocks? A case study from three Australian estuaries. Front Mar Sci 5. https://doi.org/10.3389/fmars.2018.00518

Cuellar-Martinez, T., Ruiz-Fernández, A.C., Sánchez-Cabeza, J.A., Pérez-Bernal, L., López-Mendoza, P.G., Carnero-Bravo, V., Agraz-Hernández, C.M., van Tussenbroek, B.I., Sandoval-Gil, J., Cardoso-Mohedano, J.G., Vázquez-Molina, Y., Aldana-Gutiérrez, G., 2020. Temporal records of organic carbon stocks and burial rates in Mexican blue carbon coastal ecosystems throughout the Anthropocene. Glob Planet Change 192, 103215. https://doi.org/10.1016/j.gloplacha.2020.103215

Cuervo-Robayo, A.P., Téllez-Valdés, O., Gómez-Albores, M.A., Venegas-Barrera, C.S., Manjarrez, J., Martínez-Meyer, E., 2014. Precipitación anual en México (1910-2009). escala: 1:1000000. modificado por CONABIO (2015). México, D. F. [WWW Document]. URL http://www.conabio.gob.mx/informacion/gis/?vns=gis_root/clima/precip/preanu13gw (accessed 4.13.24).

Daly, C., Neilson, R.P., Phillips, D.L., 1994. A Statistical-Topographic Model for Mapping Climatological Precipitation over Mountainous Terrain. Journal of Applied Meteorology 33, 140–158. https://doi.org/10.1175/1520-0450(1994)033<0140:ASTMFM>2.0.CO;2

Davidson, E.A., Janssens, I.A., 2006. Temperature sensitivity of soil carbon decomposition and feedbacks to climate change. Nature 440, 165–173. https://doi.org/10.1038/nature04514

DDEP, 2012. Table de radionucleides 210Pb [WWW Document]. LNE-LNHB/CEA. URL http://www.nucleide.org/DDEP_WG/ DDEPdata.htm. (accessed 1.30.22).

De la Barreda, B., Metcalfe, S.E., Boyd, D.S., 2020. Precipitation regionalization, anomalies and drought occurrence in the Yucatan Peninsula, Mexico. International Journal of Climatology 40, 4541–4555. https://doi.org/10.1002/joc.6474

Disnar, J.R., Guillet, B., Keravis, D., Di-Giovanni, C., Sebag, D., 2003. Soil organic matter (SOM) characterization by Rock-Eval pyrolysis: scope and limitations. Org Geochem 34, 327–343. https://doi.org/10.1016/S0146-6380(02)00239-5

Dittmar, T., Lara, R.J., Kattner, G., 2001. River or mangrove? Tracing major organic matter sources in tropical Brazilian coastal waters. Mar Chem 73, 253–271. https://doi.org/10.1016/S0304-4203(00)00110-9

Duarte, C.M., Cebrián, J., 1996. The fate of marine autotrophic production. Limnol Oceanogr 41, 1758–1766. https://doi.org/10.4319/lo.1996.41.8.1758

Durán-Quesada, M.A., Gimeno, L., Amador, J., 2017. Role of moisture transport for Central American precipitation. Earth System Dynamics 8, 147–161. https://doi.org/10.5194/esd-8-147-2017

Easterling, D.R., 2013. Global Data Sets for Analysis of Climate Extremes, in: AghaKouchak, A., Easterling, D., Hsu, K., Schubert, S., Sorooshian, S. (Eds.), Extremes in a Changing Climate. Detection, Analysis and Uncertainty, Water Science and Technology Library. Springer Netherlands, Dordrecht, pp. 347–361. https://doi.org/10.1007/978-94-007-4479-0

Emeis, K.-C., Struck, U., Leipe, T., Pollehne, F., Kunzendorf, H., Christiansen, C., 2000. Changes in the C, N, P burial rates in some Baltic Sea sediments over the last 150 years—relevance to P regeneration rates and the phosphorus cycle. Mar Geol 167, 43–59. https://doi.org/10.1016/S0025-3227(00)00015-3

Espitalié, J., Deroo, G., Marquis, F., 1985a. Rock-Eval pyrolysis and its applications (part one). Oil \& Gas Science and Technology-Revue d'IFPEN 40, 563–579.

Espitalié, J., Deroo, G., Marquis, F., 1985b. La pyrolyse Rock-Eval et ses applications. Deuxième partie. Revue de l'Institut français du Pétrole 40, 755–784.

Fernández, W., Chacón, R.E., Melgarejo, J.W., 1996. On the rainfall distribution with altitude over Costa Rica, in: Revista Geofisica. pp. 56–72.

Fichez, R., Archundia, D., Grenz, C., Douillet, P., Gutiérrez-Mendieta, F., Origel-Moreno, M., Denis, L., Contreras-Ruiz-Esparza, A., Zavala-Hidalgo, J., 2017. Global climate change and local watershed management as potential drivers of salinity variation in a tropical coastal lagoon (Laguna de Terminos, Mexico). Aquat Sci 79, 219–230. https://doi.org/10.1007/s00027-016-0492-1

Flores-Verdugo, F.J., 1985. Fauna survey of the decapod crustaceans, reptiles and coastal birds of the Estero el Verde, Sinaloa, Mexico, with some notes on their biology. Deep Sea Research Part B. Oceanographic Literature Review 32, 757–758. https://doi.org/10.1016/0198-0254(85)92890-0

Flores-Verdugo, F.J., Briseño-Dueñas, R., González-Farías, F., Calvario-Martínez, O., 1995. Balance de carbono en un ecosistema lagunar estuarino de boca efímera de la costa noroccidental de México (Estero El Verde, Sinaloa). Temas de oceanografía biológica en México. Universidad Autónoma de Baja California. Ensenada, 8.C., México. II.

Flores-Verdugo, F.J., Day, J.W., Briseño-Dueñas, R., 1987. Structure, litter fall, decomposition, and detritus dynamics of mangroves in a Mexican coastal lagoon with an ephemeral inlet. Mar Ecol Prog Ser 35, 83–90.

Fuentes, H., 2021. Análisis del Control de Calidad de Base de Datos Climática. [WWW Document]. Unidad de Cambio Climático Instituto Nacional de Sismología, Vulcanología, Meteorología e Hidrología. URL https://insivumeh.gob.gt/wp-content/uploads/2022/03/AnalisisControlCalidad.pdf (accessed 11.13.21).

Gilman, E.L., Ellison, J.C., Duke, N.C., Field, C., 2008. Threats to mangroves from climate change and adaptation options: A review. Aquat Bot 89, 237–250. https://doi.org/10.1016/j.aquabot.2007.12.009

Glaser, M., Krause, G., Oliveira, R.S., Fontalvo-Herazo, M., 2010. Mangroves and People: A Social-Ecological System. pp. 307–351. https://doi.org/10.1007/978-3-642-13457-9_21

Goldberg, L., Lagomasino, D., Thomas, N., Fatoyinbo, T., 2020. Global declines in human-driven mangrove loss. Glob Chang Biol 26, 5844–5855. https://doi.org/10.1111/gcb.15275

Gonneea, M.E., Paytan, A., Herrera-Silveira, J.A., 2004. Tracing organic matter sources and carbon burial in mangrove sediments over the past 160 years. Estuar Coast Shelf Sci 61, 211–227. https://doi.org/10.1016/j.ecss.2004.04.015

González-Farias, F., 1985. Importancia ecológica de la materia orgánica y su biodegradación en el estero de El Verde, Sinaloa, México. Tesis doctoral. U.A.C.P.P.-CCH, UNAM. México.

González-Farías, F., Mee, L.D., 1988. Effect of mangrove humic-like substances on biodegradation rate of detritus. J Exp Mar Biol Ecol 119, 1–13. https://doi.org/10.1016/0022-0981(88)90148-7

Guijarro, J.A., 2024. Homogenization of climatological series with Climatol Version 4.1.0 [WWW Document]. URL https://cran.r-project.org/web/packages/climatol/climatol.pdf (accessed 4.23.24).

Hannah, L., Donatti, C.I., Harvey, C.A., Alfaro, E., Rodriguez, D.A., Bouroncle, C., Castellanos, E., Diaz, F., Fung, E., Hidalgo, H.G., Imbach, P., Läderach, P., Landrum, J.P., Solano, A.L.,

2017. Regional modeling of climate change impacts on smallholder agriculture and ecosystems in Central America. Clim Change 141, 29–45. https://doi.org/10.1007/s10584-016-1867-y

Hastenrath, S.L., 1967. Rainfall distribution and regime in Central America. Archiv für Meteorologie, Geophysik und Bioklimatologie Serie B 15, 201–241. https://doi.org/10.1007/BF02243853

Herr, D., Landis, E., 2016. Coastal blue carbon ecosystems. Opportunities for Nationally Determined Contributions. Policy Brief. Gland, Switzerland and Washington, DC, USA.

Herrera-Silveira, J.A., Pech-Cardenas, M.A., Morales-Ojeda, S.M., Cinco-Castro, S., Camacho-Rico, A., Caamal-Sosa, J.P., Mendoza-Martinez, J.E., Pech-Poot, E.Y., Montero, J., Teutli-Hernández, C., 2020. Blue carbon of Mexico, carbon stocks and fluxes: a systematic review. PeerJ 8, e8790. https://doi.org/10.7717/peerj.8790

Herrera-Silveira, J.A., Teutli-Hernández, C., Camacho-Rico, A., 2017. Coastal Tidal Wetlands of Mexico : Potential Carbon Sequestration of Mangroves and Public Policies. Elementos para políticas Públicas 1, 63–68.

Hidalgo, H.G., Alfaro, E.J., Quesada-Montano, B., 2017. Observed (1970–1999) climate variability in Central America using a high-resolution meteorological dataset with implication to climate change studies. Clim Change 141, 13–28. https://doi.org/10.1007/s10584-016-1786-y

Hidalgo, H.G., Amador, J.A., Alfaro, E.J., Quesada, B., 2013. Hydrological climate change projections for Central America. J Hydrol (Amst) 495, 94–112. https://doi.org/10.1016/j.jhydrol.2013.05.004

Houghton, J.G., 1979. A Model for Orographic Precipitation in the North-Central Great Basin. Mon Weather Rev 107, 1462–1475. https://doi.org/10.1175/1520-0493(1979)107<1462:AMFOPI>2.0.CO;2

Howard, J., Hoyt, S., Isensee, K., Telszewski, M., Pidgeon, E., (eds), 2014. Coastal blue carbon: methods for assessing carbon stocks and emissions factors in mangroves, tidal salt marshes, and seagrasses. Conservational International, Intergovernmental Oceanographic Commission of UNESCO, International Union for Conservation of Nature., Arlington, Virginia, USA.

INECC–SEMARNAT, 2022. Contribución Determinada a Nivel Nacional. Actualización 2022 [WWW Document]. URL https://unfccc.int/documents/624282 (accessed 4.18.24).

INEGI, 2022. Serie histórica censal e intercensal (1990-2010) [WWW Document]. URL https://www.inegi.org.mx/programas/ccpv/cpvsh/ (accessed 4.1.22).

INEGI-INE-CONAGUA, 2007. Mapa de Cuencas Hidrográficas de México. Instituto Nacional de Estadística Geografía e Informática (INEGI), Instituto Nacional de Ecología (INE), Comisión

Nacional de Agua (CONAGUA). ElaboradO por Priego A.G., Isunza E., Luna N. y Pérez J.L [WWW Document]. URL http://www.conabio.gob.mx/informacion/gis/?vns=gis_root/hidro/chidro/cue250k_07gw (accessed 4.13.24).

Jennerjahn, T.C., 2020. Relevance and magnitude of "Blue Carbon" storage in mangrove sediments: Carbon accumulation rates vs. stocks, sources vs. sinks. Estuar Coast Shelf Sci 247, 107027. https://doi.org/10.1016/j.ecss.2020.107027

Jupin, J.L.J., Garcia-López, A.A., Briceño-Zuluaga, F.J., Sifeddine, A., Ruiz-Fernández, A.C., Sanchez-Cabeza, J., Cardoso-Mohedano, J.G., 2024. Precipitation homogenization and trends in the Usumacinta River Basin (Mexico-Guatemala) over the period 1959–2018. International Journal of Climatology 44, 108–125. https://doi.org/10.1002/joc.8318

Jupin, J.L.J., Ruiz-Fernández, A.C., Sifeddine, A., Sanchez-Cabeza, J.A., Pérez-Bernal, L.H., Cardoso-Mohedano, J.G., Gómez-Ponce, M.A., Flores-Trujillo, J.G., 2023. Anthropogenic drivers of increasing sediment accumulation in contrasting Mexican mangrove ecosystems. Catena (Amst) 226, 107037. https://doi.org/10.1016/j.catena.2023.107037

Karmalkar, A. V., Bradley, R.S., Diaz, H.F., 2011. Climate change in Central America and Mexico: Regional climate model validation and climate change projections. Clim Dyn 37, 605–629. https://doi.org/10.1007/s00382-011-1099-9

Kauffer-Michel, E.F., 2010. Hidropolítica del Candelaria: del análisis de la cuenca al estudio de las interacciones entre el río y la sociedad ribereña. Relaciones. Estudios de historia y sociedad XXXI, 187–226.

Koide, M., Bruland, K.W., Goldberg, E.D., 1973. Th-228/Th-232 and Pb-210 geochronologies in marine and lake sediments. Geochim Cosmochim Acta 37, 1171–1187. https://doi.org/10.1016/0016-7037(73)90054-9

Koné, Y.J.M., Borges, A. V., 2008. Dissolved inorganic carbon dynamics in the waters surrounding forested mangroves of the Ca Mau Province (Vietnam). Estuar Coast Shelf Sci 77, 409–421. https://doi.org/10.1016/j.ecss.2007.10.001

Kristensen, Erik, Bouillon, S., Dittmar, T., Marchand, C., 2008. Organic carbon dynamics in mangrove ecosystems: A review. Aquat Bot. https://doi.org/10.1016/j.aquabot.2007.12.005

Kristensen, E., Bouillon, S., Dittmar, T., Marchand, C., 2008a. Organic carbon dynamics in mangrove ecosystems: A review. Aquat Bot 89, 201–219. https://doi.org/10.1016/j.aquabot.2007.12.005

Kristensen, E., Flindt, M.R., Ulomi, S., Borges, A. V., Abril, G., Bouillon, S., 2008b. Emission of CO2 and CH4 to the atmosphere by sediments and open waters in two Tanzanian mangrove forests. Mar Ecol Prog Ser 370, 53–67. https://doi.org/10.3354/meps07642

Kusumaningtyas, M.A., Hutahaean, A.A., Fischer, H.W., Pérez-Mayo, M., Ransby, D., Jennerjahn, T.C., 2019a. Variability in the organic carbon stocks, sources, and accumulation rates of Indonesian mangrove ecosystems. Estuar Coast Shelf Sci 218, 310–323. https://doi.org/10.1016/j.ecss.2018.12.007

Kusumaningtyas, M.A., Hutahaean, A.A., Fischer, H.W., Pérez-Mayo, M., Ransby, D., Jennerjahn, T.C., 2019b. Variability in the organic carbon stocks, sources, and accumulation rates of Indonesian mangrove ecosystems. Estuar Coast Shelf Sci 218, 310–323. https://doi.org/10.1016/j.ecss.2018.12.007

Letourneur, Y., Briand, M.J., Guillou, G., 2018. Pathways of organic matter in an estuarine mangrove trophic network assessed by carbon and nitrogen stable isotopes. Journal of the Marine Biological Association of the United Kingdom 98, 1559–1569. https://doi.org/10.1017/S0025315417001412

Liu, S., Huang, D., Chen, A., Wei, W., Brookes, P.C., Li, Y., Wu, J., 2014. Differential responses of crop yields and soil organic carbon stock to fertilization and rice straw incorporation in three cropping systems in the subtropics. Agric Ecosyst Environ 184, 51–58. https://doi.org/10.1016/j.agee.2013.11.019

Llanes-Cárdenas, O., Gutiérrez-Ruacho, O., Montiel-Montoya, J., E., 2022. Hot Extremes and Climatological Drought Indicators in the Transitional Semiarid-Subtropical Region of Sinaloa, Northwest Mexico. Pol J Environ Stud 31, 4567–4577. https://doi.org/10.15244/pjoes/149882

Llanes-Cárdenas, O., Norzagaray-Campos, M., Muñoz-Sevilla, P., Ruiz-Guerrero, R., González-Ocampo, H., Herrera -Moreno, M., 2016. Estimating Trends and Return Periods of Daily Extreme Precipitation Associated with Tropical Cyclones in the Core North American Monsoon. Pol J Environ Stud 25, 2283–2292. https://doi.org/10.15244/pjoes/64161

López-Mendoza, P.G., Ruiz-Fernández, A.C., Sánchez-Cabeza, J.A., van Tussenbroek, B.I., Cuellar-Martinez, T., Pérez-Bernal, L.H., 2020. Temporal trends of organic carbon accumulation in seagrass meadows from the northern Mexican Caribbean. Catena (Amst) 194, 104645. https://doi.org/10.1016/j.catena.2020.104645

MacKenzie, R.A., Foulk, P.B., Klump, J. V., Weckerly, K., Purbospito, J., Murdiyarso, D., Donato, D.C., Nam, V.N., 2016. Sedimentation and belowground carbon accumulation rates in mangrove forests that differ in diversity and land use: a tale of two mangroves. Wetl Ecol Manag 24, 245–261. https://doi.org/10.1007/s11273-016-9481-3

Macreadie, P.I., Anton, A., Raven, J.A., Beaumont, N.J., Connolly, R.M., Friess, D.A., Kelleway, J.J., Kennedy, H., Kuwae, T., Lavery, P.S., Lovelock, C.E., Smale, D.A., Apostolaki, E.T., Atwood, T.B., Baldock, J.A., Bianchi, T.S., Chmura, G.L., Eyre, B.D., Fourqurean, J.W., Hall-Spencer, J.M., Huxham, M., Hendriks, I.E., Krause-Jensen, D., Laffoley, D., Luisetti, T.,

Marbà, N., Masque, P., McGlathery, K.J., Megonigal, J.P., Murdiyarso, D., Russell, B.D., Santos, I.R., Serrano, O., Silliman, B.R., Watanabe, K., Duarte, C.M., 2019. The future of Blue Carbon science. Nat Commun 10, 1–13. https://doi.org/10.1038/s41467-019-11693-w

Magaña, V.O., Vázquez, J.L., Pérez, J.L., Pérez, J.B., 2003. Impact of El Niño on precipitation in Mexico. Geofisica Internacional 42, 313–330.

Maldonado, T., Alfaro, E.J., Hidalgo, H.G., 2018. A review of the main drivers and variability of central America's climate and seasonal forecast systems. Rev Biol Trop 66, S153–S175. https://doi.org/10.15517/rbt.v66i1.33294

Maldonado, T., Alfaro, E.J., Hidalgo, J.G., 2021. Análisis de los conglomerados de precipitación y sus cambios estacionales sobre América Central para el período 1976-2015. Revista de Matemática: Teoría y Aplicaciones 28, 337–362. https://doi.org/10.15517/rmta.v28i2.42322

Marchand, C., Disnar, J.R., Lallier-Vergés, E., Lottier, N., Lallier-Vergès, E., Lottier, N., 2005. Early diagenesis of carbohydrates and lignin in mangrove sediments subject to variable redox conditions (French Guiana). Geochim Cosmochim Acta 69, 131–142. https://doi.org/10.1016/j.gca.2004.06.016

March-Mifsut, I., Castro, M., 2010. Cuenca del rio Usumacinta: Perfil y perspectivas para su conservacion y desarrollo sustentable., in: Las Cuencas Hidrográficas de México. Diagnostico y Priorización. SEMARNAT, INE, Fundación Gonzalo Río Arronte I.A.P., Mexico City, pp. 194–197.

Márdero, S., Nickl, E., Schmook, B., Schneider, L., Rogan, J., Christman, Z., Lawrence, D., 2012. Sequías en el sur de la península de Yucatán: análisis de la variabilidad anual y estacional de la precipitación. Investigaciones Geográficas 19. https://doi.org/10.14350/rig.32466

Maul, G.A., Duedall, I.W., 2019. Demography of Coastal Populations, in: Finkl, C.W., Makowski, C. (Eds.), Encyclopedia of Coastal Science. Springer International Publishing, Cham, pp. 692–700.

Meyers, P.A., 1997. Organic geochemical proxies of paleoceanographic, paleolimnologic, and paleoclimatic processes. Org Geochem 27, 213–250. https://doi.org/10.1016/S0146-6380(97)00049-1

Meyers, P.A., 1994. Preservation of elemental and isotopic source identification of sedimentary organic matter. Chem Geol 114, 289–302. https://doi.org/10.1016/0009-2541(94)90059-0

Meyers, P.A., Lallier-Vergès, E., 1999. Lacustrine sedimentary organic matter records of Late Quaternary paleoclimates. J Paleolimnol 21, 345–372. https://doi.org/10.1023/A:1008073732192

Montero-Martínez, M.J., Santana-Sepúlveda, J.S., Pérez-Ortiz, N.I., Pita-Díaz, O., Castillo-Liñan, S., 2018. Comparing climate change indices between a northern (arid) and a southern (humid)

basin in Mexico during the last decades. Advances in Science and Research 15, 231–237. https://doi.org/10.5194/asr-15-231-2018

Murray-Tortarolo, G.N., 2021. Seven decades of climate change across Mexico. Atmosfera 34, 217–226. https://doi.org/10.20937/ATM.52803

Ono, K., Mano, M., Han, G.H., Nagai, H., Yamada, T., Kobayashi, Y., Miyata, A., Inoue, Y., Lal, R., 2015. Environmental controls on fallow carbon dioxide flux in a single-crop rice paddy, Japan. Land Degrad Dev 26, 331–339.

Osland, M.J., Feher, L.C., López-Portillo, J., Day, R.H., Suman, D.O., Guzmán Menéndez, J.M., Rivera-Monroy, V.H., 2018. Mangrove forests in a rapidly changing world: Global change impacts and conservation opportunities along the Gulf of Mexico coast. Estuar Coast Shelf Sci 214, 120–140. https://doi.org/10.1016/j.ecss.2018.09.006

Osono, T., Takeda, H., Azuma, J.I., 2008. Carbon isotope dynamics during leaf litter decomposition with reference to lignin fractions. Ecol Res 23, 51–55. https://doi.org/10.1007/s11284-007-0336-5

Pérez, A., Libardoni, B.G., Sanders, C.J., 2018. Factors influencing organic carbon accumulation in mangrove ecosystems. Biol Lett 14, 20180237. https://doi.org/10.1098/rsbl.2018.0237

Phang, V.X.H., Chou, L.M., Friess, D.A., 2015. Ecosystem carbon stocks across a tropical intertidal habitat mosaic of mangrove forest, seagrass meadow, mudflat and sandbar. Earth Surf Process Landf 40, 1387–1400. https://doi.org/10.1002/esp.3745

Primavera, J.H., Friess, D.A., Van Lavieren, H., Lee, S.Y., 2019. The mangrove ecosystem. In: World Seas: An Environmental Evaluation Volume III: Ecological Issues and Environmental Impacts. 666p., 2nd ed, World Seas: An Environmental Evaluation Volume III: Ecological Issues and Environmental Impacts. Elsevier Ltd. https://doi.org/10.1016/B978-0-12-805052-1.00001-2

Purvaja, R., Ramesh, R., 2001. Natural and and anthropogenic methane emission from coastal wetlands of South India. Environ Manage 27, 547–557. https://doi.org/10.1007/s002670010169

Puvaneswaran, K.M., Smithson, P.A., 1991. Precipitation - elevation relationships over Sri Lanka. Theor Appl Climatol 43, 113–122. https://doi.org/10.1007/BF00867468

Ramos-Miranda, J., Villalobos-Zapata, G.J., 2015. Aspectos socioambientales de la región de la laguna de Términos, Campeche. Universidad Autónoma de Campeche.

Ranjan, R.K., Routh, J., Val Klump, J., Ramanathan, A.L., 2015. Sediment biomarker profiles trace organic matter input in the Pichavaram mangrove complex, southeastern India. Mar Chem. https://doi.org/10.1016/j.marchem.2015.02.001

Ray, R., Michaud, E., Aller, R.C., Vantrepotte, V., Gleixner, G., Walcker, R., Devesa, J., Le Goff, M., Morvan, S., Thouzeau, G., 2018. The sources and distribution of carbon (DOC, POC, DIC) in a mangrove dominated estuary (French Guiana, South America). Biogeochemistry 138, 297–321. https://doi.org/10.1007/s10533-018-0447-9

Riley, G., 1944. The Carbon Metabolism And Efficiency Of The Earth As A Whole. Am Sci 32, 129–134.

Rosentreter, J.A., Maher, D.T., Erler, D. V., Murray, R.H., Eyre, B.D., 2018. Methane emissions partially offset "blue carbon" burial in mangroves. Sci Adv 4. https://doi.org/10.1126/sciadv.aao4985

Rovai, A.S., Twilley, R.R., Castañeda-Moya, E., Riul, P., Cifuentes-Jara, M., Manrow-Villalobos, M., Horta, P.A., Simonassi, J.C., Fonseca, A.L., Pagliosa, P.R., 2018. Global controls on carbon storage in mangrove soils. Nat Clim Chang 8, 534–538. https://doi.org/10.1038/s41558-018-0162-5

Rovira, P., Ramón-Vallejo, V., 2002. Labile and recalcitrant pools of carbon and nitrogen in organic matter decomposing at different depths in soil: An acid hydrolysis approach. Geoderma 107, 109–141. https://doi.org/10.1016/S0016-7061(01)00143-4

RSIS, 2024a. Área de Protección de Flora y Fauna. Playa Tortuguera El Verde Camacho [WWW Document]. Ramsar Sites Information Service. URL https://rsis.ramsar.org/ris/1349 (accessed 4.23.24).

RSIS, 2024b. Área de Protección de Flora y Fauna Laguna de Términos. [WWW Document]. Ramsar Sites Information Service. URL https://rsis.ramsar.org/ris/1356 (accessed 4.23.24).

Ruiz-Fernández, A.C., Hillaire-Marcel, C., de Vernal, A., Machain-Castillo, M.L., Vásquez, L., Ghaleb, B., Aspiazu-Fabián, J.A., Páez-Osuna, F., 2009. Changes of coastal sedimentation in the Gulf of Tehuantepec, South Pacific Mexico, over the last 100 years from short-lived radionuclide measurements. Estuar Coast Shelf Sci 82, 525–536. https://doi.org/10.1016/j.ecss.2009.02.019

Ruiz-Fernández, A.C., Sánchez-Cabeza, J.A., Cuéllar-Martínez, T., Pérez-Bernal, L.H., Carnero-Bravo, V., Ávila, E., Cardoso-mohedano, J.G., Sanchez-Cabeza, J.A., Cuéllar-Martínez, T., Pérez-Bernal, L.H., Carnero-Bravo, V., Ávila, E., Cardoso-mohedano, J.G., 2020. Increasing salinization and organic carbon burial rates in seagrass meadows from an anthropogenically-modified coastal lagoon in southern Gulf of Mexico. Estuar Coast Shelf Sci 242, 106843. https://doi.org/10.1016/j.ecss.2020.106843

Salas-Flores, M.A., Hernández-Cerda, M.E., Villicaña-Cruz, J., Azpra-Romero, E., Lomas Barrié, C.T., 2014. The Influence of Strong El Nino Phases on the Rainfall over the Yucatan Peninsula, Mexico. Scientific Annals of the 'Alexandru Ioan Cuza' University of Iasi:

Geography Series / Analele Stiintifice ale Universitatii ‘Alexandru Ioan Cuza’ - Seria Geografie 60, 15–28.

Salas-Flores, M.A., Jones, P.D., 2014. The Enso Influence in the Mexican Regional Precipitation during the Instrumental Period. Scientific Annals of the “Alexandru Ioan Cuza” University of Iasi: Geography Series / Analele Stiintifice Ale Universitatii “Alexandru Ioan Cuza” - Seria Geografie 60, 29–65.

Sanchez-Cabeza, J.A., Ruiz-Fernández, A.C., 2012. 210Pb sediment radiochronology: An integrated formulation and classification of dating models. Geochim Cosmochim Acta 82, 183–200. https://doi.org/10.1016/j.gca.2010.12.024

Sanders, C.J., Maher, D.T., Tait, D.R., Williams, D., Holloway, C., Sippo, J.Z., Santos, I.R., 2016a. Are global mangrove carbon stocks driven by rainfall? J Geophys Res Biogeosci 121, 2600–2609. https://doi.org/10.1002/2016JG003510

Sanders, C.J., Maher, D.T., Tait, D.R., Williams, D., Holloway, C., Sippo, J.Z., Santos, I.R., 2016b. Are global mangrove carbon stocks driven by rainfall? J Geophys Res Biogeosci 121, 2600–2609. https://doi.org/10.1002/2016JG003510

Sasmito, S.D., Taillardat, P., Clendenning, J.N., Cameron, C., Friess, D.A., Murdiyarso, D., Hutley, L.B., 2019. Effect of land-use and land-cover change on mangrove blue carbon: A systematic review. Glob Chang Biol 25, 4291–4302. https://doi.org/10.1111/gcb.14774

Sidik, F., Friess, D.A., 2021. Dynamic Sedimentary Environments of Mangrove Coasts. Elsevier. https://doi.org/10.1016/C2018-0-00130-9

Simard, M., Fatoyinbo, L., Smetanka, C., Rivera-Monroy, V.H., Castañeda-Moya, E., Thomas, N., Van der Stocken, T., 2019. Mangrove canopy height globally related to precipitation, temperature and cyclone frequency. Nat Geosci 12, 40–45. https://doi.org/10.1038/s41561-018-0279-1

Smith, J.N., 2001. Why should we believe 210Pb sediment geochronologies? J Environ Radioact 55, 121–123. https://doi.org/10.1016/S0265-931X(00)00152-1

Smith, S. V., 1981. Marine Macrophytes as a Global Carbon Sink. Science (1979) 211, 838–840. https://doi.org/10.1126/science.211.4484.838

Smoak, J.M., Breithaupt, J.L., Smith, T.J., Sanders, C.J., 2013. Sediment accretion and organic carbon burial relative to sea-level rise and storm events in two mangrove forests in Everglades National Park. Catena (Amst) 104, 58–66. https://doi.org/10.1016/j.catena.2012.10.009

Soria-Reinoso, I., Alcocer, J., Sánchez-Carrillo, S., García-Oliva, F., Cuevas-Lara, D., Cortés-Guzmán, D., Oseguera, L.A., 2022. The Seasonal Dynamics of Organic and Inorganic Carbon along the Tropical Usumacinta River Basin (Mexico). Water (Switzerland) 14. https://doi.org/10.3390/w14172703

Soto-Galera, E., Piera, J., López, P., 2010. Spatial and temporal land cover changes in Terminos Lagoon Reserve, Mexico. Rev Biol Trop 58, 565–575. https://doi.org/10.15517/rbt.v58i2.5229

Twilley, R.R., Chen, R.. H., Hargis, T., 1992. Carbon sinks in mangroves and their implications to carbon budget of tropical coastal ecosystems. Water Air Soil Pollut 64, 265–288.

Twilley, R.R., Rovai, A.S., Riul, P., 2018. Coastal morphology explains global blue carbon distributions. Front Ecol Environ 16, 503–508. https://doi.org/10.1002/fee.1937

Tyson, R. V., 1995. Sedimentary Organic Matter, Sedimentary Organic Matter. Springer Netherlands, Dordrecht. https://doi.org/10.1007/978-94-011-0739-6

Vazquez-Molina, Y., 2019. Flujos y tendencias de la acumulación de metales pesados y carbono orgánico en manglares de Puerto Morelos, Quintana Roo, México. Universidad Nacional Autónoma De México.

Wang, B., Luo, X., Yang, Y.M., Sun, W., Cane, M.A., Cai, W., Yeh, S.W., Liu, J., 2019. Historical change of El Niño properties sheds light on future changes of extreme El Niño. Proc Natl Acad Sci U S A 116, 22512–22517. https://doi.org/10.1073/pnas.1911130116

Ward, R.D., Friess, D.A., Day, R.H., Mackenzie, R.A., 2016. Impacts of climate change on mangrove ecosystems: a region by region overview. Ecosystem Health and Sustainability 2, e01211. https://doi.org/10.1002/ehs2.1211

WMO, 2017. Guidelines on the Calculation of Climate Normals. WMO-No. 1203 1–29.

Woodroffe, S.A., Horton, B.P., Larcombe, P., Whittaker, J.E., 2005. Intertidal mangrove foraminifera from the central Great Barrier Reef Shelf, Australia: Implications for sea-level reconstruction. J Foraminifer Res 35, 259–270. https://doi.org/10.2113/35.3.259

Zavala-Hidalgo, J., de Buen-Kalman, R., Romero-Centeno, R., Hernández-Maguey, F., 2010. Tendencias del nivel del mar en las costas mexicanas. Vulnerabilidad de la zonas costeras mexicanas ante el cambio climático 249–268.

Zavala-Hidalgo, J., Ochoa de la Torre, J.L., Sánchez-Cabeza, J.L., Machain-Castillo, M.L., Ruiz-Fernández, A.C., Hernández-Maguey, F., Santiago-Santiago, J.A., Gómez-Ramos, O., Zarza-Alvarado, M.A., Gutiérrez-Quijada, S.V., Kostoglodov, V., Ortiz-Figueroa, M., Blanchon, P.A., 2015. Cambios en el nivel del mar, in: Reporte Mexicano de Cambio Climático, Grupo I Bases Científicas. Mexicano de Cambio Climático, Grupo I Bases Científicas. Modelos y Modelación. Universidad Nacional Autónoma de México/Programa de Investigación en Cambio Climático, Cuidad de México, p. 57.

LIST OF FIGURES AND TABLES

Figures

Table

APPENDICES

Supplementary Material – Chapter 1

Table S1 Meteorological stations considered for the analysis of precipitation trends in the Usumacinta River Basin (1959-2018).

Station ID	Station name	Latitude (°)	Longitude (°)	Altitude (m asl)	Period start	Period end	Missing data (%)*	Cluster
MEXICO								
4024	Palizada	18.281	-92.169	4	01/11/1944	01/12/2018	8	2
4056	Molino Chumpán	17.989	-91.761	10	01/05/1978	01/12/2018	13	2
4086	El Zapote	18.364	-91.814	10	01/01/1996	01/12/2018	16	2
7001	Abasolo Chiapas[1]	16.833	-92.222	1280	01/10/1970	01/08/2012	7	2
7004	Agua azul	16.783	-90.917	640	01/01/1961	01/02/1987	18	2
7006	Altamirano[2]	16.792	-92.078	1240	01/06/1942	01/09/2019	4	1
7017	Bonampak	16.733	-91.083	360	01/06/1965	01/02/1981	18	1
7022	Playas de Catazaja	17.833	-92.156	10	01/06/1956	01/12/2019	19	2
7028	Chacamax	17.533	-91.778	60	01/01/1969	01/09/2019	16	2
7029	Chajul	16.833	-90.933	223	01/07/1967	01/12/1988	19	1
7031	Chanal	16.747	-92.375	2100	01/01/1969	01/09/2019	18	3
7036	Chilil	16.778	-92.542	2266	01/09/1967	01/10/2016	8	3
7041	El caliente[1]	16.300	-91.467	687	01/01/1969	01/06/1980	8	1
7043	El cedro	16.417	-91.083	510	01/05/1965	01/02/1994	7	2
7044	El colorado[1]	16.150	-91.150	300	01/01/1970	01/07/1994	6	1
7046	El euseba[1]	16.217	-91.333	379	01/01/1967	01/12/1995	6	1
7047	El Jabalí[1]	16.133	-91.367	360	01/01/1969	01/07/1994	5	1
7051	El Rosario[1]	16.850	-91.783	740	01/08/1965	01/11/1993	6	2
7052	El Zapotal[1]	16.167	-91.500	500	01/03/1970	01/07/1994	4	1
7055	Finca Chayabé	16.514	-91.806	1596	01/09/1955	01/09/2019	6	1
7062	Finca La soledad	16.431	-91.975	1469	01/02/1961	01/02/2019	14	3
7076	Huixtan[1]	16.839	-92.533	1990	01/11/1964	01/11/2005	8	3
7081	Ixcán	16.833	-91.067	200	01/06/1965	01/12/1988	18	1
7089	La catarata[1]	16.217	-91.317	327	01/07/1966	01/06/1996	4	2
7096	La pimienta[1]	16.317	-91.783	1120	01/03/1964	01/07/1994	6	1
7104	Las margaritas	16.406	-92.047	1512	01/07/1962	01/06/2019	3	3

Station ID	Station name	Latitude (°)	Longitude (°)	Altitude (m asl)	Period start	Period end	Missing data (%)*	Cluster
7107	Las tazas[1]	16.836	-91.747	600	01/04/1965	01/11/1993	3	2
7108	Livingston[1]	16.767	-92.050	1200	01/04/1965	01/06/1994	5	2
7114	Yaquintela	16.994	-91.853	650	01/11/1964	01/09/2019	14	2
7118	Miramar[1]	16.383	-91.583	950	01/01/1964	01/04/1976	12	2
7121	Nueva esperanza	16.450	-91.133	1000	01/05/1957	01/12/1993	5	2
7124	Ostional	16.417	-91.250	247	01/06/1969	01/12/1983	13	2
7125	Oxchuc	16.814	-92.428	1987	01/10/1969	01/09/2019	6	2
7127	Paso Del Soldado[1]	16.117	-91.783	1485	01/03/1963	01/12/1976	12	2
7152	Santa Cecilia[1]	16.367	-91.433	254	01/03/1964	01/10/1981	7	1
7154	Santa Elena[1]	16.117	-91.483	720	01/01/1969	01/10/1994	3	1
7179	Altamirano[1]	16.683	-92.000	1250	01/12/1964	01/12/1994	13	2
7190	La Trinitaria[1]	16.128	-92.067	1540	01/01/1970	01/09/2019	13	3
7192	Ocosingo[1]	16.900	-92.100	978	01/05/1964	01/02/1989	8	3
7205	Comitán[3]	16.261	-92.142	1630	01/01/1961	01/09/2019	4	3
7215	Altamirano[3]	16.733	-92.033	1240	01/07/1973	01/12/1988	10	2
7231	Tziscao[3]	16.083	-91.667	1475	01/08/1977	01/02/2003	20	1
7337	Lacantún[3]	16.708	-90.722	120	01/06/1980	01/12/2017	8	1
7374	La Esperanza	16.192	-91.881	1500	01/06/1987	01/09/2019	19	3
7391	Yasha	16.453	-92.150	1750	01/11/1983	01/09/2019	9	3
27001	Balancán de Domínguez[2]	17.900	-91.567	18	01/08/1943	01/01/1980	18	2
27004	Boca del Cerro	17.594	-91.581	14	01/08/1948	01/10/2019	3	2
27006	Buenavista	17.678	-91.347	50	01/08/1967	01/09/2019	4	2
27021	Mactun	17.817	-91.375	29	01/06/1969	01/09/2019	18	2
27040	San Pedro	17.867	-91.233	44	01/08/1948	01/09/2019	8	2
27046	Tenosique[3]	17.533	-91.517	19	01/07/1954	01/06/1985	7	2
27050	Tres Brazos	18.392	-92.600	2	01/11/1948	01/09/2019	5	2
27088	La T	17.617	-91.550	67	01/07/1983	01/09/2019	15	2
27091	Playa larga	17.983	-91.900	5	01/07/1983	01/09/2019	16	2
GUATEMALA								
INS-020604	San Jerónimo	15.061	-90.249	1000	04/04/1970	31/12/2018	2	3
INS-141502	Chixoy	15.358	-90.662	680	01/01/1971	31/12/2018	1	2

Station ID	Station name	Latitude (°)	Longitude (°)	Altitude (m asl)	Period start	Period end	Missing data (%)*	Cluster
INS-020201	Cubulco	15.109	-90.621	994	01/01/1980	31/12/2018	3	3
INS-141001	Sacapulas	15.290	-91.092	1180	01/01/1969	31/12/2018	2	3
INS-140801	Nebaj	15.399	-91.142	1906	01/01/1969	31/12/2018	6	2
INS-110104	Flores	16.916	-89.867	123	01/01/1973	31/12/2018	2	2

m asl=meters above sea level; Administrators of the meteorological stations in Mexico: [1]CFE= Comisión Federal de Electricidad; [2]DGE= Dirección General de Estudios; [3]SMN= Servicio Meterológico Nacional; * daily missing data calculated over the operating period of each station

Table S2 Standard Precipitation Index (SPI) values and their associated conditions (WMO 2012).

SPI range	Condition
≥ 2.0	Extreme humidity
1.99 – 1.5	Severe humidity
1.49 – 1.0	Moderate humidity
0.99 – -0.99	Close to normal
-1.0 – -1.49	Moderate dry
-1.5 – -1.99	Severe dry
≤ -2.0	Extreme dry

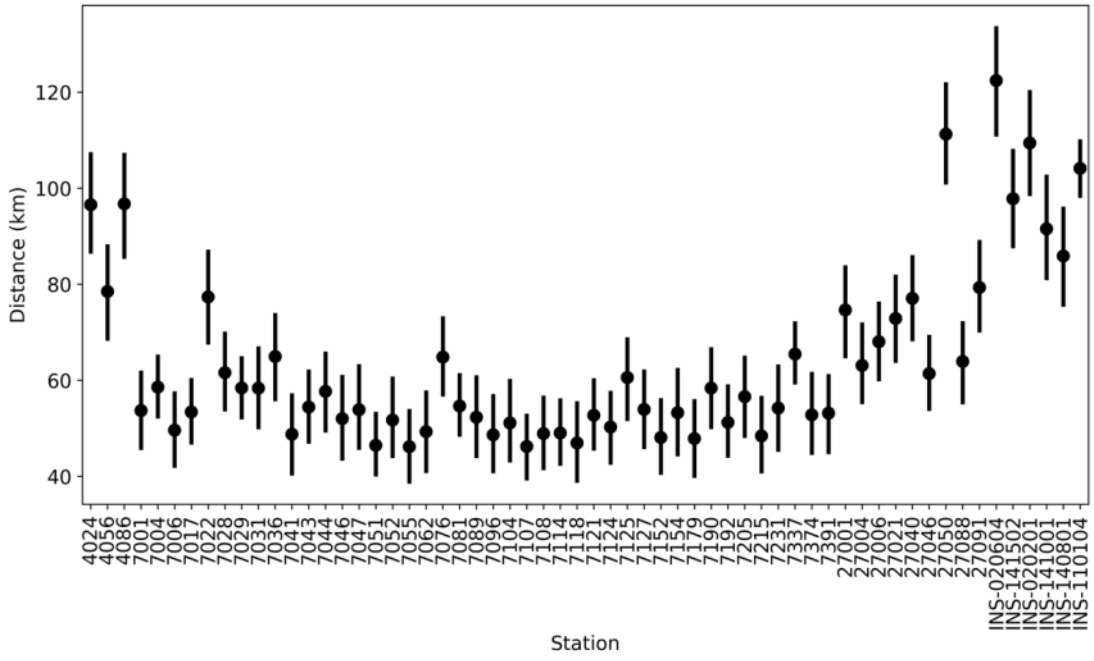

Figure S1 Mean distance to the closest station with available data in the Usumacinta River Basin over the entire study period (1959-2018). Error bars represent the 95% confidence interval.

Supplementary Material – Chapter 3

Table S1 Stable isotope values of carbon sources in study systems from Términos Lagoon (southern Gulf of Mexico) and El Verde Camacho Lagoon (entrance of the Gulf of California).

System	Source	n	$\delta^{13}C$ (‰)		$\delta^{15}N$ (‰)		References
			Mean	SD	Mean	SD	
PDE	Mangrove leaves (Rm*)	3	-30.4	0.58	3.72	0.58	Sepúlveda-Lozada et al. (2015)
	Fluvial particulate organic matter	2	-26.2	0.2	5.98	0.20	Sepúlveda-Lozada et al. (2015, 2017)
	Lagoon phytoplankton	2	-26.7	0.2	3.72	0.20	Sepúlveda-Lozada et al. (2015, 2017)
CP	Mangrove leaves (Rm, Lr, Ag*)	11	-28.4	1.0	2.62	0.75	Gonneea et al. (2004); Sepúlveda-Lozada et al. (2015)
	Fluvial particulate organic matter	2	-26.2	0.2	5.98	0.20	Sepúlveda-Lozada et al. (2015, 2017)
	Lagoon phytoplankton	7	-25.51	1.38	4.35	0.73	Gonneea et al. (2004); Sepúlveda-Lozada et al. (2015)
EV	Mangrove leaves (Rm*)	12	-29.2	0.8	4.2	0.9	Medina-Contreras et al. (2023)
	Fluvial particulate organic matter	2	-22.4	0.8	9.4	0.8	Kwak and Zedler (1997)
	Marine phytoplankton	4	-20.1	2.0	4.3	1.9	Valladolid-Garnica et al. (2023)

PDE: Palizada-del-Este System; CP: Candelaria-Panlau System; EV: El Verde Camacho.
*Rm: Rhyzophora mangle; Lr: Laguncularia racemose; Ag: Avicennia germinans.
SD: standard deviation.

Table S2: Variable characteristics in Términos Lagoon (southern Gulf of Mexico) and El Verde Camacho Lagoon (entrance of the Gulf of California).

Variable	System	Stations (Code)	Location	Period	Reference
Mass accumulation rates	PDE, CP, EV		At the sediment core location	1900-2021	Jupin et al. (2023)
Precipitation	PDE	Palizada (4024)	18°10.97; -91°02.75	1959-2018	Jupin et al. (2024)
	CP	Candelaria (SMN: 4004; CGE: 4039)	18°11.07; -91°02.77	1944-2018	SMN-CONAGUA (2022)
	EV	El Quelite CFE (25031)	23°33.43 ; -106°27.50	1961-2017	
		El Quemado (25076)	23°44.75 ; -106°28.00		
River discharge	PDE	Boca Del Cerro (B30019)	17°26.00; -91°29.00	1949-2014	CONAGUA (2020)
	CP	Candelaria (B30181)	18°11.00; -91°04.00	1953-2014	
Land-use	PDE		Palizada River basin	1968-86; 1990-99; 2001-02; 2007-08; 2011; 2014-15; 2018	INE - INEGI (1997); INEGI (2001, 2005, 2009, 2013, 2016, 2021)
	CP		Candelaria River basin		
	EV		Quelite River basin		
Population	PDE, CP		Carmen City Municipality	1900-2020	INEGI (2022)
	EV		Mazatlán Municipality	1900-2020	
Mangrove cover	PDE		Palizada River basin	1970; 2005, 2010, 2015, 2020	CONABIO (2013a, 2013b, 2013c, 2016, 2021).
	CP		Candelaria River basin		
	EV		Quelite River basin		

PDE: Palizada-del-Este System; CP: Candelaria-Panlau System; EV: El Verde Camacho.
Based on CONABIO (1998) and Priego et al. (2007), river basins were delineated to assess land-use and mangrove cover estimations.

Supplementary Material – Chapter 4

Table S1 Coefficient of determination R^2 of the fitted curve of S2 (quantity of hydrocarbon compounds produced during the Rock-Eval pyrolysis) in mangrove sediment cores from Términos Lagoon (southern Gulf of Mexico) and El Verde Camacho Lagoon (entrance of the Gulf of California).

LTMPA01		LTMPA02		LTMCA03		EVC01	
Section (cm)	R^2	Section (cm)	R^2	Section (cm)	R^2	Section (cm)	R^2
3-4	0.9994	0-1	0.9994	0-1	0.9995	0-1	0.9989
6-7	0.9995	1-2	0.9995	3-4	0.9998	1-2	0.9995
9-10	0.9995	3-4	0.9993	6-7	0.9994	3-4	0.9996
12-13	0.9996	5-6	0.9997	12-13	0.9998	5-6	0.9987
15-16	0.9995	7-8	0.9996	15-16	0.9998	7-8	0.9992
18-19	0.9996	9-10	0.9996	18-19	0.9997	9-10	0.9998
21-22	0.9995	11-12	0.9995	21-22	0.9998	11-12	0.998
24-25	0.9997	13-14	0.999	24-25	0.9997	13-14	0.9984
27-28	0.9996	15-16	0.9996	27-28	0.9996	15-16	0.9968
30-31	0.9995	17-18	0.9997	30-31	0.9996	17-18	0.9958
33-34	0.9995	19-20	0.9997	33-34	0.9996	19-20	0.995
36-37	0.9993	21-22	0.9997	36-37	0.9997	21-22	0.9959
39-40	0.9993	23-24	0.9993	39-40	0.9997	23-24	0.9973
42-42	0.9993	25-26	0.9997	42-43	0.9997	25-26	0.9983
45-46	0.9994	27-28	0.9993	45-46	0.9998	27-28	0.9974
48-49	0.9991	29-30	0.9996	48-49	0.9998	29-30	0.996
51-52	0.9992	31-32	0.9985	51-52	0.9999	31-32	0.9982
54-55	0.9985	33-34	0.9994	54-55	0.9997	33-34	0.9976
57-58	0.9979	35-36	0.9996	57-58	0.9997	35-36	0.9965
60-61	0.9979	37-38	0.999	60-61	0.9993	39-40	0.9969
63-64	0.9974	39-40	0.9996	63-64	0.9999	43-44	0.9959
66-67	0.9960	41-42	0.9994	66-67	0.9998	47-48	0.9942
67-68	0.9987	43-44	0.9996	69-70	0.9991	51-52	0.996
		45-46	0.9984	72-73	0.9996	55-56	0.9976
				74-75	0.9998	59-60	0.9969
						63-64	0.9943

Table S2 Variable characteristics for sediment cores in Términos Lagoon (southern Gulf of Mexico) and El Verde Camacho Lagoon (entrance of the Gulf of California).

Variable	System	Station (Code)	Location	Time period	Reference
Mass accumulation rate	PDE, CP, EV		Site of each sediment core	1900-2021	Jupin et al. (2023a)
Precipitation	PDE	Palizada (4024)	18°10.97; -91°02.75	1959-2018	Jupin et al. (2023b)
	CP	Candelaria (SMN:4004; CGE: 4039)	18°11.07; -91°02.77	1944-2018	SMN-CONAGUA (2022)
	EV	El Quelite CFE (25031) El Quemado (25076)	23°33.43; -106°27.50 23°44.75; -106°28.00	1961-2017	
River discharge	PDE	Boca del Cerro (B30019)	17°26.00; -91°29.00	1949-2014	CONAGUA (2020)
	CP	Candelaria (B30181)	18°11.00; -91°04.00	1953-2014	

PDE, Palizada-del-Este system; CP, Candelaria-Panlau system; EV, El Verde Camacho.

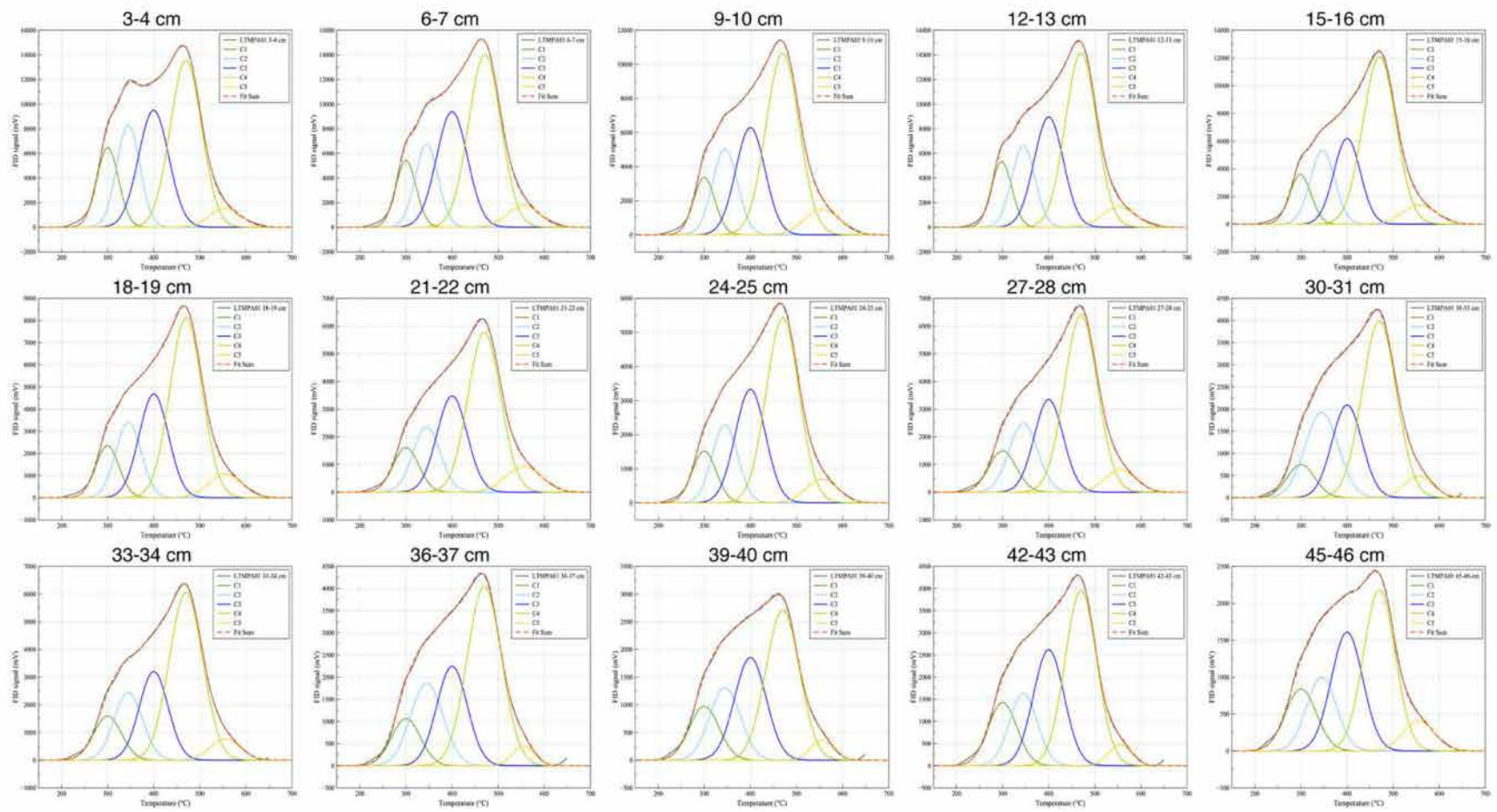

Figure S1 Deconvolution of multilobed S2 signals (representing the quantity of hydrocarbon compounds measured by a flame ionisation detector, FID, across temperature during the Rock-Eval pyrolysis) into individual cluster signals (C1 to C5) in mangrove sediment core LTMPA01 from Términos Lagoon (southern Gulf of Mexico). Cluster colors: green: C1; light blue: C2; blue: C3; light green: C3; yellow: C5; red: sum of clusters.

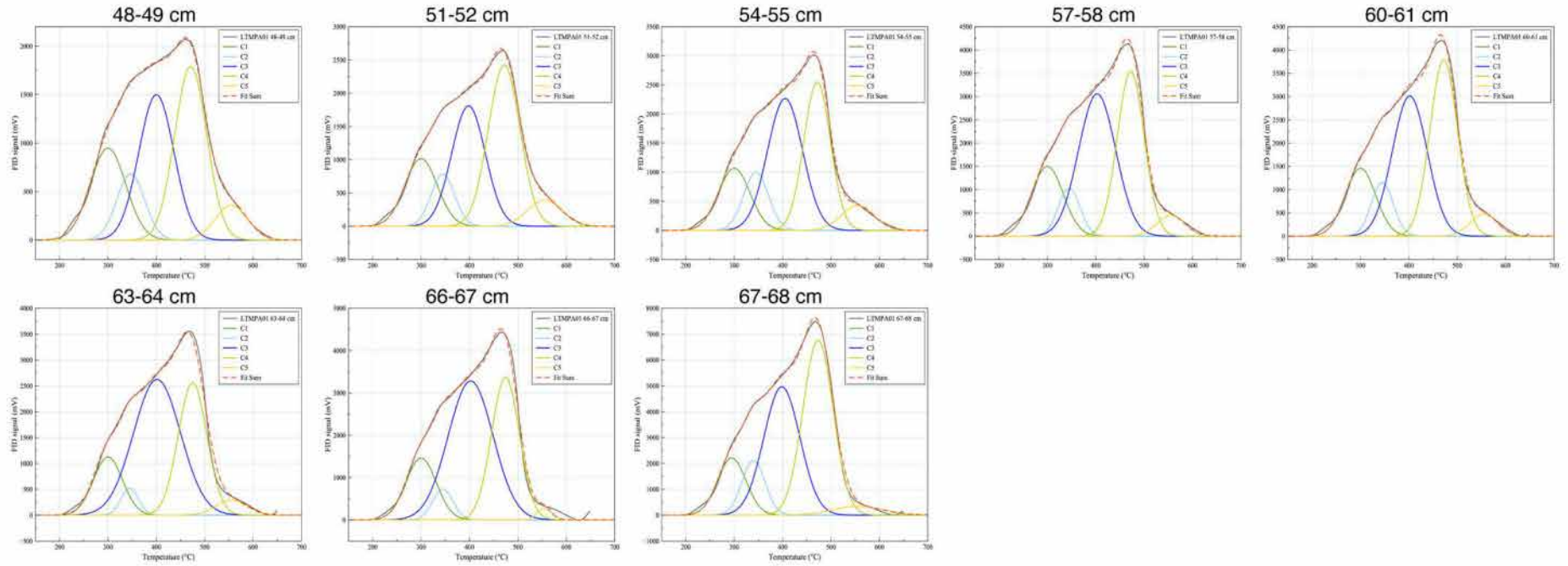

Figure S1 (continued).

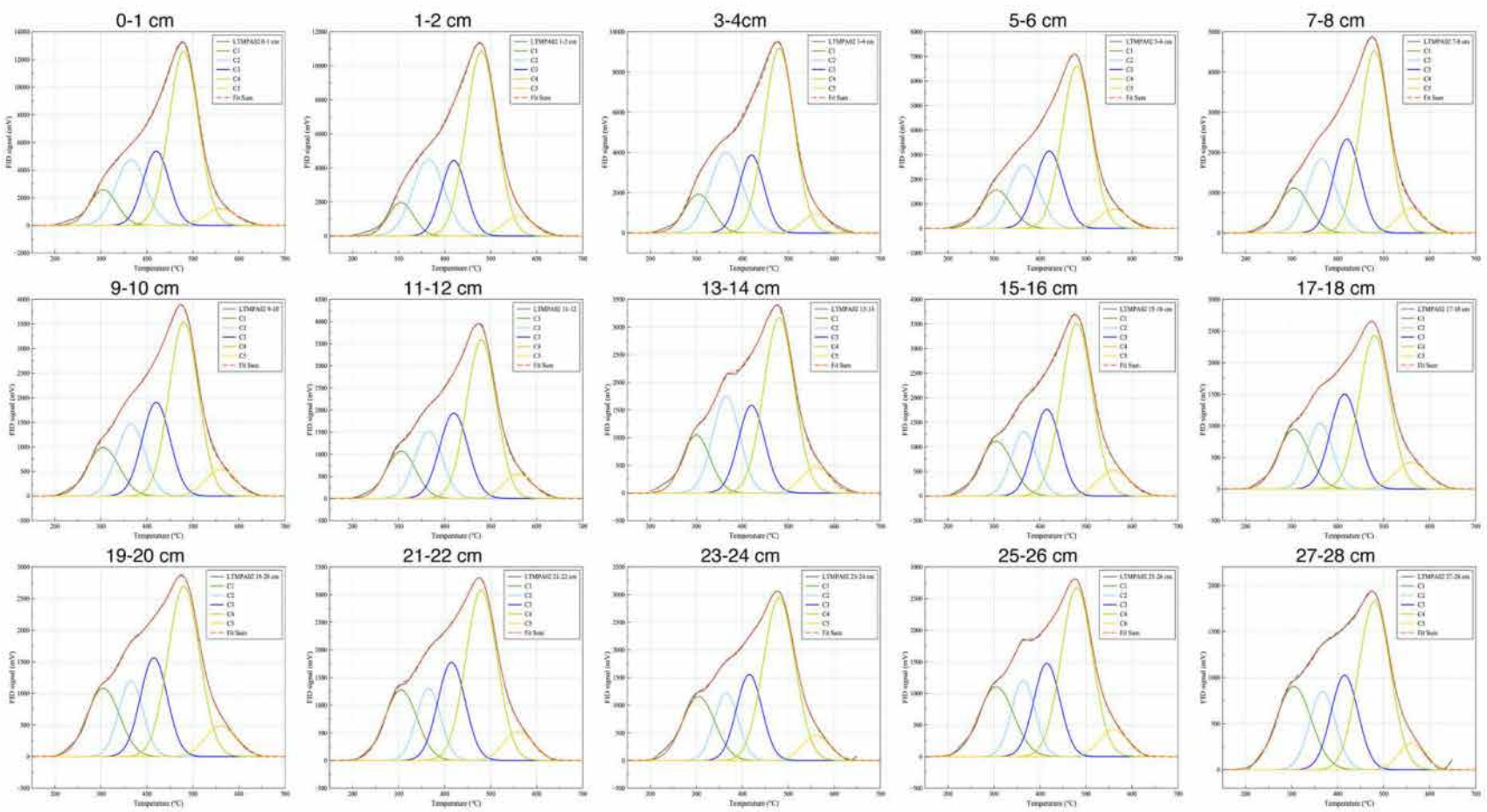

Figure S2 Deconvolution of multilobed S2 signals (representing the quantity of hydrocarbon compounds measured by a flame ionisation detector, FID, across temperature during the Rock-Eval pyrolysis) into individual cluster signals (C1 to C5) in mangrove sediment core LTMPA02 from Términos Lagoon (southern Gulf of Mexico). Cluster colors: green: C1; light blue: C2; blue: C3; light green: C3; yellow: C5; red: sum of clusters.

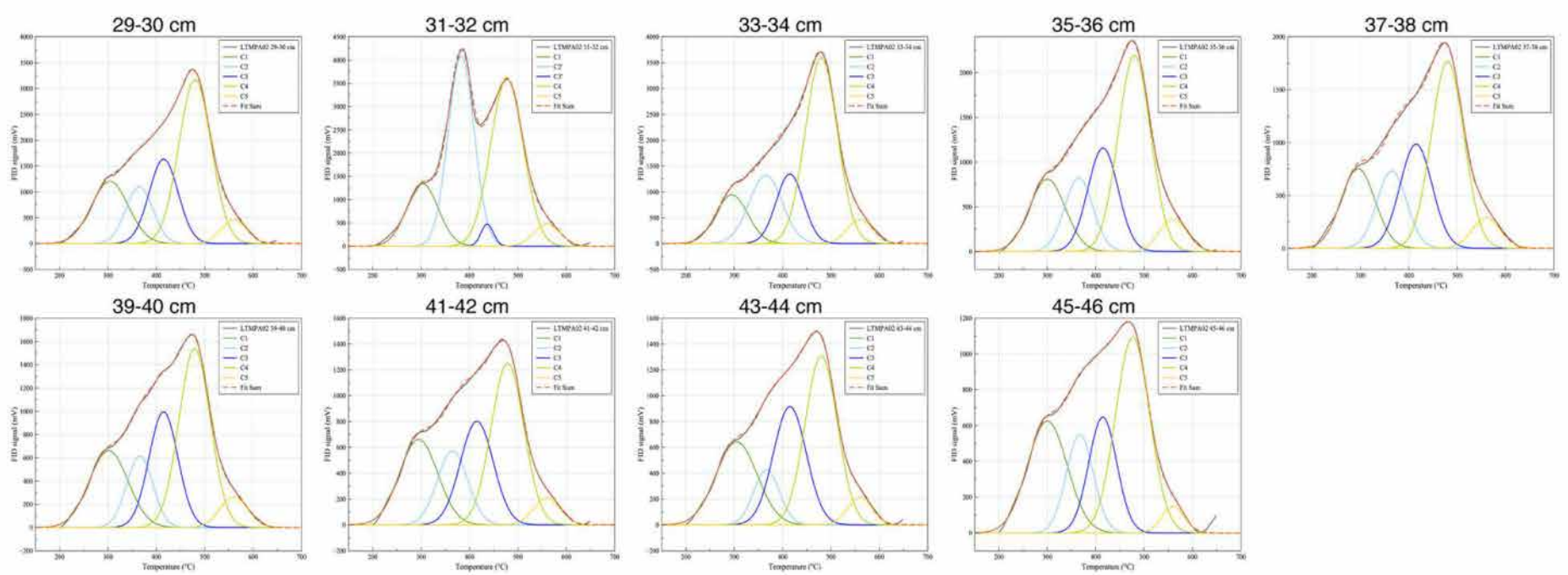

Figure S2 (continued).

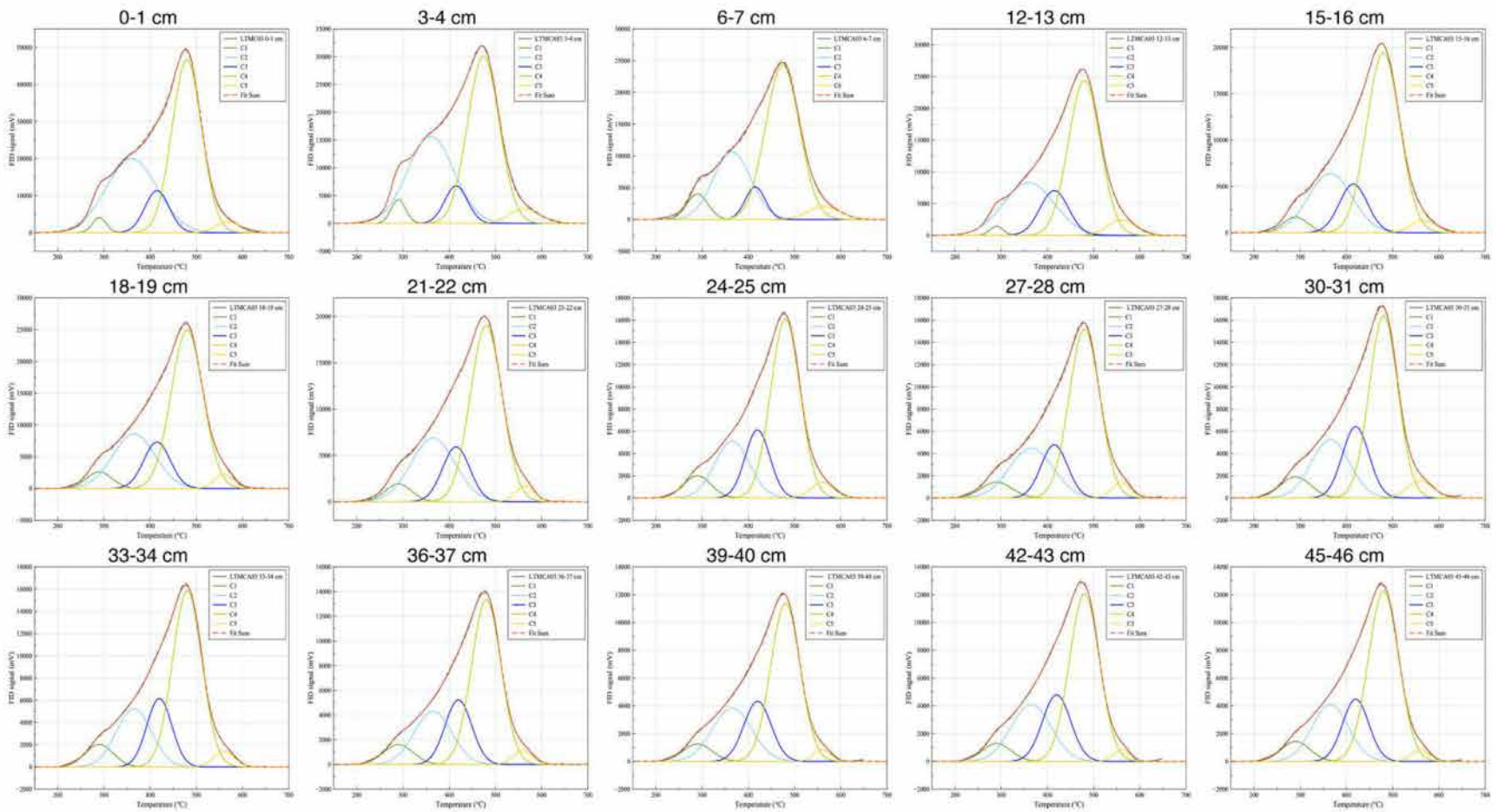

Figure S3 Deconvolution of multilobed S2 signals (representing the quantity of hydrocarbon compounds measured by a flame ionisation detector, FID, across temperature during the Rock-Eval pyrolysis) into individual cluster signals (C1 to C5) in mangrove sediment core LTMCA03 from Términos Lagoon (southern Gulf of Mexico). Cluster colors: green: C1; light blue: C2; blue: C3; light green: C3; yellow: C5; red: sum of clusters.

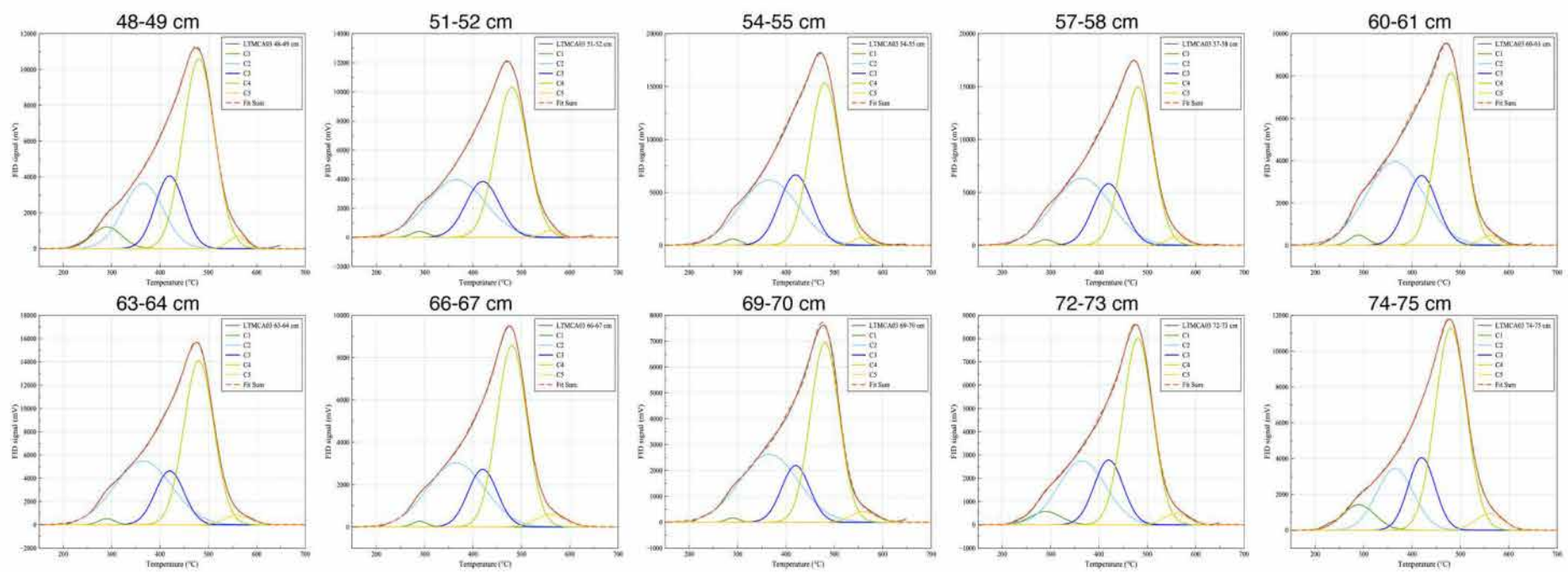

Figure S3 (continued).

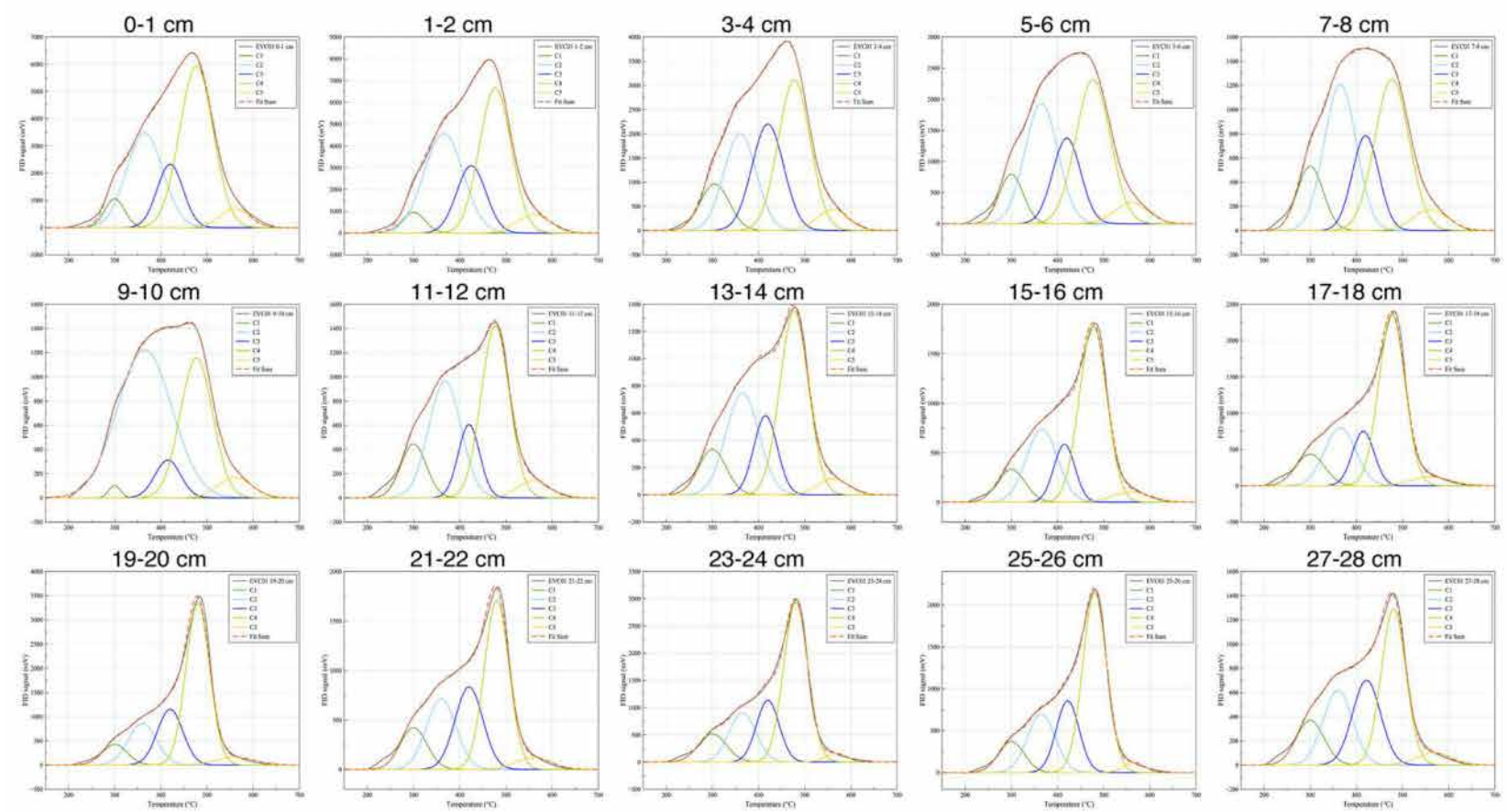

Figure S4 Deconvolution of multilobed S2 signals (representing the quantity of hydrocarbon compounds measured by a flame ionisation detector, FID, across temperature during the Rock-Eval pyrolysis) into individual cluster signals (C1 to C5) in mangrove sediment core EVC01 from El Verde Camacho Lagoon (entrance of Gulf of California). Cluster colors: green: C1; light blue: C2; blue: C3; light green: C3; yellow: C5; red: sum of clusters.

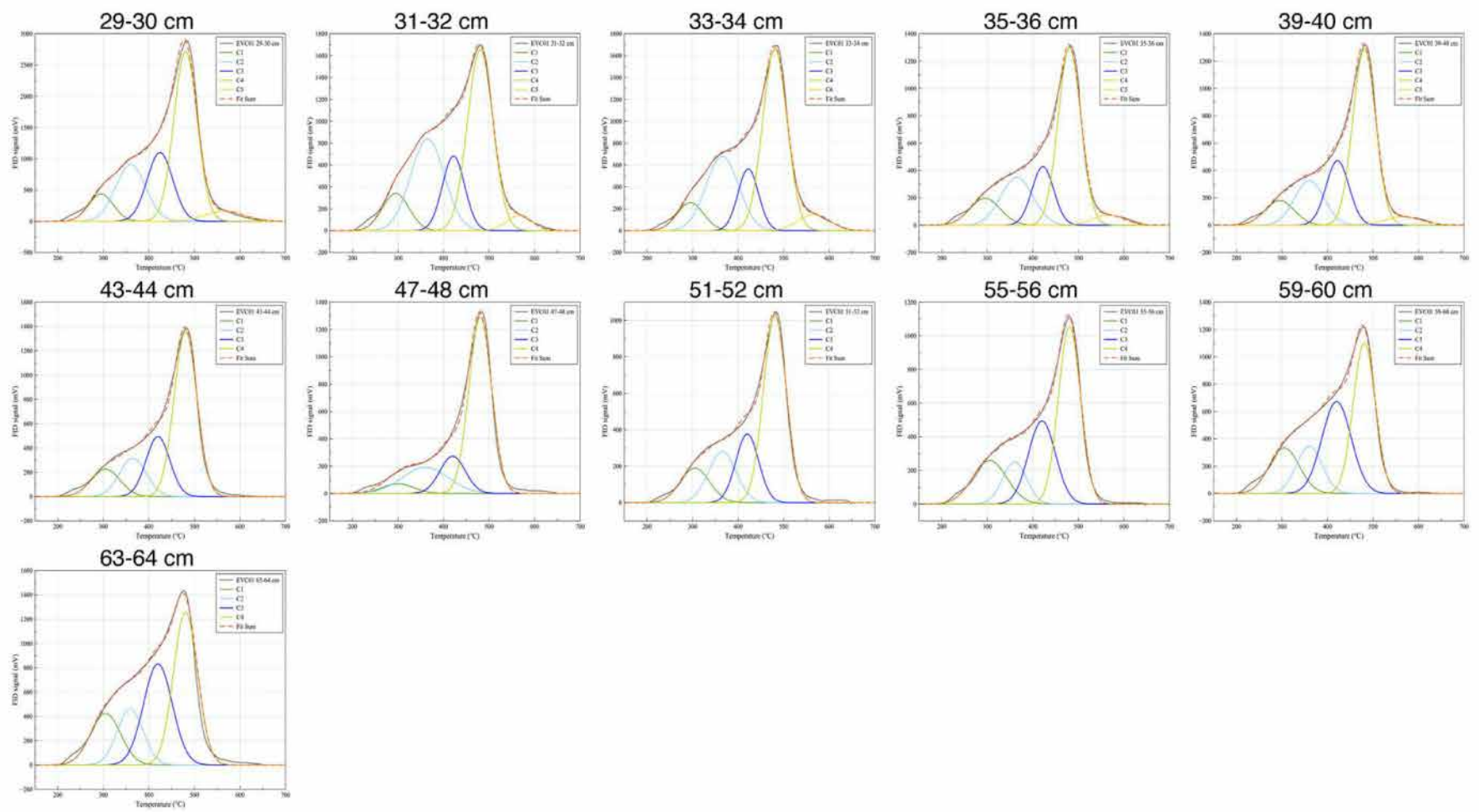

Figure S4 (continued).